Structure and Orientation of Transmembrane Peptides in Model Membrane Systems as Studied by Solid-State ^{2}H NMR and Molecular Dynamics

Structuur en oriëntatie van transmembraanpeptiden in modelmembraan systemen bestudeerd met vaste stof deuterium NMR en moleculaire dynamica

(met een samenvatting in het Nederlands)

Proefschrift ter verkrijging van de graad van doctor aan de Universiteit Utrecht op gezag van de rector magnificus, Prof. Dr. W.H. Gispen, ingevolge het besluit van het College voor Promoties in het openbaar te verdedigen op woensdag 31 januari 2007 des ochtends te 10.30 uur

door

Suat Özdirekcan

geboren op 30 december 1971,
te Montreuil, Frankrijk

Promotor: Prof. dr. J. A. Killian

Contents

Beoordelingscommissie:

Prof. dr. B. de Kruijff	(Universiteit Utrecht)
Prof. dr. M. R. Egmond	(Universiteit Utrecht)
Prof. dr. R. Boelens	(Universiteit Utrecht)
Prof. dr. S. J. Marrink	(Rijksuniversiteit Groningen)

Druk: Gildeprint Drukkerijen b.v.

ISBN: 978-90-393-4461-3

Chapter 1

General Introduction

Biomembranes

The smallest structural unit of all living organisms is the cell, which needs a wealth of biochemical processes to grow, divide, or simply to be maintained alive. A large assortment of compounds, which are nearly omnipresent in most organisms or cells, is required to ensure the wide variety of essential functions. Necessarily, cells will need a very high level of organization of cellular components to achieve their many specific tasks in a coordinated way.

Biomembranes are universal cell components that specifically bring a higher level of organization and help the coordination of events by creating cellular compartments. For example, by acting as highly selective permeability barrier, the plasma membrane allows cells to keep their specific contents different from the exterior. In eukaryotic cells, membranes in addition provide individuality to organelles, by separating their contents from the cytoplasm. This barrier function is due to the organization in a double layer of lipids, which are main constituents of membranes.

Cellular processes are localization-dependent, each cellular compartment having its own specificity of functions. Some essential processes involve selective transport of polar molecules, ions, and macromolecules across membranes. This transport is taken care of by membrane proteins that could be either channels or pumps. In addition, membrane proteins are involved in cellular and intercellular communication including hormonal reactions, signal transduction, and cell recognition. Finally, membranes are also mechanical supports for protein-mediated biochemical reactions like catalysis, biosynthesis, and degradation processes.

These examples illustrate the importance of membranes and the role of membrane proteins. In the next paragraph, the architecture of membranes will be described with special accent on their main constituents, the lipids and the proteins.

Membrane structure

The molecular composition of membranes can vary widely among organisms, but also between cells of different organs from the same organism, and between the different organelles of the same cell, reflecting the level of specialization of membranes (1,2). However, they all are essentially assemblies of two components, lipid and protein molecules, which are held together by non-covalent interactions. The basic design of lipids is amphipathic, consisting of a polar headgroup associated with a hydrophobic tail. This amphipathicity drives them to organize in a continuous double layer in which the lipids are organized with their polar headgroups pointing towards the aqueous phase and the hydrophobic acyl chains of both leaflets facing each other. Proteins that are embedded in a membrane typically have one or more hydrophobic segments that are in contact with the lipids, and residues that are more polar and that locate near the lipid headgroups of the membrane and out of the membrane.

The fluid-mosaic model, which is one of the established models describing membranes, proposed that proteins are “dissolved” in the highly dynamic lipid bilayers (3). However, recent evidence showed that neither the proteins nor the lipids are freely diffusing in the membranes. Instead, the diffusion properties of membrane components vary due to a lateral compartmentalization of lipids and proteins in domains within the bilayer (reviewed in 4).

In addition, lipids and membrane proteins can influence each other’s structure and dynamics in various ways. For example, lipid protein interactions can lead to changes of the membrane properties such as the phase or the bilayer thickness (reviewed in 5) or it can lead to protein activity modulation (6). The next paragraphs will describe the

lipids, the membrane proteins, and then the lipid parameters that affect membrane protein activity.

Lipids

The classification of membrane lipids counts several categories including phospholipids, glycolipids, and sterols. There are different classes of phospholipids based on the chemical nature of their polar headgroup and on the composition of their hydrophobic chains. In the following, the text will focus on the diacylphosphatidylcholines (PC), because they are the most common phospholipids in mammalian cells (2). Fig. 1A, shows as an example 1,2-dioleoyl-sn-glycero-3-phosphocholine (di-C18:1_c-PC). The headgroup of PC molecules consists of a phosphate diester bound on one side by a choline moiety, and on the other side by a glycerol backbone. The other two hydroxyl groups of the glycerol are esterified each with a fatty acid constituting the tail of the lipid. At physiological pH values, the headgroup of PC lipids is zwitterionic, with a negatively charged phosphate and a positive charge of the choline group. The two fatty acyl chains constitute the hydrophobic part of the molecule, which can vary in length and degree of saturation. In an aqueous environment under physiological conditions, PC lipids assemble into a bilayer, thereby minimizing energetically unfavorable interactions of acyl chains with water.

Fig. 1B, shows the time-average distribution of the different groups of di-C18:1_c-PC obtained by X-ray and neutron diffraction of the bilayer including the headgroup hydration water (7,8). The picture shows that the bilayer can be divided in two regions, one being the hydrocarbon core (between the vertical dashed lines), which is not easily accessible to water and the other one being the membrane-water interface, which can be hydrated by water molecules through hydrogen-bonding with for example the phosphate groups (7). The borderline that distinguishes the hydrocarbon core from the membrane-water interface of each leaflet is determined by the region where water molecules are able to hydrate specifically the lipid headgroups as depicted by the dotted curves.

Hydrocarbon core

Fig. 1B also illustrates the contribution of lipid structural groups to the density profile (thin lines). The biggest contribution comes from the hydrocarbon core with the methylenes and methyl groups of the acyl chains showing two peaks that have highest intensity near the interface. This pattern is typical for a “fluid” PC bilayer in the so-called liquid-crystalline phase (L_α) (7).

The fluidity of a bilayer depends on the temperature (9). At low temperatures, the kinetic energies of the acyl chains are so low that the chains become tightly packed in an extended, mostly all-trans conformation, called the gel phase (L_β). Increasing the temperature of single species bilayers will disturb the packing by increasing the degree of motion of the chains, with a very sharp transition in the motional properties at the so-called phase transition temperature. Above this temperature the lipids are in the L_α-phase. Due to the higher fluidity of bilayers in the L_α-phase, membranes are significantly thinner than in the L_β-phase. Fluid bilayers in the L_α-phase are biologically more relevant than the L_β-phase, because often cellular membranes have to be in a fluid state for cells to function (7). The length of the chains determines the number of van der Waals contacts thereby influencing the phase transition temperature, which increases with the number of carbons. Unsaturation of the acyl

chains results in a destabilization of the packing, and hence a lowering of the phase transition temperature.

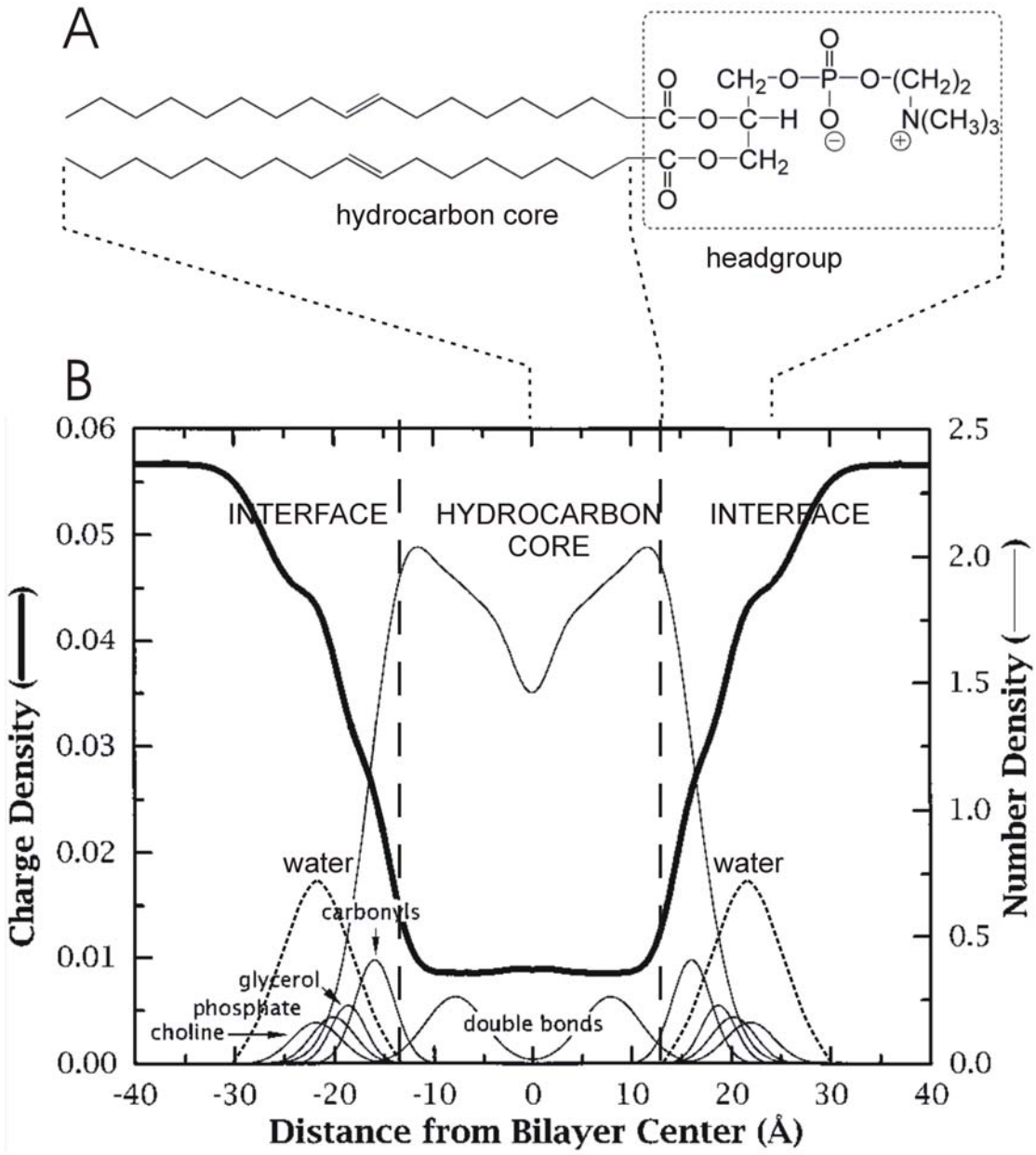

Figure 1. A. Structure of di-C18:1-PC, a zwitterionic phospholipid. B. Time-averaged distributions of the principal structural groups of di-C18:1-PC (thin lines), when the lipid is assembled into a fluid bilayer, depicted together with the resulting polarity profile (thick line). The distribution of hydrating water is indicated by the dotted lines. Adapted from (7).

As a consequence of different packing properties, lipid bilayers in the L_α-phase at an equal number of carbons in the fatty acyl chains will be generally thinner in the case of unsaturated chains than with saturated ones (10). The combined influences of the temperature, the length of the hydrophobic chains, and the degree of saturation determine the thickness of the bilayer and the packing and conformational properties of the chains. These properties in turn, will be important for the conformation and activity of proteins that are embedded in a lipid bilayer.

Interfacial region

According to Fig. 1B, approximately 50% of the total thickness of the bilayer is occupied by the interfacial regions in both membrane leaflets. A particularly important feature of the interfacial regions is their complex composition of water, phosphocholine, glyceryl, carbonyl, and the upper methylene groups. These groups offer possibilities for non-covalent interactions between lipids, proteins, or any compounds that can partition in this region.

Although this region is highly dynamic, the components of the headgroups of lipids are distributed in a rather restricted region creating a zone of intermediate polarity between the aqueous phase and the very hydrophobic region of the acyl chains. Consequently, the polarity will change very rapidly in the transition around the carbonyls from the interface to the hydrocarbon core making the polarity gradient steepest in this part. Fig. 1B, illustrates this point, where the average density of atomic partial charges (thick line) is represented for each groups of the lipids (7). In contrast, in the hydrophobic core the polarity will be negligible over a wide range of depths in the bilayer. The polarity profile is an important feature for membranes, because it strongly influences the energetics involved in the distribution of amino acids of proteins along the bilayer normal, and hence for positioning membrane proteins into lipid bilayers (11-13).

Membrane proteins

The large variety of functions of membrane proteins described earlier illustrates well how important their role is for life. Membrane proteins are commonly classified as peripheral and integral, the first category being bound to the membrane surface without traversing the lipid bilayer in contrast to integral proteins, which have one or more transmembrane segments embedded within the lipids. Therefore, integral membrane proteins are likely to be more influenced by properties of the lipid bilayer than peripheral proteins. The influence of lipids on the transmembrane parts of proteins can have important implications for the function, not only due to structural changes of the transmembrane segments, but also of the extracellular loops because they are covalently linked to the membrane-spanning parts. The rest of the introduction will treat only transmembrane segments of integral proteins.

The carbonyl and amide moieties that constitute the backbone of polypeptides are polar groups that very efficiently form H-bonds, especially with water. However, water molecules are barely present in the hydrocarbon core and they are present in small amounts only in the interfacial region. This enhances the effectiveness of carbonyls and amides to form intramolecular H-bonds within a bilayer. Formation of α-helical structures or β-sheets is favourable, because it prevents exposure of polar groups of the backbone to a hydrophobic lipid environment. As much as 80% of the structured residues in membrane proteins are in α-helices (14), the remaining 20% mainly consisting of β-strands.

General characteristics of transmembrane segments of proteins

Several studies on the amino acids composition of transmembrane parts of proteins showed that the distribution across the membrane is not random (11-13,15,16). One reason is that the energetic cost of incorporating residues of different polarity than their direct environment is unfavorable. For example, leucine and alanine, which are very hydrophobic, will partition favorably in the hydrocarbon interior, whereas aromatic amino acids are found more near the lipid-water interface.

The preferential location of residues near the membrane-water interface, whether they are charged or aromatic, is due to the possibilities for hydrogen bonding, electrostatic, dipolar, and quadrupolar interactions with the lipid headgroups (7,17), or because of the intermediate hydrophobicity of that region in the case of aromatic amino acids (18,19). Thereby, aromatic residues like tryptophan can act as membrane anchor and will resist displacement from their preferential localization in the membrane-water interface (5,17,20). Similar anchoring functions were also postulated for charged residues as lysine or arginine that often localize in the membrane-water interfacial regions of integral proteins (21).
Residues of membrane proteins that reside in regions of the membrane where they do not interact favorably will require other mechanisms for reducing the energetic cost of their presence in the lipid bilayer (22). For example, proteins that have polar amino acids in their transmembrane parts will generally be polytopic consisting of several α-helical bundles in which these residues are shielded from the surrounding lipids.
The combination of abovementioned lipid-protein interactions determines which parts of a protein incorporate in the lipid bilayers or reside in the aqueous environment and which part anchor at the interfacial region of the membrane. Typically, membrane-spanning protein segments are 20-22 residues long corresponding to the approximate hydrophobic thickness of biomembranes (22).

Lipid mediated modulation of the membrane protein structure and activity

Energetics and interaction properties will determine the way in which proteins will be accommodated in the membrane. Obviously, lipid parameters play an important role therein. Packing properties of the lipids can influence the dynamic and conformational properties of the membrane-embedded proteins, and hence modulate their activity (6). This is the case for both the hydrocarbon core and the interfacial region of the membrane.
For example, lipids like cholesterol or phosphatidylethanolamine lipids do not occupy the space as the cylindrical-shaped PC lipids, and thereby incorporation of these lipids in a PC bilayer will influence the packing properties of the lipids and the protein conformation and activity by remodeling the membrane lateral pressure profile (see (23-25) for reviews). In addition cholesterol can either affect membrane protein activity by promoting the formation of cholesterol-rich ordered domains called rafts (26-29) that are enriched in a specific set of proteins, or by directly competing with other lipids for protein binding sites (24). Furthermore, packing properties of lipids can be affected by amphipathic molecules like short chain alcohols, which partition preferentially in the interfacial region of the membrane. They are anesthetics that are known to interact with many membrane proteins influencing their activity (30) and references therein). Their partitioning in the membrane-water interface results in remodeling the lateral pressure profile (23,31-33). This in turn influences the conformational equilibria of membrane proteins that may be involved in functional properties like for example the gating mechanisms of ion channels. Small alcohols also affect the degree of association of oligomeric proteins illustrating their profound influence on membrane protein structure (23,30,32,34,35).

Bilayer thickness

One of the most extensively investigated parameters that affects membrane protein activity is the bilayer thickness. Two major contributions to the membrane positioning

of integral proteins are interfacial anchoring interactions, and hydrophobic interactions between lipids and side chains of transmembrane residues. The localization for the two types of interactions is largely depth-dependent. Consequently, a change of the bilayer thickness may cause a shift of the interaction contact interfaces between a transmembrane protein and the surrounding lipids, thereby increasing or decreasing the exposure of hydrophobic and hydrophilic parts of the protein to the aqueous phase and to the hydrophobic core of the membrane, respectively. In order to compensate for this situation, a membrane protein could either adjust its structure or cause surrounding lipids to adapt to this condition. This situation, generally designated as hydrophobic mismatch, and its consequences on lipid protein interactions, have extensively been studied since the 90's (24,36,37). The description of the "mattress model" system of membranes generally assumes that matching conditions are the most stable (38). Several studies show indeed that the stability of membrane proteins can be sensitive to mismatch (37).
A situation wherein the hydrophobic length of a transmembrane protein segment exceeds the hydrophobic thickness of the bilayer is called positive hydrophobic mismatch, whereas the opposite situation is termed negative mismatch. Although, both types of mismatch can affect membrane protein activity, the following text will focus on positive mismatch.

Positive hydrophobic mismatch
Rearrangement of the lipids and transmembrane segments of the proteins is often required for compensating the unfavorable energetic situation of hydrophobic mismatch. In the case of positive hydrophobic mismatch, limiting exposure of the transmembrane hydrophobic residues to the aqueous phase is a driving force for adaptations of the system as illustrated by Fig. 2A-F. One possible adaptation of the system to compensate for the mismatch, is by increasing the order in the lipid acyl chains, and hence the bilayer thickness (Fig. 2B). This was demonstrated with artificial single membrane-spanning α-helical peptides (5,37). Nevertheless, changing the bilayer thickness is generally not sufficient for compensating hydrophobic mismatch. Several other mechanisms such as tilting the backbone (Fig. 2C), backbone length reduction (Fig. 2D), aggregation (Fig. 2E), or non-incorporation (Fig. 2F) in a too thin bilayer have been observed for synthetic peptides (5,39-43). In particular, tilting has been suggested to be a major way in which proteins can compensate for hydrophobic mismatch.

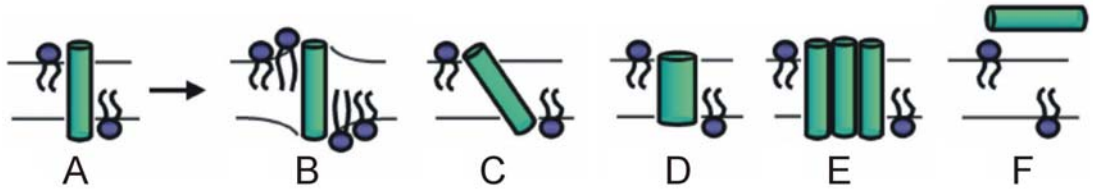

Figure 2. Schematic representation of possible responses of transmembrane segments of proteins to positive hydrophobic mismatch (A): acyl chain ordering (B), peptide tilt (C), peptide backbone deformation (D), peptide oligomerization (E), no transmembrane association (F). Adapted from (5).

Tilting backbone in response to positive mismatch
The advantage of tilting transmembrane segments under positive mismatch is that it decreases the effective hydrophobic length of the polypeptide stretch along the bilayer normal. By doing so, the exposure to a hydrophilic environment of hydrophobic

residues that flank the central segments can be reduced. This can have important consequences for membrane protein activity. Tilting motions of a segment in α-helical bundles may indeed have considerable implications on the overall three-dimensional structure and activity of the protein, since the connected parts can affect each other by structural constraints.
The importance of the tilting properties of transmembrane parts of proteins for their activity in relation to membrane properties is well illustrated by the examples described below.

The functional importance of tilting properties of membrane proteins
A striking example of a membrane protein that requires large tilt motions of its transmembrane helices for functioning as a channel is the prokaryotic large conductance mechanosensitive channel MscL (44-46). The actual trigger for the channel to function is a changed surface tension or lateral pressure profile that can arise from a drop in osmolarity of the environment. Positive mismatch can be very important in the sense that it lowers the activation energy of MscL by stabilizing a structurally distinct closed channel intermediate, which geometry is defined by different tilt angles than under matching conditions in the closed state (46).
For the Ca^{2+}-ATPase, it was reported that in case of positive hydrophobic mismatch, the protein adopts an abnormal conformation (47). The distortion in conformation of the pump could result from the requirement to tilt the longer helices to match the thinner bilayer. The functional consequence of this distortion by tilting is that the ATPase in a relatively thin bilayer binds only a single calcium ion instead of the normal two and the Ca^{2+}-ATPase activity is much less than in a thicker bilayer (48,49).
For a few membrane proteins, it was shown that only subtle fluctuations in tilt angle are responsible for functioning. This is the case for Rhodopsin, and Bacteriorhodopsin, which only require a small outward tilting of one α-helix, called the F-helix, to ensure their reprotonation as a so-called meta II or M2-state intermediate (50-56). An early study showed that positive hydrophobic mismatch slows down the transition to the M2-conformation without affecting significantly the structure (57-59).

Measuring tilt angles of transmembrane segments in model membranes

The examples above illustrate the importance of the tilt angle for the conformational changes that are associated with the functions of membrane proteins. Thus, knowledge of the tilt properties is important for understanding structure and function of membrane proteins.
In principle, tilted orientations of transmembrane segments of proteins should be predictable from molecular modeling studies either by using molecular dynamics (MD) simulations or by energy calculations (60). These computational methods can then be validated by experimental studies on macroscopic systems. However, experimental analysis of tilt angles is not straightforward, and studies on tilt properties have been mainly performed in model membranes of synthetic lipids in which either natural proteins or artificial peptides are incorporated.

Why model membranes?

The examples discussed in the previous section about the functional importance of tilting for natural membrane proteins, were derived from biophysical studies on model

membranes and complemented with crystal structures and hydrophobicity analysis of the proteins. The need for model membranes in these studies was due to the tremendous complexity of biomembranes in terms of diversity and size. Also for general investigations on lipid-protein interactions, simplified model membrane systems with a well-defined composition can be very useful. This is because they can be easily modified for studying systematically the parameters of interest. A large variety of lipid species that are usually abundant and representative in biomembranes can be synthesized and are commercially available. It is also possible by the use of standard solid phase synthesis protocols to synthesize large quantities of small proteins or peptides. Indeed, high quality α-helical transmembrane peptides of up to 31 residues have been synthesized and their properties have been widely studied in model membranes (5,61). Chemical synthesis in addition allows for site-specific labeling, which can be very valuable depending on the spectroscopic analytical method used. Thus, with the use of model membranes, it is either possible to change the composition of the lipids or the composition of the protein and to analyze the consequences of any variation in the system at a molecular level. Another advantage of model membranes is that they are relatively easy to prepare. Various protocols exist for the preparation of liposomes with transmembranously-incorporated proteins (62).

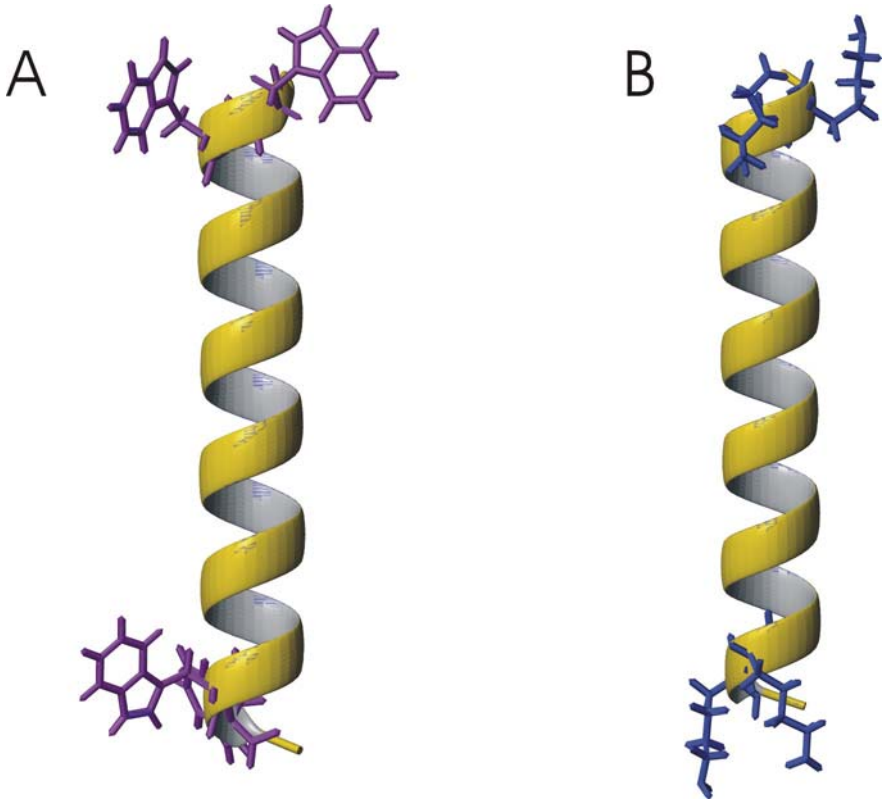

Figure 3. Structure of α-helical transmembrane model peptides flanked on both sides by two tryptophans (A) in the case of WALP, or by two lysines (B) for KALP.

Parameters that influence the tilt angle of transmembrane segments of proteins have been extensively studied in model systems. In particular, the role of hydrophobic mismatch was systematically investigated by using synthetic α-helical transmembrane in PC model membranes (5). The artificial peptides typically consist of an α-helical hydrophobic region, e.g. a sequence of alternating leucine and alanine, with variable

length, and with different flanking residues. Examples are the so-called WALP peptides (Fig. 3), which are flanked on both sides with Trp to mimic the composition of transmembrane helices in integral membrane proteins, and the KALP peptides, which are flanked by lysine residues (5,61).

Methods for measuring tilt angles

In the present section, the basic principles of different methods for measuring tilt angles of transmembrane polypeptides will be described.

Obtaining tilt angles from the depth of insertion of labels in lipid bilayers

Fluorescence spectroscopy

One of the methods to determine the position of a reporter molecule in a lipid bilayer is fluorescence spectroscopy (63). The emission properties of many fluorescent probes are sensitive to the polarity of their environment and hence to their depth in lipid bilayers. Monitoring the properties of a fluorescent label in lipid bilayers when it is attached to a synthetic α-helical peptide provides information on how deep the attachment site is inserted in the membrane. Assuming an ideal secondary structure (usually α-helical geometry), the depths obtained from fluorescent measurements of peptides labeled at different positions can be used to fit orientational parameters like the tilt angle of a transmembrane α-helix, as reported for the M13 Major coat protein (64). This method is particularly powerful because of its high sensitivity. However, it has some disadvantages for measuring tilt angles of α-helical transmembrane peptide in lipid bilayers. First, the most frequently used labels need to be linked to a cysteine, which implies that it should be either naturally present or it should be incorporated during synthesis or biosynthesis of the peptide of interest. Second, the type of reporter groups that can be attached are often bulky and aromatic, which may affect the physico-chemical properties of transmembrane peptides upon labeling. Third, this method reports information on the depth of insertion of the reporter group in the lipid bilayer. The translation of the depth to orientational constraints can be the cause of important uncertainties in the precision of the tilt angle determination.

Electron Spin resonance (ESR)

ESR techniques rely on the ability of chemical compounds having electrons with unpaired spins like nitroxide groups to interact with an applied magnetic field. Application of ESR on peptides in lipid bilayers yields valuable information on local structure based on (i) the mobility of the attached label, (ii) its accessibility to solvent molecules or lipid soluble paramagnetic species, and (iii) structural constraints related to the secondary or the tertiary structure of the protein (65). This approach can for example assess local information like distances and contacts between the transmembrane segments of proteins, which in turn can be translated to orientational constraints. Like fluorescence spectroscopy, ESR is very sensitive requiring small amounts of material, and it makes use of the depth of insertion of the labels for determining tilt angles. Therefore, ESR presents similar advantages and disadvantages as fluorescence spectroscopy, when the purpose is of determining tilt angles (see above).

Spectroscopic methods for determining tilt angles from anisotropic parameters

Attenuated total reflection Fourier Transform Infrared spectroscopy (ATR-FTIR)
Infrared spectroscopy measures the absorption caused by interaction of electromagnetic radiation with the vibrational modes of molecular bonds. Vibrational bands from a polypeptide backbone are very much influenced by the secondary structure. Applying infrared spectroscopy to macroscopically aligned lipid bilayers containing transmembrane α-helical peptides allows for determining tilt angles of the peptides with respect to the bilayer normal. This technique is very sensitive, relatively easy to apply, and it provides a wealth of structural information without need for labeling. However, also this technique has several disadvantages. First, macroscopically oriented samples are required. Second, it is difficult to discriminate between separate orientations of molecules because absorption bands represent ensembled averages. A third inconvenience is the large absorption of water in the infrared region, which limits the amount of water that can be used to hydrate the samples. (66).

Circular dichroism spectroscopy
Circular dichroism (CD) measures the differential absorption of left- and right-handed circularly polarized light of optically active compounds. The electronic environments of the chiral centers of chemical compounds like the amide groups of proteins and peptides mainly determine the resulting spectra,. The electronic properties of amides are very sensitive to different secondary structures, which result in typical spectral shapes (67). The use of CD on peptides or proteins incorporated in macroscopically oriented lipid bilayers, referred to as oriented CD, has been used for determination of peptide transmembrane orientation (68,69). Like in the case of infrared spectroscopy, the method is sensitive, albeit less than ATR-FTIR, and it requires no labeling. However, also this technique has several limitations. First, as in the case of ATR-FTIR the signals correspond to ensembled averages where the different orientations of a same moiety cannot be resolved. Furthermore, the orientational dependence of the spectral shape is rather weak. In particular, when parts of the molecule adopt different secondary structures, the interpretation of data is ambiguous. Finally, it is difficult to control full hydration conditions for oriented bilayers, which is essential for mimicking best the properties of the model membrane.

Solid State NMR

NMR is a well-established method for three-dimensional structure determination. In particular, solid state NMR is appropriate for studying macromolecules in all physical states including the liquid-crystalline environments provided by the lipids associated with membrane proteins (70). An advantage of solid state NMR for membrane systems is that both distance and orientational information can be obtained by employing labels that do not affect physico-chemical properties of the molecule under scope.
Different isotopes can be used for analysis of tilt angles by solid state NMR. Up to date, ^{15}N solid state NMR has been the most frequently used for determining tilt angles of membrane peptides (see (70,71) for reviews). However, also ^{2}H NMR is useful and has some important advantages. The next paragraphs will describe the basic principles, first of ^{15}N NMR applied to membrane peptides in lipid bilayers, and then of ^{2}H NMR.

^{15}N NMR

NMR is based on the interactions of nuclei with the magnetic field of the NMR spectrometer. In the case of ^{15}N NMR, the interactions that are measured are especially due to chemical shift (or Zeeman) interactions, but also dipolar due to the physical properties of the spin system in question. The spectral chemical shift in the absence of motion depends on the chemical nature and the orientation of the bond that carries the ^{15}N nucleus. Thus, in the case of a peptide powder labeled with ^{15}N on an individual backbone amide, an approximately 170 ppm broad ^{15}N NMR signal can be measured (Fig. 4A), representative for a random distribution of the ^{15}N-labeled bonds in space.

The anisotropic chemical shift interaction is generally described by the diagonal elements σ_{11}, σ_{22}, and σ_{33} of a 3 by 3 matrix of an orthogonal coordinate axis system called the principal axis system (PAS). These diagonal elements are the static principal elements of the chemical shift anisotropy (CSA) tensor. Since, the electron distribution of ^{15}N nuclei in molecules is not spherically symmetric, the graphical representation of the CSA tensor is an ellipse of coordinates σ_{11}, σ_{22}, and σ_{33}, of which the largest and smallest tensor elements are assigned to σ_{33} and σ_{11}, respectively (Fig. 4B). Typically, the CSA tensor ellipsoid is elongated along the N-H bond. Experimentally, σ_{11}, σ_{22}, and σ_{33} correspond to the discontinuities observed in the line shape of powdered samples, as illustrated in Fig. 4A.

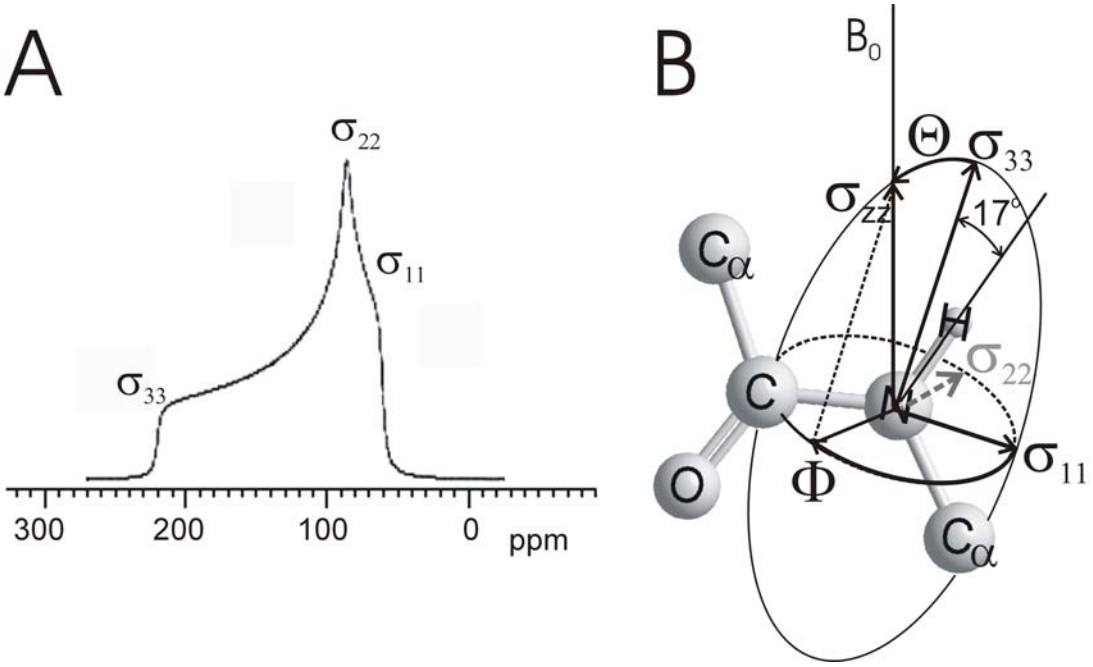

Figure 4. Static simulated ^{15}N NMR powder spectrum showing the ^{15}N NMR chemical shift tensor elements (A). Graphical representation of the ellipsoid ^{15}N NMR chemical shift tensor within a peptide bond (B).

The tensor reflects the arrangement of the nuclei and bonds within a given molecule and thereby relates the NMR interactions to the molecular coordinates. Relating the molecular coordinates of the tensor relative to the magnetic field direction of the NMR spectrometer (laboratory frame) is possible by applying Euler rotation angles (72-74). The measured NMR chemical shift value, often denoted by σ_{ZZ} (71), is the tensor component aligned with the magnetic field, which can be expressed in terms of

the Θ and Φ Euler angles (see Fig. 4B) and the principal elements of the chemical shift tensor as follows:

$$\sigma_{ZZ} = \sigma_{11} \cdot \sin^2 \Theta \cdot \cos^2 \Phi + \sigma_{22} \cdot \sin^2 \Theta \cdot \sin^2 \Phi + \sigma_{33} \cos^2 \Theta \quad (1)$$

Θ is the angle between the σ_{33} tensor element and the magnetic field, and Φ is the angle between the projection of σ_{ZZ} in the σ_{11}-σ_{22} plane and σ_{11}. In this way, it is possible to relate the measurable chemical shift σ_{ZZ} to the PAS, which in turn has a defined orientation respective to the molecular frame. For instance, σ_{11} and σ_{33} are in the plane of the peptide bond, whereas σ_{22} is perpendicular to it, and σ_{33} makes an angle of 15-20º with respect to N-H bond (75,76) within the peptide plane (the illustration in Fig. 4B shows an angle of 17º).
A parameter that can bring significant uncertainties in the estimation of the orientation of a ^{15}N labeled amide bond is the asymmetry of the chemical shift tensor. This becomes clearer when the chemical shift is expressed in the following way:

$$\sigma_{ZZ} = \sigma_{iso} + \sigma_{aniso} \cdot (3\cos^2 \Theta - 1 - \eta \cdot \sin^2 \Theta \cdot \cos 2\Phi) / 2 \quad (2)$$

where σ_{iso} is the isotropic chemical shift that corresponds to the average value of σ_{11}, σ_{22}, and σ_{33} under rapid isotropic molecular motion. σ_{aniso} is an anisotropic parameter value that corresponds to the difference between σ_{33} and σ_{iso}. The asymmetry parameter η equals $(\sigma_{22} - \sigma_{11})/\sigma_{aniso}$ and is a measure of the axial asymmetry of the CSA tensor interaction. Graphically, it means that the tensor is asymmetric if σ_{11} and σ_{22} have different values. In this case, the ellipsoid is not symmetric around the σ_{33}, which consequently will affect the ^{15}N NMR line shape.
The value of η depends on both the secondary structure and the nature of the amino acid in question. The asymmetry parameter of the amide ^{15}N chemical shift tensor in peptides varies from as low as 0.1 (mainly glycine) to as high as 0.35 (77,78) and references 14, 16, 17, 19 therein). In addition, different crystal forms of the same peptide can yield substantially different tensor element values (79). This suggests that it is important to characterize tensors not from model compounds, but from the compound of interest in the environment of interest in order to obtain precise information on the angle of a ^{15}N-labeled backbone amide bond.
Although accurate orientational information is not straightforward to obtain due to a significant asymmetry of the CSA tensor, a great advantage of ^{15}N NMR is that a single label in the sequence of an α-helical peptide is sufficient to give an estimation of the tilt angle. This is because in α-helical peptides, both the amide N-H bond and σ_{33} are almost parallel to the long axis of the molecule (70). Therefore, the tilt orientation of an α-helix will correspond roughly to the orientation of the amide N-H bond as measured by ^{15}N NMR. Fig. 5A illustrates the situation where the labeled NH bond and the helical axis are oriented in a transmembrane direction (tilt angles between 10 and 30°), which corresponds to ^{15}N resonance values above 200 ppm (71). In contrast, chemical shift values around the σ_{11} or σ_{22} values (i.e. 65 or 85 ppm, respectively) will correspond to orientations of the peptide that are perpendicular to the field (Fig. 5B).

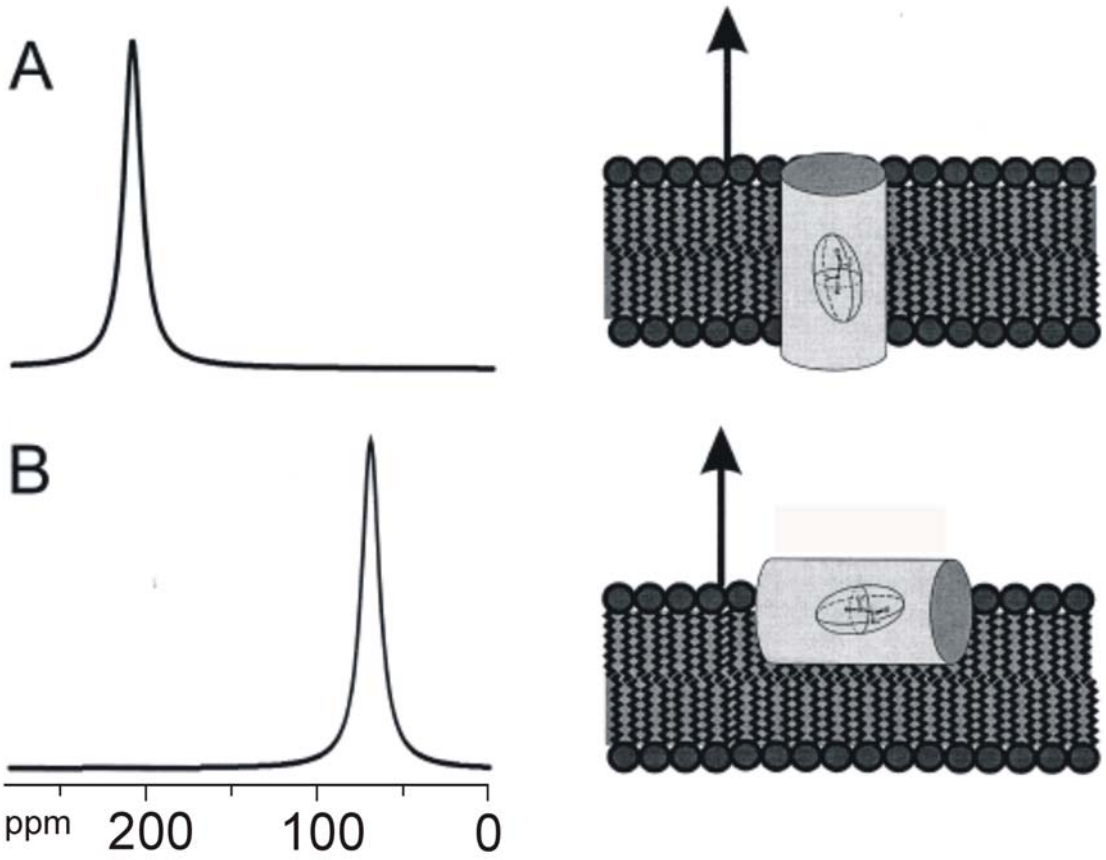

Figure 5. Simulated proton-decoupled ^{15}N solid-state NMR spectra of helical peptides ^{15}N-labeled at a single site and reconstituted into oriented membranes (illustrated to the right of the spectra). The membrane normal is aligned parallel to the magnetic field direction (arrows). (A) Transmembrane orientation of the helix axis. (B) Orientation of the peptide approximately perpendicular to the magnetic field direction.
Adapted from (80).

The fact that the long axis of the ellipsoid chemical shift tensor is nearly parallel to the α-helical axis has also a disadvantage, which is that the chemical shift anisotropy is rather insensitive to the azimuthal orientation of α-helical peptides. This implies that the ^{15}N chemical shifts for different positions of the amide labeling around the helical wheel will provide similar values. Consequently, determining the direction in which a transmembrane α-helical peptide is tilted in a lipid bilayer is rather difficult. Indeed, whereas the CSA encompasses circa 170 ppm, the maximal influence of the rotation angle is approximately only 15 ppm. This represents an important limitation if one considers that the typical line width of ^{15}N NMR peaks in macroscopically oriented samples is around 10 ppm (81,82).
An alternative way to measure tilt angles of transmembrane peptides is by measuring amide ^{15}N-^{1}H dipolar couplings. The dipolar coupling term of ^{15}N and ^{1}H nuclei in a peptide amide bond is given by:

$$D_{ZZ} = \left(\frac{\mu_0}{4\pi}\right) \cdot \frac{\gamma_1 \gamma_2 \hbar}{r^3} \cdot (3\cos^2\theta - 1) \qquad (3)$$

where μ_0 is the permeability of vacuum, $\hbar$ is the reduced Planck's constant, r is the internuclear ^{15}N-^{1}H distance, and γ_1 and γ_2 are the magnetogyric ratio of nuclei 1 and 2, respectively. Here, θ is the angle between the N-H bond and the magnetic field. The direct angular relation between the amide bond and the laboratory frame is an important advantage over the use of chemical shift and it does not suffer from symmetry issues as it is the case with the ^{15}N chemical shift tensor.

The combination of chemical shift and ^{15}N-^{1}H dipolar coupling values can be of great use as exemplified by the so-called polarity index slant angle (PISA) wheel (83,84). As illustrated in Fig. 6, when a peptide is tilted in an oriented lipid bilayer, the two-dimensional spectra of ^{15}N uniformly labeled peptides consist of a fingerprint-like pattern composed of "spots", each one corresponding to the set of ^{15}N chemical shift and ^{15}N-^{1}H dipolar coupling of one labeled residue. This two-dimensional pattern is changing its shape with the tilt angle. The use of the PISA wheel is essentially possible because of the 17° angular difference between the long axis of the ellipsoid ^{15}N chemical shift tensor σ_{33} and the amide ^{15}N-^{1}H bond within the peptide bond (70).

In any approaches based on the PISA wheel, the peak assignment is hampered by a poor resolution and the relative insensitivity of the ^{15}N chemical shift and ^{15}N-^{1}H dipolar coupling to the rotation angle. To enhance the resolution, techniques as for example polarization inversion spin-exchange at the magic angle (PISEMA) can be applied in which the bilayer normal is oriented at the magic angle (i.e. 54.7° with respect to the magnetic field) causing averaging of the dipolar interactions that at other sample orientations contribute to the broadening of the resonance lines.

An alternative way to further improve both the resolution and the sensitivity of the ^{15}N NMR techniques is by spinning samples around the magic angle. This technique called magic angle spinning NMR (MAS NMR) can average out the chemical shifts to their corresponding isotropic values and reduces the measured dipolar interactions up to zero, depending on the rotational speed that is applied to the samples. In order to maintain orientational information during fast spinning, routine protocols have been developed over the previous two decades to selectively reintroduce the dipolar interaction term (85-87). In this case, the orientation of the N-H amide bond can be related to the laboratory frame via a succession of Euler transformations as described in (88). This is more appropriately done by applying magic angle-oriented sample spinning (MAOSS) on macroscopically oriented samples, whereas spinning of non-oriented samples would lead to a spectrum consisting of side bands that correspond to the envelop of the powder pattern line shape (71). In the case of MAOSS, stacked glass plates with their normal aligned parallel to the magic angles with respect to the laboratory frame can be used (71). Alternatively, bendable plastic polymer films can be wrapped into cylinders that fit into magic angle spinning rotors (71). Thus, the use of MAOSS reduces considerably the spectral line width and the resolution is concomitantly improved to values as small as 20-30 Hz (89).

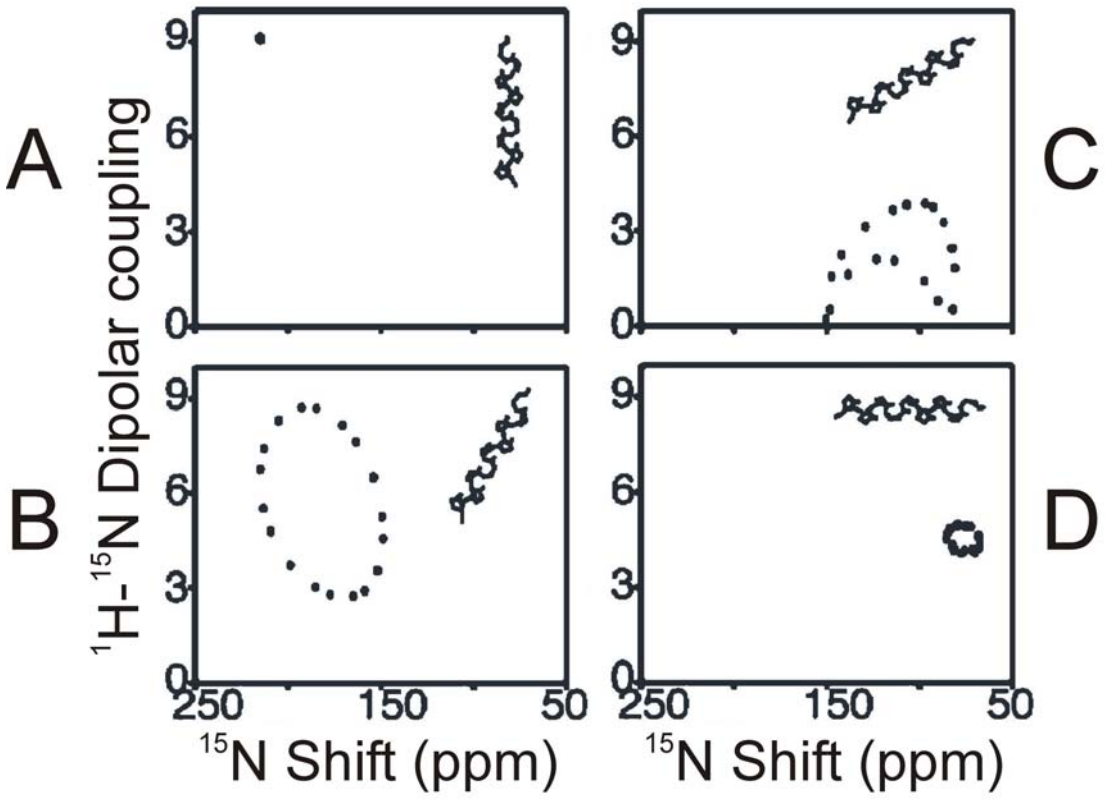

Figure 6. PISA wheels corresponding to an α-helix tilted at 0° (A), 30° (B), 60° (C), and 90° (D) with respect to the bilayer normal. Adapted from (70).

^{2}H NMR

An alternative method for determining tilt angles of transmembrane peptides in lipid bilayers with NMR spectroscopy is the use of ^{2}H NMR. When placed in a strong magnetic field of an NMR spectrometer, for nuclei like deuterium that have a spin number value *I* of 1, Zeeman interactions will split the ground state nuclear energy in three levels. Since the deuterium nucleus has an electric quadrupole moment, the nuclear Zeeman energy levels are shifted by so-called first order quadrupolar shifts. Due to this first order perturbation of the energy levels, instead of observing a single NMR peak, a doublet that appears symmetrically around the NMR resonance frequency of deuterium is observed. The peak separation between the resonance lines in terms of frequency is called the quadrupolar splitting, and corresponds to the allowed transitions upon nuclear magnetic resonance conditions. In this case, dipolar and chemical shift interactions are much smaller than the quadrupolar interaction, and are therefore negligible (90).

In the absence of motion, the value of the quadrupolar splitting of a deuteron in a carbon-deuterium (C-D) bond is a function of the orientation (angle θ) of that bond with respect to the magnetic field (Bo) and is given by (91,92):

$$\Delta\nu_q = \tfrac{3}{2}(e^2qQ/h)\{\tfrac{1}{2}([3\cos^2\theta - 1]) + \eta\sin^2\theta\cdot\cos 2\phi)\} \quad (4)$$

where *e* is the absolute value of the electron charge, *h* is the Planck constant, *Q* is the nuclear quadrupolar momentum, η is the asymmetry parameter, and ϕ is one of the Euler angles that describe arbitrary orientations of the principal axes of the electric

field gradient tensor of the deuteron. In the case of C-D bonds in aliphatic chains, $\eta = 0$ (91), which is an advantage with respect to the ^{15}N nucleus in relation to the precision of measurements of angles of labeled bonds. This reduces the equation (4) to:

$$\Delta\nu_q = \tfrac{3}{2}(e^2qQ/h)(\tfrac{1}{2}[3\cos^2\theta - 1]) \qquad (5)$$

The static quadrupolar coupling constant has a value of $e^2qQ/h \approx 168$ kHz (93). In this case, the maximum quadrupolar splitting can reach 250 kHz as illustrated in Fig. 7A, corresponding to an orientation of the C-D bond parallel to the magnetic field (i.e. $\theta = 0°$ or 180º). Equation (5) predicts also a quadrupolar splitting of -125 kHz for perpendicular orientations of the C-D bond ($\theta = 90°$ or 270º; Fig. 7B). However, it is important to note that a ^2H NMR spectrum does not allow for visual distinction between a negative and a positive quadrupolar splitting. Therefore, the sign will be omitted in the rest of the text.

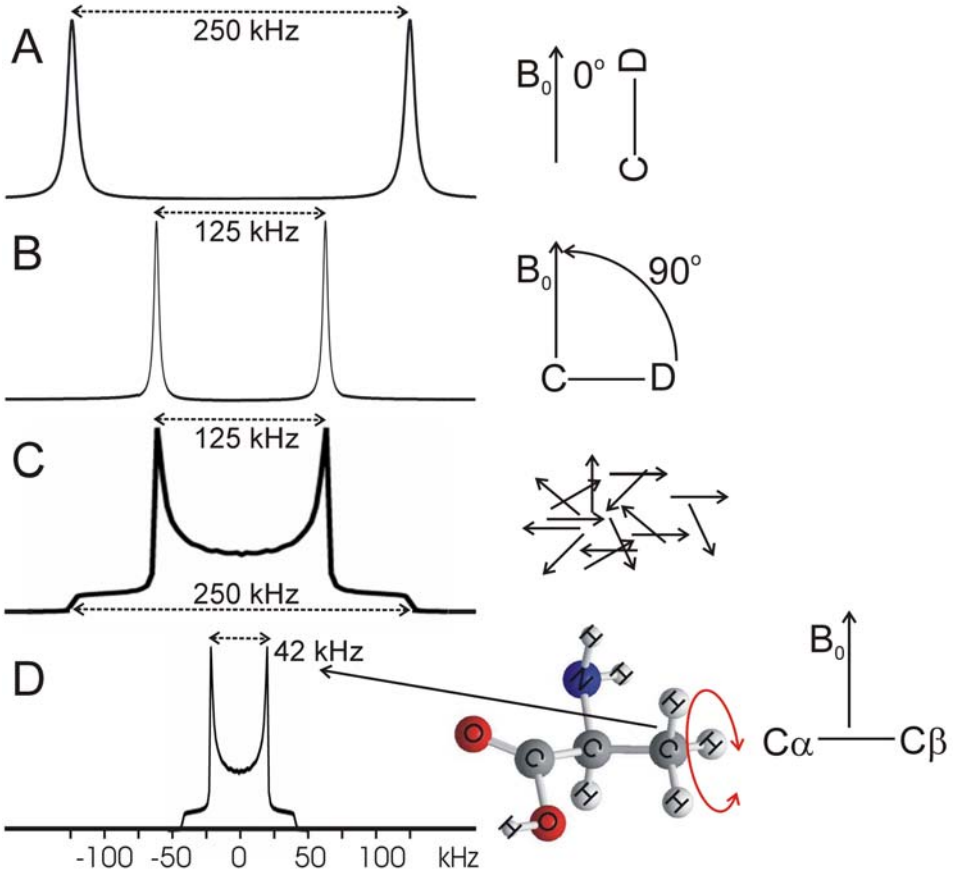

Figure 7. Simulated ^2H solid state NMR spectrum of a C-D bond parallel to the direction of the magnetic field B_0 (A), or perpendicular to the field (B). Static ^2H solid state NMR spectrum of C-D powder (C). Simulated ^2H solid state NMR spectrum of a deuterated methyl group of alanine (D).

The powder ^2H NMR pattern obtained in a randomly oriented sample is a superposition of resonances, each representing a particular orientation of the bonds containing the labeled site with respect to the magnetic field. Molecules in powder adopt orientations according to a normal distribution, which is characterized by a

majority of the bonds aligning perpendicularly to an axis of reference, like for example the static magnetic field, while bonds that are parallel to the field will represent the minority. This results in the case of a powder sample consisting of C-D labeled molecules, in the typical ^{2}H NMR powder pattern as shown in Fig. 7C.
In the case of fast motion, averaging of the quadrupolar splittings occurs. For example, in a deuterated methyl group of alanine, the fast rotation around the C^α-C^β bond averages out the signal according to (94):

$$\Delta\nu_q = \tfrac{3}{2}\cdot(e^2qQ/h)\cdot(\tfrac{1}{2}[3\cos^2\theta - 1])\cdot(\tfrac{1}{2}\cdot[3\cos^2\gamma - 1]) \qquad (6)$$

in which γ is the angle between the C-D bonds and the axis of motional averaging (along the C^α-C^β bond) and where θ is the angle between the axis of motional averaging C^α-C^β and B_0. Thus, in case of tetrahedral geometry of the methyl group (i.e. $\gamma \approx 109.5°$), the fast methyl reorientation would result in a 3-fold reduction of quadrupolar splitting (95) as illustrated by Fig. 7D. Any additional motional fluctuation would reduce this value further. It is important to note here, that because the C-D bonds are rotating fast around the C^α-C^β bond, the resulting vector corresponding to the C-D orientation defined by θ is aligned along the motional averaging axis, which in this case is parallel to C^α-C^β. Since the C^α-C^β axis is directly connected to the backbone, information on the alanine methyl groups in a peptide provide information on the motion and the orientation the peptide backbone.

Using ^{2}H-labeled alanine for tilt angle determination of α-helices in lipid bilayers
According to the principles described above, applying ^{2}H NMR on d_3-alanine labeled transmembrane peptides to measure their tilt angles in lipid bilayers should be relatively straightforward. Indeed, this method proved very successful for determining tilt angles of transmembrane α-helices in macroscopically aligned lipid samples (96,97). The principles of this approach based on the application of ^{2}H NMR and the geometric analysis of labeled alanine (GALA) will be described now.
In order to facilitate the explanation of this method, it may be helpful to use the practical case of the WALP peptide as in (97), where the peptide consists of the sequence acetyl-GWWLALALALALALALWWA-ethanolamine. This peptide is called WALP19 because it is composed of 19 residues. Let us first describe a few parameters as summarized in Table 1 and illustrated in Fig. 8, to explain the approach using the trigonometric convention of counterclockwise angles as being positive. The angle τ is the tilt angle, defined as the angle between the peptide helical axis and the bilayer normal (which is assumed to be along the magnetic field direction as indicated by the symbol N in Fig. 8A). $\in_{\|}$ is the angle between the peptide helix axis and the C^α-C^β bond vector (Fig. 8A), and δ is the rotation angle, defining the position of the bond vector around the helical axis (Fig. 8B). In turn, δ depends on three angles as shown in Fig. 8B:

$$\delta = \rho + \in_{\perp} + \varphi \qquad (7)$$

where ρ is the rotation around the α-helical axis of the C^α of Gly1 with respect to direction of the tilt, $\in_{\perp}$ is the angle of the bond vector with respect to a vector from C^α to the peptide axis, and φ is the angle between the reference point Gly1 and the labeled residue in the peptide. For a regular helix, φ is given by –(n–1)∗ψ, where n is

the residue number and ψ is the pitch angle. Using our notation, in an ideal α-helix, ψ = 100º, and $\in_{\perp}$ = -43.3 according to molecular models using Insight II database (97).

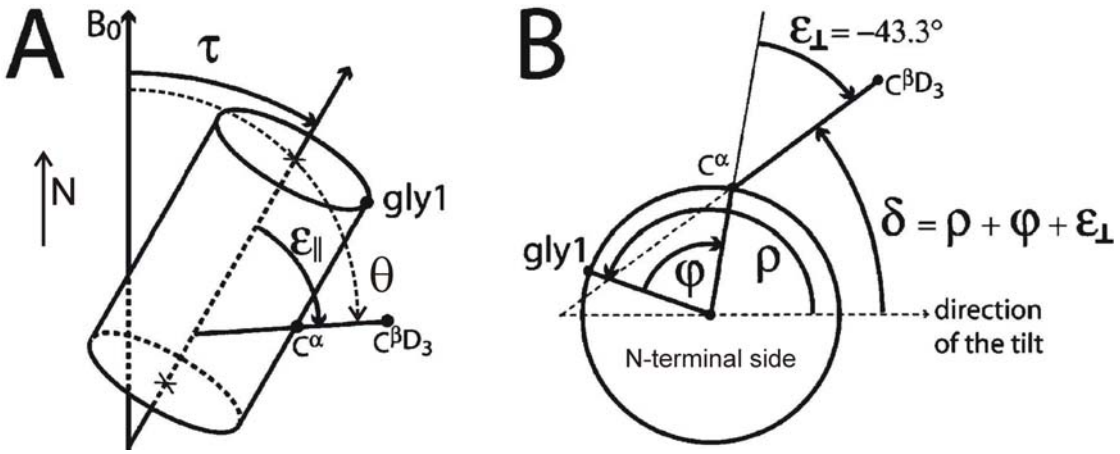

Figure 8. Definition of angles used in the calculations. (A) The tilt angle τ between the peptide axis and the bilayer normal, which is assumed to be along the magnetic field direction. The bond angle between the C-CD_3 bond and the peptide axis is denoted by $\varepsilon_{\parallel}$. (B) The rotation angle giving the orientation of the C-CD_3 bond is indicated as δ. The angle δ is determined by three contributions that are ρ, φ, and $\varepsilon_{\perp}$. ρ is the rotation of the whole peptide, and it is defined as the anticlockwise rotation angle of the C^{α} of Gly1, compared to the direction of the tilt (reference position). φ is the angle by which another amino acid residue is rotated around the peptide axis with respect to Gly1. $\varepsilon_{\perp}$ is the angle of the C^{α}-$C^{\beta}D_3$ bond projected onto a plane perpendicular to the helical axis with respect to a vector (or line) between the peptide axis and the C^{α}.

Table 1. Definitions of structural parameters used in the GALA analysis approach.

Parameters	Description
θ	Angle between the labeled C^{α}-C^{β} and the magnetic field
τ	Tilt angle of the helix, relative to the membrane normal
$\in_{\parallel}$	Angle between the alanine C^{α}-C^{β} bond and the helix axis
δ	Rotation angle, defining the position of the C^{α}-C^{β} bond vector
φ	Rotation angle between the reference point glycine 1 and the
$\in_{\perp}$	Angle between C^{α}-C^{β} and the vector pointing from the helix
ρ	Rotational angle of the helix, defined relative to glycine 1

Now, that several structural parameters inherent to the α-helical geometry have been described, it is important to see the angular relation of the C^{α}-C^{β} bond with respect to the magnetic field. From Fig. 8A, it is clear that changing the tilt (τ) and the C^{α}-C^{β} side-chain angles ($\in_{\parallel}$) will directly influence the θ angle, which determines the value of the quadrupolar splitting in equation (5) and (6). Although it appears less straightforward in Fig. 8, another important factor is the rotation angle δ when the peptide has a non-zero tilt angle. The θ angle is related to the tilt angle τ, and the rotation δ[1] by:

$$\cos^2\theta = \cos^2 \in_{\parallel} \cdot(\cos\tau - \sin\tau\cos\delta\tan \in_{\parallel})^2 \qquad (8)$$

[1] The derivation of this expression will be shown in the next chapter.

This would result in an expression relating the structural parameters of an α-helix containing a deuterium-labeled alanine in its sequence using equation (6):

$$\Delta\nu_q = \tfrac{3}{2}\cdot(e^2qQ/h)\cdot(\tfrac{1}{2}[3\cos^2\in_{\|}\cdot(\cos\tau-\sin\tau\cos\delta\tan\in_{\|})^2-1])\cdot(\tfrac{1}{2}\cdot[3\cos^2\gamma-1]) \quad (9)$$

Since a methyl group tetrahedral geometry implies a γ angle of ≈ 109.5º, the resulting equation is:

$$\Delta\nu_q = \tfrac{1}{2}\cdot(e^2qQ/h)\cdot(\tfrac{1}{2}[3\cos^2\in_{\|}\cdot(\cos\tau-\sin\tau\cos\delta\tan\in_{\|})^2-1]) \quad (10)$$

Equation (10) is the tool for simulating the quadrupolar splittings derived from all possible orientations and labeling positions. However, for a certain value of the quadrupolar splitting there can be more than a single set of tilt angle, rotation angle, and $\in_{\|}$ value. Fig. 9 illustrates this by showing a plot of simulated quadrupolar splittings at a discrete tilt angle value, where it is clear that a certain y-value of the splitting can be obtained by two different helical wheel positions. The figure also illustrates how the tilt angle, the labeling position around the helical wheel, the rotation of the helical axis, and the exact value of the α-helical parameter $\in_{\|}$ can influence the value of the ^{2}H NMR quadrupolar splitting. Consequently, a minimal number of data points is required to unambiguously determine these parameters. Thus, measurements should be performed on different peptides each of them labeled at a single different position. If $\in_{\perp}$ and $\in_{\|}$ values are fixed and if the peptide adopts an ideal α-helical geometry, in principle only two different labeling positions should be enough to determine precisely the tilt angle of a transmembrane peptide with its corresponding rotation angle.

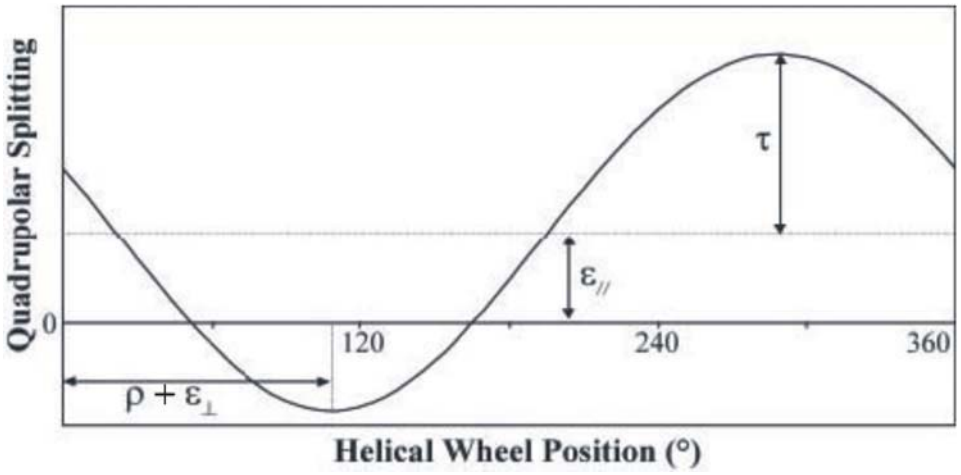

Figure 9. Dependence of the $\Delta\nu_q$ on helical wheel position and structural parameters. This figure illustrates how different conformational and structural parameters affect the dependence of the ^{2}H NMR quadrupolar splitting (adapted from 97).

From the theory described above, it can be concluded that applying GALA is only possible under certain conditions. The most important requirement is that one need a regular α-helical peptide, which does not rotate around its own axis on the NMR time scale. Otherwise, all the labels would give the same quadrupolar splitting because of averaging of the signal to the same value.

Complementary aspects of ^{2}H NMR to ^{15}N NMR for tilt angle determinations

The use of ^{2}H solid-state NMR may present several advantages over ^{15}N NMR for determining the tilt and rotation angles of transmembrane peptides in lipid bilayers. First, in the case of ^{2}H NMR, the quadrupole gradient is symmetric around the C-D bond allowing unambiguous determination of the labeled-bond angle. Second, ^{2}H NMR is a more sensitive technique than ^{15}N NMR, because of the larger gyromagnetic ratio of ^{2}H nuclei, and because of the short relaxation time of ^{2}H spins allowing much faster pulsing. Third, when the ^{2}H-label is the side chain of alanine, the presence of three chemically equivalent deuterons on the methyl group with a well-defined intrinsic mobility give rise to high intensity signals. Furthermore, ^{2}H NMR experiments are easier to set up than ^{15}N NMR experiments. Indeed, because of the poor sensitivity of the ^{15}N detection, it is necessary to transfer the magnetization of nuclei with high gyromagnetic ratio γ, such as ^{1}H to the ^{15}N label through the amide bond by solid-state NMR cross-polarization protocols to sufficiently enhance the signal (98). However, it is difficult to control the temperature of the samples in such experiments due to overheating problems. Finally, the larger angle to the peptide helix axis of the relevant C^{α}-$C^{\beta}D_3$ bond (~ 56°) causes a very high sensitivity of the ^{2}H quadrupolar splitting to the rotation angle, thereby allowing for a precise determination of the direction in which the peptide is tilted, whereas the corresponding angle for an N-H bond is only 15° (14).

However, a disadvantage of the use of ^{2}H NMR is that GALA requires the presence of alanine labels at specific positions, and therefore different peptides need to be synthesized. In the case of ^{15}N NMR, either a single labeling position or biosynthetic overall labeling provides information on the tilt angle. Thus, ^{2}H and ^{15}N NMR complement each other.

Scope of the thesis

Protein-lipid interactions play an essential role in determining the activity of membrane proteins. We described earlier several factors that can affect membrane protein activity. One of those parameters is the hydrophobic mismatch, which can influence the tilt angle of transmembrane segments of proteins. In a previous paragraph, some examples were given to illustrate the importance of the tilt angle for the structure and the function of membrane proteins. The application of GALA and the use of ^{2}H NMR is a convenient approach for a systematic determination of the tilt angle of transmembrane peptides, and thereby this approach can help understanding how tilting motions can be influenced by the lipid environment. Using ^{2}H NMR and GALA enables monitoring of small variations in tilt angle by providing detailed structural information. The present thesis explores the application of ^{2}H NMR and GALA on WALP and WALP-like peptides in lipid bilayers in the L_{α}-phase, and some implications of the results for membrane proteins structure and function are discussed.

In chapter 2, the effect of positive hydrophobic mismatch on the tilt and rotation angles of WALP23 is studied in PC-bilayers of different thickness. It is found that the tilt angle of WALP23 increases slightly but systematically with increasing positive mismatch. Interestingly, the direction in which WALP23 is tilted is the same in all studied PC-bilayers. In the same chapter, it is shown that GALA can be applied to non-oriented samples. The major advantages are that this mimics much better biological membranes, and that it allows studies of poorly orientable lipids. Also, the use of non-oriented samples enables a better control of environmental conditions such as pH and salt concentration.

In chapter 3, the GALA method is used to study the influence of flanking residues and of the hydrophobic composition of the peptide on the tilt and rotation angles by comparing the properties of WALP23 with those of the so-called KALP23, WLP23, and KLP23. The results show that the nature of anchoring residues influences not only the tilt angle but also especially the rotation angle of the model peptides. The hydrophobicity of the central part of the peptide neither influences the tilt angle, nor the azimuthal angle.
The work presented in chapter 4 uses the GALA approach to show that changing the properties of the membrane-water interfacial region by adding the anesthetic model molecule 2, 2, 2-trifluoroethanol to the model membranes affects the orientational behaviour of the model peptides depending on the nature of the interfacial anchoring residues. The alcohol interferes with the interfacial interactions of tryptophan-flanked peptides like WALP23, whereas lysine equivalents are insensitive to its presence.
Finally, chapter 5 is a molecular dynamic study of a system composed of WALP23 and di-C14:0-PC. This chapter complements the experimental studies using the GALA method and aims at giving insights into the molecular and atomistic mechanisms by which the WALP23 peptide is interacting with the surrounding lipids. The results emphasize the importance of the secondary structure on the structure and the orientation of WALP23 in a lipid bilayer. In general, the length of simulations is an important issue for giving a representative view on the lipid-peptide interactions events in the system. Also, some insight is gained on the interfacial interactions and energetic aspects that influence the tilt and rotation angles and the secondary structure.
Chapter 6 is a summarizing discussion of the results presented in all previous chapters where different parameters that influence the tilt and rotation angles of transmembrane peptides in lipid bilayers are described, and where future perspectives for the development of the methodology are presented.

References

1. Daum, G. (1985) *Biochim Biophys Acta* 822(1), 1-42
2. White, D. A. (1973) *in The Phospholipid Composition of Mammalian Tissues. Form and Function of Phospholipids*, (Ansell, G. B., Hawthorne, J. N., and Dawson, R. M. C., Eds). 2nd Ed., pp. 441-482, Elsevier.
3. Singer, S. J., and Nicolson, G. L. (1972) *Science* 175(23), 720-731
4. Vereb, G., Szöllõsi, J., Matkó, J., Nagy, P., Farkas, T., Vígh, L., Mátyus, L., Waldmann, T. A., and Damjanovich, S. (2003) *Proc Natl Acad Sci U S A* 100(14), 8053-8058
5. de Planque, M. R., and Killian, J. A. (2003) *Molecular membrane biology* 20(4), 271-284
6. Lee, A. G. (2004) *Biochim Biophys Acta* 1666(1-2), 62-87
7. White, S. H., and Wimley, W. C. (1998) *Biochim Biophys Acta* 1376(3), 339-352
8. Wiener, M. C., and White, S. H. (1992) *Biophys J* 61(2), 434-447
9. Gennis, R. B. (1989) *Biomembranes: molecular structure and function.*, Springer-Verlag, New York.
10. Niemelä, P. S., Hyvönen, M. T., and Vattulainen, I. (2006) *Biophys J* 90(3), 851-863
11. Landolt-Marticorena, C., Williams, K. A., Deber, C. M., and Reithmeier, R. A. (1993) *J Mol Biol* 229(3), 602-608
12. Reithmeier, R. A. (1995) *Curr Opin Struct Biol* 5(4), 491-500
13. von Heijne, G. (1994) *Annu Rev Biophys Biomol Struct* 23, 167-192
14. Mesleh, M. F., Lee, S., Veglia, G., Thiriot, D. S., Marassi, F. M., and Opella, S. J. (2003) *J Am Chem Soc* 125(29), 8928-8935

15. Sakai, H., and Tsukihara, T. (1998) *J Biochem (Tokyo)* 124(6), 1051-1059
16. Wallin, E., Tsukihara, T., Yoshikawa, S., von Heijne, G., and Elofsson, A. (1997) *Protein Sci* 6(4), 808-815
17. de Planque, M. R., Bonev, B. B., Demmers, J. A., Greathouse, D. V., Koeppe, R. E., 2nd, Separovic, F., Watts, A., and Killian, J. A. (2003) *Biochemistry* 42(18), 5341-5348
18. Persson, S., Killian, J. A., and Lindblom, G. (1998) *Biophys J* 75(3), 1365-1371
19. Yau, W. M., Wimley, W. C., Gawrisch, K., and White, S. H. (1998) *Biochemistry* 37(42), 14713-14718
20. Kachel, K., Asuncion-Punzalan, E., and London, E. (1995) *Biochemistry* 34(47), 15475-15479
21. Spruijt, R. B., Wolfs, C. J., Verver, J. W., and Hemminga, M. A. (1996) *Biochemistry* 35(32), 10383-10391
22. Arkin, I. T., and Brunger, A. T. (1998) *Biochim Biophys Acta* 1429(1), 113-128
23. Cantor, R. S. (1999) *Chem Phys Lipids* 101(1), 45-56
24. Lee, A. G. (2003) *Biochim Biophys Acta* 1612(1), 1-40
25. van den Brink-van der Laan, E., Killian, J. A., and de Kruijff, B. (2004) *Biochim Biophys Acta* 1666(1-2), 275-288
26. Foster, L. J., De Hoog, C. L., and Mann, M. (2003) *Proc Natl Acad Sci U S A* 100(10), 5813-5818
27. Hooper, N. M. (1999) *Molecular membrane biology* 16(2), 145-156
28. Xu, X., Bittman, R., Duportail, G., Heissler, D., Vilcheze, C., and London, E. (2001) *J Biol Chem* 276(36), 33540-33546
29. Xu, X., and London, E. (2000) *Biochemistry* 39(5), 843-849
30. van den Brink-van der Laan, E., Chupin, V., Killian, J. A., and de Kruijff, B. (2004) *Biochemistry* 43(20), 5937-5942
31. Barry, J. A., and Gawrisch, K. (1994) *Biochemistry* 33(26), 8082-8088
32. Cantor, R. S. (2002) *Biophys J* 82(5), 2520-2525
33. Feller, S. E., Brown, C. A., Nizza, D. T., and Gawrisch, K. (2002) *Biophys J* 82(3), 1396-1404
34. Cantor, R. S. (1997) *Biochemistry* 36(9), 2339-2344
35. Spelbrink, R. E., Kolkman, A., Slijper, M., Killian, J. A., and de Kruijff, B. (2005) *J Biol Chem* 280(31), 28742-28748
36. Dumas, F., Lebrun, M. C., and Tocanne, J. F. (1999) *FEBS Lett* 458(3), 271-277
37. Killian, J. A. (1998) *Biochim Biophys Acta* 1376(3), 401-415
38. Mouritsen, O. G., and Bloom, M. (1984) *Biophys J* 46(2), 141-153
39. Belohorcova, K., Davis, J. H., Woolf, T. B., and Roux, B. (1997) *Biophys J* 73(6), 3039-3055
40. Park, S. H., and Opella, S. J. (2005) *J Mol Biol* 350(2), 310-318
41. Shen, L., Bassolino, D., and Stouch, T. (1997) *Biophys J* 73(1), 3-20
42. Zhang, Y. P., Lewis, R. N., Hodges, R. S., and McElhaney, R. N. (1992) *Biochemistry* 31(46), 11579-11588
43. Zhang, Y. P., Lewis, R. N., Hodges, R. S., and McElhaney, R. N. (1995) *Biochemistry* 34(7), 2362-2371
44. Betanzos, M., Chiang, C. S., Guy, H. R., and Sukharev, S. (2002) *Nat Struct Biol* 9(9), 704-710
45. Perozo, E., Cortes, D. M., Sompornpisut, P., Kloda, A., and Martinac, B. (2002) *Nature* 418(6901), 942-948
46. Perozo, E., Kloda, A., Cortes, D. M., and Martinac, B. (2002) *Nat Struct Biol* 9(9), 696-703
47. Lee, A. G. (2002) *Biochim Biophys Acta* 1565(2), 246-266
48. Starling, A. P., East, J. M., and Lee, A. G. (1993) *Biochemistry* 32(6), 1593-1600
49. Starling, A. P., Khan, Y. M., East, J. M., and Lee, A. G. (1994) *Biochem J* 304 (Pt 2), 569-575

50. Gordeliy, V. I., Labahn, J., Moukhametzianov, R., Efremov, R., Granzin, J., Schlesinger, R., Buldt, G., Savopol, T., Scheidig, A. J., Klare, J. P., and Engelhard, M. (2002) *Nature* 419(6906), 484-487
51. Hashimoto, S., Sasaki, M., Takeuchi, H., Needleman, R., and Lanyi, J. K. (2002) *Biochemistry* 41(20), 6495-6503
52. Moukhametzianov, R., Klare, J. P., Efremov, R., Baeken, C., Goppner, A., Labahn, J., Engelhard, M., Buldt, G., and Gordeliy, V. I. (2006) *Nature* 440(7080), 115-119
53. Spudich, J. (2002) *Nat Struct Biol* 9(11), 797-799
54. Subramaniam, S., and Henderson, R. (2000) *Nature* 406(6796), 653-657
55. Wegener, A. A., Chizhov, I., Engelhard, M., and Steinhoff, H. J. (2000) *J Mol Biol* 301(4), 881-891
56. Wegener, A. A., Klare, J. P., Engelhard, M., and Steinhoff, H. J. (2001) *Embo J* 20(19), 5312-5319
57. Baldwin, P. A., and Hubbell, W. L. (1985) *Biochemistry* 24(11), 2633-2639
58. Baldwin, P. A., and Hubbell, W. L. (1985) *Biochemistry* 24(11), 2624-2632
59. Lewis, B. A., and Engelman, D. M. (1983) *J Mol Biol* 166(2), 203-210
60. Ulmschneider, M. B., Sansom, M. S., and Di Nola, A. (2006) *Biophys J* 90(5), 1650-1660
61. Killian, J. A. (2003) *FEBS Lett* 555(1), 134-138
62. Deamer, P. W., and Uster, P. S. (1983) *in Liposome Preparation: Methods and Mechanisms. Liposomes* (Ostro, M. J., Ed.) pp.27-51, Marcel Dekker, New York.
63. Lakowicz, J. R. (1999) *Principles of Fluorescence Spectroscopy*, 2nd Ed. Kluwer Academic/Plenum Publishers, New York.
64. Koehorst, R. B., Spruijt, R. B., Vergeldt, F. J., and Hemminga, M. A. (2004) *Biophys J* 87(3), 1445-1455
65. Stopar, D., Štrancar, J., Spruijt, R. B., and Hemminga, M. A. (2005) *J Chem Inf Model* 45(6), 1621-1627
66. Kosters, P. G. H. (2000) FT-IR Spectroscopy of Thin Biological Layers. PhD-thesis. In.
67. Frasman, G. D. (1996) *Circular Dichroism and the Conformational Analysis of Biomolecules*, Plenum Press, New York.
68. de Jongh, H. H., Brasseur, R., and Killian, J. A. (1994) *Biochemistry* 33(48), 14529-14535
69. de Jongh, H. H., Goormaghtigh, E., and Killian, J. A. (1994) *Biochemistry* 33(48), 14521-14528
70. Opella, S. J., and Marassi, F. M. (2004) *Chem Rev* 104(8), 3587-3606
71. Bechinger, B., Aisenbrey, C., and Bertani, P. (2004) *Biochim Biophys Acta* 1666(1-2), 190-204
72. Mehring, M. (1983) *Principles of High Resolution NMR in Solids*, Springer, Berlin.
73. Rose, M. E. (1963), Elementary Theory of Angular Momentum, John Wiley, New York.
74. Schmidt-Rohr, K., and Spiess, H. W. (1994) *Multidimensional Solid-State NMR and Polymers*, Academic Press, London.
75. Marassi, F. M. (2002) *Concepts Magn. Reson.* 14, 212–224.
76. Wu, C. H., Ramamoorthy, A., Gierasch, L. M., and Opella, S. J. (1995) *J. Am. Chem. Soc.* 117, 6148-6149
77. Hong, M., Gross, J. D., Hu, W., and Griffin, R. G. (1998) *J Magn Reson* 135(1), 169-177
78. Shoji, A., Ozaki, T., Fujito, T., Deguchi, K., Ando, S., and Ando I. (1990) *J. Am. Chem. Soc.* 112, 4693-4697.
79. Hiyama, Y., Niu, C. H., Silverton, J. V., Bavoso, A., and Torchia, D. A. (1988) *J. Am. Chem. Soc.* 110, 2378–2383.
80. Bechinger, B. (1999) *Biochim Biophys Acta* 1462(1-2), 157-183
81. Song, Z., Kovacs, F. A., Wang, J., Denny, J. K., Shekar, S. C., Quine, J. R., and Cross, T. A. (2000) *Biophys J* 79(2), 767-775

82. Wasniewski, C. M., Parkanzky, P. D., Bodner, M. L., and Weliky, D. P. (2004) *Chem Phys Lipids* 132(1), 89-100
83. Marassi, F. M., and Opella, S. J. (2000) *J Magn Reson* 144(1), 150-155
84. Wang, J., Denny, J., Tian, C., Kim, S., Mo, Y., Kovacs, F., Song, Z., Nishimura, K., Gan, Z., Fu, R., Quine, J. R., and Cross, T. A. (2000) *J Magn Reson* 144(1), 162-167
85. Griffin, R. G. (1998) *Nat Struct Biol* 5 Suppl, 508-512
86. McDowell, L. M., and Schaefer, J. (1996) *Curr Opin Struct Biol* 6(5), 624-629
87. Smith, S. O., Aschheim, K., and Groesbeek, M. (1996) *Q Rev Biophys* 29(4), 395-449
88. Baldus, M. (2002) *Progress in Nuclear Magnetic Resonance Spectroscopy* 41(1-2), 1-47
89. Mason, A. J., Grage, S. L., Straus, S. K., Glaubitz, C., and Watts, A. (2004) *Biophys J* 86(3), 1610-1617
90. Davis, J. H. (1983) *Biochim Biophys Acta* 737(1), 117-171
91. Seelig, J. (1977) *Q Rev Biophys* 10(3), 353-418
92. Smith, R. L., and Oldfield, E. (1984) *Science* 225(4659), 280-288
93. Burnett, L. J., and Muller, B. H. (1971) *The Journal of Chemical Physics* 55(12), 5829-5831
94. Keniry, M. A., Kintanar, A., Smith, R. L., Gutowsky, H. S., and Oldfield, E. (1984) *Biochemistry* 23(2), 288-298
95. Killian, J. A., Taylor, M. J., and Koeppe, R. E., 2nd. (1992) *Biochemistry* 31(46), 11283-11290
96. Jones, D. H., Barber, K. R., VanDerLoo, E. W., and Grant, C. W. (1998) *Biochemistry* 37(47), 16780-16787
97. van der Wel, P. C., Strandberg, E., Killian, J. A., and Koeppe, R. E., 2nd. (2002) *Biophys J* 83(3), 1479-1488
98. Pines, A., Gibby, M. G., and Waugh, J. S. (1973) *The Journal of Chemical Physics* 59(2), 569-590

Chapter 2

Tilt Angles of Transmembrane Model Peptides in Oriented and Non-Oriented Lipid Bilayers as Determined by ^{2}H Solid-State NMR

Taken from
Biophysical Journal (2004) 86, 3709-3721

Abstract

Solid-state NMR methods employing ^{2}H NMR and geometric analysis of labeled alanines (GALA) were used to study the structure and orientation of the transmembrane α-helical peptide acetyl-GWW(LA)$_8$LWWA-amide (WALP23) in phosphatidylcholine (PC) bilayers of varying thickness. In all lipids the peptide was found to adopt a transmembrane α-helical conformation. A small tilt angle of 4.5° was observed in di-18:1-PC, which has a hydrophobic bilayer thickness that approximately matches the hydrophobic length of the peptide. This tilt angle increased slightly but systematically with increasing positive mismatch to 8.2° in di-C12:0-PC, the shortest lipid used. This small increase in tilt angle is insufficient to significantly change the effective hydrophobic length of the peptide and thereby to compensate for the increasing hydrophobic mismatch, suggesting that tilt of these peptides in a lipid bilayer is energetically unfavorable. The tilt and also the orientation around the peptide axis were found to be very similar to the values previously reported for a shorter WALP19 peptide (GWW(LA)$_6$LWWA). As also observed in this previous study, the peptide rotates rapidly around the bilayer normal, but not around its helix axis. Here we show that these properties allow application of the GALA method not only to macroscopically aligned samples but also to randomly oriented samples, which has important practical advantages. A minimum of four labeled alanine residues in the hydrophobic transmembrane sequence was found to be required to obtain accurate tilt values using the GALA method.

Introduction

Membrane proteins perform many important functions in cells, but relatively little is known about the mechanisms by which they work. To understand the mode of action of membrane proteins on a molecular level, it is important to have a detailed knowledge of the structural properties of these proteins, such as precise backbone structure and tilt angles of the transmembrane segments. In addition, since membrane proteins are embedded in a lipid bilayer, it is important to know how and to what extent these properties can be influenced by the lipid environment. An important factor could be, for example, the extent of hydrophobic matching (reviewed in 1). If the hydrophobic part of a transmembrane segment is long with respect to the thickness of the bilayer formed by the surrounding lipids, the protein may adopt a tilted orientation to achieve hydrophobic matching. Alternatively, such a mismatch could lead to (local) changes in peptide backbone structure which might decrease the effective length of the protein. Clearly, both types of mismatch responses could have functional consequences because they could influence the structure, and hence the activity of the protein.

Since large proteins are difficult to study in detail, a number of groups have started to study single transmembrane helices that mimic the transmembrane segments of membrane proteins (2-9; reviewed in 10). One example of these model peptides is the family of α-helical transmembrane model peptides called WALP, with an amino acid sequence given in Table 1. These peptides have a hydrophobic transmembrane stretch of alanines and leucines of variable length and are flanked on both sides by tryptophan residues. These flanking residues were chosen because aromatic amino acid residues are frequently found at the interfacial region in membrane proteins (11,12), where they are believed to have favorable interactions with the lipid-water interface (13,14). Also in the WALP peptides interfacial anchoring properties of the

tryptophan residues have been shown to play an important role in the interaction of the peptides with surrounding lipids (15).

Table 1. Amino acid sequences of the peptides used.

Peptide	Sequence
WALP19	Acetyl-GWW$(LA)_6$LWWA-ethanolamine
WALP23	Acetyl-GWW$(LA)_8$LWWA-amide

The use of peptide families, such as the WALP peptides, allows systematic analysis of the effects of the lipid environment on structural and dynamic properties of transmembrane segments of α-helical membrane proteins. WALP peptides have been studied extensively in lipid bilayers with a variety of biophysical methods (5,15-20). Circular dichroism and Fourier transform infrared experiments have shown that WALP peptides are mostly transmembrane and α-helical (5,21,22). Recently, a solid-state NMR method was developed, based on geometric analysis of labeled alanines (GALA) to study the orientation and backbone structure of transmembrane peptides (23). The method uses CD_3 labels on different alanine residues in the transmembrane part of peptides. The peptide-containing bilayers are macroscopically oriented between glass plates, and the quadrupolar splittings from ^2H NMR spectra are measured for each labeled position. The results are analyzed based on a peptide model with α-helical geometry. Due to this geometry, GALA is a very sensitive method to study peptide tilt and backbone conformation, allowing a high resolution of the tilt angle. Detection of changes in the tilt for a specific peptide, assuming that the dynamics do not change significantly, can be made with a resolution of <1º. The method was applied to study the backbone and tilt angle of WALP19 in lipid bilayers of phosphatidylcholine with different lengths of the hydrocarbon chains (23). The tilt was found to be essentially independent of the lipid length, and even in the relatively short di-C12:0-PC only a very small tilt and no backbone distortions were found (23).
In the present study a longer peptide, WALP23, is used together with the same lipids as in the previous WALP19 study, resulting in peptide/lipid systems with a significantly larger positive mismatch. Therefore, if hydrophobic mismatch is important for determining the tilt angles, a significant tilt could be expected for this peptide, in particular in the shortest lipids. WALP23 also has more alanines in the hydrophobic region, giving more potential data points to use in the analysis. Since this feature would yield more data points than would be required to determine the tilt angle for a regular α-helix, application of this method to WALP23 allows a detailed analysis of possible deviations from an α-helical structure if small changes in the backbone structure would occur. In addition, we explore the possibility of analyzing tilt and precise backbone structure by using non-oriented bilayers. Such an approach would not only have practical advantages; such samples also better mimic the situation in biological membranes, in terms of water content and lipid packing.
Our results show that analysis of peptide tilt in unoriented bilayers indeed is possible. In all lipid systems investigated, only a small tilt of WALP23 was observed, which increased slightly with the extent of mismatch. The results will be compared with those previously obtained on WALP19 and discussed in light of other hydrophobic mismatch responses.

Materials and Methods

Materials

WALP23 (amino acid sequence acetyl-GWW$(LA)_8$LWWA-amide) was synthesized using Fmoc/tBu solid phase peptide synthesis and purified as described elsewhere for related KALP peptides (22). Deuterated L-alanine-d_4 was obtained from Sigma-Aldrich (St. Louis, MO) and its amino functionality was protected by an 9-fluorenylmethyloxycarbonyl (Fmoc) group as described by Ten Kortenaar et al. (1986) before being used in the synthesis (24). The WALP peptides were isotopically labeled with one of the alanine residues in the transmembrane domain deuterium-labeled. 1,2-dilauroyl-*sn*-glycero-3-phosphatidylcholine (di-C12:0-PC), 1,2-ditridecanoyl-*sn*-glycero-3-phosphatidylcholine (di-C13:0-PC), 1,2-dimyristoyl-*sn*-glycero-3-phosphatidylcholine (di-C14:0-PC), and 1,2-dioleoyl-*sn*-glycero-3-phosphatidylcholine (di-C18:1-PC) were purchased from Avanti Polar Lipids (Alabaster, AL) and used without further purification. Trifluoroacetic acid (TFA) and 2,2,2-trifluoroethanol (TFE) were obtained from Merck (Darmstadt, Germany). Deuterium-depleted water was obtained from Sigma Aldrich. All other chemicals were of analytical grade. Water was deionized and filtered with a Milli-Q Water purification system from Millipore (Bedford, MA).

Methods

Sample preparation

Stock solutions were prepared of the lipid in chloroform and the amount of lipid was checked by a phosphorus assay. To remove residual traces of TFA in the peptide powder after synthesis, peptides were dissolved in 1 ml TFE and dried to a film in a rotavapor and resolubilized in TFE. This procedure was repeated twice. The peptide solution was then added to an appropriate amount of the lipid solution. The mixture was vortexed and dried to a film in a rotavapor. The samples were further dried overnight under vacuum.

For oriented samples, the dry lipid-peptide film was redissolved in 2 ml methanol/chloroform (1:1 volume ratio) and the solution was spread on 50 glass plates of size 24 × 4.8 × 0.07 mm (Marienfeld Laboratory Glassware, Lauda-Koenigshofen, Germany). Dry peptide/lipid films were obtained by subsequent air-drying followed by drying under vacuum overnight. The dry plates were stacked in a 27 × 6 × 6 mm glass cuvette under a N_2(g) flow and hydrated with deuterium-depleted water to get a hydration of 40% (w/w). The cuvette was sealed with an end-glass plate using fast-drying epoxy glue. Samples were allowed to equilibrate at 37ºC for typically one week, until they became transparent, which is an indication for good alignment on the glass plates. Subsequently samples were stored at room temperature before measurements. Typically 2 μmol of peptide and40 μmol of lipid was used for each sample. Lower P/L ratios were tried in a few samples, by keeping the amount of peptide constant while increasing the lipid content. However, this resulted in less-well-oriented samples, probably due to the high amount of sample material per glass plate.

For unoriented samples, the dry lipid-peptide film was hydrated in 200–300-ml deuterium-depleted water and the suspension was transferred to7-mm diameter glass tubes. The pH of the suspension was checked to be at 6 or above. The tubes were sealed with a silicon stopper and epoxy glue. In unoriented samples, typically 1 μmol of peptide and 100 μmol of lipid was used for each sample, with a peptide/lipid molar

ratio of 1:100. In a test series with P/L between 1:20 and 1:200 it was found that P/L = 1:100 or lower gave better resolved splittings, whereas the value of the splitting did not depend on the peptide concentration in this range.

NMR spectroscopy

NMR experiments were carried out on a Bruker Avance 500 MHz NMR spectrometer (Bruker Biospin, Karlsruhe, Germany). Unless stated otherwise, measurements were performed at 40ºC. Samples were allowed to equilibrate at this temperature for at least 10 min before measurements.

^{31}P NMR experiments were performed at 202.5 MHz using a one-pulse experiment with a 13.4-μs 90º pulse, 1.3-s relaxation delay time, 100-kHz spectral width, 1024 data points, and gated proton-noise decoupling. Between 200 and 2000 scans were collected. Spectra were processed on the spectrometer by DC offset correction, zero-filling to 2048 data points, and a 50-Hz exponential multiplication before Fourier transformation.

^{2}H NMR experiments were performed at 76.78 MHz using a quadrupolar echo experiment with a 5.6-ms 90º pulse, an echo delay of 50 ms, a 100-ms relaxation delay time, 1 MHz spectral width, and 1024 data points. Between 200,000 and 1,000,000 scans were collected. Acquisition was started before the echo and the time domain data was left-shifted to get the FID starting at the echo maximum before further processing by zero-filling to 8192 data points and a 100-Hz exponential multiplication followed by Fourier transformation.

Calculations

Quadrupolar splittings from the labeled positions were measured from ^{2}H NMR spectra. The data were fitted to a model of an α-helix in a manner that parallels the previous procedure (23), with small modifications. In oriented spectra the quadrupolar splittings from samples oriented with the bilayer normal parallel to the magnetic field direction were used. For unoriented samples, the measured splittings were multiplied with 2 to obtain comparable splittings. Data were fitted to the equation

$$\Delta\nu_q = (3/4)K(3\cos^2\varepsilon_{\|}(\cos\tau - \sin\tau\cos\delta\tan\varepsilon_{\|})^2 - 1) \quad (1)$$

Equation 1 is similar to the treatment of Jones et al. (1998) and Whiles et al.(2002) (25,26), and is derived in the Appendix. Here, $\Delta\nu_q$ is the quadrupolar splitting, K is a constant with dimension frequency, and the angles τ, $\varepsilon_{\|}$, and δ depend on the peptide geometry and orientation, and are defined in Fig. 1.The τ is the tilt angle, defined as the angle between the peptide helical axis and the bilayer normal (which is assumed to be along the magnetic field direction, Fig. 1 A), $\varepsilon_{\|}$ is the angle between the peptide helix axis and the C^{α}-CD_3 bond vector (Fig. 1 B), and δ is the rotation angle, defining the position of the bond vector around the helical axis (Fig. 1 C). In turn, δ depends on three angles as shown in Fig. 1 D,

$$\delta = \rho + \varepsilon_{\perp} + \varphi \quad (2)$$

where ρ is the rotation of the helix compared to a standard orientation with C^{α} of Gly1 in the *xz* plane, $\varepsilon_{\perp}$ is the angle of the bond vector with respect to a vector from C^{α} to the peptide axis, and φ is the angle between the reference point Gly1 and the labeled

residue in the peptide. For a regular helix, φ is given by –(n–1)ψ, where *n* is the residue number and ψ is the pitch angle. Using our notation, in an ideal α-helix, ψ = 100º, which value was used in the calculations unless otherwise stated; $\varepsilon_\perp$ was estimated from molecular models using Insight II database to be –43.3º, which was used in all calculations; and τ, ρ, and $\varepsilon_\parallel$ were used as fitting parameters in the calculations (see also 23).

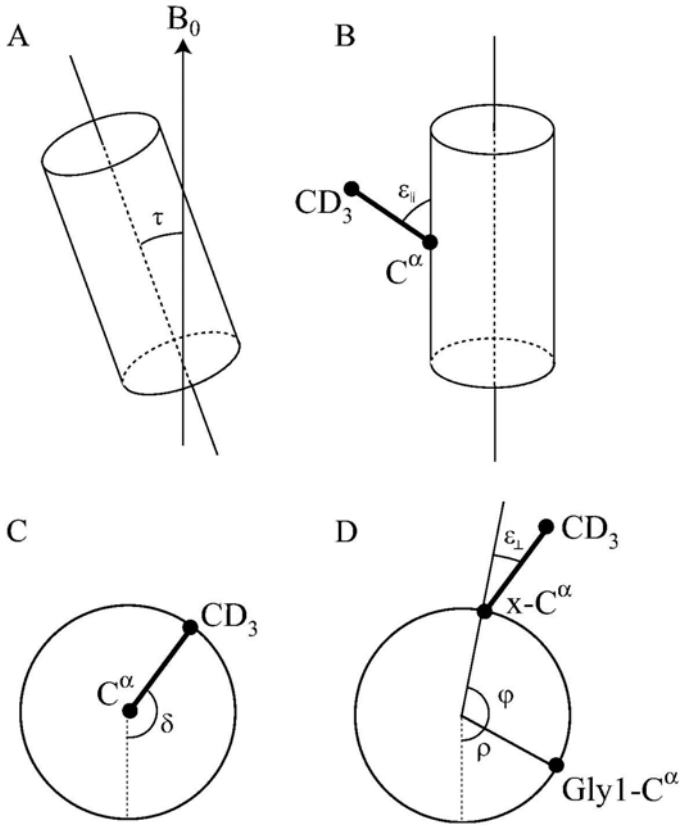

Figure 1. Definition of angles used in the calculations. (A) The tilt angle τ between the peptide axis and the bilayer normal (assumed to be along the magnetic field direction). (B) The bond angle $\varepsilon_\parallel$ between the C-CD_3 bond and the peptide axis. (C) The rotation angle δ giving the orientation of the C-CD_3 bond. (D) The angle δ is determined by three contributions: ρ is the rotation of the whole peptide, defined as the anticlockwise rotation angle of C^α of Gly1, compared to the reference position; φ is the angle by which another amino acid residue is rotated around the peptide axis compared to Gly1; and $\varepsilon_\perp$ is the angle of the C^α-CD_3 bond projected onto a plane perpendicular to the helical axis compared to the direction from the peptide axis to the C^α. (Angles in the figure are chosen for clarity and do not represent real values.)

The constant K is defined as

$$K = (e^2qQ/h)S \qquad (3)$$

where e^2qQ/h is the quadrupolar coupling constant and *S* is an order parameter taking into account the molecular motion. For a deuterium bound to a carbon, the quadrupolar coupling constant is 167 kHz (27). In the case of methyl groups, this value is averaged by the fast rotation of the methyl groups giving a third of this value, or 56 kHz. Additional motions or a small deviation from tetrahedral geometry can

cause further averaging, which is here included in the order parameter *S*. It was previously shown for WALP19 peptides that the fitting procedure was not very sensitive to changes of the value of *K* between 47 and 56 kHz (23). In this study a *K*-value of 49 kHz was used, corresponding to $S = 0.875$, which was obtained from the splittings in a powder sample of dry WALP23-Ala-d_4 peptide (data not shown). Optimum values for τ, ρ, and $\varepsilon_{||}$ were calculated to minimize the error function

$$Error = \sum_i \left[\Delta\upsilon_{q,i}^{\exp} - \Delta\upsilon_{q,i}^{calc}\left(\tau,\rho,\varepsilon_{||}\right)\right]^2 \qquad (4)$$

where the sum is over all labeled positions. All angles were varied in steps of 0.1º, τ was varied in the range 0–45º, and ρ in the range 0–360º, whereas $\varepsilon_{||}$ was only varied within a few degrees from 56.2º (the value for Ala in the Insight II database) until a minimum was found. The error values for best-fits will be presented as root mean square deviations (RMSD), defined as $RMSD = (Error/number\ of\ data\ points)^{1/2}$.

Results

WALP23 in di-C14:0-PC

WALP23 was labeled at different positions with deuterated alanine. As shown in Fig. 2 in a helical wheel model, these deuterated sites are regularly distributed around the helical axis.

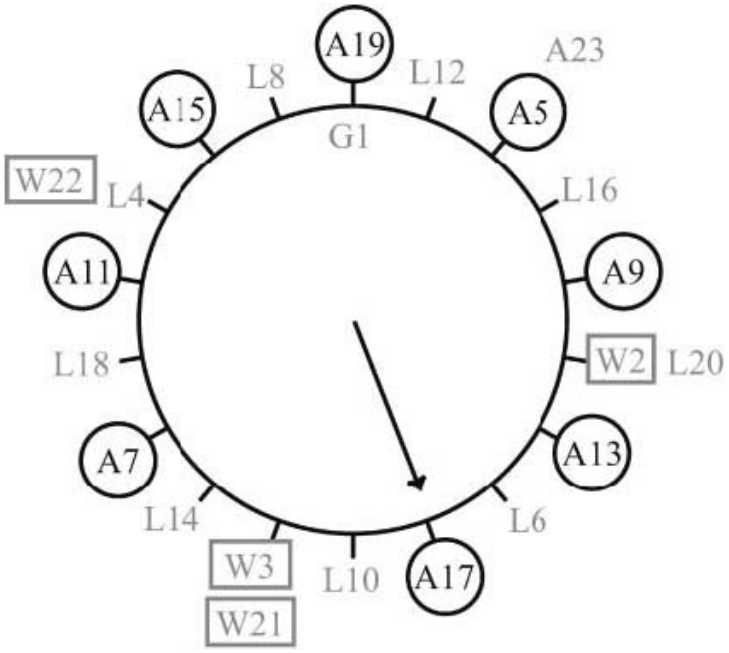

Figure 2. Helical wheel projection of WALP23, with Gly1 at the top. The positions of the labeled alanine residues are marked with circles, and the tryptophan residues are marked with rectangles. The arrow marks the side of the peptide pointing away from the membrane normal in di-C14:0-PCbilayers.

Oriented samples were prepared of all labeled peptides in di-C14:0-PC. The bilayer organization of the lipids and their predominant orientation with their long axis perpendicular to the glass plates was confirmed by ^{31}P NMR (data not shown). ^{2}H NMR spectra of these samples, measured with the orientation of the bilayer normal parallel to the external magnetic field (Fig. 3, left column), show that the magnitude

of the ^{2}H splittings varies with the position of the labeled site around the helical axis, as was previously also observed for WALP19 (23). The distribution of splittings is clearly nonrandom, with every other alanine showing a large splitting, and with small splittings for the intervening alanines. Since the angular distance between two consecutive alanines in a regular α-helix is 200º (Fig. 2), this pattern suggests that alanines on one face of the peptide exhibit larger splittings, whereas on the opposite face the splittings are smaller. Such a behavior would be consistent with that of a helix that is tilted away from the bilayer normal.

When oriented samples are measured with the orientation of the bilayer normal perpendicular to the external magnetic field (Fig. 3, middle column), the quadrupolar splittings are reduced with a factor of two, within the margin of error (see below) of the measurements (Table 2). This observation indicates that the peptides are rotating fast with respect to the bilayer normal (23,28). The results also indicate that the peptide does not rotate around its own helical axis, since this motion would average all the splittings to the same value, at least for a regular α-helix conformation. An implication of fast rotation about the bilayer normal, but not around the helical axis, is that it should be possible to obtain similar information from quadrupolar splittings in non-oriented samples as from oriented samples. In unoriented samples, the main splittings should correspond to those from oriented samples for which the bilayer normal is perpendicular to the magnetic field. The right column of Fig. 3 shows spectra from unoriented samples, and the splittings are indeed close to those of the middle column, as shown in Table 2.

Table 2. Measured ^{2}H NMR splittings of unoriented and oriented di-C14:0-PC samples in kHz

Peptide	di-C14:0-PC oriented 0º	di-C14:0-PC oriented 90º	***di-C14:0-PC unoriented***
WALP23A5	9.3	4.3	4.7
WALP23A7	1.0*	0.5*	0.5*
WALP23A9	11.3	5.8	6.6
WALP23A11	2.0*	1.0*	2.3
WALP23A13	12.8	5.65	7.75
WALP23A15	1.0*	0.5*	0.5*
WALP23A17	12.3	6.0	6.5
WALP23A19	2.0	1.5	0.6

Splittings that could not be resolved are marked with an asterisk and an estimated value is given.

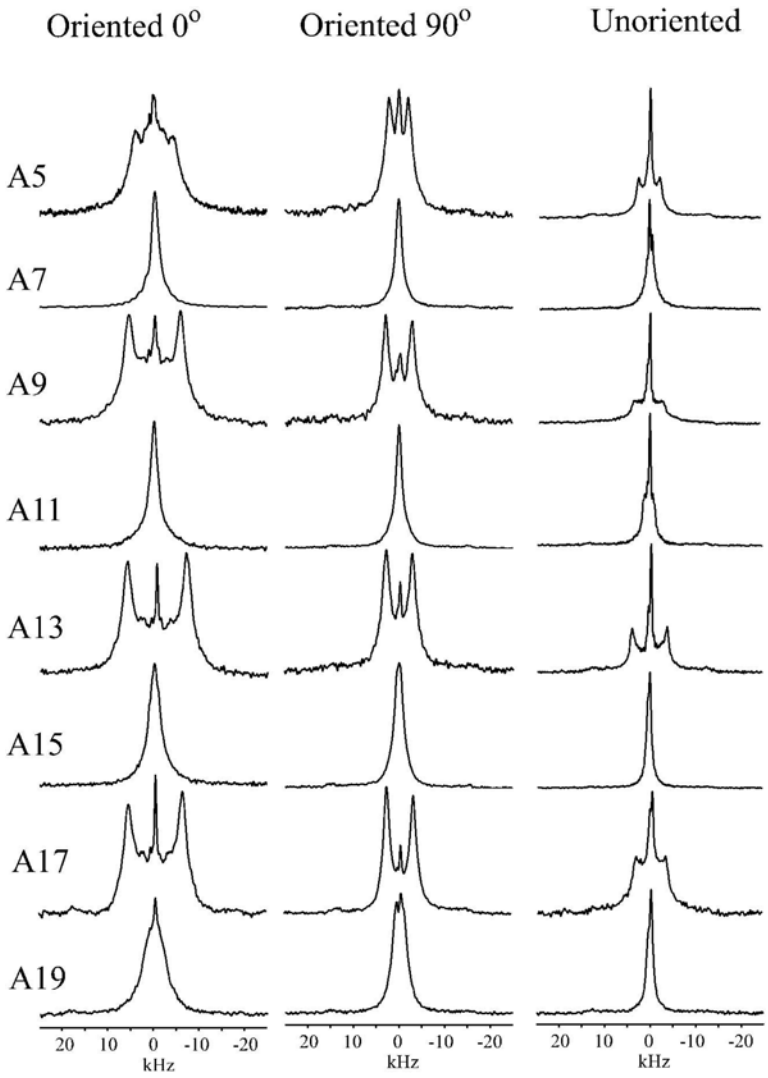

Figure 3. ^{2}H NMR spectra of WALP23/di-C14:0-PC for the different labeled alanine residues. The row with a deuterium label at position 5 is indicated by A5, etc. (Left column) Oriented samples with the bilayer normal parallel to the magnetic field. (Middle column) Oriented samples with the bilayer normal perpendicular to the magnetic field. (Right column) Unoriented samples. The isotropic peak in the middle of the spectra originates from residual deuterium in H_2O.

WALP23 in different lipid systems

Next, samples were studied using unoriented di-C12:0-PC, di-C13:0-PC, and di-C18:1-PC bilayers. Control experiments using ^{31}P NMR demonstrated that in all of these samples the lipids are organized in a bilayer (data not shown). Fig. 4 shows selected ^{2}H NMR spectra. The splittings for all labeled positions in WALP23 in unoriented samples for di-C12:0-PC, di-C13:0-PC, di-C14:0-PC and di-C18:1-PC are given in Table 3. It can be noted that splittings are rather similar in di-C14:0-PC and di-C18:1-PC samples, with slightly larger splittings for di-C14:0-PC. Along the peptide sequence, the splittings again vary systematically between large and small for every other splitting.

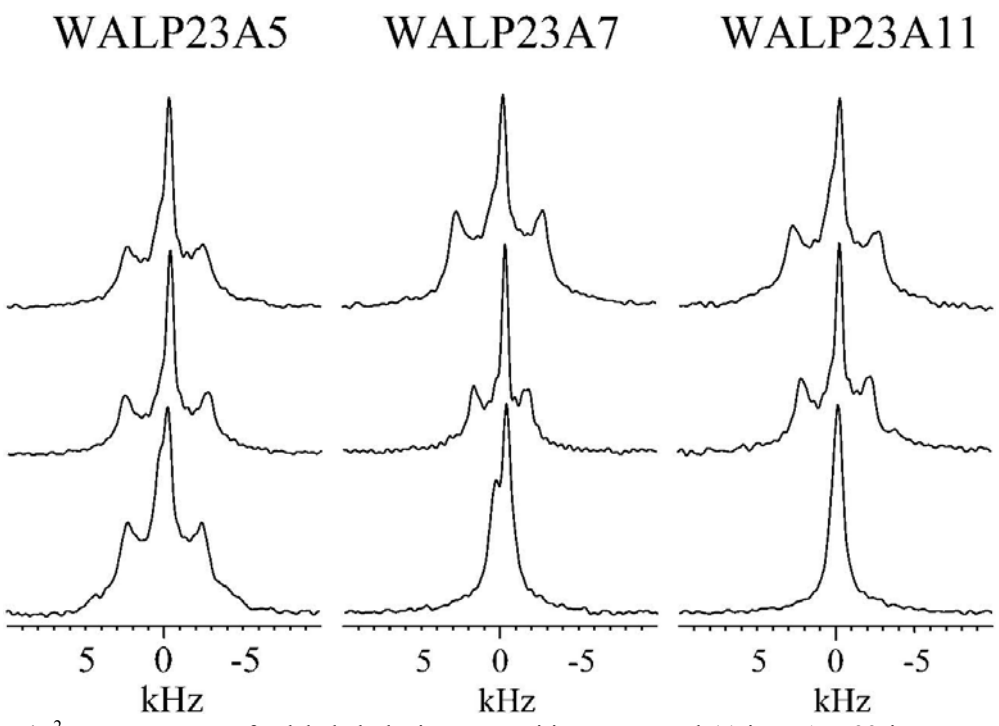

Figure 4. ^{2}H NMR spectra for labeled alanines at positions 5, 7, and 11 in WALP23 incorporated in bilayers of di-C12:0-PC (top row), di-C13:0-PC (middle row), or di-C18:1-PC (bottom row). For details see text.

Table 3. Measured ^{2}H NMR splittings of unoriented samples in kHz

	di-C12:0-PC unoriented	di-C13:0-PC unoriented	di-C14:0-PC unoriented	***di-C18:1-PC unoriented***
WALP23A5	4.75	5.3	4.7	4.7
WALP23A7	5.5	3.5	0.5*	0.35
WALP23A9	7.6	7.5	6.6	5.9
WALP23A11	5.45	4.4	2.3	0.5*
WALP23A13	8.65	8.7	7.75	6.7
WALP23A15	2.05	1.65	0.5*	0.5*
WALP23A17	7.1	6.7	6.5	5.6
WALP23A19	0.75	0.75	0.6	1.65

Splittings that could not be resolved are marked with an asterisk and an estimated value is given.

In the series of saturated lipids of different length, di-C12:0-PC, di-C13:0-PC, and di-C14:0-PC, most splittings are similar but there are some systematic differences. In general, the splittings are larger in shorter lipids. In particular, WALP23A7 and WALP23A11 show a small splitting in di-C18:1-PC, but the splitting increases considerably as the lipids are shortened, as illustrated in Fig. 4. Interestingly, these two positions, 7 and 11, are approximately one helical turn from each other and on the same face of the helix (Fig. 2).

In the case of di-C14:0-PC, the full series of labeled positions have been examined in both oriented and unoriented samples. For each of the other lipids, three oriented samples of different labeled peptides were also made for a comparison with the unoriented samples. In all cases the observed quadrupolar splittings differed <0.5 kHz between oriented and unoriented samples (data not shown), indicating that the peptides behave very similarly in the two types of sample systems.

Error estimate

The error in the measurement of the quadrupolar splitting in each data point is estimated from duplicate samples to be ~0.5 kHz. An error of this size must be considered rather small, because at the sensitive region around $\varepsilon_{||} = 56^{\circ}$ a change in the peptide tilt of only 1º can already change the splitting up to 2 kHz, depending on the position around the peptide axis. The splitting is also very sensitive to the exact value of $\varepsilon_{||}$. Assuming that the peptide does not significantly change its structure and dynamics, the GALA method is able to detect very small changes in, for example, tilt angles.

Calculation of tilt angles

Next, the experimental values of the quadrupolar splittings were fitted to a model of an α-helical peptide in a tilted membrane-spanning orientation as described above. Experimental data from WALP23 in unoriented di-C14:0-PC bilayers are presented in Fig. 5 together with the theoretical best-fit curve. In this figure, data are given for the different alanine positions according to their relative positions around the helical axis. In this case, the position of the residue Gly1 is defined as 0º, placing Trp3 at 200º, Ala5 at 400º (= 40º), and so on.

Best-fit values for WALP23 in all lipid systems investigated are given in Table 4. The results clearly show that there is a change to larger tilt angles of WALP23 when shorter lipids are used. The changes are small, as the tilt angle only changes from 4.4º to 8.2º. The rotation angle is similar in different lipids, indicating that the peptide is tilting in almost the same direction in all cases.

The angle between the C^{α}-CD_3 bond and the helix axis ($\varepsilon_{||}$ in Eq. 1) is difficult to determine with a high accuracy from existing experimental data; for example, from crystal structures of membrane proteins. According to the Insight II database the angle is 56.2º, but this angle may fluctuate or deviate (the Insight II database gives values between 55º and 60º for different side chains in an α-helix). For di-C14:0-PC and di-C18:1-PC, a bond angle of ~58º was found to give the best fit to the experimental data, in good agreement with our earlier findings of 58.8º and 59.2º for WALP19 in di-C14:0-PC and di-C18:1-PC, respectively (23). For the shorter di-C13:0-PC and di-C12:0-PC lipid systems, slightly smaller $\varepsilon_{||}$-angles were suggested by the calculations. Also the RMSD values were found to increase with shorter lipids, suggesting that perhaps slight distortions of the backbone occur with increasing mismatch. However, in all lipids, the RMSD values can be reduced to zero if each of the backbone angles is allowed to fluctuate slightly from its average value. For di-C18:1-PC a fluctuation of only ~0.4º in $\varepsilon_{||}$ would be required to obtain an RMSD value of zero; in di-C14:0-PC the errors are larger and a fluctuation of 0.9º is required, but even for the worst fit, in di-C12:0-PC, a maximum deviation of only ~±1.8º would be sufficient. It is important to note that, although varying the $\varepsilon_{||}$-angle within a few degrees resulted in improved fits (lower RMSDs), it did not influence the optimal values of tilt angle and rotation angle. For example, if $\varepsilon_{||}$ was set to 55º (uniformly for all residues) in di-C14:0-PC, the best-fit values were $\tau = 5.4^{\circ}$ and $\rho = 149.8^{\circ}$, very close to the optimal values, even though the RMSD error was as large as 5.21 kHz.

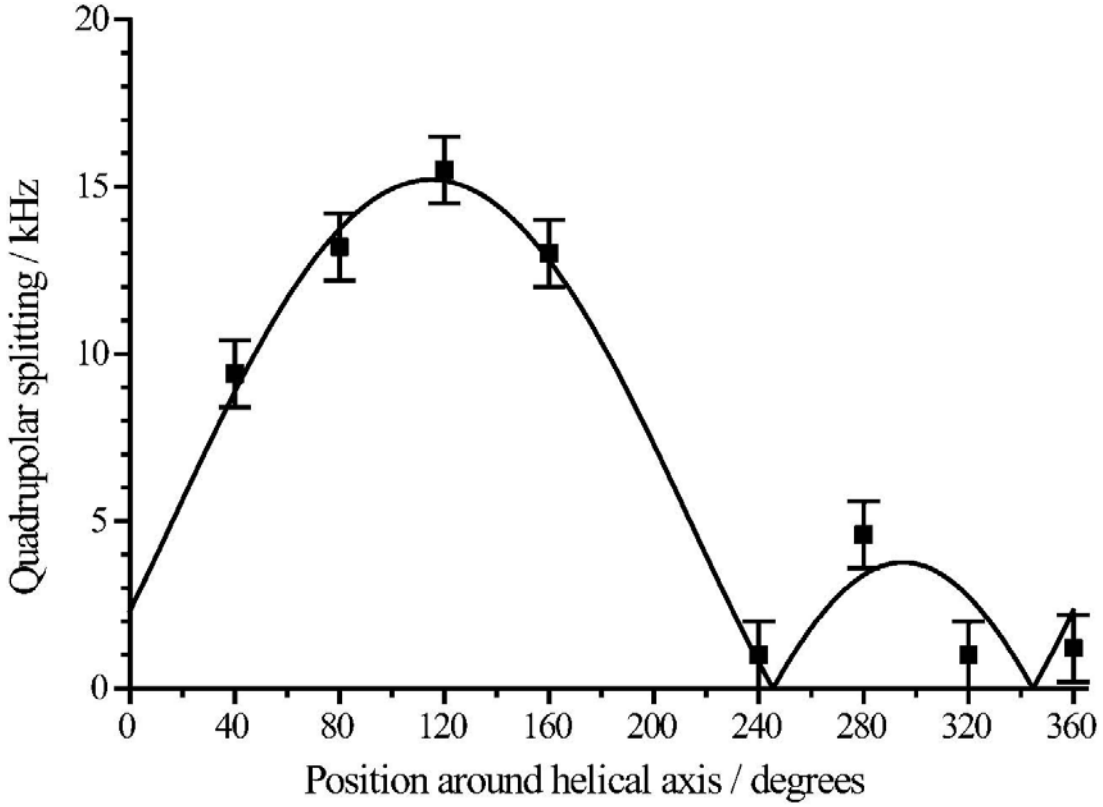

Figure 5. Data of WALP23 in unoriented di-C14:0-PC bilayers given together with a theoretical best-fit curve corresponding to a tilt angle of 5.5º, a rotation angle of 158.3º, and a bond angle $\varepsilon_{\|}$ of 58.2º. The error bar shows 1 kHz.

Table 4. Best-fit results for WALP23 (unoriented) using data from all labeled positions.

	Tilt angle τ/º	Rotation angle ρ/º	RMSD error (kHz)	Bond angle $\varepsilon_{\|}$/º
di-C12:0-PC	8.2	143	2.19	56.9
di-C13:0-PC	7.4	145	1.41	57.4
di-C14:0-PC	5.5	158	0.90	58.2
di-C18:1-PC	4.4	154	0.48	58.1
di-C14:0-PC oriented	4.5	158	0.73	58.0

The molecular model that we used per se does not assume a specific type of helix, but in all fits shown until this point, the angle between consecutive amino acid residues was fixed to 100º, the value for an α-helix. When this angle (ψ) was also allowed to vary, together with the backbone/side-chain angle ($\varepsilon_{\|}$), it was found that the angle between consecutive residues giving the best-fit remains near 100º for di-C18:1-PC, di-C14:0-PC, and di-C13:0-PC, as illustrated in Fig. 6 for di-C14:0-PC. A large region of (ψ, $\varepsilon_{\|}$) space was sampled where different helical structures are located. In the figure is shown the most relevant region where RMSD values below 4 kHz were found. Low RMSD values were also found in mirror regions (not shown) at the line ψ = 90º, which was due to the symmetry of the equations, and around the magic angle at $\varepsilon_{\|}$ = 54.7º, where there is a pseudo-mirror symmetry due to the lack of sign of the quadrupolar splitting. The fit indicates that the structure is not changed to another type

of helix. However, for di-C12:0-PC, there was not a good fit, and there was no clear minimum, which could indicate a distortion of the peptide backbone for large mismatch. The most likely position for such a distortion would be near Ala7 and Ala11, because at this position a prominent increase of the splittings was found upon decreasing lipid-chain length (Table 3).

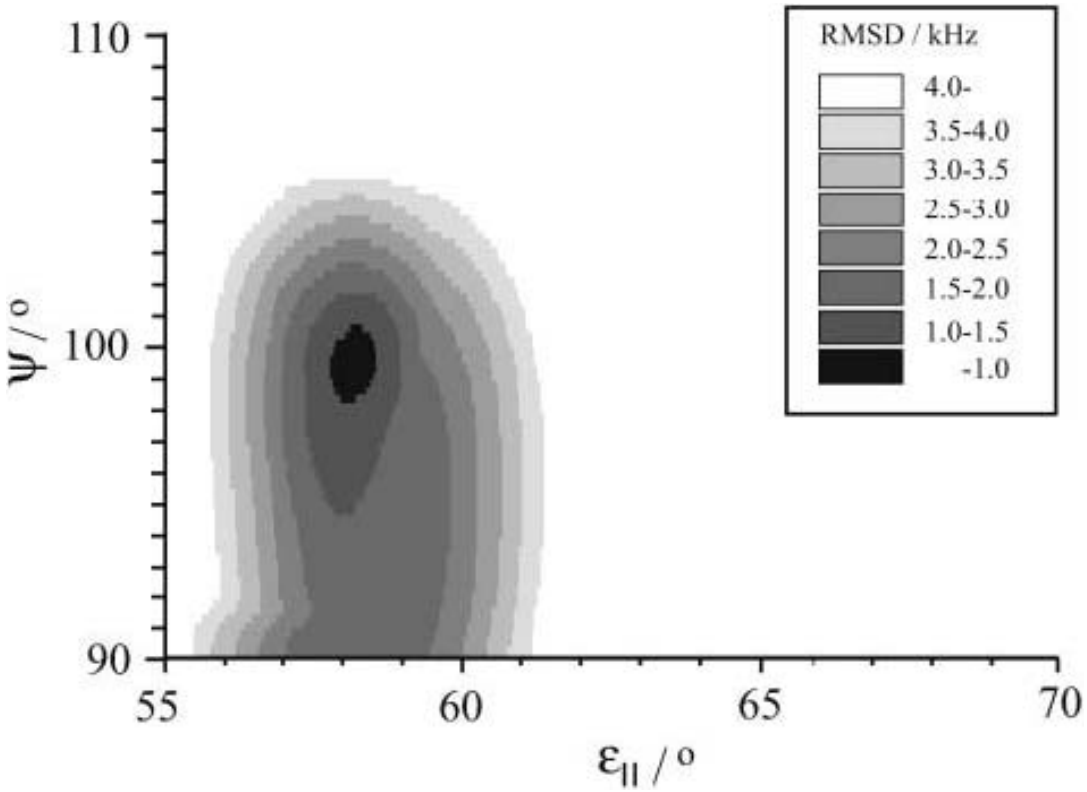

Figure 6. Figure of best fit for different pitch angle (ψ) and bond angles ($\varepsilon_{||}$) for WALP23 in unoriented di-C14:0-PC. The best fit is found for ψ = 99.5º, corresponding closely to an α-helical configuration of the peptide. The scale is RMSD error in kHz.

Combined analysis in different lipid systems

The results above used eight data points in each lipid system to get a fit, giving four separate fits where not only the tilt angle but also the bond and rotation angles were allowed to vary between lipid systems. Using the assumption that the peptide structure is the same and that only the tilt of the peptide should change depending on the lipid chain length, another fit was made, using the data from all lipid systems, keeping the bond and rotation angles the same and only allowing variation of the tilt angle in each lipid system. In this way, 32 data points are used to obtain six parameters in total. Interestingly, values of the rotation and bond angle were found that corresponded to an average of the values obtained in the individual lipid systems ($\varepsilon_{||}$ = 57.6º and ρ = 146.9º). The four tilt angles were found to be almost exactly the same as in the separate fits: 4.4º in di-C18:1-PC, 5.5º in di-C14:0-PC, 7.5º in di-C13:0-PC, and 8.3º in di-C12:0-PC. The RMSD error in this combined fit was quite large, 1.71 kHz. A more detailed analysis indicated that most of the error was due to the problem of fitting data from Ala7 and Ala11 in the shortest lipids. When these two residues were not included in the fit, using the other 24 data points a much smaller RMSD of 0.61 kHz was found, together with $\varepsilon_{||}$ = 58.3º and ρ= 157.8º, which is close to the values found in di-C14:0-PC or di-C18:1-PC. The best-fit tilt angles in this latter analysis

were 4.3º in di-C18:1-PC, 5.3º in di-C14:0-PC, 6.4º in di-C13:0-PC, and 6.6º in di-C12:0-PC. This fit suggests that there indeed could be some local distortion of the peptide at positions 7 and 11 in shorter lipids, possibly affecting the $\varepsilon_{\|}$-angles at these positions, whereas the rest of the peptide is well described by an ideal α-helix.

Number of data points required for accurate tilt angle determination

In WALP23 eight positions have been deuterium-labeled, giving eight data points to use in the fits for each lipid system. An analysis was made of how the results depend on the number of data points used. Since the best fit was found for di-C18:1-PC and the worst for di-C12:0-PC, a comparison was made for these two lipid systems. The results are shown in Fig. 7 as a plot of the maximum and minimum values of tilt, rotation angles, and RMSD error, obtained for different combinations of different numbers of the eight data points. For each parameter, the range of values is clearly decreasing using more data points.

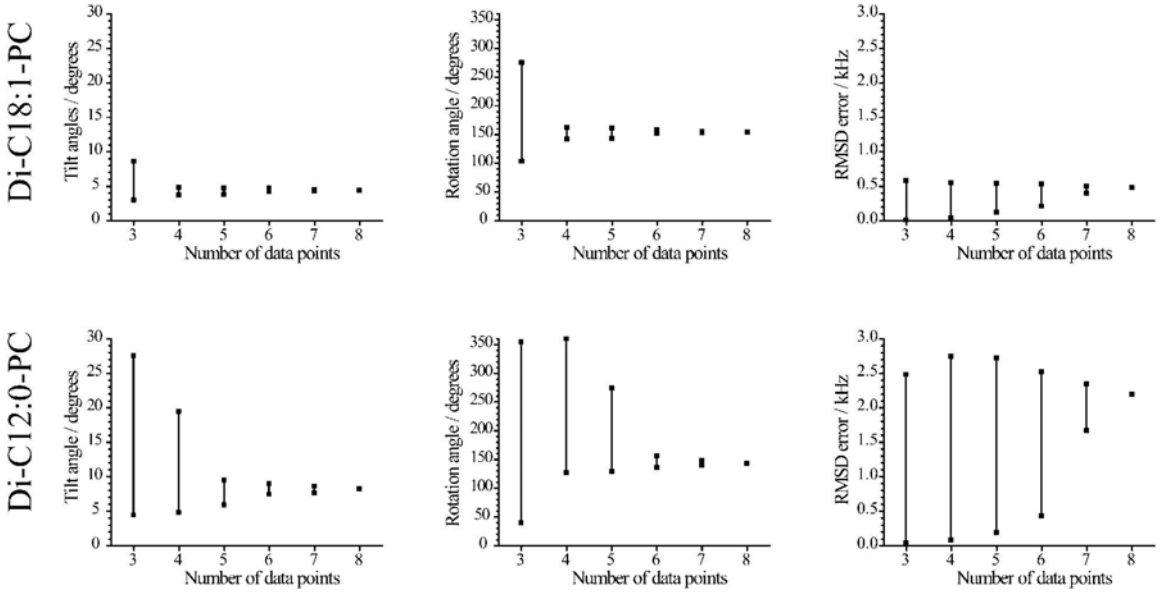

Figure 7. Results when a different number of data points were used in the fits, in di-C18:1-PC (top row) and di-C12:0-PC lipids (bottom row). For a certain number of data points, all different combinations of data points were used to get best-fit results. The squares indicate the maximum and minimum values, and the lines indicate the region where values are found, of each parameter for each number of data points used. In all cases the $\varepsilon_{\|}$-angle was fixed to the optimal value from Table 4.

For di-C18:1-PC, using all eight data points, the fit yields a tilt angle of 4.4º. Using all possible combinations of only three data points yields tilt angles between 3.0º and 8.6º. However, even in this case, 54 of 56 choices of the set of the three data points gave tilt angles between 3.0º and 4.9º (not shown). Using four data points, the calculated tilt is between 3.7º and 4.8º, in reasonably good agreement with the best fit from all eight data points. In all cases the maximum RMSD value is small, near 0.6 kHz. Thus, it would seem that using four labels is sufficient to get a reasonably reliable determination of the tilt angle for WALP23 in di-C18:1-PC.

For di-C12:0-PC, the fit is much less good than for di-C18:1-PC, as seen from the much larger RMSD error. For this system, six data points seem to be required to narrow the range to only ±0.8º from the value of 8.2º that is obtained with all data points. Five data points gives a range of ±1.3º and four or fewer data points gives a very wide range of values.

A similar behavior is found for the rotation angle, where the use of more data points narrows the range of the best-fit values. For di-C18:1-PC already at four data points a narrow range of rotation angles close to 150º is observed, but for di-C12:0-PC six data points are required to obtain such a narrow range.
The RMSD error for a smaller data set can be either larger or smaller than for the full set of eight data points, which is expected if there is a random error in each data point. This means that for some small sets of data, a very small RMSD error may be found fortuitously, even if the calculated tilt and rotation angles are far away from the ‘‘real’’ values. For example, the combination of three data points (residues 5, 17, and 19) giving the most deviating values for di-C18:1-PC, gave a tilt of 8.6º and ρ = 274.5º while showing a very small RMSD value of 0.06 kHz.
As a conclusion, it would seem that, depending on the experimental errors (or on how close the peptide conformation resembles an ideal α-helix), six data points are sufficient to obtain a reliable value of the tilt angle, and four labeled positions is probably a minimum. Results from three or fewer labeled positions should be used only with great caution.

Calculation for the N- and C-terminal parts of the peptide
The result above that four labeled positions can be enough for the analysis, allowed us to test the possibility of a bent or kinked helix. This possibility was investigated by independent calculations of the tilt and rotation angles for the four N-terminal labeled residues (5, 7, 9, 11) and the four C-terminal labels (13, 15, 17, 19). In these calculations the same $\varepsilon_{||}$-angles were used for the different lipid systems as the best-fit values in Table 4. For WALP23 in di-C18:1-PC, di-C14:0-PC, and di-C13:0-PC bilayers the tilt differed <1º between the two parts of the peptide, and the rotation angle differed <10º. This is within the error of the method and indicates that the peptide is very straight and regular in all these lipid systems. In contrast, for WALP23 in di-C12:0-PC, the best-fit value of the tilt was 19.4º for the N-terminal part of the peptide and 7.7º for the C-terminal part. The rotation angles changes from 201º in the N-terminal part to 139º in the C-terminal part. This could be an indication that the peptide forms a kink, or bends when the hydrophobic mismatch is too large. It should be noted, however, that this model gives only a slight decrease in the overall RMSD for WALP23 in di-C12:0-PC, from 2.19 to 1.65 kHz, which is still higher than in the other lipid systems (see Table 4).

Discussion

In this study, we use solid-state NMR on isotopically labeled WALP23 peptides to study the structure and dynamics of transmembrane peptides in a lipid bilayer. First, we will discuss the results from oriented and unoriented samples in di-C14:0-PC. Then we will discuss the effect of hydrophobic mismatch, as investigated by using lipids with different chain length. The results will be compared to those obtained from the shorter WALP19 peptide (23). Finally we will discuss some advantages and disadvantages of different NMR methods to study tilt of transmembrane peptides.

Behavior of WALP23 in di-C14:0-PC
The ^{2}H NMR spectra of the WALP23 peptide in all investigated lipid systems shows a variation of quadrupolar splittings from different labeled alanine positions. For a peptide with a regular α-helical structure this indicates that the peptide is tilted and not rotating fast around the peptide axis. The tilt is quite small (4.4–8.2º) and

comparable to that previously obtained for the shorter but otherwise similar WALP19 (3.6–4.0º; see ref. 23). Oriented samples give rise to twice-as-large quadrupolar splittings when the bilayer normal is oriented parallel to the magnetic field than when oriented perpendicular, indicating that the peptide is rotating fast around the bilayer normal. A similar peptide motion was found previously for WALP19 (23) as well as for other synthetic transmembrane peptides (8,25,26,29-31). These are nontrivial results; for if the peptide axis is not tilted with respect to the bilayer normal, then the two motions, rotation about the bilayer normal and rotation about the helix axis, would be identical.

The rotational motion could be explained by a random diffusion of the peptide in the bilayer, while tilted in a specific preferred direction. The reason for this preferred rotational angle could be a favorable conformation of the large and bulky flanking tryptophan residues, in combination with a favorable interaction with the lipid/water interface, where tryptophans have been proposed to anchor. The best-fit value of the rotation angle in each lipid (Table 4) can be visualized as the direction of tilt of the peptide, telling which residue is pointing up against the bilayer normal in the tilted peptide. In Fig. 2, the rotation angle for WALP23 in unoriented di-C14:0-PC bilayers is indicated with an arrow. In other words, C^{α} of Ala17 is in the plane formed by the bilayer normal and the peptide axis, pointing away from the membrane normal, where the maximum splittings are found. It is likely that some (limited) rotational motion around the peptide axis is present, and that the observed value is an average orientation. The fit is much less sensitive to the parameter ρ than to the tilt angle τ, and a small change does not much influence the fit. It is therefore interesting that the rotation angle is very similar in all lipid systems for WALP23, ~150º ±8º. This is somewhat lower than the rotation angles found forWALP19 in the same lipid systems, ~192º ±20º.

Comparison of oriented and unoriented systems

It is shown here that the GALA experiments can be performed on both oriented and unoriented samples. The same information is obtained, but the use of unoriented samples has a number of practical advantages: 1), it allows a wider application of the method, e.g., to investigate the effects of lipids that are notoriously difficult to orient or to analyze the effects of environmental factors such as salt concentration or pH; 2), it is less time-consuming to prepare samples; 3) using the same sample volume, much more material may be used, allowing us to obtain a better signal/noise ratio or save spectrometer time; and 4), unoriented samples better mimic biological membranes in terms of hydration and lipid packing. In the literature there are several examples where such unoriented systems have been successfully used to investigate structure and dynamics of single-span membrane peptides by solid-state NMR methods (8,25).

The splittings are rather similar in oriented and unoriented samples, especially considering the fact that they are very sensitive to small changes in tilt or $\varepsilon_{\|}$. Indeed, there is only a small change of best-fit tilt value for WALP23 in di-C14:0-PC from 4.5º in oriented samples to 5.5º in non-oriented samples. A possible explanation for the difference is that in the oriented samples the bilayer thickness is larger because the lipids are more ordered. It is also possible that the macroscopic orientation of lipid bilayers on glass plates can make the bilayers less flexible, which could make it more difficult for peptides to tilt. The lower water content in the oriented samples may have a similar effect. It may also be noted that the peptide concentration is lower in the unoriented samples where *P/L* = 1:100 whereas in the oriented samples *P/L* = 1:20. In

total, the changes of splittings are small and the peptide tilt seems not to be much affected by the different conditions between oriented and unoriented samples.

Effects of hydrophobic mismatch

Hydrophobic mismatch is expected to be energetically unfavorable, and therefore there should be some compensating mechanism to minimize it. A too-long peptide could tilt, which would reduce the effective hydrophobic length. The nonzero tilt of WALP19 was found to be close to 4º in oriented samples of di-C12:0-PC, di-C14:0-PC, and di- C18:1-PC (23). In the case of WALP19 it could be that the mismatch is small enough to be compensated by other mechanisms. WALP23 has four more amino acids in the α-helix, increasing its length with 6 Å, so for this peptide a much larger mismatch is expected. As shown in Table 4, the tilt in di-C18:1-PC is still low, ~4.5º, but it increases in the shorter lipids. However, much larger tilt angles would be needed to provide a considerable relief of the mismatch. In a simple model, the effective hydrophobic length is the projection of the peptide length in the membrane, $L_{eff} = L_p \cos\tau$, where L_p is the peptide length, τ is the tilt angle, and L_{eff} should be equal to the lipid bilayer hydrophobic thickness. Let us assume that WALP23 in di-C18:1-PC is matching when the tilt is the 4.4º found in this study. The hydrophobic thickness of di-C18:1-PC is 27 Å (32). This implies that to get matching conditions for WALP23 in di-C12:0-PC, with a hydrophobic thickness of 20 Å (16), the peptide needs to tilt by 42º. The much smaller change from 4.4º to 8.2º observed here would only change L_{eff} from 27.0 Å to 26.8 Å.

The system should proceed to a state of lowest free energy, and apparently a tilt of the peptide will not give the lowest energy, even if it results in a decrease of the mismatch. Either there are other mechanisms to relieve mismatch, or peptide tilt is more unfavorable than mismatch. Indeed, it is quite feasible that there is some energy term that makes tilting unfavorable, such as problems with lipid packing around a tilted peptide. Such packing problems may be less for peptides that form oligomeric structures, such as the M2 transmembrane peptide from *Influenza A* virus, for which rather large tilt angles were observed (29). Packing problems of course could be lipid-specific, and therefore it would be interesting to also investigate tilting of peptides in other lipid systems. The use of unoriented samples will make it possible to study a wide range of different lipids and different environmental conditions.

In principle, besides tilting, the peptides could also change their length by a change of conformation, which would mean to distort the backbone configuration away from an ideal α-helix. Our results show that the peptides do not change their helical pitch: they remain in a very stable α-helical conformation. However, there are some variations in the bond angle ($\varepsilon_{\|}$). The results suggest a tendency of the angle to increase with decreasing mismatch. This was also observed for WALP19 (23) and suggests that there may be very small, but systematic changes in backbone structure with increasing mismatch. Such changes would be extremely small because they could not be observed by Fourier transform infrared spectroscopy (21).

Overall, the results suggest that the WALP peptides form surprisingly regular α-helices without distortions or kinks when there is a moderate extent of mismatch. However, for the shorter lipids the observed increase of the RMSD value may indicate slight local distortions of the backbone at increasing mismatch. The largest variations in quadrupolar splitting in different lipid systems are found at positions 7 and 11. When these positions are excluded from the fitting procedure, almost no difference in best-fit parameters is found in di-18:1-PC lipids, and the whole peptide fits very well

with an ideal α-helical structure. In shorter lipids, these two residues yield increasingly larger quadrupolar splittings that are also increasingly away from the best-fit curve using the other six residues. One explanation would be that the bond angles $\varepsilon_{\|}$ at positions 7 and 11 become distorted in shorter lipids, although leaving the backbone structure mostly intact. Since Ala7 and Ala11 are at the same face of the peptide (see Fig. 2), we may speculate that they could be part of a site of peptide-peptide interactions, and that the occurrence of such interactions may become more likely as the hydrophobic mismatch increases. Such peptide-peptide interactions may reduce the sensitivity of the peptide to mismatch, as was previously proposed for the *Influenza* M2 peptide (29).

Another possible explanation for the large RMSD values in the shortest lipids would be that the peptide changes from a straight to a bent helix. The calculations of tilt for the first and last part of the helix indicated that the peptide is not bent in the longer lipid systems, where the tilt of the first and second part of the helix was within the error of the method. Only in di-C12:0-PC was there a large difference between the N- and C-terminal parts, which could indicate that the peptide is bent or kinked. However, the fit is not very good even when a kink is included in the model, indicating some more distortions are present. A kinked α-helix has recently been observed by solid-state NMR methods in the channel-forming transmembrane domain of virus protein **u** (Vpu) of HIV-1 (33).

Our experiments indicate that mismatch does not result in significant tilting or in clearly observable backbone adaptation, at least in the systems that we used here. Other mechanisms to compensate for hydrophobic mismatch could include stretching or compressing of the lipid acyl chains. However, results from ^{2}H NMR studies on effects of different length WALP peptides on acyl chain order of perdeuterated lipids in unoriented peptide/lipid systems indicated systematic, but only very small mismatch-dependent, changes in bilayer thickness (16). Moreover, in a recent x-ray diffraction study (34), using oriented peptide/lipid bilayers and a lower water content, no change at all was found in bilayer thickness upon incorporation of different length WALP peptides.

Still another possible explanation for the lack of large mismatch-dependent effects is related to the observation that Trp-interfacial anchoring effects are more dominant than hydrophobic mismatch effects for peptides with a hydrophobic Leu-Ala core (15). We speculate that, although Trp may prefer a defined localization at the interface, it can be located within a rather broad interfacial region >10 A° wide (14), at only a relatively small energetic cost, which may be further minimized by allowing reorientation of the Trp χ_1 and χ_2 side-chain angles. If the peptide is too long for the outer limit of this permitted range, mismatch effects like lipid stretching, peptide tilt, or other structural changes could become more pronounced. Thus, larger tilt values might be found in systems with an even larger mismatch than in this study.

Tilt determination of α-helices using different NMR methods

The GALA method to study tilt, rotation, and backbone conformation of transmembrane peptides uses CD_3-labeled peptides studied by ^{2}H NMR. So far, ^{15}N in the peptide backbone amide has been the most commonly used isotopic label for NMR studies of peptides in lipid bilayers. The GALA method can complement ^{15}N NMR experiments.

A practical advantage of the GALA method is that the labeled methyl groups, due to their intrinsic mobility and the presence of three chemically equivalent deuterons in

each side chain, give rise to high intensity signals, which can easily be monitored in a simple one-dimensional NMR experiment. The low sensitivity of ^{2}H is partly compensated by a short relaxation time. On the other hand, ^{15}N is a label that can be incorporated in any peptide, irrespective of the content of alanine residues, also biosynthetically.

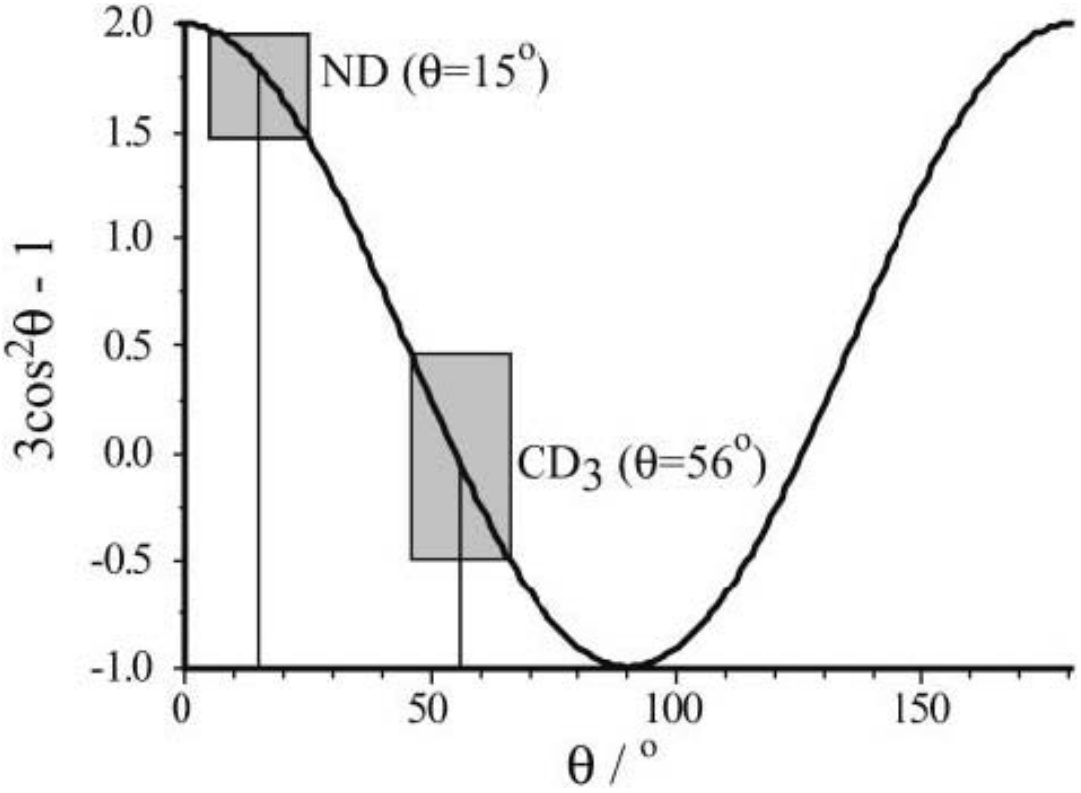

Figure 8. A plot of the function 3 $\cos^2\theta$ –1, illustrating why Ala-CD_3 labels are more sensitive to small tilt values than ^{15}N labels. The boxes represent ±10º in θ and the corresponding changes in the value of 3 $\cos^2\theta$ –1. The slope at 56º is approximately twice as large as at 15º.

The two labels are independent, with the relevant C-CD_3 bond forming an angle to the peptide helix axis of ~58º (this article), whereas the corresponding angle for an NH bond is only ~15º (35). To illustrate the importance of this, consider a peptide in oriented bilayers. When the peptide is tilted, for example, 10º, the angle θ between the N-H or C-CD3 bond vector and the magnetic field will vary around the helix axis. The N-H θ angle will vary between 5º and 25º, and the C–CD_3 θ-angle will vary between 48º and 68º. There is a (3 $\cos^2\theta$ –1) variation of the measured value (quadrupolar splitting for ^{2}H and chemical shift for ^{15}N), and from the graph of this function (Fig. 8) it is clear that the slope is higher close to 58º, whereas at 15º the function changes more slowly. In this respect, CD_3 is a more sensitive probe.

A curve as in Fig. 8 can also be used to explain why the results for the GALA method in oriented bilayers will not be extremely sensitive to the orientation of the glass plates in the magnetic field. If the angle between the bilayer normal and the magnetic field is denoted β, there is a 3 $\cos^2\beta$ –1 dependence of the splittings. Thus, for glass plates oriented with their normal vector at an angle of 0º or 90º to the magnetic field direction, a deviation of the glass plates' orientation with 5º will only lead to a decrease of $\Delta\nu_q$ of 1%.

Although a larger value of $\varepsilon_{\|}$ increases the sensitivity to tilt angles, small values of $\varepsilon_{\|}$, as for NH labels, have the advantage that there is not a large change in quadrupolar splittings or chemical shift between amide labels at different positions around the helix. This means that a single ^{15}N label allows a rough estimate of the tilt of an α-helical peptide (shown for several peptides in 36), which is not the case for alanine-d_3 labels. It must also be noted that two-dimensional methods, where ^{15}N-^{1}H dipolar couplings are measured together with ^{15}N CSA, are able to provide atomic resolution structures of peptides and proteins in lipid bilayers (37,38). The tilt and rotation of peptides and proteins can be accurately determined using PISEMA/PISA wheel, or dipolar wave experiments (35,39-42). In conclusion, our results show that GALA is a useful method to obtain high resolution information on the structure and orientation of peptides in lipid bilayers, with high precision and sensitivity. Hence, the method may allow monitoring of very subtle changes in tilt angle or backbone conformation of transmembrane segments that can be important for functional activity of membrane proteins. The method is complementary to previously used ^{15}N NMR methods.

Appendix

Derivation of an expression for the quadrupolar splitting in terms of tilt, rotation, and bond angles

In the derivation a methyl (CD_3) group will be assumed, but it is equally valid for a carbon-deuterium bond (CD). The same angles defining the peptide orientation and structure as illustrated in Fig. 1 will be used throughout this derivation.

The quadrupolar splitting $\Delta\nu_q$ is given by

$$\Delta\upsilon_q = (3/4)K\left(3\cos^2\theta - 1\right) \tag{A1}$$

where K is a strength constant as defined in Methods and θ is the angle between the C-CD_3 bond and the magnetic field direction.

The bond vector of length r can now be located around the cone shown in Fig. 9 A. The z direction is defined to be along the magnetic field and the x axis is defined so that the center of the cone lies in the xz plane. The center of the cone is defined by the angle τ, the width of the cone by the angle $\varepsilon_{\|}$, and the position of the bond around the cone by the angle δ. (Note that the values of the angles in the figures are chosen for clarity and may not be realistic.) From Fig. 9 A it can be seen that the angle θ is given by

$$\cos\theta = z/r \tag{A2}$$

where z is the projection of the bond vector to the z axis. The next step is to find an expression for z.

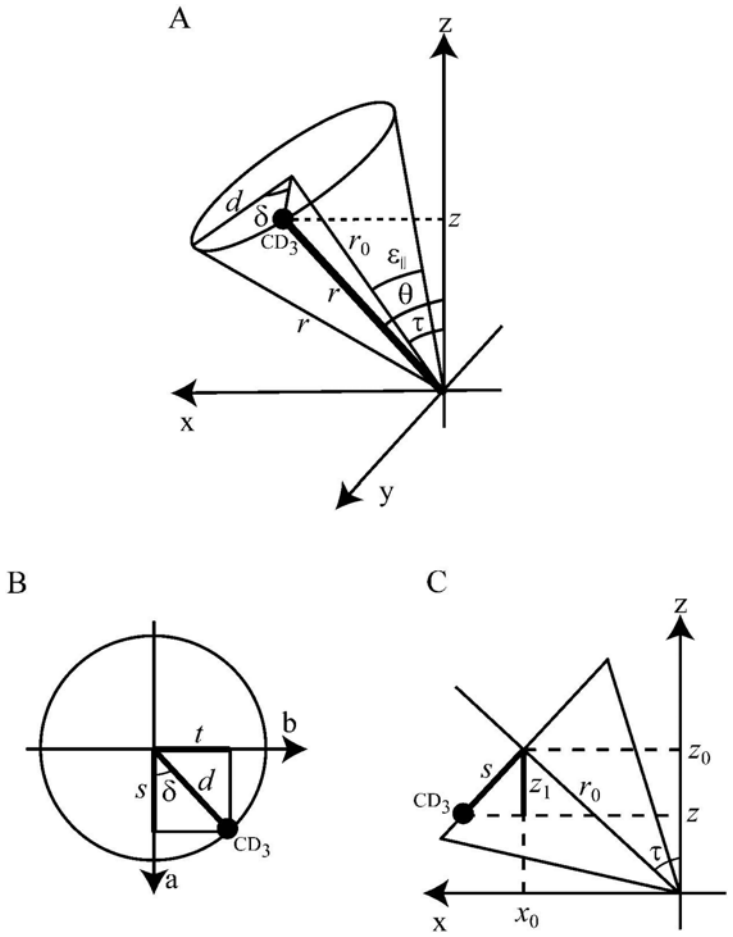

Figure 9. (A) The cone formed by the possible orientations of the C-CD_3 bond vector. (B) The circle where the CD_3 group can be located. (C) The circle in B shown from the side. The angles and distances are described in the text.

First, the CD_3 group can be located on a circle of radius *d* shown in Fig. 9 B. As seen in Fig. 9 B, δ is defined as the anticlockwise angle between the bond and the *a* axis, with the a axis lying in the xz plane. Fig. 9 C gives the projection of the circle in Fig. 9 B to the xz plane. It is clear that

$$z = z_0 - z_1 \tag{A3}$$

where z_0 is the position of the center of the circle. From Fig. 9 C we get

$$z_0 = r_0 \cos\tau \tag{A4}$$

$$z_1 = s \sin\tau \tag{A5}$$

From Fig. 9 B we get

$$s = d \cos\delta \tag{A6}$$

And from Fig. 9 A we see

$$r_0 = r \cos\varepsilon_{\|} \tag{A7}$$

$$d = r\sin\varepsilon_{\|} \tag{A8}$$

We can now combine Eqs. A4 and A7 to get

$$z_0 = r\cos\varepsilon_{\|}\cos\tau \tag{A9}$$

and from Eqs. A5, A6, and A8 we get

$$z_1 = r\sin\varepsilon_{\|}\cos\delta\sin\tau \tag{A10}$$

Combining Eqs. A2, A3, A9, and A10 we get the expression

$$\cos\theta = z/r = (z_0 - z_1)/r = \cos\varepsilon_{\|}\cos\tau - \sin\varepsilon_{\|}\cos\delta\sin\tau \tag{A11}$$

which gives

$$\cos^2\theta = \cos^2\varepsilon_{\|}(\cos\tau - \sin\tau\cos\delta\tan\varepsilon_{\|})^2 \tag{A12}$$

The final expression, Eq. 1, is now obtained by combining Eqs. A1 and A12:

$$\Delta\upsilon_q = (3/4)K\left(3\cos^2\varepsilon_{\|}(\cos\tau - \sin\tau\cos\delta\tan\varepsilon_{\|})^2 - 1\right) \tag{A13}$$

References

1. Killian, J. A. (1998) *Biochim Biophys Acta* 1376(3), 401-415
2. Caputo, G. A., and London, E. (2003) *Biochemistry* 42(11), 3275-3285
3. Harzer, U., and Bechinger, B. (2000) *Biochemistry* 39(43), 13106-13114
4. Huschilt, J. C., Millman, B. M., and Davis, J. H. (1989) *Biochim Biophys Acta* 979(1), 139-141
5. Killian, J. A., Salemink, I., de Planque, M. R., Lindblom, G., Koeppe, R. E., 2nd, and Greathouse, D. V. (1996) *Biochemistry* 35(3), 1037-1045
6. Liu, F., Lewis, R. N., Hodges, R. S., and McElhaney, R. N. (2001) *Biochemistry* 40(3), 760-768
7. Mall, S., Broadbridge, R., Sharma, R. P., East, J. M., and Lee, A. G. (2001) *Biochemistry* 40(41), 12379-12386
8. Sharpe, S., Barber, K. R., Grant, C. W., Goodyear, D., and Morrow, M. R. (2002) *Biophys J* 83(1), 345-358
9. Subczynski, W. K., Pasenkiewicz-Gierula, M., McElhaney, R. N., Hyde, J. S., and Kusumi, A. (2003) *Biochemistry* 42(13), 3939-3948
10. de Planque, M. R., and Killian, J. A. (2003) *Molecular membrane biology* 20(4), 271-284
11. Arkin, I. T., and Brunger, A. T. (1998) *Biochim Biophys Acta* 1429(1), 113-128
12. Landolt-Marticorena, C., Williams, K. A., Deber, C. M., and Reithmeier, R. A. (1993) *J Mol Biol* 229(3), 602-608
13. Persson, S., Killian, J. A., and Lindblom, G. (1998) *Biophys J* 75(3), 1365-1371
14. Yau, W. M., Wimley, W. C., Gawrisch, K., and White, S. H. (1998) *Biochemistry* 37(42), 14713-14718
15. de Planque, M. R., Bonev, B. B., Demmers, J. A., Greathouse, D. V., Koeppe, R. E., 2nd, Separovic, F., Watts, A., and Killian, J. A. (2003) *Biochemistry* 42(18), 5341-5348

16. de Planque, M. R., Greathouse, D. V., Koeppe, R. E., 2nd, Schafer, H., Marsh, D., and Killian, J. A. (1998) *Biochemistry* 37(26), 9333-9345
17. Demmers, J. A., Haverkamp, J., Heck, A. J., Koeppe, R. E., 2nd, and Killian, J. A. (2000) *Proc Natl Acad Sci U S A* 97(7), 3189-3194
18. Morein, S., Koeppe, I. R., Lindblom, G., de Kruijff, B., and Killian, J. A. (2000) *Biophys J* 78(5), 2475-2485
19. Rinia, H. A., Kik, R. A., Demel, R. A., Snel, M. M., Killian, J. A., van Der Eerden, J. P., and de Kruijff, B. (2000) *Biochemistry* 39(19), 5852-5858
20. Strandberg, E., Morein, S., Rijkers, D. T., Liskamp, R. M., van der Wel, P. C., and Killian, J. A. (2002) *Biochemistry* 41(23), 7190-7198
21. de Planque, M. R., Goormaghtigh, E., Greathouse, D. V., Koeppe, R. E., 2nd, Kruijtzer, J. A., Liskamp, R. M., de Kruijff, B., and Killian, J. A. (2001) *Biochemistry* 40(16), 5000-5010
22. de Planque, M. R., Kruijtzer, J. A., Liskamp, R. M., Marsh, D., Greathouse, D. V., Koeppe, R. E., 2nd, de Kruijff, B., and Killian, J. A. (1999) *J Biol Chem* 274(30), 20839-20846
23. van der Wel, P. C., Strandberg, E., Killian, J. A., and Koeppe, R. E., 2nd. (2002) *Biophys J* 83(3), 1479-1488
24. Ten Kortenaar, P. B. W., van Dijk, B. G., Peters, J. M., Raaben, B. J., Adams, P. J. H. M., and Tesser, G. I. (1986) *Int. J. Pept. Protein Res.* 27, 398–400.
25. Jones, D. H., Barber, K. R., VanDerLoo, E. W., and Grant, C. W. (1998) *Biochemistry* 37(47), 16780-16787
26. Whiles, J. A., Glover, K. J., Vold, R. R., and Komives, E. A. (2002) *J Magn Reson* 158(1-2), 149-156
27. Davis, J. H. (1983) *Biochim Biophys Acta* 737(1), 117-171
28. Killian, J. A., Taylor, M. J., and Koeppe, R. E., 2nd. (1992) *Biochemistry* 31(46), 11283-11290
29. Kovacs, F. A., Denny, J. K., Song, Z., Quine, J. R., and Cross, T. A. (2000) *J Mol Biol* 295(1), 117-125
30. Morrow, M. R., and Grant, C. W. (2000) *Biophys J* 79(4), 2024-2032
31. Sharpe, S., Grant, C. W., Barber, K. R., Giusti, J., and Morrow, M. R. (2001) *Biophys J* 81(6), 3231-3239
32. Nagle, J. F., and Tristram-Nagle, S. (2000) *Curr Opin Struct Biol* 10(4), 474-480
33. Park, S. H., Mrse, A. A., Nevzorov, A. A., Mesleh, M. F., Oblatt-Montal, M., Montal, M., and Opella, S. J. (2003) *J Mol Biol* 333(2), 409-424
34. Weiss, T. M., van der Wel, P. C., Killian, J. A., Koeppe, R. E., 2nd, and Huang, H. W. (2003) *Biophys J* 84(1), 379-385
35. Mesleh, M. F., Lee, S., Veglia, G., Thiriot, D. S., Marassi, F. M., and Opella, S. J. (2003) *J Am Chem Soc* 125(29), 8928-8935
36. Bechinger, B., Gierasch, L. M., Montal, M., Zasloff, M., and Opella, S. J. (1996) *Solid State Nucl Magn Reson* 7(3), 185-191
37. Ketchem, R. R., Lee, K. C., Huo, S., and Cross, T. A. (1996) *J Biomol NMR* 8(1), 1-14
38. Zeri, A. C., Mesleh, M. F., Nevzorov, A. A., and Opella, S. J. (2003) *Proc Natl Acad Sci U S A* 100(11), 6458-6463
39. Marassi, F. M., and Opella, S. J. (2000) *J Magn Reson* 144(1), 150-155
40. Tian, F., Song, Z., and Cross, T. A. (1998) *J Magn Reson* 135(1), 227-231
41. Wang, J., Denny, J., Tian, C., Kim, S., Mo, Y., Kovacs, F., Song, Z., Nishimura, K., Gan, Z., Fu, R., Quine, J. R., and Cross, T. A. (2000) *J Magn Reson* 144(1), 162-167
42. Wu, C. H., Ramamoorthy, A., and Opella, S. J. (1994) *Journal of Magnetic Resonance, Series A* 109(2), 270-272

Chapter 3

Influence of Flanking Residues on Tilt and Rotation Angles of Transmembrane Peptides in Lipid Bilayers. A Solid State ^{2}H NMR Sudy

Taken from

Biochemistry (2005) 44, 1004-1012

Abbreviations
NMR, nuclear magnetic resonance; TFA, Trifluoroacetic acid; TFE, 2,2,2-trifluoroethanol. HEPES, N-(2-Hydroxyethyl)piperazine-N'-(2-ethanesulfonic acid); tBu, tertButyl; d_4-Ala, deuterated L-alanine-d_4; Fmoc, 9-fluorenylmethyloxycarbonyl; di-C12:0-PC, 1,2-dilauroyl-*sn*-glycero-3-phosphocholine; di-C13:0-PC, 1,2-ditridecanoyl-*sn*-glycero-3-phosphocholine; di-C14:0-PC, 1,2-dimyristoyl-*sn*-glycero-3-phosphocholine; di-C18:1-PC, 1,2-dioleoyl-*sn*-glycero-3-phosphocholine.

Abstract
To gain insight into the parameters that determine the arrangement of proteins in membranes, ^{2}H NMR experiments were performed to analyze tilt and rotation angles of membrane-spanning α-helical model peptides upon incorporation in diacylphosphatidylcholine bilayers with varying thickness. The peptides consisted of the sequence acetyl-$GW_2(LA)_8LW_2A$-NH_2 (WALP23) and analogs thereof, in which the interfacial Trp residues were replaced by Lys (KALP23) and/or the hydrophobic sequence was replaced by Leu (WLP23 and KLP23). The peptides were synthesized with a single deuterium labeled alanine at four different positions along the hydrophobic segment. For all peptides a small but systematic increase in tilt angle was observed upon decreasing the bilayer thickness. However, significantly larger tilt angles were obtained for the Lys-flanked KALP23 than for the Trp-flanked WALP23, suggesting that interfacial anchoring interactions of Trp may inhibit tilting. Increasing the hydrophobicity resulted in an increase in tilt angle for the Trp-flanked analog only. For all peptides the maximum tilt angle obtained was remarkably small (less than 12^o), suggesting that further tilting is inhibited, most likely due to unfavorable packing of lipids around a tilted helix. The results furthermore showed that the direction of tilt is determined almost exclusively by the flanking residues: Trp- and Lys-flanked peptides were found to have very different rotation angles, which were neither influenced significantly by hydrophobicity of the peptides nor by the extent of hydrophobic mismatch. Finally, very small changes in the side chain angles of the deuterated alanine probes were observed in Trp-flanked peptides, suggesting that these peptides may decrease their hydrophobic length to help them adapt to thin membranes.

Introduction
Membrane proteins carry out many essential functions in cells. In the specific case of integral proteins, the membrane spanning parts of these molecules are in direct contact with acyl chains and head groups of the surrounding lipids. Consequently, the lipid environment can modulate structure and dynamics, hence activity of membrane proteins (1). For example, changes in hydrophobic thickness of a lipid bilayer can affect the structure of an integral membrane protein by causing a hydrophobic mismatch between the bilayer thickness and the length of the membrane spanning parts of that protein (reviewed in (2-4) Understanding the molecular basis of how lipids influence membrane proteins requires precise information on structural properties of transmembrane segments of proteins and knowledge of how these properties are sensitive to protein and lipid composition. It is most suitable to perform such experiments on model membranes of synthetic lipids and transmembrane peptides, since both the composition of lipids and peptides can be systematically varied. Model membranes, made of phosphatidylcholine derivatives (PC) and model

transmembrane peptides, have already been extensively studied to investigate the effects of hydrophobic mismatch on lipid-peptide interactions (5-15) and reviewed in (2-4). In particular, the so-called WALP peptides have been used as tools to monitor the consequence of hydrophobic mismatch for the organization of peptides and lipids in model membranes (reviewed in 8). WALP peptides are a family of α-helical transmembrane model peptides made of a central leucine alanine stretch that is flanked by two tryptophan residues on each side.

Recently, a technique based on solid-state ^{2}H NMR using deuteriated alanines has been developed to analyze structural properties of transmembrane peptides in model membranes (12,13,15,16). This method, called geometric analysis of labeled alanines (GALA) allows for very accurate determination of tilt angles of WALP peptides in either oriented or non-oriented PC-bilayers (13,15). In addition, the direction in which the peptides are tilted, as determined by their rotation angles, can be analyzed with this method. Previous results (13) showed that when the hydrophobic length of WALP peptides exceeds the bilayer thickness (i.e. under conditions of positive hydrophobic mismatch) the peptides are more tilted in the thinnest bilayers with a preferential rotation angle that is independent of mismatch. However, the tilt angles were much too small to compensate for hydrophobic mismatch suggesting that tilting is also affected by other parameters than the hydrophobic thickness of the membrane. One such parameter is likely to be the amino acid composition of the peptides. For instance, aromatic residues are thought to have a preference for the lipid-water interface in PC-bilayers (2,17,18) and therefore the flanking tryptophan residues in WALP peptides could influence the way that these peptides are positioned in the membrane. In addition, other features such as hydrophobicity of the peptide might play a part in this process. To gain insight into the role of amino acid composition in determining the arrangement of peptides in membranes, we performed in the present study ^{2}H NMR experiments on transmembrane model peptides of different composition in unoriented PC-bilayers, using a similar approach as in Strandberg et al. (13). All experiments were conducted in PC-bilayers with varying acyl-chain length in their liquid-crystalline phase. Comparison of the mismatch dependent behavior of Trp- and Lys-flanked transmembrane peptides showed that besides hydrophobic mismatch, flanking residues play an important role in determining both the tilt and rotation angles of the peptides. In contrast, hydrophobicity of the transmembrane part seemed to have at most a small effect on the arrangement of the different peptides in the lipid bilayer. Finally, small changes in the side chain angles of the deuterated alanine probes in the helix suggest that, in contrast to their Lys-flanked counterparts, Trp-flanked peptides may slightly decrease their hydrophobic length to help them adapt to the thinnest lipid bilayers.

Materials and Methods

Materials

WALP23, KALP23, WLP23 and KLP23 (for amino acid sequence see table 1) were synthesized using Fmoc/tBu solid phase peptide synthesis as described elsewhere for related KALP peptides (19). Deuterated L-alanine-d_4 was obtained from Sigma Aldrich and 9-fluorenylmethyloxycarbonyl (Fmoc) was used to protect its amino functionality as described by Ten Kortenaar et al. (20) before being used in the synthesis. The peptides were isotopically labeled with one deuterium labeled alanine residue at different positions in the transmembrane domain. 1,2-dilauroyl-*sn*-glycero-

3-phosphocholine (di-C12:0-PC), 1,2-ditridecanoyl-*sn*-glycero-3-phospholcholine (di-C13:0-PC), 1,2-dimyristoyl-*sn*-glycero-3-phosphocholine (di-C14:0-PC) and 1,2-dioleoyl-*sn*-glycero-3-phosphocholine (di-C18:1-PC) were purchased from Avanti Polar Lipids Inc. (Alabaster, AL) and used without further purification. Trifluoroacetic acid (TFA) and 2,2,2-trifluoroethanol (TFE) were obtained from Merck (Darmstadt, Germany). Deuterium depleted water was obtained from Cambridge Isotope Laboratories, Inc. All other chemicals were of analytical grade. Water was deionized and filtered with a Milli-Q Water purification system from Millipore (Bedford, MA, USA).

Table 1. Amino acid sequences of the peptides used.

Peptide	Design
Ac-WALP23-d_4-Ala-NH_2	Acetyl-GWWL**A**L**A**LALAL**A**L**A**LALALWWA-NH_2[a]
Ac-KALP23-d_4-Ala-NH_2	Acetyl-GKKL**A**L**A**LALAL**A**L**A**LALALKKA-NH_2[a]
Ac-WLP23-d_4-Ala-NH_2	Acetyl-GWWLLLLLLL**LLLL**LLLLLLWWA-NH_2[b]
Ac-KLP23-d_4-Ala-NH_2	Acetyl-GKKLLLLLLL**LLLL**LLLLLLKKA-NH_2

[a] Underlined letters indicated in bold are positions where the peptides have been labeled with d_4-Ala.

[b] Underlined bold characters indicate the residues that have been replaced by d_4-Ala for single labeling. If not deuterium labeled, leucine residues occupied those positions.

Methods

NMR sample preparation

Stock solutions were prepared of ca. 10 mM phospholipid in chloroform and the exact concentrations of the phospholipid stocks were determined by a phosphorous assay (21). For each sample 1 μmol of peptide was used, which was dissolved in 1 ml TFE and dried to a film in a rotavapor twice in order to remove residual traces of TFA . Subsequently, the peptide film was dissolved in 1 ml TFE and added to a lipid solution containing 100 μmol of phospholipid to achieve a peptide to lipid molar ratio of 1:100. The mixture was vortexed and dried to a film in a rotavapor. Traces of solvent in samples were further evaporated overnight under vacuum (ca. 1.10^{-2} bar).

The lipid-peptide films were hydrated in either 100 μl of deuterium-depleted water for WALP23 samples or deuterium-depleted buffer for KALP23 samples (25 mM HEPES, 100 mM NaCl, pH 7.4) and the suspension was transferred to 7 mm diameter glass tubes. Control experiments with KALP23 samples were performed with and without buffer to show that the buffer does not affect the ^{2}H NMR signal (data not shown). The peptide/lipid suspensions did not affect the pH of either the buffer or the water that was used for hydration. The tubes were sealed under a N_2 atmosphere with a silicon stopper and epoxy glue. Samples were freeze-thawed at least 10 times to promote sample homogeneity.

NMR measurements

NMR experiments were carried out on a Bruker Avance 500 MHz NMR spectrometer. Unless stated otherwise, measurements were performed at 40ºC. Samples were allowed to equilibrate at this temperature for at least 10 minutes before measurements. ^{31}P NMR experiments were performed as described (13) on all samples used. In all cases the spectra were similar to those reported previously for WALP/DMPC samples (9), confirming a bilayer organization of the lipids (data not shown).

^{2}H NMR experiments were performed at 76.78 MHz using a quadrupolar echo sequence as described previously (13).

Calculations

Quadrupolar splittings from the labeled positions were measured from ^{2}H NMR spectra. As in previous work (15), the splitting of the backbone deuteron could not be observed and the ^{2}H NMR signals were assigned to the deuterons of the alanine side-chain methyl group. The data were fitted to a model α-helix, similar as in previous studies (12,13,15,16). In particular, data were fitted to the equation

$$\Delta\nu_q = ½ \{(3/4)K(3\cos^2\varepsilon_{\|} (\cos\tau - \sin\tau \cos\delta \tan\varepsilon_{\|})^2 - 1)\} \quad (1)$$

$\Delta\nu_q$ is the quadrupolar splitting as measured in unoriented samples. K is a constant with a frequency dimension. The angles τ, $\varepsilon_{\|}$ and δ depend on the peptide geometry and orientation (Figure 1). The tilt angle denoted τ is defined as the angle between the peptide helical axis and the bilayer normal and $\varepsilon_{\|}$ is the angle between the peptide helix axis and the C^{α}-$C^{\beta}D_3$ bond vector (Figure 1 A). δ is the rotation angle of the labeled bond vector around the helical axis with respect to the direction of the tilt (Figure 1 B). As depicted in Figure 1 B, three angles are contributing to δ:

$$\delta = \rho + \varepsilon_{\perp} + \varphi \quad (2)$$

where ρ is the rotation around the helical axis of the C^{α} of Gly1 with respect to the direction of the tilt, $\varepsilon_{\perp}$ is the angle of the bond vector C^{α}-$C^{\beta}D_3$ with respect to a vector from C^{α} to the peptide axis. φ is the pitch (or rotation) angle between both C^{α} of the reference Gly1 and of the labeled residue in the peptide. For a regular helix

$$\varphi = -(n\text{-}1)\psi \quad (3)$$

where n is the residue number and ψ is the pitch angle between two neighboring residues. In an ideal α–helix ψ = 100º. The value of $\varepsilon_{\perp}$, which has been estimated from molecular models using Insight II database was kept constant at -43.3º for all calculations (15). τ and ρ were used as the fitting parameters in the calculations and $\varepsilon_{\|}$ was allowed to vary in a range between 51° and 64° based on modeling of typical transmembrane α-helical structures (see below). The constant K is defined as

$$K = (e^2qQ/h)S \quad (4)$$

where e^2qQ/h is the quadrupolar coupling constant and S is an order parameter that accounts for molecular motion. In this study a K value of 49 kHz was used, as in a previous study (15). This corresponds to S = 0.875, which was obtained from the splittings in dry powder samples of the peptides. The splittings were similar for WALP23 and KALP23 at different label positions (data not shown).

Values for τ, ρ and $\varepsilon_{\|}$ were calculated to minimize the error function

$$\text{Error} = \Sigma_n [\Delta\nu_{q,n}^{exp} - \Delta\nu_{q,n}^{calc}(\tau, \rho, \varepsilon_{\|})]^2 \quad (5)$$

where the sum is over all labeled positions denoted by the index n in analogy to the n-value for φ (of equation 3). Angles were varied in steps of 0.1º in the range 0-45º and 51-64° for τ and $\varepsilon_{\|}$ (see modeling below), respectively. ρ was varied in the range 0-360º in steps of 1°. The error values for the best fits are presented as RMSD, root mean square deviations. This is defined here as RMSD=(Error/number of data points)$^{1/2}$. An in-house computer program written in Python 2.3 was designed to select the best fit values of τ, ρ and $\varepsilon_{\|}$ corresponding to the lowest RMSD.

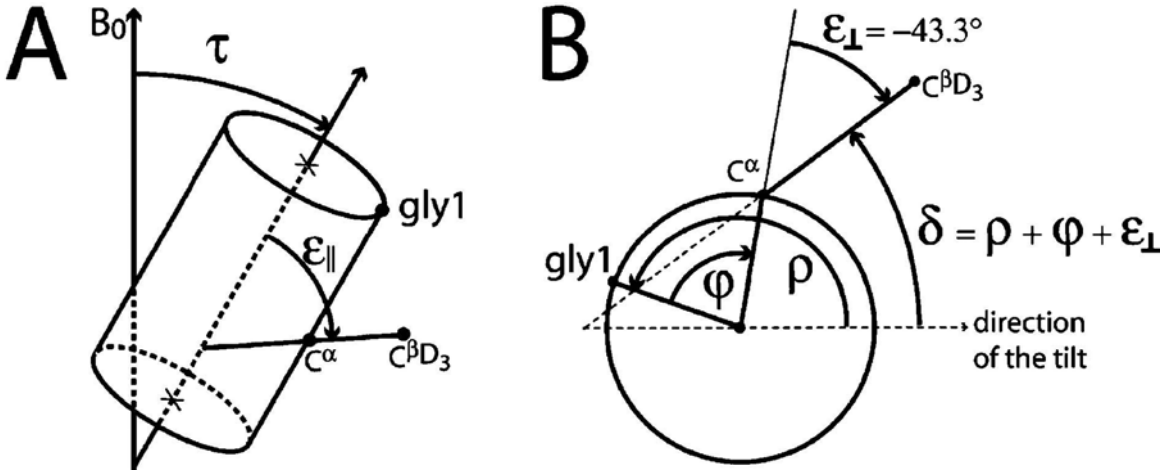

Figure 1. Definition of angles used in the calculations. (A) The tilt angle τ between the peptide axis and the bilayer normal, which is assumed to be along the magnetic field direction. The bond angle between the C-CD_3 bond and the peptide axis is denoted by $\varepsilon_{\|}$. (B) The rotation angle giving the orientation of the C-CD_3 bond is indicated as δ. The angle δ is determined by three contributions that are ρ, φ and $\varepsilon_{\perp}$. ρ is the rotation of the whole peptide, and it is defined as the anti-clockwise rotation angle of C^{α} of Gly1, compared to the direction of the tilt (reference position). φ is the angle by which another amino acid residue is rotated around the peptide axis with respect to Gly1. $\varepsilon_{\perp}$ is the angle of the C^{α}-CD_3 bond projected onto a plane perpendicular to the helical axis with respect to a vector (or line) between the peptide axis and the C^{α}. (Angles in the figure are chosen arbitrarily for clarity)

Error estimates in fitting

The maximum deviation for the best fit was evaluated by implementing the error of measurement in the calculations. This error is estimated to be 0.5 kHz based on duplicate measurements or duplicate samples. Calculations were performed with data set combinations of the average values of WALP23 for eight labeled positions in di-12:0-PC from previous work (13) ± the error. The data from the four labeled positions in our work were similar to those of the previous study. In that way for each peptide three experimental data were assigned according to:

$$\Delta\nu_{q,\,n} = \Delta\nu_{q,\,n,\,experimental} + m*0.5 \qquad (6)$$

where n is the residue number, m can be either –1, 0 or +1 for an error of –0.5, 0, and 0.5 kHz, respectively. In that way, 3^n data sets were fitted to determine the maximal deviation inherent to this method. The maximal deviations thus calculated were ± 0.4°, ± 3° and ± 0.3° for the tilt angle τ, the rotation angle ρ and $\varepsilon_{\|}$, respectively.

Analysis of the relationship between $\varepsilon_{//}$-values and hydrophobic length of WALP23 based on molecular modeling

To determine a realistic range of $\varepsilon_{||}$-values for calculation on a transmembrane peptide model, WALP23 has been modeled based on typical parameters of crystal structures of transmembrane helices (22). The modeling was performed in DeepView/Swiss-PdbViewer, generating Pdb-structures by varying the ϕ- and ψ-Ramachandran parameters. In order to encompass the values of the so-called membrane coils, the α-helical parameters were allowed to vary by steps of 0.5° around the average values of $-64.5° \pm 8.5°$ and $-41° \pm 9.5°$ for ϕ and ψ, respectively. $\varepsilon_{||}$-values of all the generated structures were calculated using a program written in Python 2.3 (kindly provided by Aalt-Jan van Dijk). The range of $\varepsilon_{||}$-values was calculated to be between 51° and 64°. The distance between both C^{α} of the outer leucines of all these structures was monitored under DeepView/Swiss-PdbViewer. $\varepsilon_{||}$-values were plotted versus peptide lengths of corresponding structures to determine the relationship between both parameters.

Results

Influence of flanking residues on tilt and rotation angles

WALP23 and KALP23 were labeled with a single d_4-Ala at 4 different positions as indicated in Table 1 for each peptide. The choice of labeling position was such to have a homogeneous distribution around the helical wheel (Figure 2A).

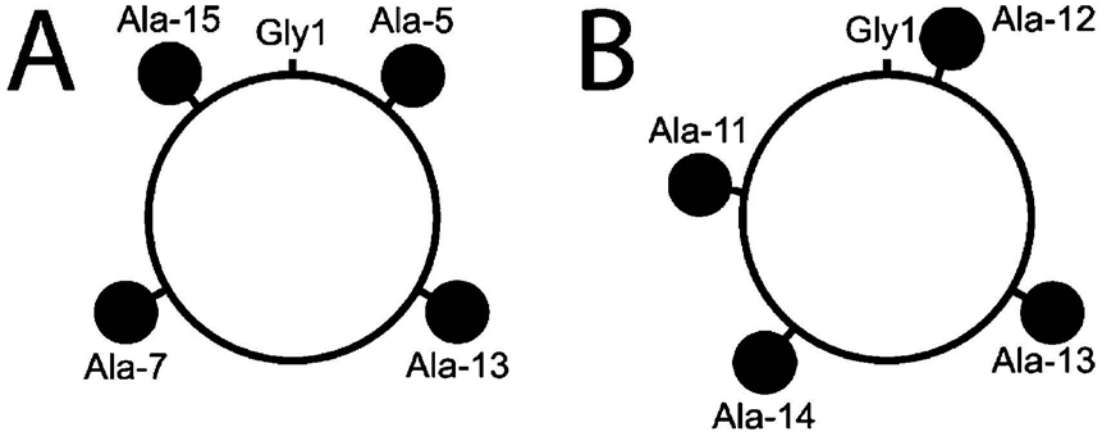

Figure 2. Top view from N-terminus of helical wheel showing the d_4-Ala labeling positions in WALP23 and KALP23 (A) and in WLP23 and KLP23 (B) as indicated by circles.

Figure 3 shows ^2H NMR spectra of the four different WALP23 and KALP23 peptides in unoriented samples of di-12:0-PC. For both types of peptides defined quadrupolar splittings can be observed, the magnitude of which vary with the position of the label. Also in di-13:0-PC, di-14:0-PC and di-18:1-PC bilayers a label-position dependent variation of quadrupolar splittings was observed, as quantified in Table 2. If one assumes that the peptides adopt a regular α-helical structure then the observation of a position dependent variation of $\Delta\nu_q$ implies that both the WALP23 and KALP23 peptides are tilted and that they do not rotate fast around their own axis because otherwise all values of $\Delta\nu_q$ would have been similar. Measurements on oriented samples for the four types of peptides showed that instead the peptides undergo fast reorientation about the bilayer normal, in agreement with earlier studies on these and similar peptides (12,13,15).

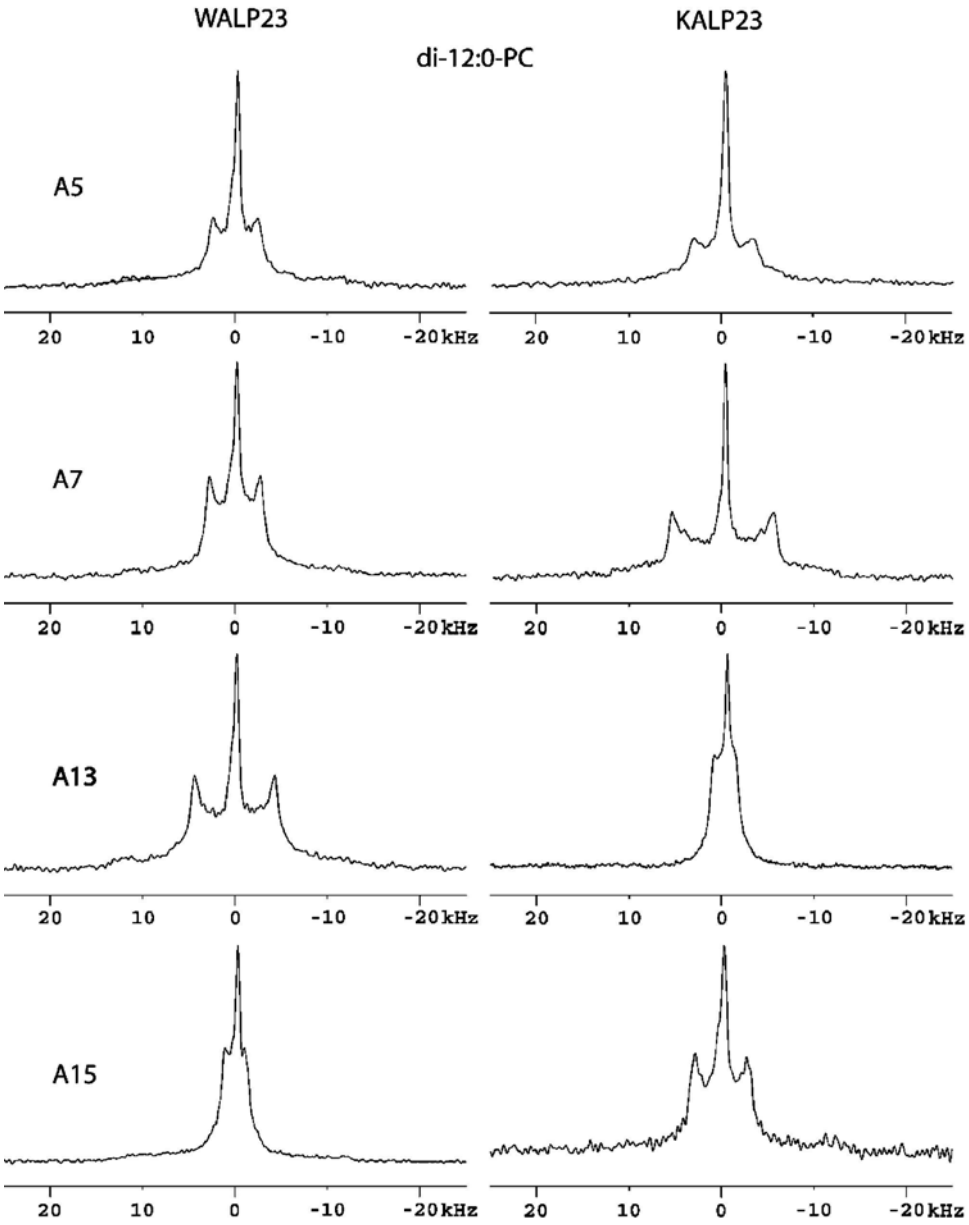

Figure 3. ^{2}H NMR spectra for labeled alanines at position 5, 7, 13 and 15 in WALP23 (left panel) and in KALP23 (right panel) incorporated in bilayers of di-12:0-PC at a peptide to lipid molar ratio of 1/100. The labels on the left indicate the position of the d_4-labeled alanine along the peptide sequence. The isotropic peak in the middle of the spectra is assigned to residual deuterium in H_2O.

Table 2 shows that for almost all labeled positions systematic changes in quadrupolar splitting occur, whereby the quadrupolar splitting decreases with increasing bilayer thickness from di-12:0-PC to di-18:1-PC. From the quadrupolar splittings obtained for the different labeled positions, tilt and rotation angles were calculated based on an α-helical geometry of the peptides and on a geometric analysis of labeled alanine (GALA) (13). The results are shown in Table 3. When the acyl chain length is increased, the calculated tilt angle of both peptides decreases, suggesting that the changes in tilt angle are a response to hydrophobic mismatch. For WALP23 the tilt angle varies from 8.2° to 4.4° with increasing hydrophobic thickness of the membrane and the tilt angle of KALP23 changes from 11.2° to 4.8°. Although the calculated tilt

angles are quite small, KALP23 tilts significantly more than WALP23 in the thinner membranes.

Table 2. Measured ^{2}H NMR splittings of d_4-Ala labeled WALP23 (A) and KALP23 (B) peptides in unoriented PC-bilayers in kHz.

A		Labeled residue			
Phospholipids	Peptide	5	7	13	15
di-12:0-PC	WALP23[a]	4.75	5.5	8.65	2.05
di-13:0-PC	WALP23[a]	5.3	3.5	8.7	1.65
di-14:0-PC	WALP23[a]	4.7	0.5[b]	7.75	0.5[b]
di-18:1-PC	WALP23[a]	4.7	0.35[b]	6.7	0.5[b]
B					
di-12:0-PC	KALP23	6.6	11.4	1.9	5.6
di-13:0-PC	KALP23	4.45	10.3	1.3	4.6
di-14:0-PC	KALP23	3	9.7	0[b]	3.9
di-18:1-PC	KALP23	0.2	7.9	1.9	3.1

[a] Data as in ref. 13.
[b] Splittings that could not be resolved and for which an estimated value is given.

In contrast to the tilt angles, the rotation angles of both WALP23 and KALP23 are relatively independent of the type of phospholipid bilayer (Table 3). The rotation of Gly1 in WALP23 around the helical axis has an angle between 134° and 155° with respect to the direction of the tilt, whereas the range of the rotation angles of KALP23 lies between 273° and 286°. The rotation angles are defined by the direction of the tilt as is depicted in Figure 4. This figure shows that WALP23 and KALP23 are tilted in a completely different direction when compared to each other, suggesting a strong influence of the flanking residues in orienting the peptides in membranes.

Table 3. Fit results using data from the four labeled positions summarized in Table 2 for WALP23 (A) and KALP23 (B)

A					
Phospholipids	Peptide	Tilt angle	Rotation	CD_3 angle	RMSD
di-12:0-PC	WALP23	8.1	134	56.5	2.2
di-13:0-PC	WALP23	7.5	139	57.4	1.3
di-14:0-PC	WALP23	5.2	155	58.5	0.3
di-18:1-PC	WALP23	4.8	146	57.9	0.13
B					
Phospholipids	Peptide	Tilt angle	Rotation	CD_3 angle	RMSD
di-12:0-PC	KALP23	11.2	286	58.0	0.2
di-13:0-PC	KALP23	9	286	58.0	0.5
di-14:0-PC	KALP23	7.6	281	58.3	0.8
di-18:1-PC	KALP23	4.8	273	58.8	0.9

Table 3 also shows the values used for the side chain angles of the deuterated alanine ($\varepsilon_{||}$) to obtain the best fit. Values for WALP23 seem to increase slightly with increasing bilayer thickness for di-12:0-PC, di-13:0-PC and di-14:0-PC, while for KALP23 such dependence is less evident. This may suggest small adaptations of backbone structure for WALP peptides under conditions of positive mismatch.
Root mean square deviation (RMSD) values are also summarized in Table 3 as indication of quality of the fits. RMSD-values of WALP23 increase with thinner bilayers as observed previously (13). In the case of KALP23, RMSD-values are rather small for all bilayer thicknesses indicating a good fit.

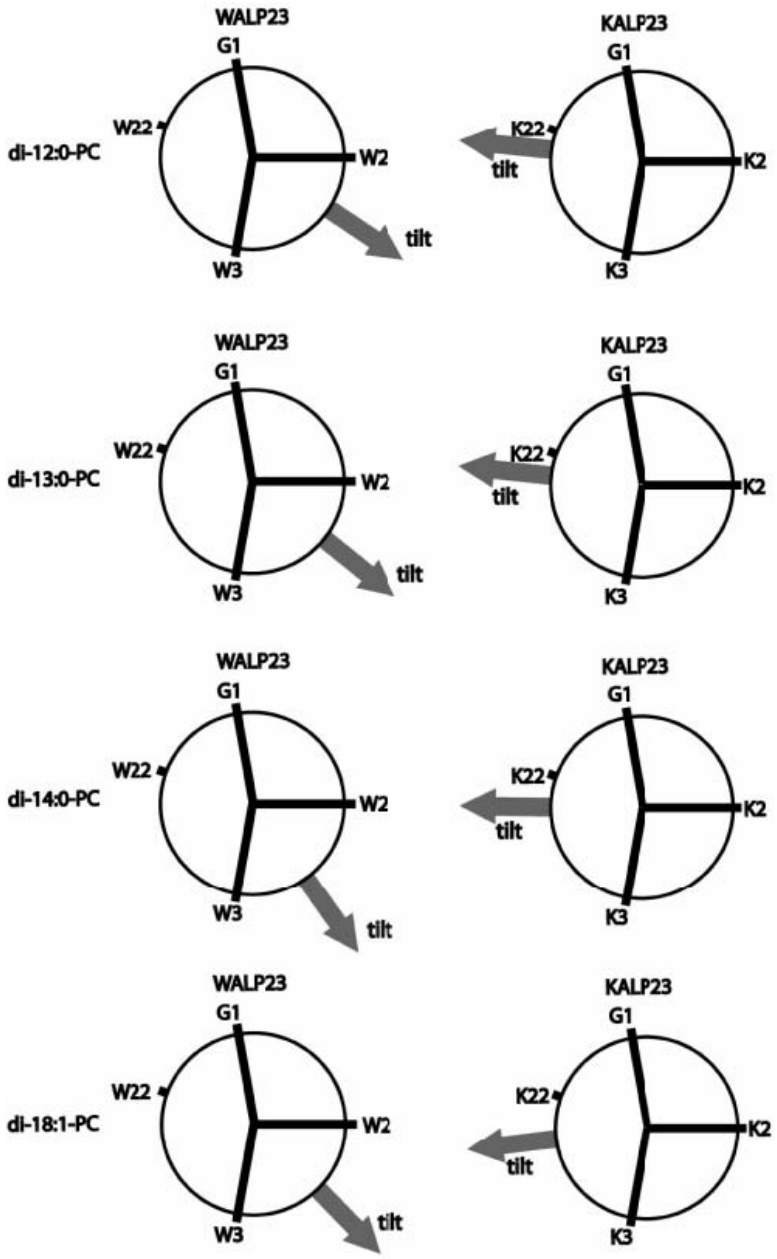

Figure 4. View of helical wheel for WALP23 (left column) and KALP23 (right column) from the N-terminal side with the direction of the tilt indicated with respect to the Gly1 residue, representing the rotation angle. The orientation of tryptophans and lysines at positions 2, 3 and 22 are indicated. From top to bottom, results in di-12:0-PC, di-13:0-PC, di-14:0-PC, and di-18:1-PC are presented.

Effects of peptide hydrophobicity on tilt and rotation angles

Next, we investigated the effect of hydrophobicity by changing the leucine alanine repeat (poly-LA) of the hydrophobic central core of the peptides for poly-leucine stretches (poly-L), in which a d_4-Ala label was incorporated at a suitable position (Table 1). For each peptide the choice of labeling position was such that a homogeneous distribution around the helical wheel is obtained (Figure 2B) and that a relatively symmetrical distribution of the hydrophobicity along the central poly-L stretch is ensured. Measurements were performed for each peptide in di-12:0-PC, di-13:0-PC, di-14:0-PC, and di-18:1-PC. Figure 5 shows selected ^{2}H NMR spectra of d_4-Ala14 labeled peptides in the different lipid systems.

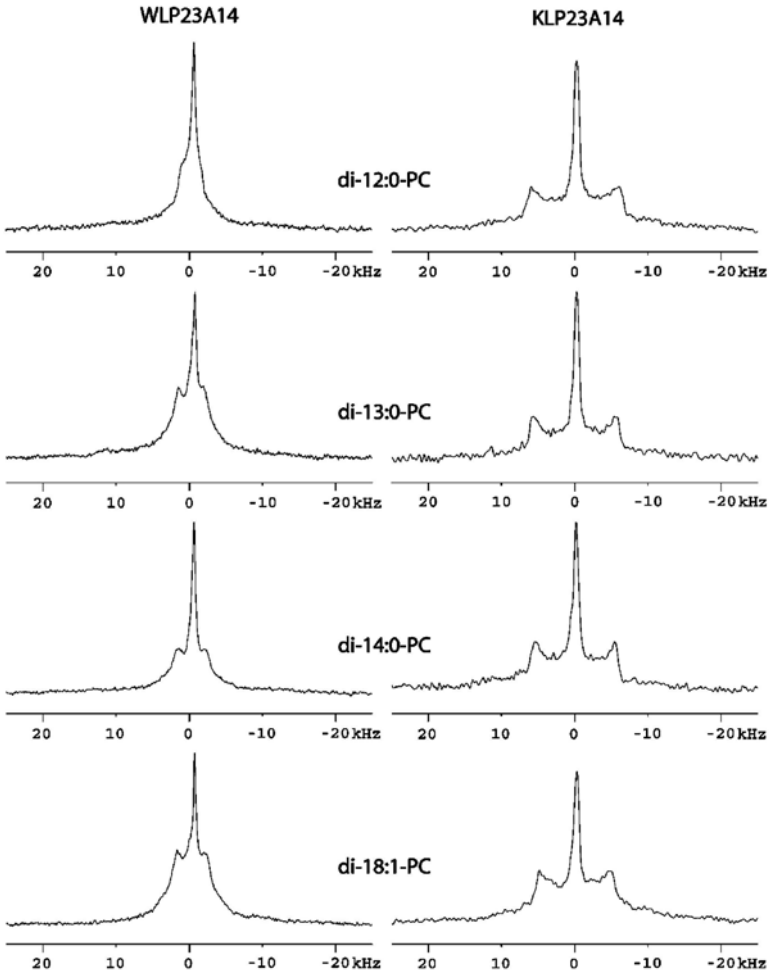

Figure 5. ^{2}H NMR spectra for WLP23 (left panel) and KLP23 (right panel) labeled at position 14 and incorporated in bilayers of di-12:0-PC, di-13:0-PC, di-14:0-PC, and di-18:1-PC (from top to bottom).

The quadrupolar splitting varies with hydrophobic thickness of the membrane for both Trp- and Lys-flanked peptides, as quantified in Table 4 for all labeled positions. As is the case for WALP23 and KALP23, WLP23 and KLP23 had different $\Delta\nu_q$-values depending on the position of the label, indicating that the peptides are tilted in the membrane and that they do not rotate fast around their own axis.

Table 4. Measured ^2H NMR splittings of d_4-Ala labeled WLP23 (A) and KLP23 (B) peptides in unoriented PC-bilayers in kHz.

A		Labeled residue			
Phospholipids	Peptide	11	12	13	14
di-12:0-PC	WLP23	7.3	1.6	10.5	2.4
di-13:0-PC	WLP23	4.1	1.4	10.0	3.1
di-14:0-PC	WLP23	2.7	1.2	9.6	4.4
di-18:1-PC	WLP23	1	2.5	7.7	4.6
B					
di-12:0-PC	KLP23	7.9	5.3	1.3	12.0
di-13:0-PC	KLP23	7.6	4.0	2.2	11.3
di-14:0-PC	KLP23	7.3	2.7	2.6	10.9
di-18:1-PC	KLP23	6.6	0.85	3.1	9.8

Calculations based on an α-helical geometry of the peptides are summarized in Table 5. When the acyl chain length is increased, the calculated tilt angle of both peptides decreases, consistent with a response to hydrophobic mismatch. The tilt angles vary from 11.4° to 4.5° for WLP23 and from 10.6° to 6.4° for KLP23. Comparison of tilt angles between WALP23 and WLP23 shows that the substitution of poly-LA by poly-L produces considerably larger tilt angles in the thinner bilayers (Table 3A and Table 5A). Their Lys-flanked counterparts, KALP23 and KLP23 show more similar tilting behavior when compared to each other (Table 3B and Table 5B). Like in the poly-LA analogs the rotation angles of WLP23 and KLP23 are very different and appear to be independent of hydrophobic mismatch. Directions of tilt of these peptides are illustrated in Figure 6. Comparison of the rotation angles of WLP23 and KLP23 to those of their respective poly-LA counterparts shows that the direction of the tilt is hardly influenced by the hydrophobicity of the central stretch (table 3 and table 5). Instead the rotation angles seemed to be determined almost exclusively by the flanking residues.

Table 5. Fit results using data from all labeled positions for WLP23 (A) and KLP23 (B).

A					
Phospholipids	Peptide	Tilt angle	rotation	CD3 angle	RMSD
di-12:0-PC	WLP23	11.4	175	56.5	0.1
di-13:0-PC	WLP23	8.9	170	58.3	0.2
di-14:0-PC	WLP23	8.1	176	58.7	0.4
di-18:1-PC	WLP23	4.5	179	59.4	0.1
B					
Phospholipids	Peptide	Tilt angle	rotation	CD3 angle	RMSD
di-12:0-PC	KLP23	10.6	267	58.4	0.9
di-13:0-PC	KLP23	9.4	265	58.9	0.6
di-14:0-PC	KLP23	8.3	265	59.3	0.7
di-18:1-PC	KLP23	6.4	265	59.5	0.8

Comparison of the $\varepsilon_{\|}$-values of WLP23 and KLP23 shows again somewhat larger fluctuations for the Trp-flanked peptide than for the Lys-flanked one, similar as for the poly-LA analogs WALP23 and KALP23. RMSD-values for both poly-L analogs were small, indicating a good quality of the fit even in 12:0-PC under the largest mismatch conditions.

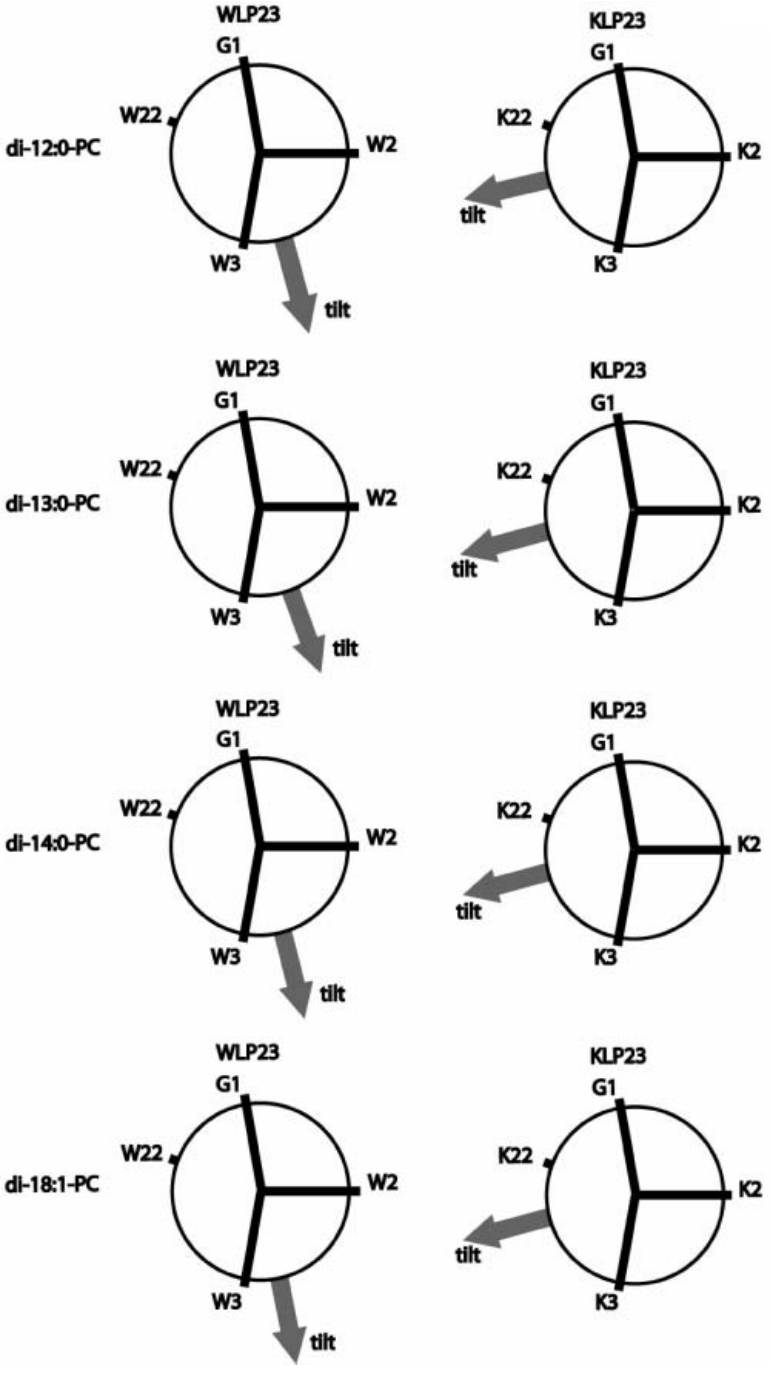

Figure 6. View of helical wheel for WLP23 (left column) and KLP23 (right column) from the N-terminal side with the direction of the tilt indicated with respect to the Gly1 residue, representing the rotation angle. The rotation of tryptophans and lysines at positions 2, 3 and 22 are indicated. From top to bottom, results in di-12:0-PC, di-13:0-PC, di-14:0-PC, and di-18:1-PC are presented.

Discussion

In this study, we have investigated the importance of flanking residues and hydrophobicity of transmembrane peptides for influencing tilt and rotation angles in lipid bilayers as a function of bilayer thickness. For this, we have used solid-state deuterium NMR on isotopically labeled transmembrane peptides analogous to WALP23. Our approach is based on GALA, a recently developed method (15) to study tilt and rotation angles that can only be applied on transmembrane peptides when they have a more or less regular α-helical structure. Indeed, circular dichroism spectra showed patterns that were typical of α-helical structures for all studied peptides in small unilamellar vesicles made of di-12:0-PC and di-18:1-PC at a peptide to lipid molar ratio of 1/100 (data not shown). The spectra were similar to those previously reported for WALP23 and KALP23 in di-14:0-PC bilayers (19).

The regular α-helical character of the peptides is particularly important for the use of GALA if a limited number of data points are available. GALA has been recently applied to WALP23 in similar PC-bilayers as in this work using singly labeled peptides with deuteriated alanine at 8 different positions, hence using 8 data points (13). That study showed that the method is applicable to a minimum of 4 data points, whereby the quality of the fit as reflected by the RMSD-values may decrease when there are local distortions from the regular α-helical geometry. In the present study, the RMSD-values are generally low, indicating that there is no significant distortion from a regular α-helical structure (table 3 and table 5), and the fit parameters could be determined with high precision. The maximal errors in fit parameters for all samples were estimated to be very low: ± 0.4°, ± 3° and ± 0.3° for the tilt angle τ, the rotation angle ρ and $\varepsilon_{\|}$, respectively (see materials and methods). This allows us to differentiate between very small variations in fit parameters that reflect subtle changes in lipid peptide interactions. We will now discuss how flanking residues and hydrophobicity when analyzed as a function of hydrophobic mismatch can modulate tilt, rotation and backbone structure.

Tilt angles

When the hydrophobic length of a transmembrane peptide exceeds the hydrophobic thickness of a bilayer, it may be expected to tilt. Recently, the tilt angles of WALP23 were analyzed in bilayers of different thickness (13). A small non-zero tilt angle was obtained in the absence of hydrophobic mismatch. This was also observed for the shorter WALP19 (15). Here we show that when the tryptophan residues in WALP23 are replaced by lysines (KALP23) a similar non-zero tilt angle is adopted in di-18:1-PC bilayers (table 3). These results suggest that a small non-zero tilt under matching conditions can be an intrinsic property of transmembrane peptides, which may be attributed to a non-symmetrical distribution of the amino acids along the helical axis.

When the bilayer thickness was decreased, both WALP23 and KALP23 showed a small but systematic increase in tilt angle in response to positive hydrophobic mismatch. However, the tilt angle of KALP23 showed a significantly larger mismatch sensitivity. KALP23 tilt angles varied from about 5° to 11° with decreasing bilayer thickness, while tilt angles of WALP23 varied from about 4° to 8° (table 3). The 3° difference in tilt between the two peptides in the thinnest bilayers is likely to be effectively larger, because the effective hydrophobic length of KALP23 is smaller than that of WALP23 due to the more hydrophobic character of Trp-residues and their preferred positioning near the interface (19,23). The relatively weak sensitivity to mismatch for WALP23 suggests that under positive mismatch conditions, Trp-

residues may inhibit tilting of transmembrane segments of membrane proteins. The reason for this is not known, but one might speculate that the preferred positioning of Trp at the interface (24) in combination with distinct, energetically favored torsion angles of the side chain may render tilt unfavorable.

The main reason for a transmembrane peptide to tilt in response to hydrophobic mismatch is to limit the energetic penalty due to exposure of its hydrophobic regions to a polar interfacial environment. Enhancing the hydrophobicity of the transmembrane part may be expected to increase this penalty, hence to increase the tilt angle. Our results showed that in the matching di-18:1-PC bilayer the tilt angle of WLP23 is similar to the one of WALP23, but that when positive mismatch is achieved by using shorter phospholipids, the tilt angle of WLP23 indeed becomes systematically larger than for WALP23. In contrast, hydrophobicity did not seem to significantly affect tilt of Lys-flanked peptides. The maximum tilt angles for both peptides are around 11° in a di-12:0-PC membrane, similar to the maximum tilt angle of WLP23. These tilt angles are small considering the fact that a tilt angle of about 40° would be required to fully match the hydrophobic thickness by tilting (13). Together, the results suggest that the energy barrier for adopting tilt angles above 11-12° is rather high. One might speculate that this energy barrier is related to packing properties of the lipids. The insertion of a transmembrane peptide with a large tilt angle would severely perturb the packing of the lipids surrounding the peptide, which in turn would perturb lipid-lipid interactions with neighboring lipids.

The results obtained for KALP can be compared with literature data that are available on other Lys-flanked peptides in slightly different peptide/lipid systems. Using solid state NMR on Lys-flanked peptides with deuteriated alanines, but using fewer label positions, Sharpe and coworkers also reported a relatively small tilt angle in bilayers of 16:0/18:1_c-PC (12) for a peptide with the same hydrophobic length as KALP23, while a slightly larger tilt angle was observed for a five amino acids longer peptide, in agreement with the mismatch dependence of the results presented here. Our results are also consistent with tilt angles determined from ^{15}N NMR on Lys-flanked peptides of varying length in unsaturated bilayers of varying thickness (6). Although the precise tilt angle could not be determined in these samples, because the rotation angle was not known, the minimum values obtained for the tilt angles in this study were close to the values obtained in our study.

Rotation angles

When a transmembrane peptide is tilted in a bilayer and it is not rotating around its long axis, it has a preferential direction of tilt with respect to the membrane. This rotation angle is another important determinant for lipid peptide interactions.

The rotation angles of WALP23 and KALP23 are rather constant in the studied bilayers, suggesting that the direction of the tilt is independent of hydrophobic mismatch. Interestingly, comparison of the rotation angles of WALP23 and KALP23 shows that they differ from each other. This demonstrates that lipid-peptide interactions at the membrane-water interface play a dominant role in determining the direction in which a peptide is tilted in a membrane. This is further supported by the observation that also the hydrophobicity does not significantly affect the rotation angle. Although rotation angles of transmembrane segments of proteins have been determined before by solid state NMR techniques (25,26) to our knowledge this is the first time that parameters that determine rotation angles have been investigated.

Effects of flanking residues on the backbone structure

As mentioned earlier, the fit procedure includes a value of $\varepsilon_{||}$, which is the side-chain angle of the deuteriated alanine with respect to the helix axis. The results suggest that the $\varepsilon_{||}$-values of Trp-flanked peptides may be more sensitive to bilayer thickness than those of their Lys-analogs. When a grid of α-helical structures is produced, as described in materials and methods, using any realistic ϕ and ψ Ramachandran parameters, and $\varepsilon_{||}$-values of these structures are plotted against the calculated distance between the outer C_α-carbons of the outer leucines in the sequence, a nearly linear relationship is obtained (Figure 7). From this relationship it can be estimated that WALP23 and WLP23 in di-12:0-PC correspond to structures that have a slightly shorter hydrophobic length (up to 1.8 Å) than their Lys-flanked counterparts. This suggests that the anchoring of the tryptophan residues to the membrane-water interface may cause the peptides to help adapt to mismatch by slightly reducing their length in addition to tilting.

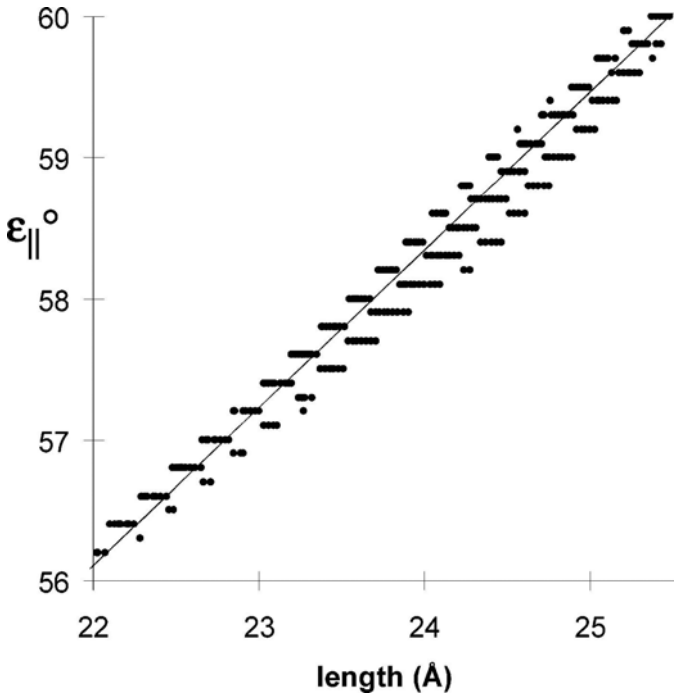

Figure 7. Relation between the alanine side chain angle with respect to the helix axis ($\varepsilon_{||}$) and the length of α-helical structures, calculated as the distance in Å between the C_α of the outer leucines, as described in the methods section. Dots represent calculated values and the straight line represents a regression line. Only the range that encompasses the experimental $\varepsilon_{||}$-values as listed in table 3 and table 5 is represented.

Such small adaptations of peptide length were not measurable by ATR-FTIR in very similar peptide-lipid systems (27), which illustrates the exceptional sensitivity of the GALA method to very small changes in backbone structure. The observation of small changes in backbone structure for Trp-flanked peptides but not for Lys-flanked peptides is consistent with the postulated strong interaction of Trp with the interface (24). Interestingly, from this strong interaction one would predict more tilting of the WALP23 peptide in response to mismatch as compared to KALP23, instead of inhibition of the tilt, as we observed. We propose that the preferred positioning of Trp at the interface (24) in combination with distinct, energetically favored torsion angles of the side chain may render tilt of transmembrane segments with Trp as flanking

residues less sensitive to positive mismatch, and that instead other responses are favored, such as adaptation of the peptide backbone and ordering and stretching of the lipid chains (24).

Implications for membrane proteins

In this study we have determined both tilt and rotation angles of α-helical transmembrane segments in different peptide/lipid model systems with high accuracy. Rather surprisingly, in all peptides we observed only very small changes in peptide tilt and rotation as function of lipid length. Nevertheless, in biological membranes such subtle changes may be important because they can be sufficient for modulating activity of membrane proteins. Examples of proteins that require only small structural changes for activity are bacteriorhodopsin upon transition to an intermediate state of its photocycle (28) and the rhodopsin II–transducer complex, in which light activation may trigger a signal cascade by inducing a small tilt movement, which in turn initiates a rotation of transmembrane helices (29,30).

In contrast to the relatively small effect of lipid length, we observed large effects when the flanking Trp residues were replaced by Lys, including a significant increase in the extent of tilting, and a completely different direction of tilt, or rotation angle. These results may be important to help understanding and predicting the precise arrangement of transmembrane segments of membrane proteins in lipid bilayers and how this arrangement can be modulated by interactions with surrounding lipids. An interesting example is the mechanosensitive channel MscL, which experiences conformational changes involving large tilt and twist rotation motions of its transmembrane regions upon changes in membrane tension (31,32). MscL is one of the few membrane proteins of which the transmembrane segments are not enriched in aromatic amino acids as flanking residues, and it was recently shown that introduction of Trp or Tyr at these positions can result in loss of functionality of the protein (33). Our observations that Trp seems to inhibit tilting of transmembrane segments and that the flanking residues are important for determining the rotation angle, provides a plausible explanation for this effect.

Acknowledgements

We thank Aalt-Jan van Dijk for kindly providing a Python program for angle calculations and we thank Ben de Kruijff, Alexandre Bonvin, and Erik Strandberg for helpful discussions.

References

1. Lee, A. G. (2003) *Biochim Biophys Acta* 1612(1), 1-40
2. de Planque, M. R., and Killian, J. A. (2003) *Molecular membrane biology* 20(4), 271-284
3. Dumas, F., Lebrun, M. C., and Tocanne, J. F. (1999) *FEBS Lett* 458(3), 271-277
4. Killian, J. A. (1998) *Biochim Biophys Acta* 1376(3), 401-415
5. Caputo, G. A., and London, E. (2003) *Biochemistry* 42(11), 3275-3285
6. Harzer, U., and Bechinger, B. (2000) *Biochemistry* 39(43), 13106-13114
7. Huschilt, J. C., Millman, B. M., and Davis, J. H. (1989) *Biochim Biophys Acta* 979(1), 139-141
8. Killian, J. A. (2003) *FEBS Lett* 555(1), 134-138
9. Killian, J. A., Salemink, I., de Planque, M. R., Lindblom, G., Koeppe, R. E., 2nd, and Greathouse, D. V. (1996) *Biochemistry* 35(3), 1037-1045

10. Liu, F., Lewis, R. N., Hodges, R. S., and McElhaney, R. N. (2001) *Biochemistry* 40(3), 760-768
11. Mall, S., Broadbridge, R., Sharma, R. P., East, J. M., and Lee, A. G. (2001) *Biochemistry* 40(41), 12379-12386
12. Sharpe, S., Barber, K. R., Grant, C. W., Goodyear, D., and Morrow, M. R. (2002) *Biophys J* 83(1), 345-358
13. Strandberg, E., Özdirekcan, S., Rijkers, D. T., van der Wel, P. C., Koeppe, R. E., 2nd, Liskamp, R. M., and Killian, J. A. (2004) *Biophys J* 86(6), 3709-3721
14. Subczynski, W. K., Pasenkiewicz-Gierula, M., McElhaney, R. N., Hyde, J. S., and Kusumi, A. (2003) *Biochemistry* 42(13), 3939-3948
15. van der Wel, P. C., Strandberg, E., Killian, J. A., and Koeppe, R. E., 2nd. (2002) *Biophys J* 83(3), 1479-1488
16. Jones, D. H., Barber, K. R., VanDerLoo, E. W., and Grant, C. W. (1998) *Biochemistry* 37(47), 16780-16787
17. Persson, S., Killian, J. A., and Lindblom, G. (1998) *Biophys J* 75(3), 1365-1371
18. Yau, W. M., Wimley, W. C., Gawrisch, K., and White, S. H. (1998) *Biochemistry* 37(42), 14713-14718
19. de Planque, M. R., Kruijtzer, J. A., Liskamp, R. M., Marsh, D., Greathouse, D. V., Koeppe, R. E., 2nd, de Kruijff, B., and Killian, J. A. (1999) *J Biol Chem* 274(30), 20839-20846
20. Ten Kortenaar, P. B. W., van Dijk, B. G., Peters, J. M., Raaben, B. J., Adams, P. J. H. M., and Tesser, G. I. (1986) *Int. J. Pept. Protein Res.* 27, 398–400.
21. Rouser, G., Fleisher, S., and Yamamoto, A. (1970) *Lipids* 5, 494-496
22. Hildebrand, P. W., Preissner, R., and Frommel, C. (2004) *FEBS Lett* 559(1-3), 145-151
23. Strandberg, E., Morein, S., Rijkers, D. T., Liskamp, R. M., van der Wel, P. C., and Killian, J. A. (2002) *Biochemistry* 41(23), 7190-7198
24. de Planque, M. R., Bonev, B. B., Demmers, J. A., Greathouse, D. V., Koeppe, R. E., 2nd, Separovic, F., Watts, A., and Killian, J. A. (2003) *Biochemistry* 42(18), 5341-5348
25. Kovacs, F. A., Denny, J. K., Song, Z., Quine, J. R., and Cross, T. A. (2000) *J Mol Biol* 295(1), 117-125
26. Marassi, F. M., and Opella, S. J. (2000) *J Magn Reson* 144(1), 150-155
27. de Planque, M. R., Goormaghtigh, E., Greathouse, D. V., Koeppe, R. E., 2nd, Kruijtzer, J. A., Liskamp, R. M., de Kruijff, B., and Killian, J. A. (2001) *Biochemistry* 40(16), 5000-5010
28. Dencher, N. A., Dresselhaus, D., Zaccai, G., and Buldt, G. (1989) *Proc Natl Acad Sci U S A* 86(20), 7876-7879
29. Klare, J. P., Gordeliy, V. I., Labahn, J., Buldt, G., Steinhoff, H. J., and Engelhard, M. (2004) *FEBS Lett* 564(3), 219-224
30. Wegener, A. A., Klare, J. P., Engelhard, M., and Steinhoff, H. J. (2001) *Embo J* 20(19), 5312-5319
31. Sukharev, S., Durell, S. R., and Guy, H. R. (2001) *Biophys J* 81(2), 917-936
32. Valadié, H., Lacapčre, J. J., Sanejouand, Y. H., and Etchebest, C. (2003) *J Mol Biol* 332(3), 657-674
33. Chiang, C., Shirinian, L., and Sukharev, S. (2004) *Biophys J* 86(1), 546A-546A (part 542 Suppl. S)

Chapter 4

Influence of 2,2,2,-Trifluoroethanol on Membrane Interfacial Anchoring Interactions of Transmembrane α-Helical Peptides

Submitted to Biophysical Journal

Abbreviations
The abbreviations used are: PC, phosphatidylcholine; NMR, nuclear magnetic resonance; TFA, trifluoroacetic acid; TFE, 2,2,2-trifluoroethanol; HEPES, *N*-(2-hydroxyethyl)piperazine-*N*′-2-ethanesulfonic acid; tBu, *tert*-butyl; d_4-Ala, deuterated L-alanine-d_4; Fmoc, 9-fluorenylmethyloxycarbonyl; di-C14:0-PC, 1,2-dimyristoyl-*sn*-glycero-3-phosphocholine; di-C14:0-PC-d_{27}, 1-myristoyl-2-perdeuteriomyristoyl-*sn*-glycero-3-phosphocholine; Trp, tryptophan; LUVs, Large Unilamellar Vesicles.

Abstract
Interfacial anchoring interactions between aromatic amino acid residues and the lipid-water interface are believed to be important determinants for membrane protein structure and function. Thus, it is possible that molecules that partition into the lipid-water interface can influence membrane protein activity simply by interfering with these anchoring interactions. Here we tested this hypothesis by investigating the effects of a small alcohol, 2,2,2-trifluoroethanol (TFE), on the interaction of a Trp-flanked synthetic transmembrane peptide (acetyl-$GW_2(LA)_8LW_2A$-NH_2) with model membranes of dimyristoylphosphatidylcholine. Two striking observations were made. First, using ^2H nuclear magnetic resonance (NMR) on acyl chain deuterated lipids, we found that addition of 4 or 8 volume % of TFE completely abolishes the ability of the peptide to order and stretch the lipid acyl chains in these relatively thin bilayers. Second, we observed that addition of 8 volume % TFE reduces the tilt angle of the peptide from 5.3° to 2.5°, as measured by ^2H NMR on Ala-d_4 labeled peptides. The 'straightening' of the peptide was accompanied by an increased exposure of Trp to the aqueous phase, as shown by Trp-fluorescence quenching experiments using acrylamide. The observation of a reduced tilt angle was surprising, because we also found that TFE partioning results in a significant thinning of the membrane, which would increase the extent of hydrophobic mismatch. In contrast to the Trp-flanked peptide, no effect of TFE was observed on the interaction of a Lys-flanked analog (acetyl-$GK_2(LA)_8LK_2A$-NH_2) with the lipid bilayer. These results emphasize the importance of interfacial anchoring interactions for membrane organization and provide new insights into how molecules like TFE that can act as anesthetics, may affect the behavior of membrane proteins that are enriched in aromatic amino acids at the lipid-water interface.

Introduction
Membrane proteins are involved in a large variety of cellular processes where they fulfill many different functions. Most membrane proteins are embedded in the membrane with one or more hydrophobic segments that are in contact with the lipid acyl chains. It has been shown that the extent of matching between the length of these hydrophobic transmembrane segments and the hydrophobic thickness of the bilayer can influence the activity of membrane proteins, and hence their structural and/or dynamic properties (1-3). However, it is not only the consequences of hydrophobic mismatch itself that can result in modulation of membrane protein structure and function. A mismatch also results in a change in the positioning of the residues that flank the hydrophobic transmembrane segments with respect to the lipid-water interface. Thus, hydrophobic mismatch may in addition affect the behavior of membrane proteins by disturbing any 'anchoring' interactions of these flanking residues with the interfacial region of the membrane. Such anchoring interactions may

be in particular relevant for aromatic amino acids, which in virtually all integral membrane proteins are found to be preferentially positioned at the lipid-water interface (4-6). It was even suggested that interfacial anchoring interactions could dominate over effects of hydrophobic mismatch in case of Trp-flanked transmembrane segments (7,8).

On a molecular level, relatively little is known about how interfacial anchoring interactions can influence properties of membrane proteins. A useful approach to gain insight into this is by using synthetic peptides that mimic the transmembrane segments of membrane proteins. Such peptides typically consist of an α-helical hydrophobic region, e.g. a sequence of alternating leucine and alanine, with variable length, and with different flanking residues (7-12). Examples are the so-called WALP peptides, which are flanked on both sides with Trp, and the KALP peptides, which are flanked by lysine residues (reviewed in 13 and 14). By using these peptides it was possible to demonstrate that interfacial interactions indeed play a role in membrane organization. For example, for the Trp-flanked WALP peptides it was shown that a positive mismatch, i.e. the situation where the hydrophobic length of the peptide is larger than the hydrophobic thickness of the bilayer, results in small but systematic increases in acyl chain order with increasing mismatch (7,15), whereas for the analogous Lys-flanked peptides no significant stretching of the lipids was observed. In addition, both the extent and direction of tilt of these peptides in lipid bilayers were found to depend on the nature of the flanking residues (16,17).

The importance of interfacial anchoring interactions for membrane organization suggests that molecules that modify the physico-chemical properties of the membrane-water interface may thereby also modify the behavior of integral membrane proteins. Candidate molecules, which partition at the interface and therefore may interfere with interfacial anchoring, are short chain alcohols, like 2,2,2-trifluoroethanol (TFE). These molecules, which are known to have anesthetic properties, can strongly influence properties of membrane proteins. An example is the high potency of TFE and other small alcohols to dissociate oligomeric membrane proteins (18,19). As a possible mechanism for this effect it was proposed that the partitioning of these alcohols in the interfacial region changes the packing properties of the lipids (20,21) or the lateral pressure profile across the lipid bilayer (18,19), thereby affecting the lipid-protein interactions. However, alternatively it is possible that small alcohols act by interfering with the interfacial anchoring properties of membrane proteins. In the present work, we investigated this possibility by analyzing how modification of the interface by addition of small amounts of TFE affects peptide/lipid interactions for Trp-flanked WALP and Lys-flanked KALP peptides in dimyristoylphosphatidylcholine (di-C14:0-PC) model membranes. One advantage of using these model peptides instead of a large natural membrane protein is that it allows detailed analysis of the effects of the alcohol on a molecular level by using different biophysical approaches. An even more important advantage is that it facilitates interpretation of the results, because the behavior of these single span peptides is expected to be insensitive to changes in lateral pressure. This is because effects of lateral pressure are believed to be transmitted through changes in shape or depth-dependent cross-sectional area of membrane proteins (22,23). In multi-span proteins this can be accomplished by changes in tilt and rotation angles of individual transmembrane segments. However, for single-span peptides the cross-sectional area will be largely unchanged as long as the peptide retains its α-helical conformation.

The results show that the presence of TFE strongly affects the membrane interaction of WALP peptides by interfering with their acyl chain ordering effect and by influencing their orientation in the membrane. In contrast, TFE does not affect the membrane interaction of analogous KALP peptides. These results provide new insights into the importance of interfacial anchoring interactions for the structure and function of membrane proteins and may help to understand the molecular mechanism by which small solutes such as alcohols may act as general anaesthesia.

Experimental procedures

Materials

WALP23 and KALP23 (for amino acid sequence, see Table 1) were synthesized using Fmoc/tBu solid-phase peptide synthesis as described elsewhere (24). The purity was analyzed by analytical high-performance liquid chromatography and electrospray mass spectrometry and MALDI-TOF (24,25). Deuterated L-alanine-d_4 (d_4-Ala) was obtained from Sigma Aldrich, and 9-fluorenylmethyloxycarbonyl (Fmoc) was used to protect its amino functionality as described in (26) before being used in the synthesis. Deuterium-labeled peptides were isotopically labeled with one deuterium-labeled alanine residue at different positions in the transmembrane domain. 1,2-dimyristoyl-*sn*-glycero-3-phosphocholine (di-C14:0-PC), and 1,2-dimyristoyl-glycero-3-phosphocholine with a perdeuterated *sn-2* chain (1-myristoyl-2-perdeuteriomyristoyl-*sn*-glycero-3-phosphocholine; di-C14:0-PC-d_{27}) were purchased from Avanti Polar Lipids Inc. (Alabaster, AL) and used without further purification. Trifluoroacetic acid (TFA) and 2,2,2-trifluoroethanol (TFE) were obtained from Merck (Darmstadt, Germany). Deuterium-depleted water was obtained from Cambridge Isotope Laboratories, Inc. All other chemicals were of analytical grade. Water was deionized and filtered with a Milli-Q Water purification system from Millipore (Bedford, MA).

Table 1. Amino acid sequences of the peptides used.

Peptide	Design
Ac-WALP23-d_4-Ala-NH_2	Acetyl-GWWL**A**L**A**L**A**L**A**L**A**LAL**A**L**A**LWWA-NH_2[a]
Ac-KALP23-d_4-Ala-NH_2	Acetyl-GKKL**A**L**A**LALAL**A**L**A**LALALKKA-NH_2[a]

[a] Underlined letters indicated in bold are positions where the peptides have been labeled with d_4-Ala.

Methods

NMR Sample Preparation

Lipid stock solutions were prepared of ca. 10 mM phospholipid in chloroform, and the exact concentrations of the phospholipid stocks were determined by a phosphorus assay as described in (27).

For ^{2}H NMR experiments on Ala-d4 labeled peptides and for ^{31}P NMR measurements with unlabeled WALP23 and KALP23, samples were prepared as follows. An amount of 1 μmol of peptide was dissolved in 1 mL of TFE and dried to a film in a rotavapor twice in order to remove residual traces of TFA. The peptide films were dissolved in 1 mL of TFE, transferred to glass tubes and mixed with lipid solutions containing 30 and 100 μmol of phospholipid to achieve peptide to lipid molar ratios of 1/30 and 1/100 for ^{31}P NMR and ^{2}H NMR, respectively. The mixtures were vortexed and dried to films under a nitrogen flow to evaporate solvents more efficiently. Traces of

solvent in samples were further evaporated overnight under vacuum ($0.5–1\times10^{-2}$ bar). The lipid-peptide films were hydrated in 500 μL of deuterium-depleted water, kept at room temperature for at least an hour in a N_2 atmosphere to equilibrate, and centrifuged 10–20 minutes at 2880*g* to collect the maximal amount of sample at the bottom of the tubes. Subsequently, the samples were lyophilized overnight. The lipid-peptide films were then hydrated in 100 μL of deuterium-depleted buffer (25 mM *N*-(2-hydroxyethyl)piperazine-*N*′-2-ethanesulfonic acid (HEPES), 100 mM NaCl, pH 7.4), and the suspensions were transferred to NMR glass tubes. The tubes were airtight sealed under a N_2 atmosphere with silicon stoppers. Samples were freeze-thawed at least 10 times to promote sample homogeneity.

For the determination of acyl chain parameters by ^{2}H NMR, the procedure was identical with the following exceptions. Unlabeled WALP23 or KALP23 (0.1 μmol) in 60 µl TFE was mixed to a lipid solution containing 3 μmol of di-C14:0-PC-d_{27} in 300 µl chloroform to achieve a peptide to lipid molar ratio of 1/30. The mixtures were vortexed and dried to a film evaporating solvents under a constant N_2-flow. The samples were vacuum-dried overnight after which they were hydrated in 200 μL of deuterium-depleted buffer (25 mM TRIS, 100 mM NaCl, pH 7.4) and transferred to NMR glass tubes. The tubes were sealed under a N_2 atmosphere with a silicon stopper and were freeze-thawed at least 10 times. The same procedures were used for the preparation of samples containing only the di-C14:0-PC-d_{27} suspensions.

NMR Measurements

NMR experiments were carried out on a Bruker Avance 500 MHz NMR spectrometer. Samples were allowed to equilibrate at 40 °C for at least 10 min before measurements. ^{31}P NMR experiments were performed as described (16) on all samples used.

^{2}H NMR experiments on deuterated peptides were performed at 76.78 MHz using a quadrupolar echo sequence as described previously (16). The measurements were performed with a 5.8 μs 90° pulse, an echo delay of 40 μs, a recycling delay of 100 ms, 1 MHz spectral width, and 4096 data points. Typically, between 200,000 and 1,000,000 scans were collected. Acquisition was started at the echo maximum and further processed by zero-filling to 16384 data points, and using a 100-Hz exponential multiplication followed by Fourier transformation.

^{2}H NMR experiments on di-C14:0-PC-d_{27} phospholipid samples were carried out using the same quadrupolar echo sequence with identical parameters as above, except that a spectral width of 500 kHz, and a recycling time of 600 ms were used.

Calculation of peptide structural parameters

Quadrupolar splittings ($\Delta\nu_q$, kHz) of seven or four labeled positions were measured from ^{2}H NMR spectra of WALP23 and KALP23, respectively (see Table 1). ^{2}H NMR signals were assigned to the deuterons of the alanine side-chain methyl group as in previous work, since the splitting of the backbone deuteron was not observed (28). The $\Delta\nu_q$-values for unoriented samples were fitted to a model α-helix to determine the tilt (τ), rotation (ρ) and the labeled alanine side chain ($\in_{\|}$) angles as in (16,17).

The tilt angle is defined as the angle between the peptide helical axis and the bilayer normal and $\in_{\|}$ is the angle between the peptide helix axis and the C^{α}-$C^{\beta}D_3$ bond vector. The angle ρ is the angle of rotation around the α-helical axis that is necessary to minimize the root mean square deviation (RMSD, kHz) between experimental and simulated $\Delta\nu_q$-values for discrete values of τ and $\in_{\|}$ (17). The fitting procedure was

based on the $\Delta\nu_q$-values of the four labeled positions as indicated in Table 1 using an in-house computer program written in Python 2.3.
The errors in τ, ρ, and $\in_{\|}$ were estimated, deviations being ± 0.4°, ± 3° and ± 0.3°, respectively (17).

Analysis of ^{2}H NMR spectra for determination of acyl chain parameters
The recorded ^{2}H-NMR powder spectra were numerically deconvoluted to yield the θ = 0° spectra (29,30), resulting in so-called de-Paked spectra. Using the Peak-Fitting Module in Origin 7.5 we deconvoluted the de-Paked spectra in order to assign the peaks to carbon atoms along the *sn-2* acyl chain. The quadrupolar splittings determined from the de-Paked spectra were used to calculate the order parameter, $S_{CD(i)}$, according to:

$$\Delta\nu_{Q(i)} = \frac{3}{4}(e^2qQ/h)(3\cos^2\theta - 1)S_{CD(i)} \quad (1)$$

where e^2qQ/h = 167 kHz for $\theta = 0°$ (29) From the determined order parameters we estimated the hydrocarbon thickness of one monolayer according to the method described in (31-33). To estimate the hydrocarbon thickness per monolayer the following equation was used:

$$D_C = \frac{n_C l_0}{q} \quad (2)$$

where the factor n_C is the number of carbons per acyl chain (i.e. 14 for di-C14:0-PC), and the maximum segmental projection l_0, was 1.27 Å. The factor q was approximated from:

$$q \approx 3 - 3\langle\cos\beta\rangle + \langle\cos^2\beta\rangle \quad (3)$$

described by Brown and co-workers (31). In equation 3, the first $\langle\cos\beta\rangle$ and the second moment $\langle\cos^2\beta\rangle$ are given by:

$$\langle\cos\beta\rangle = \frac{1}{2}\left(1 + \sqrt{\frac{-8S_{CD} - 1}{3}}\right) \quad (4)$$

$$\langle\cos^2\beta\rangle = \frac{1 - 4S_{CD}}{3} \quad (5)$$

where the order parameter, S_{CD}, of the plateau region is used to avoid complication of chain upturns, early terminations and interdigitation (31-33).

Steady State Fluorescence
All fluorescence experiments were performed at 30° C using a QuantaMaster QM-1/2005 spectrofluorometer (Photon Technology International, NJ) in a quartz cuvette. The samples were excited at 295 nm and emission spectra were collected between 300 and 400 nm. The bandwidths for both excitation and emission monochromators were 5 nm. Acrylamide quenching of tryptophan fluorescence was performed to check the accessibility of tryptophans in lipid bilayers as a function of TFE. Samples for

fluorescence experiments were prepared as follows: di-C14:0-PC and WALP23 were mixed in TFE/chloroform at a peptide to lipid molar ratios of 1/100. The mixture was dried to a film that was rehydrated in buffer (25 mM TRIS, 100 mM NaCl, pH 7.4). The samples were freeze-thawed ten times, extruded through a 200 nm membrane filters (Anotop 10, Whatman, Maidstone UK), and diluted in 1.25 ml of buffer to achieve a final WALP23 concentration of 2.5 μM. The samples were treated with 4 or 8 vol% TFE. Acrylamide was added in aliquots from a 3 M stock solution to each sample up to a concentration of about 70 mM. The Stern-Volmer equation was used to analyze the quenching data (34):

$$F_0/F = 1 + K_{SV}[Q] \qquad (6)$$

where F_0 is the Trp fluorescence in the absence of quencher and F is the observed fluorescence at the concentration $[Q]$ of the quencher. K_{SV} is the collisional quenching constant, which was determined from the slope of Stern-Volmer plots. As a control, similar experiments were performed for a L-Trp solution (10 μM). All data were corrected for inner filter effects as described previously (34).

Results

Influence of TFE on phospholipid bilayer

Before studying how TFE influences the interaction between WALP and KALP peptides with lipid bilayers, we first analyzed the influence of this small alcohol on the properties of the lipids themselves. For this purpose, ^{31}P NMR experiments were performed at 40°C on samples made of di-C14:0-PC in the absence of peptides at different TFE concentrations.

All spectra up to 30 vol % TFE showed an anisotropic pattern with a low field shoulder and a high field peak, which are typical of multilamellar vesicle (MLV) bilayers in the liquid crystalline phase (35). Selected spectra are shown in Figure 1A. As plotted in Figure 1B, the chemical shift anisotropy (CSA) decreases gradually upon addition of TFE in the range of 0 to 30 vol % TFE. At 50 vol % TFE, vesicles are disrupted, resulting in an optically clear solution of di-C14:0-PC, which gives rise to an isotropic peak (Figure 1A).

The observed decrease in CSA may imply either a decrease in particle size, which would result in motional averaging due to Brownian tumbling of the entire vesicles and lateral diffusion of the lipids (36) or to a decreased order in the lipid headgroup region of the bilayers. To discriminate between these two possibilities, we performed ^{31}P NMR experiments with flat oriented bilayers of di-14:0-PC as described in (16). In these systems the motional axis of the phospholipids is oriented parallel to the magnetic field, giving rise to a low field ^{31}P NMR peak. Upon addition of TFE we observed an upfield shift of this peak (data not shown). In these systems averaging of the CSA by a decreased particle size is excluded because the motional axis of the phospholipids will remain parallel to the magnetic field. Therefore the most logical explanation for the decreased CSA is that TFE affects the order in the headgroup region of the phospholipid bilayer.

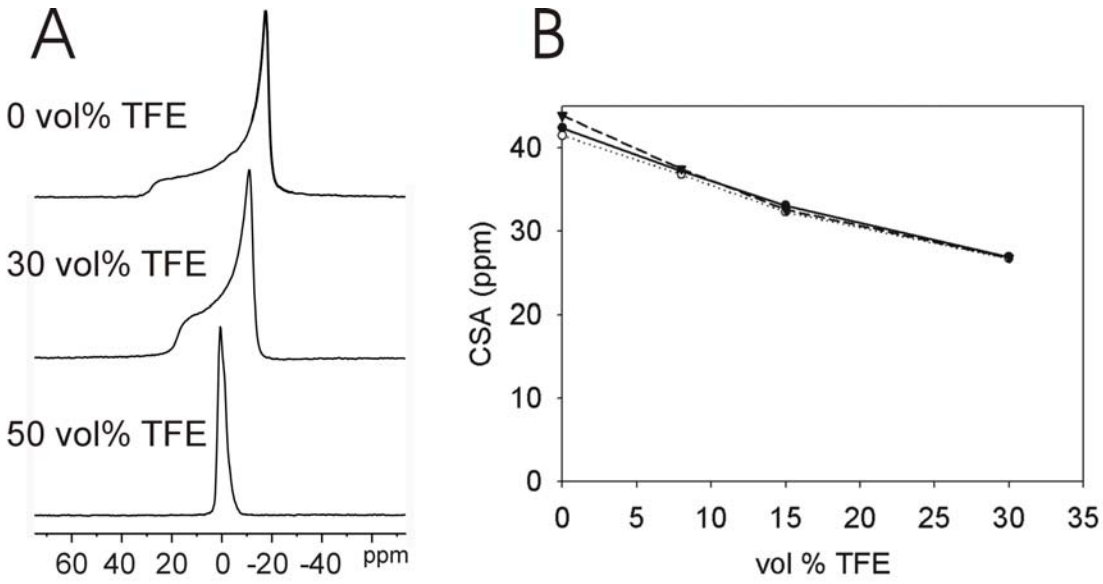

Figure 1. Influence of increasing concentration of TFE on ^{31}P NMR CSA of di-C14:0-PC bilayers at 40°C. Selected spectra of di-C14:0-PC multilamellar vesicles (panel A). Graph of ^{31}P NMR CSA versus TFE vol % of di-C14:0-PC for pure lipids (▼), for lipids with WALP23 (●), and for lipids with KALP23 (○) (panel B).

We performed similar ^{31}P NMR experiments as above by adding TFE to MLV suspensions made of WALP23 or KALP23 in di-C14:0-PC in a peptide to lipid molar ratio of 1:30. All samples gave rise to typical 'bilayer' spectra up to a TFE concentration of 30 vol %. Figure 1B shows that the presence of either KALP23 or WALP23 in di-C14:0-PC slightly reduces the CSA when no TFE is present. However, when TFE is added the effect of peptides on the CSA is removed and samples of pure lipids and lipids containing peptides behave similarly regardless of the amount of TFE that is added. This indicates that the presence of peptide does not interfere with the influence of TFE on the lipid headgroup organization.

Influence of TFE on the order in the phospholipid acyl chains

Recent work showed that the presence of TFE in a membrane increases the disorder of the acyl chains of unsaturated phospholipids (18). Here we investigated the effect on the saturated lipid di-C14:0-PC by performing ^{2}H NMR on di-C14:0-PC-d_{27} (*sn*-2 chain deuterated) bilayers, as described in (15,25,31). Experiments were first performed in the absence of peptide.

^{2}H NMR spectra of di-C14:0-PC-d_{27} multilamellar vesicles with and without TFE are shown in Figure 2A. The lineshape and the quadrupolar splittings from the different labeling positions along the acyl chains for the pure lipid dispersion are in good agreement with results from a previous study of di-C14:0-PC-d_{27} (15,25,31). The addition of 4 vol % of TFE clearly reduces all the splittings, indicating an increased averaging of the signals from the acyl chains. In addition, some changes are observed in the ^{2}H NMR lineshape, which can be ascribed to a depth-dependent influence of TFE on the di-C14:0-PC bilayers.

To facilitate data analysis and assignment of the quadrupolar splittings that were difficult to resolve, the spectra were de-Paked (Figure 2B). The resulting spectra would correspond to aligned bilayers with their normal parallel to the magnetic field. Assuming a monotonic variation of the order parameters ($S_{CD}^{(i)}$) along the acyl chains, the peak assignment was based on the sequence of the labels along the acyl chain. The

largest splittings were assumed to be from the labels closest to the headgroup region in the membranes.

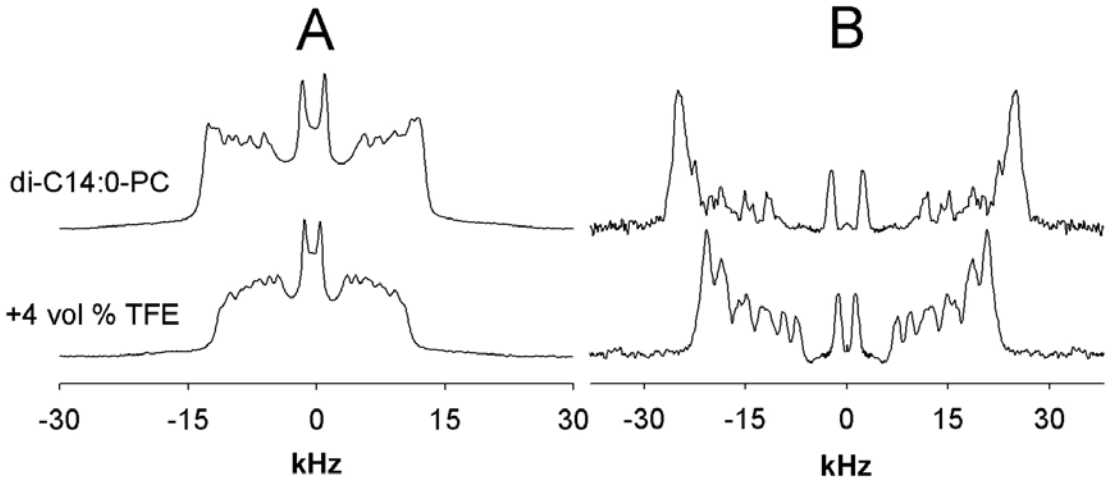

Figure 2. ^{2}H-NMR spectra of di-C14:0-PC-d_{27} at 40 °C with or without 4 vol % TFE in TRIS buffer pH = 7.4. In panel A, original spectra are represented. In panel B, dePaked deuterium spectra were obtained as described in (30) by using the GRAMS software.

From the splittings, corresponding $S_{CD}^{(i)}$-values were calculated of the di-C14:0-PC-d_{27} lipids in the absence and presence of TFE (Figure 3). A plateau region characterizes the order profile of the lipids in the absence of TFE, indicating a relatively high chain order near the bilayer interface. This is followed by a rapid decrease towards the end of the acyl chain in the core of the bilayer. As shown in Figure 3, the order parameters are in general reduced by the addition of TFE. Note also that adding TFE shortens the plateau. Increasing the TFE concentration up to 8 vol % resulted in a further reduction of the order of the acyl chains.

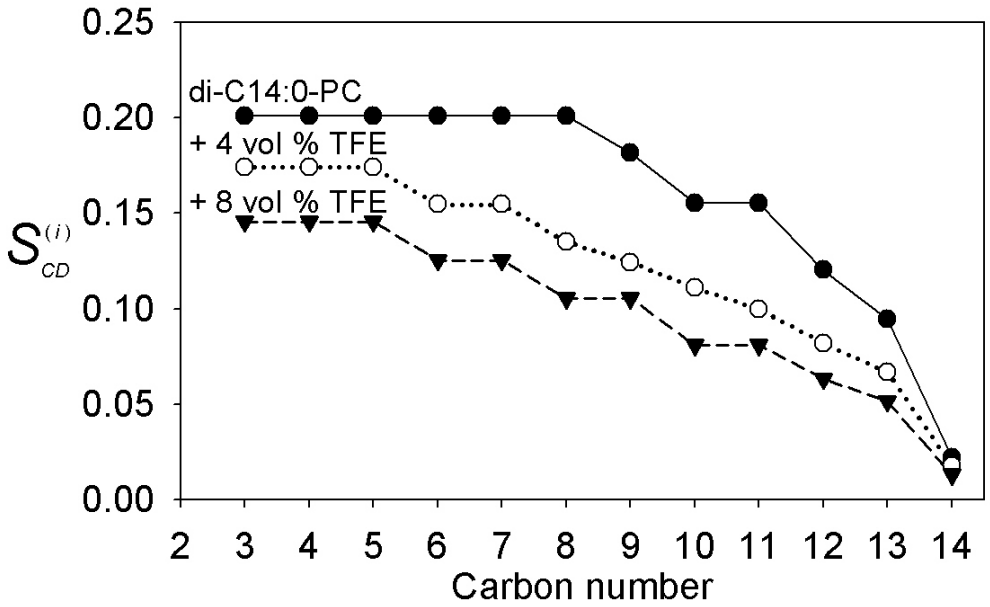

Figure 3. Order parameter profiles in di-C14:0-PC-d_{27} bilayers at 40 °C in TRIS buffer with pH = 7.4. Plotted values were calculated as described in (31-33) for di-C14:0-PC-d_{27} (●), di-C14:0-PC-d_{27} + 4 vol % TFE (○), and di-C14:0-PC-d_{27} + 8 vol % TFE (▼).

Next, we used the order parameters to estimate the bilayer thickness as described in (31-33). As shown in Table 2, the estimated bilayer thickness of di-C14:0-PC-d_{27} membranes at 40°C decreases from 25.0 Å to 21.2 Å upon addition of 8 vol % TFE, showing that the TFE-induced disorder in the membrane results in a significant reduction of the bilayer thickness.

Table 2. Estimation of the di-C14:0-PC bilayer thickness at 313 K deduced from order parameters according to reference 31. The peptide to lipid molar ratio of samples containing peptides was 1 to 30.

Sample		Bilayer thickness $2\times D_C$[a] (Å)
di-C14:0-PC		25.0 (25.6[b] & 24.0 [c])
	+ 4% TFE	23.4
	+ 8% TFE	21.2
WALP23		26.4
	+ 4% TFE	23.2
	+ 8% TFE	21.6
KALP23		25.2
	+ 8% TFE	21.0

[a] D_C represents the distance in Å of the carbonyl atom to the center of the bilayer (31-33).

[b] Data from (31) at 30°C.

[c] Data from (31) at 50ºC.

Effects of peptide incorporation on lipid order in the presence of TFE

To investigate the influence of TFE on the interaction of the peptides with the lipids, we performed ^{2}H NMR experiments on samples of WALP23 an KALP23 in di-C14:0-PC-d_{27}. After recording the ^{2}H NMR spectra of the lipid-peptide suspensions, further measurements were performed on the same samples with 4 or 8 vol % TFE added. Figure 4 shows selected de-Paked deuterium spectra. Experiments without peptide in the membrane are included for comparison.

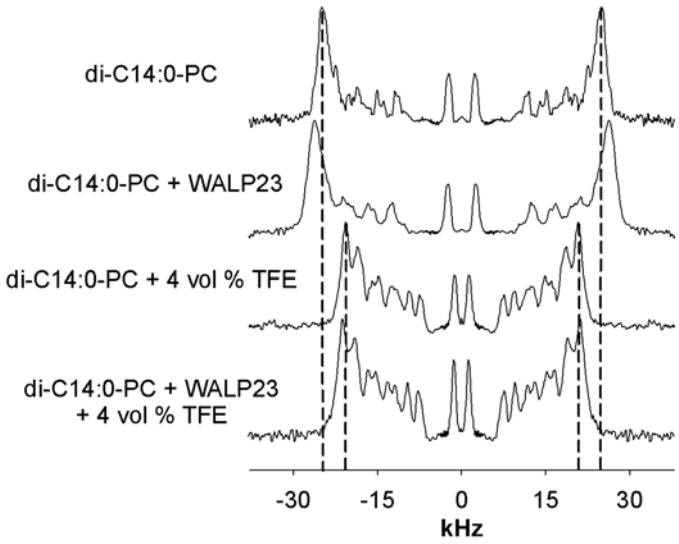

Figure 4. DePaked ^{2}H-NMR spectra of di-C14:0-PC-d_{27} and di-C14:0-PC-d_{27} with WALP23 at 40 °C with or without 4 vol % TFE in TRIS buffer pH = 7.4. DePaking the spectra were performed by using the GRAMS software as described in (30).

Introduction of WALP23 at a 1 to 30 peptide to lipid molar ratio increases the order in the acyl chains. This is illustrated by the increase of ^{2}H NMR quadrupolar splittings with respect to those in the pure di-C14:0-PC-d_{27} suspension, which is in good agreement with previous observations (25). When 4 % TFE is added, the quadrupolar splittings are reduced, but now the spectra are very similar in the absence and presence of peptide. Similar behavior was observed for 8 vol% TFE (spectra not shown).

The loss of the ordering effect is also apparent from the order parameter profiles (Figure 5A). When no TFE is added, incorporation of the peptide results in a plot that is characterized by a plateau region with higher $S_{CD}^{(i)}$ -values than for the pure di-C14:0-PC-d_{27} suspensions, indicating an increased order in the acyl chains. Towards the bilayer core, the order parameters of both types of samples converge gradually. In the presence of TFE, the order parameter profiles of di-C14:0-PC-d_{27} and di-C14:0-PC-d_{27}/WALP23 samples look very similar.

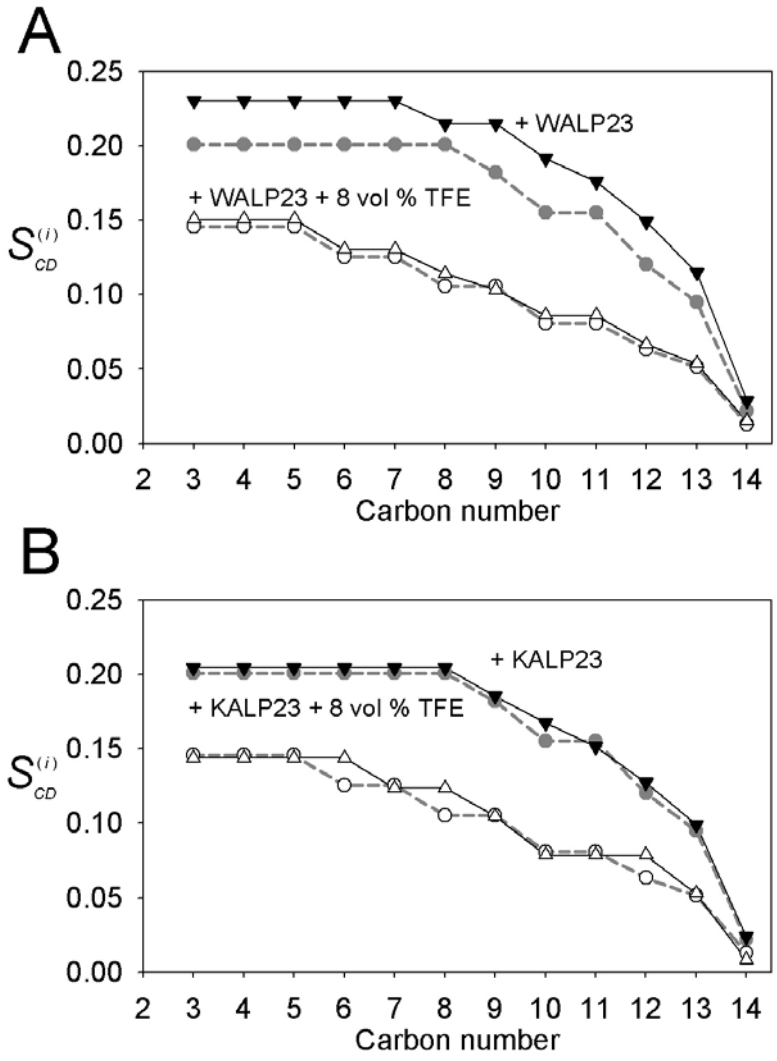

Figure 5. Order parameter profiles in di-C14:0-PC-d_{27} bilayers at 40 °C in TRIS buffer with pH = 7.4. The order parameters for di-C14:0-PC-d_{27} (dashed grey line, ●), and di-C14:0-PC-d_{27} + 4 vol % TFE (dashed grey line, ○) are plotted for comparison issues in panel A and B. Plotted values for di-C14:0-PC-d_{27} + WALP23 (solid line, ▼), and di-C14:0-PC-d_{27} + WALP23 + 8 vol % TFE (solid line, △) are represented in panel A. Order parameter profiles for di-C14:0-PC-d_{27} + KALP23 (solid line, ▼), and di-C14:0-PC-d_{27} + KALP23 + 8 vol % TFE (solid line, △) are shown in panel B.

As shown in Table 2, the incorporation of WALP23 in di-C14:0-PC-d_{27} causes an estimated increase in bilayer thickness from 25.0 to 26.4 Å, in agreement with previous observations (25). Addition of TFE reduces the estimated bilayer thickness to values that are very similar to those obtained in the absence of peptide. These results clearly show that TFE dissipates the ordering effect and hence interferes with the lipid-peptide interactions in case of WALP23.
Previously, it was observed that KALP23 peptides in contrast to WALP23 do not significantly influence lipid chain order in di-C14:0-PC (25). Our results show that the order parameter profiles (Figure 5B) or the bilayer thickness (Table 2) in the presence of TFE are also unaffected by KALP23.

Influence of TFE on Tilt Angle of WALP23 and KALP23
We next investigated how the presence of TFE affects properties of the peptides. In particular, we used ^{2}H NMR on d_4-Ala-labeled peptides to monitor effects of TFE on tilt angles of the peptides. Each peptide was labeled with a single d_4-Ala as indicated in Table 1 for WALP23 and KALP23 at seven and four different positions, respectively. The labeling positions were chosen to enable precise determination of the tilt angles of the peptides in membrane bilayers and the direction in which they tilt, as represented by rotation angles of the α-helix axis with respect to the plane of tilt (16,17,28). Selected ^{2}H NMR spectra are shown in Figure 6 for two labeling positions of both the WALP23 and the KALP23, with 0 and 8 vol % TFE in the di-C14:0-PC suspensions. For both peptides in the absence of TFE, the spectra with corresponding quadrupolar splittings were in good agreement with earlier results (16,17). When 8 vol % TFE was added changes in the quadrupolar splitting values could be observed for all the labels of WALP23 (Table 3). This effect was much less pronounced for KALP23, which was rather insensitive to the presence of TFE.

Table 3. Measured ^{2}H NMR splittings of d_4-Ala-labeled WALP23 peptides in unoriented PC bilayers with and without addition of TFE in kHz.

A. WALP23		Labeled residue						
Phospholipids	TFE vol %	5	7	9	11	13	17	19
di-14:0-PC	0	4.3	0.7*	6.8	0.9	7.5	6.9	1.0
di-14:0-PC	8	2.2	0.0*	3.5	0.2	4.0	3.8	1.7

B. KALP23		Labeled residue			
Phospholipids	TFE vol %	5	7	13	15
di-14:0-PC	0	3.2	9.6	0.5*	3.9
di-14:0-PC	8	2.5	9.6	0.0*	5.0

* Quadrupolar splittings that could not be resolved and for which an estimated value is given.

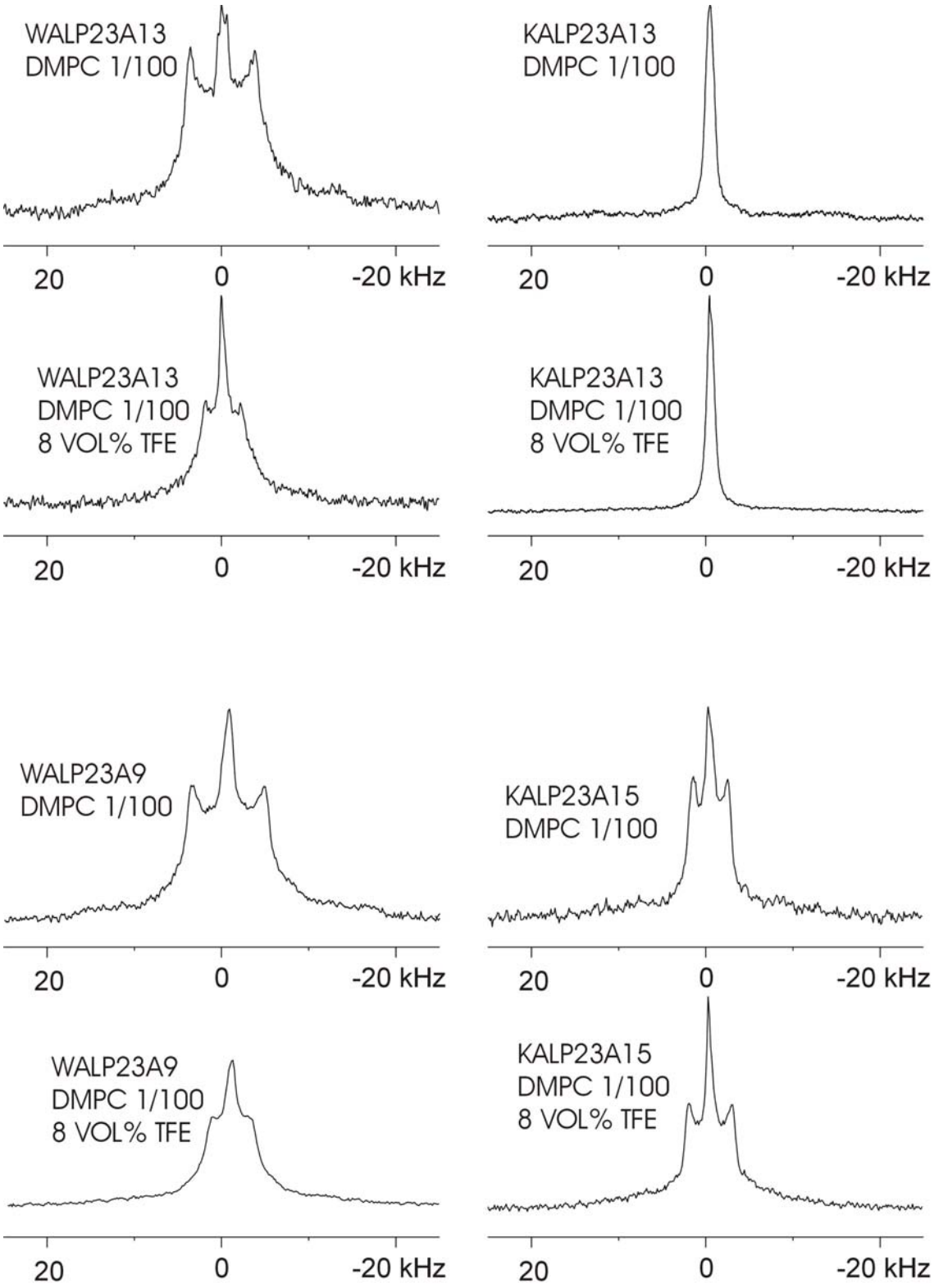

Figure 6. ^{2}H NMR spectra for labeled alanines at positions 9, and 13 of WALP23 and 13 and 15 of KALP23 incorporated in di-14:0-PC without and with 8 vol % of TFE at a peptide to lipid ratio of 1/100. The isotropic peak in the middle of the spectra is assigned to residual deuterium in H_2O.

We calculated the tilt (τ), the rotation (ρ) and the labeled side chain angles ($\in_{\|}$) in the absence and the presence of TFE assuming a regular α-helical geometry of the peptides, as described (16,17,28). The results are shown in Table 4. When no TFE is

added, a relatively small tilt angle is observed of 5.3º, in agreement with previous results (17). The presence of 8 vol % TFE results in a decrease of the tilt angle to 2.5º without a significant change of the rotation angle. In contrast, for KALP23 the addition of 8 vol % TFE neither changes the tilt angle nor the rotation angle.

Table 4. Fit results using data from the four-labeled positions summarized in Table 3 for WALP23 (A), KALP23 (B).

A. WALP23		Fit parameters			
Phospholipids	TFE vol %	Tilt angle	Rotation angle	$\in_{\|\|}$ angle	RMSD (kHz)
di-14:0-PC	0	5.3	162	58.4	0.4
di-14:0-PC	8	2.5	154	56.8	0.8
B. KALP23					
di-14:0-PC	0	7.8	278	58.5	0.4
di-14:0-PC	8	7.5	286	58.7	0.3

Table 4 also shows that the angle $\in_{\|}$ of the labeled alanines of WALP23 decreases slightly when TFE is added. A similar effect was recently also observed for WALP23 and a Trp-flanked polyleucine analog of this peptide (WLP23) upon reducing the bilayer thickness from di-C14:0-PC to di-C12:0-PC (17). In this case the reduction of $\in_{\|}$ was proposed to be a possible indication of a reduction in the length of the backbone of Trp-anchored transmembrane peptides to help the system adapt to mismatch when the phospholipid bilayers are too thin to accommodate the whole hydrophobic length of a transmembrane peptide. In the case of KALP23, $\in_{\|}$ appears to be insensitive to the presence of TFE. This is in line with the previous observation that $\in_{\|}$ in KALP23 is insensitive to bilayer thickness (17). These results might suggest that WALP23 senses mismatch more than KALP23 even though it does not react to it by tilting.

Influence of TFE on the positioning of the tryptophans

The deuterium NMR results suggest that WALP23 reduces its tilt angle when TFE is added, even though the bilayer gets thinner. To determine whether TFE has an influence on the positioning of tryptophans in lipid bilayers we performed tryptophan fluorescence experiments. In di-C14:0-PC membranes, WALP23 exhibits an emission maximum at about 334 nm, which is typical for positioning of tryptophans in the interfacial region (37). When TFE is added to samples containing large unilamellar vesicles (LUVs) composed of WALP23 and di-C14:0-PC in a 1/100 peptide to lipid molar ratio, the fluorescence intensity decreases (Figure 7A). In addition, a red shift of the emission spectrum (~ 2 nm) is observed, indicating a more polar environment. This decrease in fluorescence intensity is not due to a direct effect of TFE, because for free L-Trp in buffer, which shows an emission maximum at 350 nm in a more hydrophilic environment, neither the fluorescence intensity nor the wavelength of the emission maximum is affected by this solvent (Figure 7B).

The effects of TFE on the local environment of Trp were further investigated by monitoring Trp accessibility using the aqueous quencher acrylamide. Figure 8A

shows the Stern-Volmer quenching plots of WALP23 in di-C14:0-PC (1/100 molar ratio), in which F_0/F is plotted against the acrylamide concentration in the absence and presence of TFE. Addition of 4 vol% TFE increased the quenching constant (K_{SV}) from 5.2 ± 0.2 to 6.0 ± 0.1 M^{-1}, and at 8 vol% it was further increased to 6.7 ± 0.5 M^{-1}. A qualitatively similar effect was observed for a sample with a higher peptide/lipid molar ratio of 1/30 (data not shown). Again this was not a direct effect of TFE, since experiments on L-Trp in buffer (Figure 8B) show no effect of TFE addition on acrylamide accessibility (K_{SV} = 20.7 ± 1.4 M^{-1} in the absence of TFE and 20.5 ± 1.1 M^{-1} and 20.4 ± 0.4 M^{-1} in the presence of 4 and 8 vol% TFE, respectively). Thus, the fluorescence data are fully consistent with an increased exposure of Trp in WALP peptides to the aqueous environment and support our notion that TFE addition results in a more upright position of WALP peptides in a di-C14:0-PC bilayer.

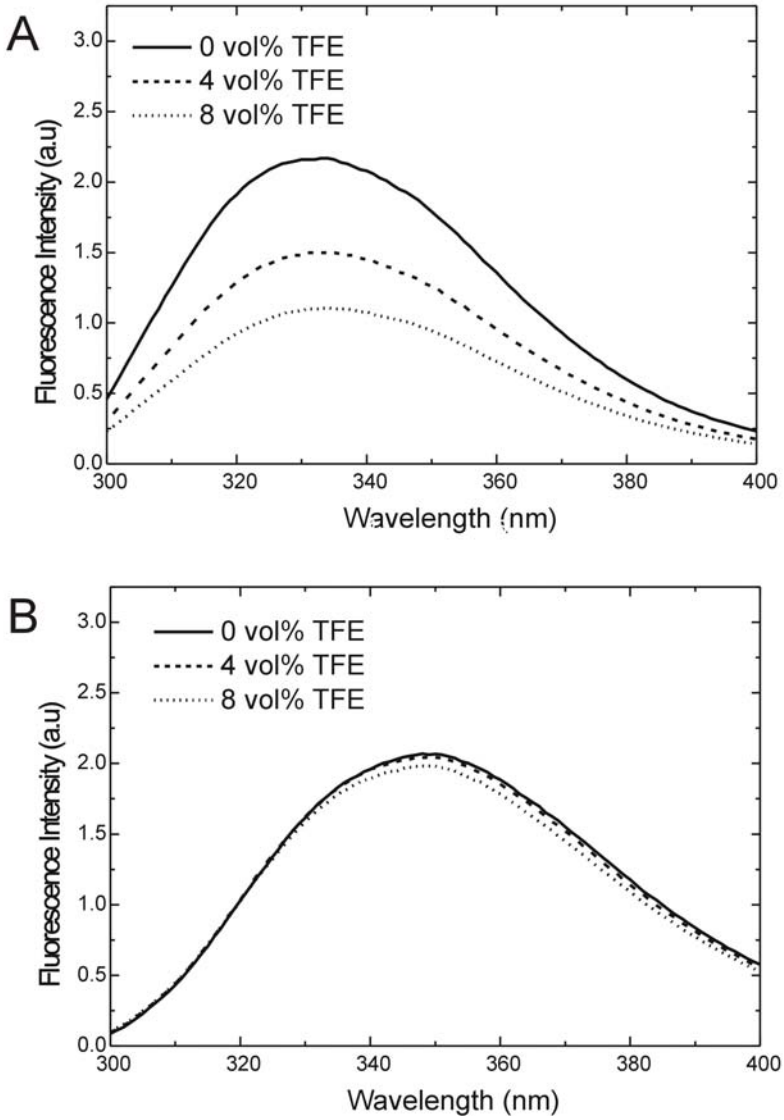

Figure 7. The effect of TFE on fluorescence emission spectra of WALP23 in di-C14:0-PC (A) and L-Trp in buffer (B). The peptide to lipid ratio of WALP23 in di-C14:0-PC was 1/100. The corrected spectra and the effects of 4 and 8 vol% TFE on the fluorescence intensities are shown.

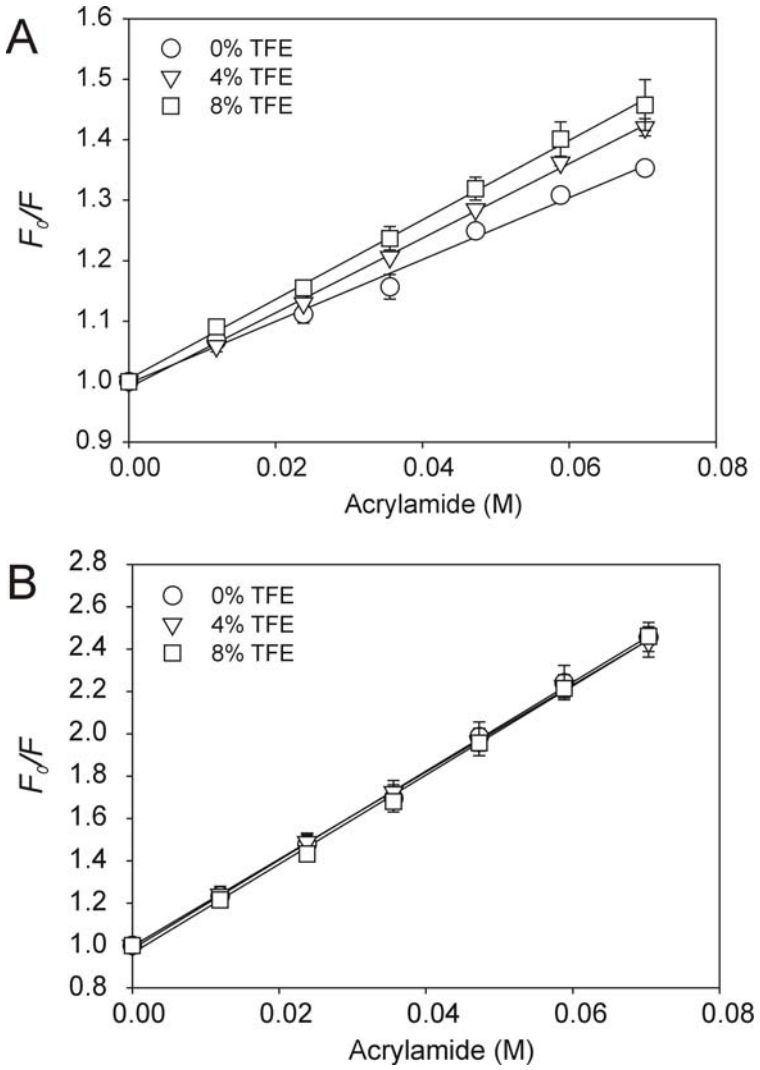

Figure. 8. Stern-Volmer plots of Trp fluorescence quenching by acrylamide. Both WALP23 in di-C14:0-PC (A) or L-Trp in buffer (B) and were investigated with or without 4 or 8 vol% TFE. The WALP23:di-C14:0-PC ratio was 1/100. Mean values ± standard deviation from three experiments is given.

Discussion

In this work, we have used NMR to investigate how TFE influences the structure of phosphatidylcholine bilayers and how it affects the interactions of the lipids with peptides that mimic transmembrane segments of membrane proteins. The results show that TFE has drastic effects on membrane organization. We will first discuss the consequences of the partitioning of TFE in the interfacial regions of the bilayer for the properties of the lipids. Next, we will describe how TFE can affect the properties of the peptides by interfering with their interactions with the lipid-water interface. Finally, we propose a model for the mechanism by which TFE influences anchoring interactions in particular of Trp-flanked peptides with the lipid-water interface.

Partitioning of TFE into the membrane-water interface and implications for the behavior of the lipids

In the first part of this study, we observed that the presence of TFE decreases the order of both the lipid headgroups and the acyl chains in phosphatidylcholine bilayers.

Similar disordering effects were previously observed in different phospholipid bilayers for diverse short-chain alcohols like ethanol (18,21). Since TFE and ethanol are expected to have rather similar physico-chemical properties, knowledge of how ethanol affects phosphatidylcholine bilayers may help to understand the mechanism by which TFE affects lipid systems.
It has been shown that ethanol partitions predominantly in the membrane-water interface near the glycerol backbone and the carbonyl moieties and to a slightly lower extent near the phosphates (20,38). Although ethanol also can partition in the hydrophobic core of the bilayer and in water, this occurs to a much lower extent than in the headgroup region. Consequently, it has been suggested that there might be a continuous remodeling of the lipid packing around the permanently migrating ethanol molecules resulting in conformational changes of the headgroup as observed with ^{2}H NMR on headgroup deuterated di-C14:0-PC-d_5 (21). The partitioning in the interfacial region also leads to an increased disorder of the acyl chains and consequently a decrease in bilayer thickness (21,39).
Like ethanol, TFE is amphiphilic, and its electrostatic properties are similar. Both molecules have octanol-water partitioning coefficients and dielectric constants favorable for localizing in a relatively hydrophobic environment such as membrane-water interfaces (40-42). However, TFE has a stronger hydrogen-bond donating hydroxyl group than ethanol (43) and a significantly higher octanol-water partitioning coefficient that may favor the distribution in the interface more than for its non-fluorinated analog (40). The more efficient partitioning in membranes of TFE with respect to ethanol might explain the larger efficacy of TFE to influence the order of the acyl chains and consequently to reduce bilayer thickness, as measured by ^{2}H NMR (18).

Effects of TFE on the behavior of transmembrane peptides
In the second part of our study we analyzed the influence of TFE on the interaction of the peptides with lipid bilayers by ^{2}H NMR and fluorescence techniques. From the NMR experiments two striking results were obtained in particular. First, we found that addition of TFE results in a complete loss of the acyl chain ordering effect of WALP23. Second, although the bilayer becomes more disordered and hence is expected to become thinner upon TFE addition, the peptide was found to tilt less. This was supported by results from fluorescence quenching experiments, which showed an increased exposure of Trp to the aqueous environment upon TFE addition. How can we understand this behavior? The simplest interpretation of the first observation is that TFE inhibits acyl chain adaptation by interfering with the anchoring interactions of Trp with the interface. Under conditions of positive mismatch, the peptide thus behaves similarly as a KALP peptide, which does not have strong interfacial anchoring interactions. However, an explanation for the second observation is more challenging. Why would the peptide tilt less if the bilayer becomes thinner? We will discuss several possibilities to explain the effect of TFE on a molecular level.
One possible explanation is that TFE actively drives the peptide to adopt a more upright orientation because of packing constraints in the interfacial region. The bulky indole rings of Trp require much space in the tightly packed lipid-water interface and partitioning of TFE into this region will reduce the available space even more. Such packing constraints are not present for KALP peptides, which only require the charged amine groups of the lysines to reach the hydrophilic surface of the membrane (7).

A second possible explanation for the decreased tilt involves interference of TFE with specific anchoring interactions of Trp residues with the interface. Properties of the interfacial region that are important for anchoring interactions include the characteristic polarity gradient (44) and the electrostatic properties of the lipid-water interface, which offer possibilities for dipolar and quadrupolar interactions and for hydrogen-bonding (7). Like ethanol, TFE will displace interfacial water molecules and thereby it will change the electrostatic properties and render the polarity gradient at the interface less steep by distributing in a gradient-like manner towards the exterior of the membrane. As a result of these changes, the preference for a specific orientation and localization of the indole groups may become lost, which ultimately may result in a decrease of the tilt angle.
A third possible explanation for the reduction of tilt could simply be that the presence of TFE, which results in a less hydrophilic environment at the interface, might reduce the penalty for mismatch, thereby allowing the peptide to be less tilted. However, in that case one might expect that also the KALP peptides become less tilted, which was not observed.

Influence of TFE on dynamics of the peptide
In principle it is possible to explain the smaller tilt angle, as observed by the ^{2}H NMR studies, by assuming that the presence of TFE in the lipid bilayer results in an increased mobility of the peptides with large fluctuations around average tilt and rotation angles. This would lead to an increased motional averaging of the observed quadrupolar splittings and consequently to an underestimation of the 'true' tilt angle. Besides the results from the fluorescence studies, there are two important reasons why we believe that the observed reduction of the tilt angle of WALP23 in the presence of TFE is not just an artefact due to increased motional averaging. First, such increased motional averaging should lead to a reduction of all the quadrupolar splittings, which is not observed, as illustrated by the effects of TFE on label 19 (see Table 3). Second, if indeed the presence of TFE leads to an increased peptide mobility, one would also expect this apparent reduction of tilt angle to occur for KALP23. We found that the tilt angle of KALP23 is insensitive to high concentrations of TFE (up to 30 vol%; data not shown).
It may be worthwhile to note that even if TFE would lead to an underestimated value of the tilt angle by increasing the motional freedom of WALP23, it clearly does not affect the motional freedom of KALP23. Therefore, independent of the considerations above, this would still support the hypothesis that TFE interferes with the anchoring properties of interfacially localized Trp.

Biological implications
Like ethanol and other short chain alcohols, TFE is believed to act as anesthetic in a lipid-mediated way, although direct interactions with membrane proteins cannot be excluded (45-47). Recently, an attractive mechanism was postulated for a lipid-mediated effect, related to remodeling of the lateral pressure profile of the lipids in the bilayer, which in turn can influence the conformation of the transmembrane parts of membrane proteins (18,22). By using single span α-helical transmembrane peptides, which are expected to be relatively insensitive to changes in lateral pressure profile, we investigated here whether small alcohols can also act by simply interfering with interfacial anchoring properties of membrane proteins. We found indeed that TFE can influence properties of transmembrane peptides and that the effect depends on the

nature of the flanking residues. We propose that TFE may act on transmembrane protein segments specifically through membrane-anchoring residues like Trp or Tyr, by disturbing their interactions with the lipid-water interfacial region. Thus, membrane proteins that are rich in aromatic anchoring residues may be more efficiently affected by the presence of TFE or other small amphiphilic solutes, than proteins of which the transmembrane segments are flanked by charged residues like Arg or Lys.

Recently, it was observed that TFE and other small alcohols can influence the association of oligomeric membrane proteins in a way that is related both to their anesthetic potency and to their lipid disturbing effect (18). Our results suggest that interference with anchoring properties of aromatic amino acids may also be involved in the ability of these small alcohols to dissociate membrane protein complexes (19).

In conclusion, our results emphasize the importance of specific lipid-peptide interactions at the complex lipid-water interfacial region for the organization of proteins and lipids in membranes, and they shed new light on the possible roles of aromatic amino acids as flanking residues in membrane proteins.

Acknowledgments

We thank Hans Meeldijk and Loes Kroon-Batenburg for stimulating discussions about the influence of alcohols on the macroscopic structure of bilayers and we thank Erica Kremer for her help in performing some of the control experiments. We acknowledge Ben de Kruijff for helpful discussions throughout the course of this work.

References

1. Lee, A. G. (2003) Biochim. Biophys. Acta 1612, 1-40
2. Dumas, F., Lebrun, M. C., and Tocanne, J. F. (1999) *FEBS Lett.* 458, 271-277
3. Killian, J. A. (1998) *Biochim. Biophys. Acta* 1376, 401-416
4. Landolt-Marticorena, C., Williams, K. A., Deber, C. M., and Reithmeier, R. A. F. (1993) *J. Mol. Biol.* 229, 602-608
5. von Heijne, G. (1994) *Annu. Rev. Biophys. Biomol. Struct.* 23, 167-192
6. Reithmeier, R. A. F. (1995) *Curr. Opin. Struct. Biol.* 5, 491-500
7. de Planque, M. R. R., Bonev, B. B., Demmers, J. A. A., Greathouse, D. V., Koeppe, R. E., II, Separovic, F., Watts, A., and Killian, J. A. (2003) *Biochemistry* 42, 5341-5348
8. Demmers, J. A. A., Van Duijn, E., Haverkamp, J., Greathouse, D. V., Koeppe II, R. E., Heck, A. J. R. & Killian, J. A. (2001) *J. Biol. Chem.* 276, 34501-34508
9. Davis, J. H., Clare, D. M., Hodges, R. S. and Bloom, M. (1983) *Biochemistry* 22, 5298-5305
10. Webb, R. J., East, J. M., Sharma, R. P. and Lee, A. G. (1998) *Biochemistry* 37, 673-679
11. Ren, J., Lew, S., Wang, J. and London, E. (1999) *Biochemistry* 38, 5905-5912
12. Zhang, Y. P., Lewis, R. N., Hodges, R.S. and McElhaney, R. N. (1995) *Biochemistry* 34, 2362-2371
13. de Planque, M. R. R., and Killian, J. A. (2003) *Mol. Membr.Biol.* 20, 271-284
14. Killian, J. A. (2003) *FEBS Lett.* 555, 134-138
15. de Planque, M. R., Greathouse, D. V., Koeppe, R. E., II, Schafer, H., Marsh, D., and Killian, J. A. (1998) *Biochemistry* 37*,* 9333-9345
16. Strandberg, E., Özdirekcan, S., Rijkers, D. T. S., van der Wel, P. C. A., Koeppe, R. E., II, Liskamp, R. M. J., and Killian, J. A. (2004) *Biophys. J.* 86, 3709-3721

17. Özdirekcan, S., Rijkers, D. T. S., Liskamp, R. M. J., and Killian, J. A. (2005) *Biochemistry* 44, 1004-1012
18. van den Brink-van der Laan, E., Chupin, V., Killian, J. A., and De Kruijff, B. (2004) *Biochemistry* 43, 5939-5942
19. Spelbrink, R. E. J., Kolkman, A., Slijper, M., Killian, J. A. and De Kruijff, B. (2005) *J. Biol. Chem.* 280, 28742-28748
20. Feller, S. E., Brown, C. A., Nizza, D. T., and Gawrisch, K. (2002) *Biophys J.* 82, 1396-1404
21. Barry, J. A., and Gawrisch, K. (1994) *Biochemistry* 33, 8082-8088
22. Cantor, R. S. (1997) *Biochemistry* 36, 2339-2344
23. Cantor, R. S. (2002) *Biophys. J.* 82, 2520-2525
24. Rijkers, D. T. S., Kruijtzer, J. A. W., Killian, J. A., and Liskamp, R. M. J. (2005) *Tetrahedron Lett.* 46, 3341-3345
25. de Planque, M. R. R., Kruijtzer, J. A. W., Liskamp, R. M. J., Marsh, D., Greathouse, D. V., Koeppe, R. E., II, de Kruijff, B., and Killian, J. A. (1999) *J. Biol. Chem.* 274, 20839-20846
26. Ten Kortenaar, P. B. W., van Dijk, B. G., Peters, J. M., Raaben, B. J., Adams, P. J. H. M., and Tesser, G. I. (1986) *Int. J. Pept. Protein Res.* 27, 398-400
27. Rouser, G., Fleisher, S., and Yamamoto, A. (1970) *Lipids* 5, 494-496
28. Van der Wel, P. C. A., Strandberg, E., Killian, J. A., and Koeppe, R. E., II (2002) *Biophys. J.* 83, 1479-1488
29. Davis, J. H. (1983) *Biochim. Biophys. Acta.* 737, 117-171
30. Sternin, E., Bloom, M., and Mackay, A. L. (1983) *J. Magn. Reson.* 55, 274-282
31. Petrache, H. I., Dodd, S. W., and Brown, M. F. (2000) *Biophys. J.* 79, 3172-3192
32. Henzler-Wildman, K. A., Martinez, G. V., Brown, M. F., and Ramamoorthy, A. (2004) *Biochemistry* 43, 8459-8469
33. Rajamoorthi, K., Petrache, H. I., McIntosh, T. J., and Brown, M. F. (2005) *J. Am. Chem. Soc.* 127, 1576-1588
34. Lackowicz, J. R. (1999) *Principles of Fluorescence Spectroscopy*, Kluwer Academic/Plenum, New York
35. Seelig J. (1978) *Biochim. Biophys. Acta* 515, 105-140
36. Burnell, E. E., Cullis, P. R., and de Kruijff B. (1980) *Biochim. Biophys. Acta* 603*,* 63-69
37. de Planque, M. R. R., Goormaghtigh, E., Greathouse, D. V., Koeppe II, R. E., Kruijtzer, J. A. W., Liskamp, R. M. J., de Kruijff, B., Killian, and J. A. (2001) *Biochemistry* 40*,* 5000-5010
38. Holte, L. L., and Gawrisch, K. (1997) *Biochemistry* 36, 4669–4674
39. Lafleur, M., Fine, B., Sternin, E., Cullis, P. R., and Bloom, M. (1989) *Biophys. J.* 56, 1037-1041
40. Abraham, M. H., Chadha, H. S., Whiting, G. S., and Mitchell, R. C. (1994) *J. Pharm. Sci.* 83, 1085-1100
41. Åkerlöf, G. (1932) *J. Am. Chem. Soc.* 54, 4125-4139
42. Hong, D.-P., Hoshino, M., Kuboi, R., and Goto, Y. (1999) *J. Am. Chem. Soc.* 121*,* 8427-8433
43. Mukherjee, L. M., and Grunwald, E. (1958) *J. Phys. Chem.* 62, 1311-1314
44. White, S. H., and Wimley, W. C. (1998) *Biochim. Biophys. Acta* 1376, 339-352
45. Meyer, H. H. (1899) *Arch. Exp. Pathol. Pharmakol.* 42, 109-118
46. Overton, E. (1901) Studien uber die Narkose, Zugleich ein Beitrag zur allgemeinen Pharmakologie. Gustav Fischer, Jena, Germany
47. Dluzewski, A. R., Halsey, M. J., and Simmonds, A. C. (1983) *Mol. Aspects Med.* 6, 461-573

Chapter 5

Molecular Dynamics on Membrane Peptides under Positive Hydrophobic Mismatch: Insights from Long Time Scale Trajectories

Manuscript in preparation

Abstract

A model membrane system consisting of a transmembrane polypeptide in a 1,2-dimyristoyl-sn-glycero-3-phosphocholine (di-C14:0-PC) was investigated by two long time-scale molecular dynamics (MD) simulations. The peptide consisted of the sequence acetyl-$GW_2(LA)_8LW_2A$-NH_2 (WALP23). In particular, we investigated the influence of the peptide on lipid organization, and we analyzed the secondary structure of the peptide, its length and insertion in the lipid bilayer, the tilt and azimuthal angles, and the behavior of the alanine and tryptophan side chains. The data suggest that the peptide is able to order and stretch the lipid acyl chains, consistent with results from experimental ^{2}H NMR studies on WALP23 in di-C14:0-PC with deuterated acyl chains (chapter 4). We observed in one of the simulations after a period of 190 ns the formation of a kink in the α-helical structure on the N-terminus of WALP23 accompanied with anti-snorkeling behavior of the N-terminal tryptophan side-chains, illustrating the importance of interfacial anchoring interactions. The loss of α-helical structure was followed by an increase in hydrophobic length, a reduction of the tilt angle, and the adoption of a rotation angle that is very similar to the one obtained experimentally by ^{2}H NMR on WALP23 with deuterated alanine side chains (chapter 2). However, we observed a large difference between the tilt angles obtained by MD and ^{2}H NMR. This discrepancy may be ascribed to non-optimal MD parameters, and/or too short simulation lengths although we simulated up to 400 ns. A second simulation of 190 ns did not show the occurrence of the kink in the peptide structure and behaved similarly as in the longest simulation before the loss of α-helical structure, which suggests that the orientational and dynamical parameters that stabilize after the kink formation were strongly related to its happening. In addition, the fact that the kink happens only after 190 ns and not in a second simulation raises the questions of how reproducible the event of kinking is, and how long its correlation time, and hence how long MD simulations should be to stabilize to a state that is representative for describing important factors that influence lipid-peptide interactions in model systems.

Introduction

A large variety of cellular processes involves membrane proteins. A majority of these membrane proteins have one or more of their hydrophobic segments crossing the lipid bilayer, and thereby are in contact with the lipid acyl chains and headgroups. Typically, membrane-spanning protein segments consist of an α-helical stretch of 20-22 hydrophobic residues flanked by polar or aromatic residues and approximately matching the hydrophobic thickness of biomembranes (1-6). It has been well documented that the structure and activity of integral proteins can be influenced by the extent of mismatch between the hydrophobic length of transmembrane segments of a protein and the hydrophobic thickness of a lipid bilayer (7-9), whereby also the interactions of the flanking residues with the lipid-water interface can play an important role (10,11).

In order to study how the structural and/or dynamic properties of membrane proteins are influenced by the interactions with the surrounding lipids, several groups used designed α-helical peptides that mimic the transmembrane segments of proteins in synthetic lipid bilayers (10-18). Examples are the so-called WALP peptides, which are composed of leucine-alanine repeats with variable lengths that are flanked on both sides by Trp residues, respectively (13,14). These peptides were used to investigate

the role of interfacial interactions in membrane organization by studying the consequences of the hydrophobic mismatch between the hydrophobic lengths of the peptides and lipid acyl chains (13,14).

In the case of WALP peptides that have a hydrophobic length longer than the hydrophobic thickness of the lipid bilayer (i.e. positive mismatch) a variety of responses to mismatch was observed. ^{2}H NMR experiments on acyl chain deuterated diacylphosphatidylcholine (PC) lipids showed small but systematic increases in acyl chain order indicating a stretching of the lipids with increasing mismatch (10,19). ^{2}H NMR experiments on the 23-amino acids long peptides WALP23 that were deuterated on alanine side chains demonstrated in addition small but systematic increases in tilt angle of WALP23 with increasing hydrophobic mismatch (Chapter 2). In addition, a study based on NMR methods and hydrogen/deuterium exchange in combination with mass spectrometry suggested that WALP23 has strong interfacial anchoring interactions, which are modulated by the flanking Trp-residues (10).

Over the last decade many different properties of model systems of WALP peptides in lipid bilayers have been characterized using different spectroscopic techniques. However, systematic analysis of all potentially important parameters using experimental methods is difficult because most techniques enable investigation of only one or few aspects at a time. In the case of molecular dynamics (MD) studies, a complete description of the system is obtained including not only structural properties, but also the dynamics and energetic parameters, albeit on relatively short times scales.

In an earlier MD study on WALP peptides of variable length in PC bilayers of different thickness (20), it was found that the bilayer thickness increases monotonically with increasing length of the WALP peptides, and that the peptides tilt in response to hydrophobic mismatch. Although the tilt angles were found to correlate with an earlier experimental study using infrared spectroscopy (21), these findings are not in agreement with results obtained more recently for WALP23 and the four-residue shorter WALP19 by ^{2}H NMR, which is considered to be a more reliable technique for analysis of peptide tilt angles (Chapter 2 and ref. 22). In addition, the simulations were run only for 1.5 ns. Due to the extraordinary development of computational calculation capacities over the last years, much longer simulation times on model membrane systems are nowadays easily amenable, as exemplified by the recent work of Kandasamy and Larson (23). In this study the influence of hydrophobic mismatch was investigated on analogous Lys-flanked (KALP) peptides of variable length in PC-bilayers of different hydrophobic thickness, reaching time scales of 50 to 200 ns. The use of these relatively long time scales enabled the analysis of dynamical parameters that were only observable after tens of ns.

In the present study we used long time scale simulations to analyze a system of a WALP peptide in a di-C14:0-PC bilayer at a peptide to lipid molar ratio of 1 to 100, which corresponds to a situation wherein no spontaneous peptide aggregation occurs in experimental studies (24). The system represents a situation of positive though small hydrophobic mismatch that is very well characterized experimentally. It thus allows for comparison with experimental studies as well as with the above-mentioned work on KALP peptides. In addition it allows comparison with recent studies using an implicit membrane generalized Born model and replica-exchange (25) in a system that has a hydrophobic thickness corresponding to a di-C14:0-PC bilayer (21). Also in this latter study a much larger tilt angle was obtained than determined by ^{2}H NMR. However, the implicit character of such MD models does not enable for detailed description of the lipid-peptide interactions.

The results show an increased order of the acyl chains and of the bilayer thickness of the di-C14:0-PC bilayer due to the presence of WALP23, which decreases with the distance from the peptide. After almost 200 ns of simulation the α-helical secondary structure of WALP23 was perturbed drastically by the formation of a kink at the N-terminus. The azimuthal rotation angle of the peptide (i.e. the direction in which WALP23 tilts) stabilized after the appearance of the kink to a value similar to the one determined by ^{2}H NMR (chapter 2). However, the tilt angle of the peptide obtained by MD was found to be larger than determined by recent ^{2}H NMR studies.
These results together with further observations help to rationalize structural and dynamical parameters involved in lipid-peptide interactions in model membranes.

Methods

Molecular dynamics

Pure lipid systems

Molecular dynamics (MD) simulations were performed with GROMACS 3.2.1 (26-28). First, the simulations were run with pure bilayers using the parameters of Berger (29), surrounded by Single Point Charge (SPC) water (30). The starting lipid structures and parameters were taken from the website of Peter Tieleman's group (http://moose.bio.ucalgary.ca/index.php?page=Downloads). The simulation box originally consisting of 128 di-C14:0-PC lipid molecules (64 in each leaflet) and 3655 water molecules was cut at each edge in order to have 118 lipids (59 in each leaflet), which gave 3274 water molecules (or 27-28 water molecules per lipid). The system was then energy minimized and a production run was done for 10 to 50 ns.

WALP23 lipid systems

For the simulations of the peptide/ lipids/water systems we used the so-called 'ffgmx' force field derived from GROMOS87 force field (31), that is usually used for peptides/proteins in conjunction with the Berger lipids (29). First, the peptide was constructed in a perfect α-helix of sequence acetyl-$GW_2(LA)_8LW_2A$-NH_2 (ϕ = -57° ; ψ = -47°) and minimized with a few steps of steepest descent. We took a structure of equilibrated bilayer of di-C14:0-PC (after 10 to 50 ns) in which a hole was created by removing 18 lipids in the center (9 from each leaflet) resulting in a system of 100 lipids. The peptide was then vertically inserted within the bilayer (i.e. along the z-axis, which almost perfectly coincides with the bilayer normal) by adjusting the center of mass of this latter with that of the bilayer. We thus obtained a system consisting of one WALP peptide, 100 lipids and 3274 water molecules (32-33 water molecules per lipid) for a total of 14,652 atoms. After a few steps of steepest descent, a 10 ns equilibration was performed by holding the peptide fixed with some position restraints of 1000 $kJ.mol^{-1}.nm^{-2}$ on each heavy atom, while lipids and water molecules were allowed to move freely. For the production runs, the position restraints were then removed and simulations of 190 to 400 ns were performed.
In all simulations, periodic boundary conditions were applied. A 2 fs time step was used for the leap frog algorithm integration. All bonds were constrained by using the LINCS algorithm (32) and the water molecules were kept rigid using the SETTLE algorithm (33). The initial velocities were generated at the wanted temperature following a Maxwellian distribution. The simulations were done under the NPT ensemble using the weak coupling method of Berendsen for both temperature and pressure (34). For the pressure, semi-isotropic coupling was used. The peptide, lipids

and solvent molecules were coupled separately to a temperature bath with a time constant of 0.1 ps. The pressure was coupled to an external bath at 1 bar with a time constant of 1.0 ps and a compressibility of 4.5×10-5 bar^{-1}. For the electrostatics, we used two techniques to take into account the long range interactions (beyond the cut-off). First, we used a generalized reaction field (RF) (35) with a 1.0 nm cut-off for the van der Waals interactions and the non bonded list was updated every 10 steps. Beyond the 1.0 nm cut-off, a dielectric constant of 54 was chosen (36,37). Other simulations using the Particle Mesh Ewald (PME) (38,39) were also done with a cut-off of 1.0 nm for the electrostatics, a Fourier spacing of 0.12 nm for the FFT grid and an order of 4 for the interpolation of charges between points of the grid; for these simulations, the Van der Waals interactions and the non-bonded list were treated in a similar way as for the RF simulations. The simulations were performed in both RF and PME conditions in order to provide these simulations with a mutual control experiment and due to the fact that a PME treatment of electrostatics requires more computational time due to scaling problems. In addition, although it is quite common to realize MD simulations of membrane systems using PME conditions, Anezo et al. (2003) showed that lipid parameters obtained by applying RF are in very good agreement with results obtained by PME (40).
The simulations were performed in parallel on a LINUX cluster (Intel Xeon 2.4 GHz processors) or on Power4 P690 CPUs (1.3 GHz) at the french national supercomputer center IDRIS (Orsay). As a CPU cost indication, 1 ns took about 6 h for the simulations using RF on our LINUX cluster on 4 CPUs, and ~ 8h for the PME simulations on 16 CPUs at IDRIS, for a total of time of approximately 160 CPU days.

Trajectory analysis

Almost all the analyses were done using the programs within the GROMACS package, except for the tilt angle, as well as the angle between each Trp ring and the normal to the membrane. For the tilt, a specific program was developed in C within the GROMACS package, which allowed us to read directly the compressed trajectories (in the xtc format). Basically, we first calculated the helix axis by taking the first eigenvector of the inertia matrix (defined by the heavy atoms of the backbone). Unless stated otherwise, we used the sequence defined from Trp3 to Trp21. The normal to the membrane was calculated by taking the third eigenvector of the inertia matrix defined by all phosphorous atoms (the first two eigenvectors basically define the best plane containing all phosphorous atoms). Similar results were obtained when, as an alternative the Z direction was directly used as the normal to the membrane. For the angle between a given Trp ring and the normal to the membrane, we used a similar approach as for the tilt angle: the normal to the Trp ring was determined as the third eigen vector of the inertia matrix considering each heavy atom of the ring; for the normal to the membrane, we used the same procedure as for the tilt. In general, the statistic analyses are accompanied by the estimated standard deviation around the average values, which represents the extent of fluctuations. In the specific case of the tilt angle and rotation angle analyses, the averages are calculated over a range of ± 5 ns.

Fitting simulated d_3-Alanine ^2H NMR quadrupolar splittings to a tilted α-helix

The methyl side chains of the alanines were treated as they were deuterated. The calculations of the ^{2}H NMR quadrupolar splittings ($\Delta\nu_q$, kHz) from the simulations of the eight alanine positions comprised between the Trp-residues were based on the C^α-

$C^{\beta}H_3$ bond coordinates, which correspond to the ^2H NMR signals that would arise from the deuterons of the alanine side-chain methyl group in NMR experiments (Chapter 2) if those would be deuterated. The $\Delta\nu_q$-values were calculated from the equation:

$$\Delta\nu_q = \tfrac{3}{4} \cdot K(3\cos^2\theta - 1) \quad (1)$$

where θ is defined as the angle between the magnetic field and the C^{α}–C^{β} bond of the alanine (22). The constant K is defined as:

$$K = (e^2qQ/h)S \quad (2)$$

where e^2qQ/h is the quadrupolar coupling constant and S is an order parameter that accounts for molecular motion. In this study a K value of 49 kHz was used corresponding to S = 0.875, as in the ^2H NMR studies we refer to (22).
In order to fit the simulated ^2H NMR quadrupolar splittings to a tilted α-helical model peptide, we used the next equation:

$$\Delta\nu_q = \tfrac{3}{4} \cdot K(3\cos^2 \in_{\parallel} (\cos\tau - \sin\tau \cdot \cos\delta \cdot \tan \in_{\parallel})^2 - 1) \quad (3)$$

The tilt angle τ is defined as the angle between the peptide helical axis and the bilayer normal and $\in_{\parallel}$ is the angle between the peptide helix axis and the C^{α}-$C^{\beta}D_3$ bond vector. δ is the rotation angle of the labeled bond vector around the helical axis with respect to the direction of the tilt and is related to the azimuthal angle ρ of WALP23 by:

$$\delta = \rho + \in_{\perp} + \varphi \quad (4)$$

where $\in_{\perp}$ is the angle of the C^{α}-$C^{\beta}D_3$ bond vector with respect to a vector from the C^{α} to the peptide axis, and φ is the pitch angle between both C^{α} of the reference Gly1 and C^{α} of the labeled residue in the peptide. The values of $\in_{\perp}$ and φ were similarly used as in Chapter 2 and 3.
The angle ρ was varied in order to minimize the root mean square deviation (RMSD, kHz) between MD-simulated and calculated $\Delta\nu_q$-values (equation 3) for discrete values of τ and $\in_{\parallel}$ as in (Chapter 3). The fitting procedure was based on eight $\Delta\nu_q$-values (unless otherwise stated) of the alanine positions in the central Leucine-alanine stretch using an in-house computer program written in C.
In order to be able to assign positive or negative values to the ^2H NMR quadrupolar splittings, experimental tilt, and rotation angles were used in the equation that determines the expected quadrupolar splitting arising from a ^2H-labeled alanine in a regular α-helix as described in (Chapter 2).

Results

Pure lipid systems and WALP23/lipid systems were investigated in the presence of excess of water (see methods). The simulations were performed with both the reaction field (RF) and the particle mesh Ewald (PME) for the treatments of electrostatic

interactions, giving generally very similar results concerning the lipid parameters. However, we will generally present the results focused on our longest simulation, which was performed under semi-isotropic and RF conditions and was by far the longest (400 ns). The results will be compared to those obtained in the PME simulation only in the discussion to illustrate the importance or reproducibility of specific events.
We will first present the results of the effect of WALP23 incorporation on the lipids, and we will then focus on the effect of the lipids on the conformation and orientation of WALP23 within the membrane.

Influence of WALP23 on the lipids
Experimental parameters that are often used for describing the structure of a lipid bilayer are the ^{2}H NMR order parameters of the acyl chains and the bilayer thickness. These parameters are interrelated structural properties of lipid bilayers. Our molecular dynamic simulations provided us a way to investigate these parameters independently from each other, and to compare systematically our results to experimentally determined data (see Chapter 4).

^{2}H NMR order parameter
The ^{2}H NMR order parameter profiles for the *sn*-2 chain methylene deuterons in positions 2 to 14 in the absence of WALP23 of either the RF or PME simulations (data not shown) were very similar. The results for the RF simulations with and without peptides are presented in Figure 1, where the two solid lines indicate simulated order profiles of pure lipids (open circles) and the lipid bilayer including WALP23 (open squares). In both cases a plateau region characterizes the order profile of the lipids, indicating a relatively high chain order near the bilayer interface, which is followed by a rapid decrease towards the end of the acyl chain in the core of the bilayer. The introduction of WALP23 in the lipid bilayer at a 1 to 100 peptide to lipid molar ratio increases the order parameters with respect to those in the pure di-C14:0-PC bilayer.
We then compared the simulated order parameters to experimental data of the corresponding systems plotted as dashed lines (Chapter 4). Although the order parameters of our simulations with and without peptide incorporated are in general slightly lower than in ^{2}H NMR experiments, the shape of the curves is rather similar with a plateau region for the upper methylenes, and a comparable decrease of order towards the center of the bilayer converging to similar values for both the experimental study and our simulations. Also, in both cases incorporation of WALP23 leads to an increase in chain order. In the simulations this is slightly less than in the experimental study, but this may be expected due to the lower peptide to lipid molar ratio of 1/100 in the simulations as compared to the 1 to 30 peptide to lipid molar ratio in the experiments.

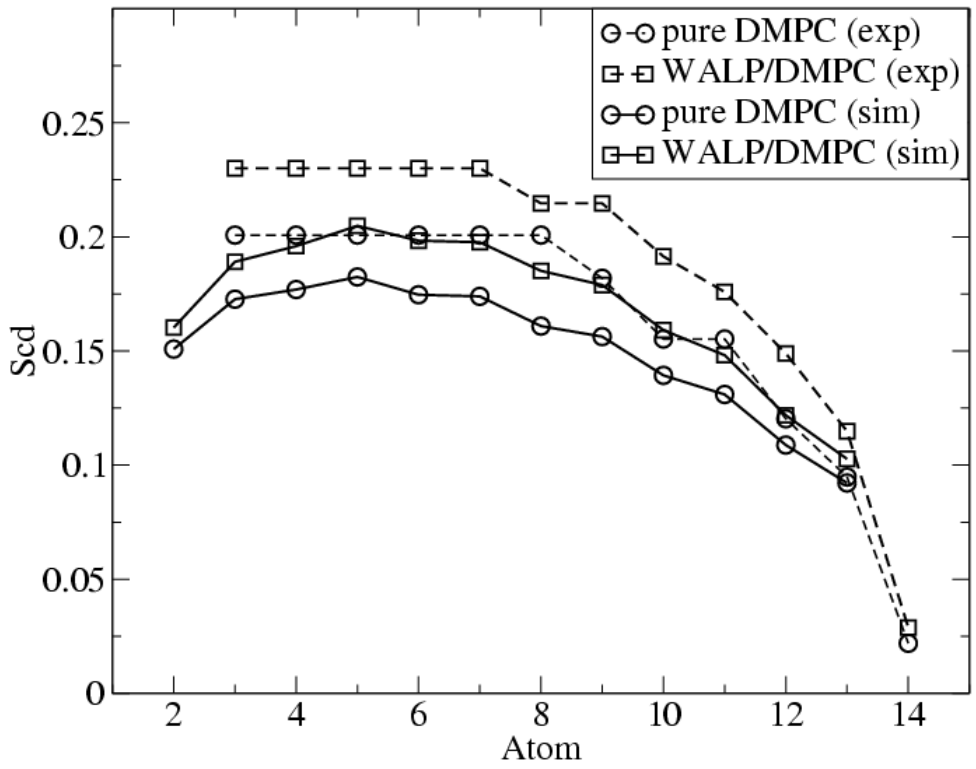

Figure 1. ^{2}H NMR order parameter profiles of the *sn*-2 myristoyl chain of di-C14:0-PC for both simulations (solid lines) and experiments (dotted lines) in the absence (circle shapes) and in the presence (open squares) of WALP23 in the bilayer. Note that molecular dynamics can simulate the carbons only from C2 to C13, whereas the experimental approach allowed for plotting the order parameters from C3 to C14. Experimental data are taken from Chapter 4 and were measured at a 1/30 (P/L) ratio, while the MD simulation of the peptide-lipid system was at a 1/100 ratio.

Bilayer thickness

Table 1 summarizes the bilayer thickness obtained with and without peptide in the bilayer, as average distance both between the carbonyl carbon atoms of the acyl chains (41) and between its nearest methylene neighboring group (carbon number 2) from one leaflet to the other (13,23).

An estimate of the bilayer thickness as defined by the average distance between the carbonyl groups of each leaflet (i.e. between C1 atoms of both the *sn*1 and the *sn*2 chains) can be determined experimentally by using ^{2}H NMR experiments (41). In this way, we see in Table 1 that a pure di-C14:0-PC bilayer gives a value of 25.6 ± 0.5 Å (*sn*1 and *sn*2 average C1 position), which is very similar to the experimental 25.0 Å (Chapter 4) from which the error estimate may probably overlap with the error range of our simulation value.

Introduction of WALP23 at a peptide to lipid molar ratio of 1 to 100 only increases the thickness of the bilayer from 25.6 Å to 25.9 Å. When we calculate the bilayer thickness in the proximity of the peptide (i.e. within a radius of 18 Å around the center of mass of the peptide), the thickness increases to 26.5 Å. Considering that these conditions would correspond to a peptide to lipid molar ratio of approximately 1 to 30, as in the ^{2}H NMR experiments, this is almost exactly the experimental value. Distant lipids (i.e. above the region of 18 Å from the center of mass of the peptide)

adopt a bilayer thickness of 25.6 Å as in the simulation without peptide. When the bilayer thickness is expressed in terms of distance between the carbons of the first methylenes (C2) of the acyl chains of opposing leaflets, similar effects are observed upon the incorporation of WALP23 (Table 1).

Table 1. Average bilayer thickness of di-C14:0-PC or di-C14:0-PC/WALP23 systems.

	Reference carbons	Pure lipids	Lipids + WALP23	Lipids + WALP23 (close lipids)	Lipids + WALP23 (distant lipids)
Simulation	*sn*1 & *sn*2 C1 average position	25.6 Å (± 0.5)	25.9 Å (± 0.5)[a]	26.5 Å (± 0.9)[c]	25.6 Å (± 0.6)[d]
	*sn*1 & *sn*2 C2 average position	23.3 (± 0.5)	24.1 Å (± 0.5)[a]	24.8 Å (± 0.9)[c]	23.9 Å (± 0.6)[d]
Experimental ^{2}H NMR	*sn*1 & *sn*2 C1 average position	25.0 Å	26.4 Å[b]	-	-

[a] Peptide-to-lipid molar ratio of 1 to 100 averaged from 20 to 400 ns from the RF simulation.

[b] Peptide-to-lipid molar ratio of 1 to 30 (Chapter 4).

[c] Thickness determined for lipids that are within 18 Å from the center of mass of the peptide averaged from 20 to 400 ns from the RF simulation.

[d] Thickness determined for lipids that are beyond 18 Å from the center of mass of the peptide averaged from 20 to 400 ns from the RF simulation.

Influence of the lipids on the structure of the peptide

In the following, we will show the influence of the lipids on the structure, energy of interactions of the amino acids, and on the tilt and rotation angles of WALP23 within the membrane. Finally, we will describe the behavior of the side chains of the tryptophans.

Secondary structure

WALP23 was reported to be highly α-helical in di-C14:0-PC based on circular dichroism analysis and supported by two ^{2}H NMR studies (42) and Chapter 2 and Chapter 3). Indeed, during the first 190 ns, WALP23 adopted an α-helical conformation as illustrated in the snapshot of the simulation at 30 and 63 ns (Figure 2, A and B). The peptide experienced also large fluctuations in the tilt angle. After 190 ns of simulation, the structure lost some α-helicity on the N-terminus side with the formation of a kink in the structure (Figure 2, C and D). This kink remained present till the end of the simulation. As we can see from the snapshots of the structure after 289 and 400 ns of simulation, the axis of the backbone is bent on the N-terminal side disrupting the overall straight "rod-like" geometry of the α-helix structure in contrast to the regular structures at 30 and 63 ns. We can also see that the N-terminal Tryptophan 2 residue is buried deeper in the bilayer than without a kink in the structure by comparing the kinked structures in panel C and D with the structure in panel A and B. Another observation was that in general, after the occurrence of the kink, smaller tilt angles were more often visited than before the kink formation (illustrated in Figure 2C).

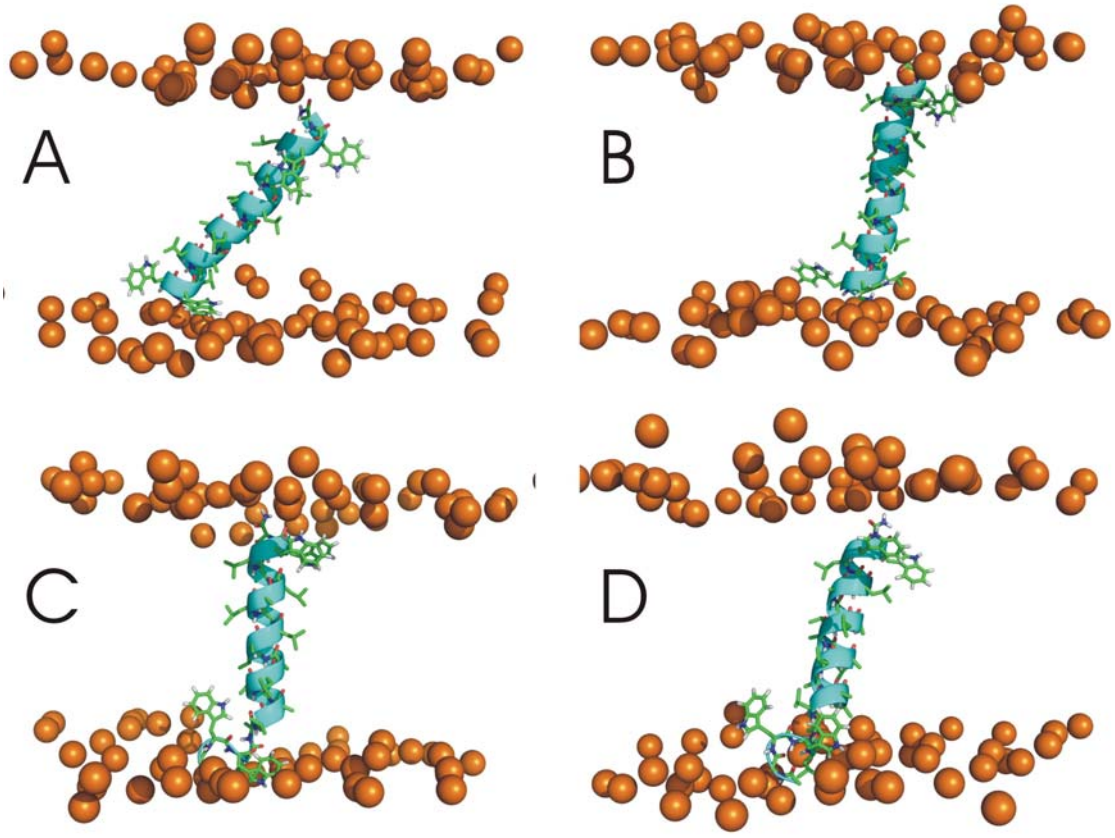

Figure 2. Snapshot of WALP23 in a di-C14:0-PC bilayer at different stages during the 400 ns semi-isotropic RF simulation. The system is represented at 30, 63, 289, and 400 ns in panel A, B, C, and D, respectively. The peptide backbone is represented in cartoon, the peptide bonds are drawn as sticks. The flanking tryptophans are clearly visible; to give an idea of the bilayer plane phosphorus atoms are depicted as Van der Waals spheres. A kink appears on the N-terminal side represented below here. This snapshot was rendered with the PyMOL program (W. L. DeLano, The PyMOL Molecular Graphics System, 2002, http://www.pymol.org).

The detailed secondary structure analysis of WALP23 in our di-C14:0-PC system is depicted in Figure 3, where the different conformations are reported as lines with different levels of darkness. In general the central leucine-alanine stretch is highly α-helical except for Leu4 and Ala5, which are quite unstable in their secondary structure forming together with the N-terminal Trp-residues a kinked region of the peptide. The secondary structure of the anchoring Trp-residues is rather unstable especially on the N-terminal side of the peptide. The Gly1 and Ala23 ends do not adopt a regular secondary structure.
The kink together with the changes in secondary structure will affect the length of the peptide and thereby the extent of hydrophobic mismatch. This will be discussed in the next paragraph.

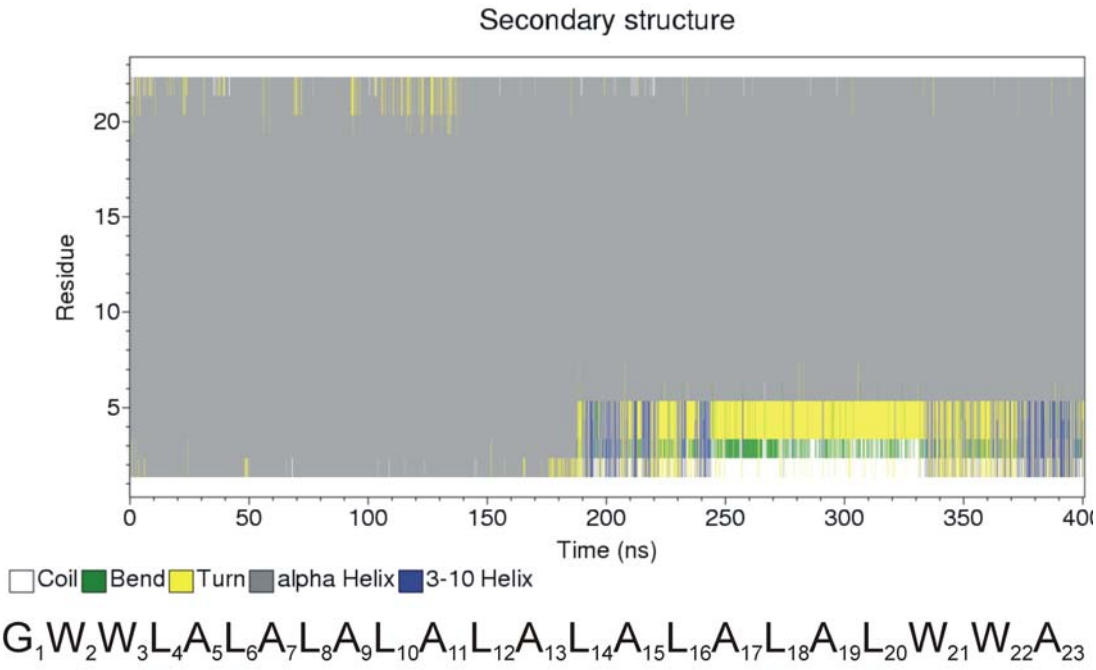

Figure 3. Evolution of secondary structures along the trajectory. The sequence with corresponding residue numbers are indicated below the diagram.

Hydrophobic length of WALP23

The peptide length was typical of an α-helix with an overall rise per residue of 1.5 Å up to 190 ns when the kinked structure was formed. When the kink appeared, the rise per residue remained constant only from Ala5 to Trp22, the remaining on the N-terminal side showing an irregular and non-linear increase in length along the peptide long axis. We analyzed the length of WALP23 along the whole trajectory and estimated the extent of hydrophobic matching based on the bilayer thickness obtained by our molecular dynamics simulations.

Figure 4 shows the graphs of the distance of the C^{α} of each residue from the C^{α} of the Gly1 residue. The distance is estimated along the α-helical axis. The solid line represents the length of a perfect α-helix, whereas the circles and the crosses correspond to the length of WALP23 before and after the kink, respectively. As expected the plot for the non-kinked structure is very similar to the case of a perfect α-helix with a length of 24.1 Å ± 0.5 from Leu4 to Leu20, which corresponds to a 1.5 Å rise per residue. The Leu4-Leu20 fragment is commonly used as the reference for the hydrophobic length of model peptides (13,20,23). In the case of the kinked structure, the distance between the C^{α}'s of Leu4 and Leu20 was 25.9 ± 0.4Å, which was slightly longer than either Trp3-Leu20 or Trp2-Leu20. This suggests that the N-terminal tryptophans may be inserted deeper in the membrane than Leu4. When the vector that links the C^{α}'s of Leu4 and Leu20 is projected onto the z-axis (coinciding with the bilayer normal) the distance between both residues is 24.0 Å ± 1.1 after the occurrence of the kink, which matches the hydrophobic thickness of the bilayer (24.1 Å ± 0.5; see Table 1). This reinforces the idea that using the inter-leaflet distance between the C2-methylenes is appropriate to specify the hydrophobic bilayer thickness.

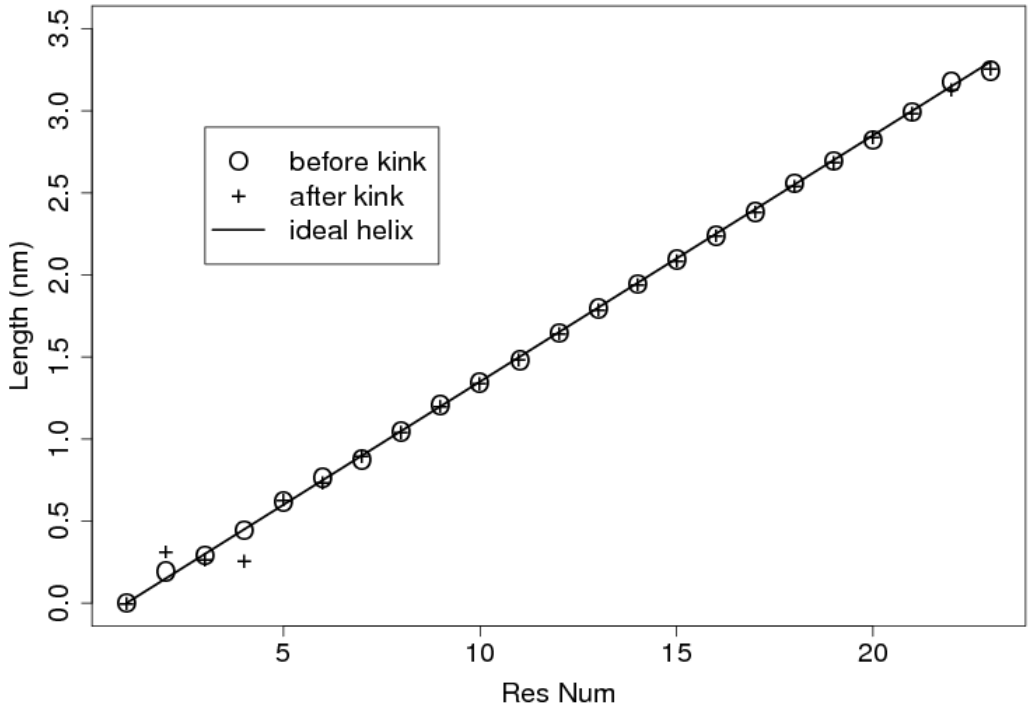

Figure 4. Projection of the distance in Å along the α-helical axis between the C^{α}'s of residues along the sequence of WALP23 and Gly1. The x-axis indicates the residue numbers.

Insertion depth of WALP23 in di-C14:0-PC

The fact that the length of the WALP23 segments starting from the N-terminal Trp-residues is shorter than fragments starting from Leu4 implies that the peptide is accommodated in the membrane in such a way that Trp2 and Trp3 are buried even further away from the aqueous phase than Leu4. This can also be seen in the density profile in Figure 5. The Trp2, Trp3, and Leu4 density lines are indicated by arrows in the picture. In the case of the C-terminal residues, the Leu20 is as expected inserted deeper in the membrane than the aromatic flanking residues.

Another interesting feature of the density profile is that the C-terminal side of the peptide is more inserted in the bilayer (see legend). This can be clearly seen from the two external peaks. The peak that is the most on the left corresponds to the C-terminal part (at ~ -10 Å) and is closer to the bilayer center (at 0 nm) than the furthest peak on the right corresponding to the N-terminal part (at ~ 14.5 Å).

In addition, even though we can observe that Trp2 is as deeply inserted as Trp21 and Trp22, the average insertion of the Trp-residues on the N-terminal is shallower due to the position of Trp3. These results are consistent with previous observations using fluorescence spectroscopy that the C-terminal flanking Trp-residues of WALP23 are exposed to a more hydrophobic environment than on the N-terminal side, and from ESR measurements, suggesting that the peptide is slightly shifted with respect to the middle of the membrane (24,43,44).

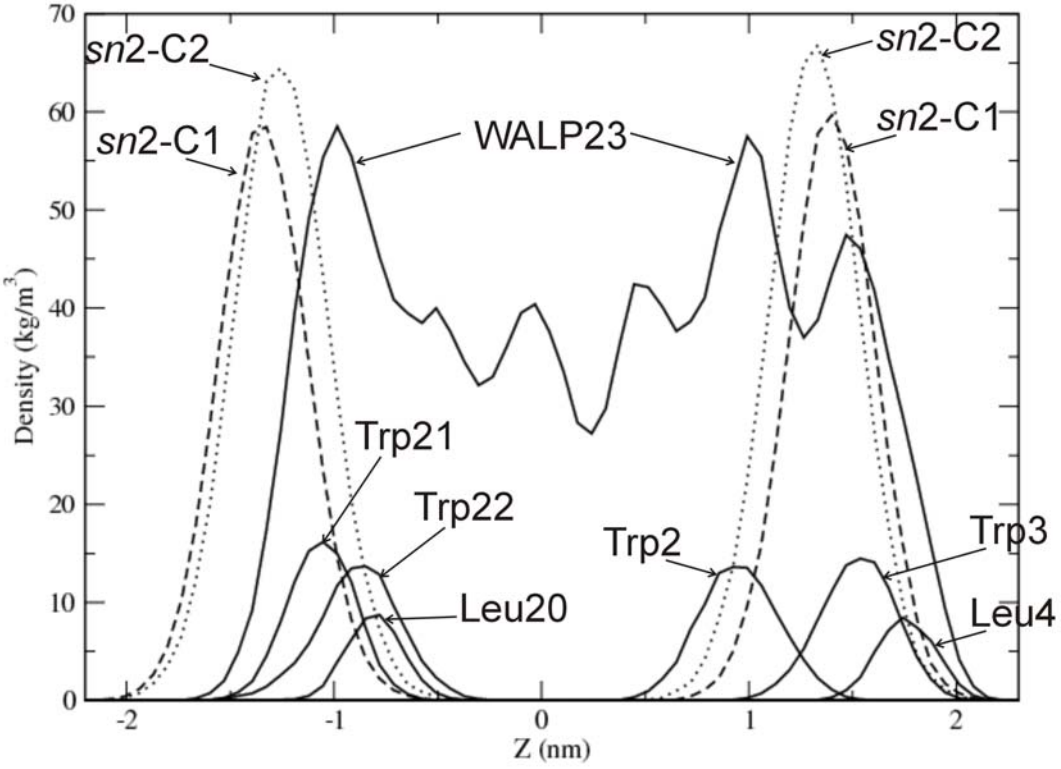

Figure 5. Density profiles of different groups of the di-C14:0-PC/WALP23 system after the apparition of the kink (from 190 ns to 400 ns). The different amino acids and the lipid groups are indicated by arrows and legends in the picture. Note that for each amino-acid trace (the various Trp and Leu), only the side chain was used to evaluate the density, while for the trace 'WALP23' all the atoms (backbone + side chains) of the peptide were taken into account.

Tilting of WALP23: a consequence of hydrophobic mismatch?

The hydrophobic length of the peptide (25.9 Å ± 0.4) is longer than its projection along the normal to the bilayer (24.0 ± 1.1 Å) implying a non-zero tilt angle and the value of the projection along the bilayer normal is very close to the hydrophobic thickness of 24.1 Å ± 0.5 (Table 1; C2 used as a reference of opposite leaflets). Thus, it seems that the energetically unfavorable situation of a positive mismatch resulting from the hydrophobic length of WALP23 being larger than the hydrophobic thickness of a di-C14:0-PC bilayer is compensated by a significant tilt angle of the peptide. For the kinked peptide after 190 ns of simulation, the tilt angle of 24.5° ± 7 was determined by using the coordinates of the vector defining the α-helix on the fragment Ala7-Trp22, which excludes the kinked part of the structure. When we compare this value to the one obtained by ^{2}H NMR (i.e. 5.5°; chapter 2) there is an significant discrepancy. A possible explanation could be related to the difference in approach to calculate the tilt. The ^{2}H NMR approach makes use of the ^{2}H NMR quadrupolar splittings of side chain labeled alanine residues and fits the data to the geometry of a tilted regular α-helix. Therefore, we also calculated the tilt angle of WALP23 from the ^{2}H NMR quadrupolar splittings as back calculated from the simulation (See Methods), using a similar fitting procedure as in chapter 2. By this approach, we obtained a tilt angle of 26.4° (± 8.7). This value was slightly reduced to 23.3º (± 7.4) if residue Ala5 was omitted. Because of the kink formation, and hence

the loss of α-helicity at the level of Ala5, in the following part a definition is used that discards Ala5 from the calculations, unless otherwise stated.

Figure 6 shows the evolution in time of the tilt angle as measured by defining the α-helical axis from the peptide coordinates in the simulation box and by fitting the simulated ^{2}H NMR quadrupolar splittings of deuterated alanine. We observe in the first part of the curve relatively high tilt angles with some fluctuations: 31.4° (± 3.8) until approximately 190 ns, which corresponds to the appearance of the kink as indicated by the vertical dashed line. After the kink formation, the tilt angle decreases significantly to the value mentioned above. Before the kink formation, the direct tilt angle is larger than the fitted value, whereas the values are very similar after 190 ns. The difference between directly calculated tilt angles and fitted values can be due to deviations from ideal α-helical geometry or due to averaging of the ^{2}H NMR quadrupolar splittings. In the range of the angles of the deuterated bonds that are measured, the ^{2}H NMR quadrupolar splittings are sensitive to the rotation angle of the peptide (See chapter 1). This sensitivity is stronger at larger tilt angles. Therefore, large fluctuations around the average rotation angles of the peptide could reduce the ^{2}H NMR quadrupolar splittings significantly, thereby leading to an underestimation of the tilt angle when it is estimated by the fitting procedure. In the simulation, fluctuations around the average of the rotation angle are observed of ± 20º and ± 12º before and after the kink formation, respectively. When the influence of such fluctuations is tested on the tilt angle as calculated directly from the orientation of the defined α-helical axis, we indeed find back similar tilt angles as obtained by fitting the simulated ^{2}H NMR quadrupolar splittings. However, these fluctuations around the average rotation angle are too small to explain the discrepancies between experimental values obtained by ^{2}H NMR (Chapter 2) and simulated values obtained in the present work.

Since the fitting procedure is independent of the definition of the α-helix axis, and because a kinked structure was observed, we preferred the use of the fitting procedure to obtain the tilt angles. This procedure has the additional advantage that it is more convenient for the determination of the rotation angles (see next). In addition, the use of the ^{2}H NMR quadrupolar splittings is the best way to compare our results with the experimentally obtained ^{2}H NMR data (Chapter 2). Therefore, we also analyzed the evolution of every ^{2}H NMR quadrupolar splitting that would arise from a ^{2}H-labeling of the side chains of alanines as in the experimental study of WALP23 in PC-bilayers (Chapter 2). The quadrupolar splittings for each alanine are plotted in Figure 7 as bar graphs, representing the distribution of ^{2}H NMR quadrupolar splitting values that were adopted during the whole length of the simulation.

In general, the simulated ^{2}H NMR quadrupolar splittings converge rather quickly to an equilibrium value except in the case of Ala5 and Ala7 that are located near to or in the kinked region of the peptide but which values converge rapidly to their equilibrium after the formation of the kink. The distribution of the quadrupolar splittings in the simulations is clearly different before (grey bars) and after the kink (white bars), in particular for residues 7, 11, 15 and 19, which are on the same face of an α-helical wheel (See Figure 2 in Chapter 2). If simulated and experimental (vertical lines) values after the kink formation are compared from Figure 7, we see in general very large discrepancies, the absolute value of the simulation values being much larger. However, we notice that the trend of the ^{2}H NMR splitting values between experiments and simulations after the kink formation is similar. Indeed, alanine positions that are on one face of the α-helical wheel, 5, 9, 13, and 17 have

simulated values that are on the left side of the vertical lines (experimental values) on the graphs, whereas positions 7, 11, 15, and 19 on the other face of the helix are mostly on the right of the vertical lines. Similarly, experimental values for positions 5, 9, 13, and 17 have splittings on the left side of the values obtained experimentally for positions 7, 11, 15, and 19, which correspond to the other face of the peptide. This indicates that the direction in which WALP23 in the simulation will tilt after kink formation is the same as determined by experiments (Chapter 2). This will be further discussed in the paragraph about the rotation angle.
We conclude that the large discrepancies between the experimental and simulated values after the kink are mainly due to a larger tilt angle in the simulations. This larger tilt angle increases the sensitivity of the ^{2}H NMR quadrupolar splittings to the position around the α-helical wheel especially in the region at which the Alanine side chains at position 7, 11, 15 and 19 are located, which would explain the wide range of values observed for these residues.

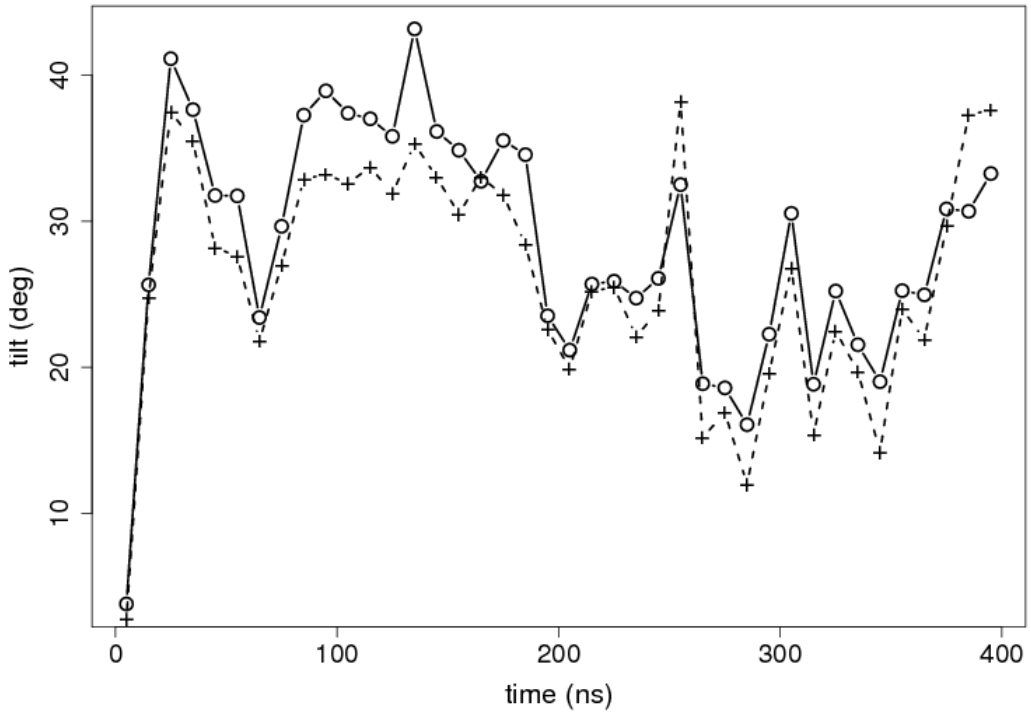

Figure 6. Tilt angle as measured by defining the α-helical axis from the peptide coordinates in the simulation box (solid line) and by fitting the simulated ^{2}H NMR quadrupolar splittings of deuterated alanine (dashed line). The vertical dotted line indicates the simulation time of 190 ns when the structure started to kink. Data points on this graph are averages of the tilt angle over a range of ± 5 ns for each point.

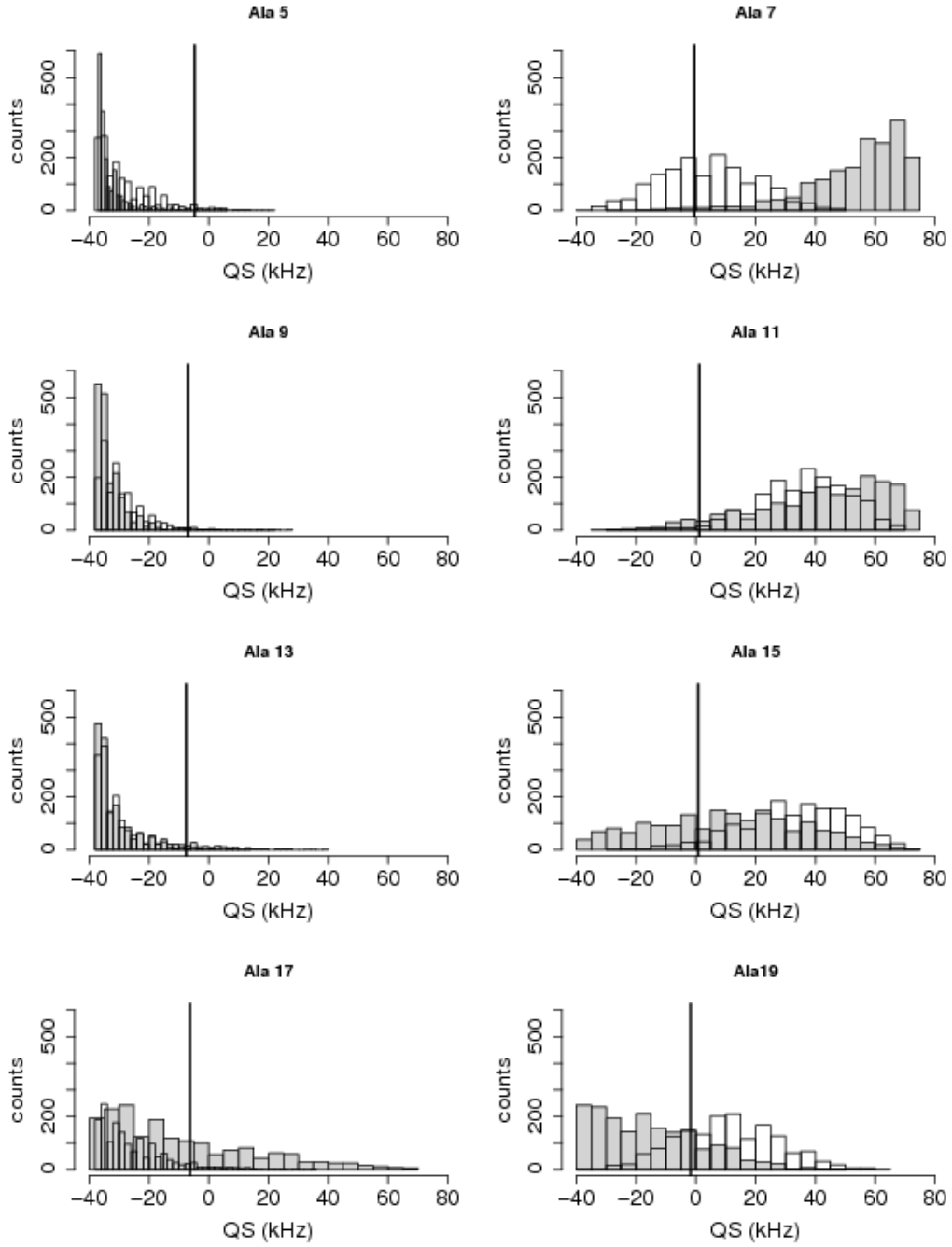

Figure7. Distribution of simulated ^{2}H NMR quadrupolar splittings for the ^{2}H-labeled side chains of alanines. The vertical line represents the experimental value. The grey and white bars are the results obtained before the appearance of the kink and after, respectively. Note that ^{2}H NMR values can also be negative.

Rotation angle and the side-chains conformation of Alanines

Next, we used the ^{2}H NMR data to analyze the time course of the rotation angle using the same reference 0º rotation angle as in Chapter 2, and the ^{2}H NMR quadrupolar splittings obtained by the simulations. The result of the RF simulation is depicted in Figure 8 for the complete trajectory. Interestingly, we see that the rotation angle average of 116° (± 20) before kink converged to 166° (± 12) after the kink formation

in at 190 ns, which is very similar to the experimental 158º azimuthal angle (Chapter 2). This suggests that the formation of the kink in the α-helical structure may be necessary to reproduce experimental conditions or alternatively that reaching the right rotation angle has a relaxation time of a few hundreds of nanoseconds.

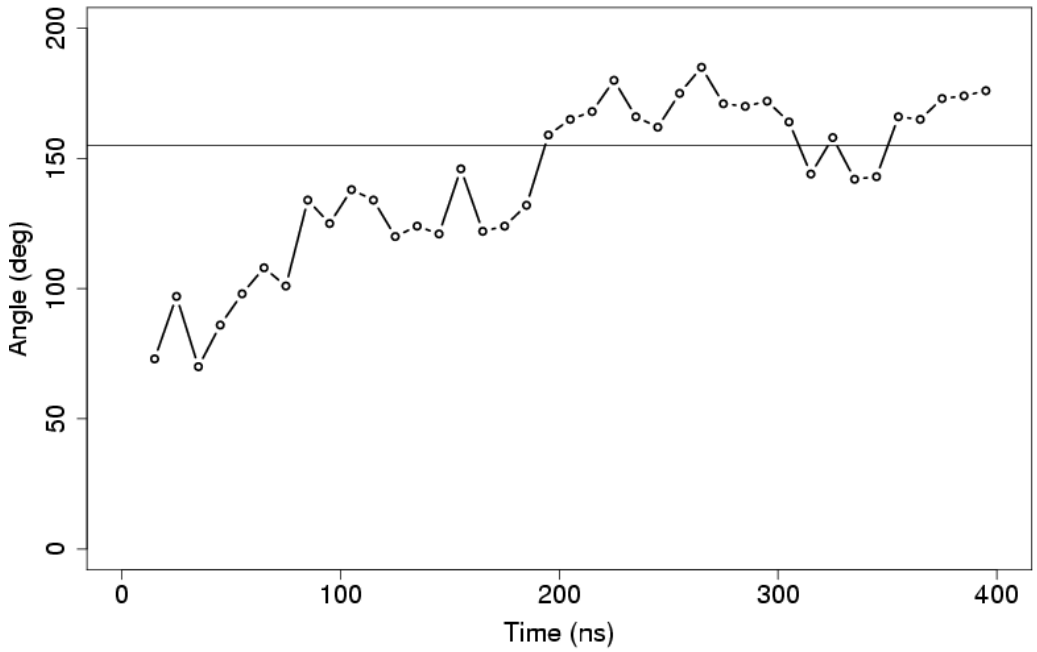

Figure 8. Rotation angle of WALP23 in a di-C14:0-PC bilayer determined by fitting ^{2}H NMR quadrupolar splittings obtained by molecular dynamic simulations. The horizontal line represents the experimental value as determined by (Chapter 2). Note that the point representing the ten first nanoseconds has been removed since the peptide was held vertically, and hence the azimuthal rotation was undefined.

Local conformation of Alanines in the transmembrane segment

Another parameter that is important for refining the calculations in the determination of the tilt and rotation angles by the use of ^{2}H NMR is the angle of the side-chain C^{α}–C^{β} with respect to the α-helical axis. This angle was denoted by $\in_{||}$ in previous studies (ref. 22, Chapter 2 and Chapter 3) where the value was fitted to 58.2º for WALP23 in di-C14:0-PC. In our simulations, using the fitting procedure, before the kink formation the average value was approximately 53.5º (± 1.6) and it increased to 58.1º (± 2.2) after the kink appeared. The average value of $\in_{||}$ after the kink approaches more the experimental value than before the apparition of the kink suggesting that the kink formation may be an important event in the incorporation of WALP23 in a di-C14:0-PC bilayer.

Conformation of Trp-residues: a monitor for interfacial interactions

Experimental studies showed that the peptide conformation and orientation is largely influenced by the four tryptophans that have a role in anchoring the peptide in the interfacial region (Chapter 3). The fact that Trp-residues are strongly anchored at the membrane-water interfacial region (10) may imply that they are involved in the formation of the kink in the tilted peptide structure. Figure 3 shows indeed that the N-

terminal tryptophans lose their α-helicity. Therefore, it may be interesting to study which particular event was accompanied with their changed secondary structure. To get more insight into the behavior of these residues and their interactions with the lipid/water interface, we analyzed the orientation of each ring with respect to the normal to the membrane. In Figure 9, the distribution of the angle between the normal of each Trp ring and the normal to the membrane is shown before (grey bars) and after the kink (white bars). For all Tryptophan side chains, before the kink the distributions are quite wide indicating that the motional freedom of the rings is very large. Introduction of the kink dramatically influences the behavior of Trp2 and Trp3: they change their orientation and thereby adopt a more defined orientation than both C-terminal Trp-residues. The largest change due to the kink occurs for Trp2, which adopts a preferential orientation of its indole rings plane parallel to the membrane normal. Such a preferential orientation of the indole rings of Trp-residues has been proposed in the literature (45,46). In the case of Trp3, the normal to the indole ring plane is at ca. 45º with respect to the bilayer normal. In contrast, the C-terminal Trp-residues showed a large distribution of orientations throughout the simulation suggesting no stabilization of the indole side chain ring direction. The lack of preferential orientation of the C-terminal Trp-rings, as opposed to the more oriented and stable N-terminal ones, suggests that the N-terminal residues may be more strongly anchored in the interfacial regions.

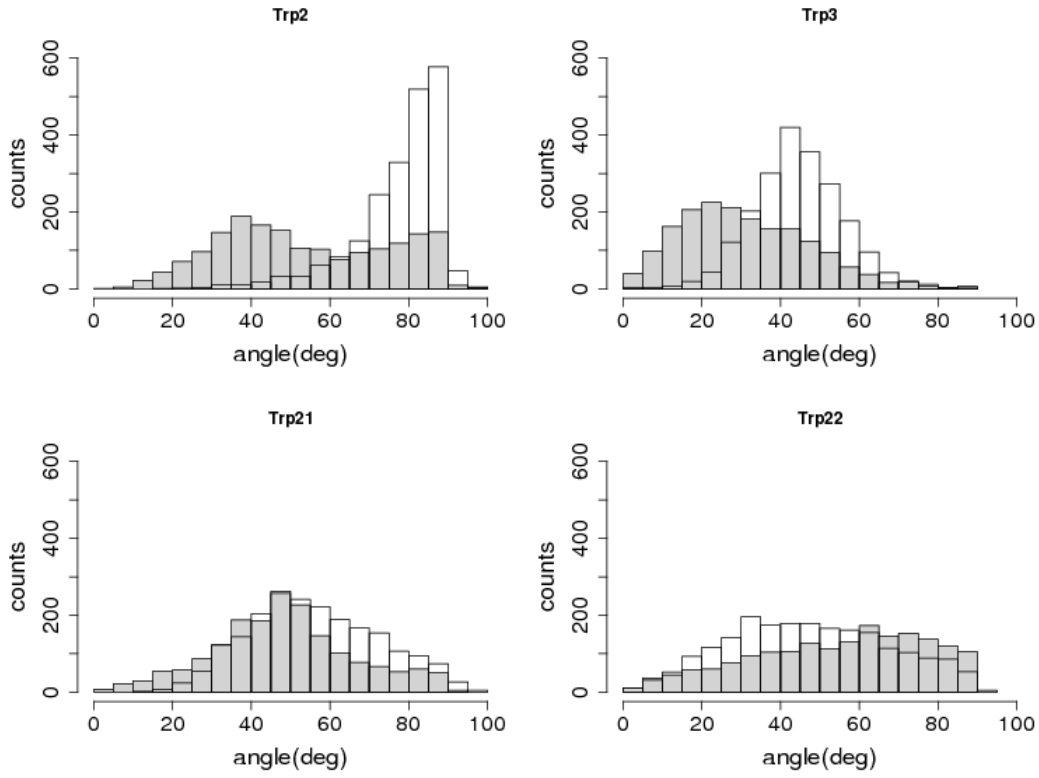

Figure 9. Distribution of the angle between the normal to the ring of each Trp and the normal to the membrane. The grey and white bars are the results obtained before the appearance of the kink and after, respectively. The height of the bar is indicative of the frequency of occurrence of the corresponding orientation of the indole ring.

Energetics of the lipids amino acids interactions

Up till now, we have described several parameters that all seemed to be largely affected by the occurrence of the kink on the N-terminal side of the peptide. Apparently, the deviation from the α-helical structure has important consequences for the structure, orientation, and the dynamics of the WALP23, and is thereby probably accompanied by a considerable redistribution of the energies of the system.

Energy profiles of the lipid amino acid interactions are depicted in Figure 10. In general, the potential energy decrease at the beginning of the simulation for every residue was due to the dramatic starting conditions created by the presence of the hole in the membrane that initially housed the peptide. In most cases, it took up to tens of ns to reach the best packing conditions with the surrounding lipids and stabilize the energy level. Before the occurrence of the kink, all central alanines and leucines presented similar interaction energies (~ -30 $kJ.mol^{-1}$ for Ala and ~ -50 $kJ.mol^{-1}$ for Leu) indicating homogeneous packing and energetic properties along the central hydrophobic stretch (Leu4 to Leu20). When WALP23 started to kink in the N-terminal region a spectacular decrease of the interaction energies with lipids was observed for the residues from Leu4 to Ala9 indicating that breaking the α-helical structure in this region was energetically favourable (Figure 10). Interestingly, this dramatic change in the secondary structure did not affect the energetic state of any other residue along the whole sequence including the N-terminal Trp-residues. Indeed, the Trp-residues reached very rapidly their equilibrium level, which remained unaffected even in the very close vicinity of the N-terminal kink. This suggests that in general, the Trp-residues were already positioned in a favourable surrounding near the lipid-water interfacial region, which is consistent with anchoring interactions.

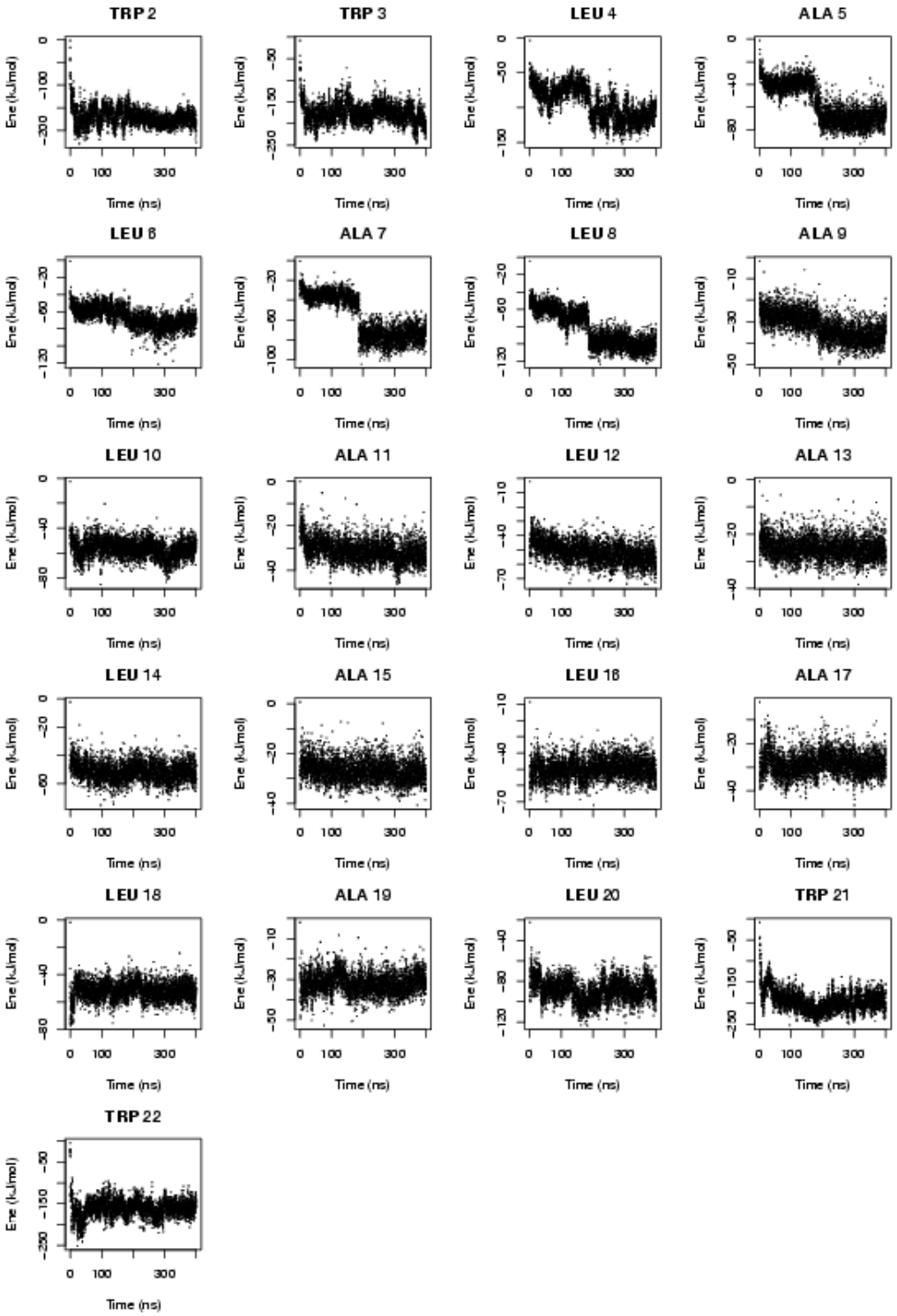

Figure 10. Interaction energy between each residue of the peptide with lipids. This interaction energy has been calculated as the sum of each non-bonded (van der Waals and electrostatics) interaction between one given residue (including backbone and side chain), with all lipids lying within the cutoff distance.

Discussion

In this chapter, we have used MD simulations to investigate how the WALP23 peptide interacts with di-C14:0-PC lipids and which factors are important for this interaction. Lipid parameters took tens of ns before stabilization, whereas some peptide properties like tilt and azimuthal orientation were only stable after several hundreds of ns. We found that the secondary structure of WALP23 and the energetics of the peptide-lipid interactions play an important role in stabilizing the macroscopic parameters such as the tilt and azimuthal rotation angles as exemplified by the events that follow the formation of a kink in the α-helical structure. The ab initio vicinity of the Trp-residues to the interfacial region was favourable as confirmed by the rapid reaching of the lipid-tryptophan interaction energies to equilibrium values. We will now describe these effects in more detail and compare them with experimental results on the same systems. Finally, we will discuss the possibilities for future MD simulations that would enable better understanding of the discrepancies between simulated parameters and experimental ones such as the tilt angle.

Influence of the presence of WALP23 on lipid packing

It was shown experimentally that WALP23 can increase at a 1/30 peptide to lipid molar ratio the bilayer thickness and the order of the acyl chains of di-C14:0-PC. We see in our MD study that it also happens at a lower peptide to lipid molar ratio of 1/100, but to an extent at which it will be difficult to detect with experimental methods. An increase of chain order or bilayer thickness with a concomitant decrease of area per lipid is consistent with a tighter packing of the acyl chains. We observed that the influence of WALP23 on both chain order and lipid packing decreases with the distance from the peptide. However, the tighter packing of the lipids near the peptide that we observed may be an overestimation because the combination of the Berger lipids (29) with the ffgmx force field (31) might cause artefacts that reinforce the packing of lipids around the peptide (47). Nevertheless, when the influence of WALP23 on the bilayer thickness and on the simulated ^{2}H NMR order parameters was analyzed, we obtained effects of the same order of magnitude as experimentally determined (Chapter 4) indicating that our simulations rather accurately reproduce the experimental conditions.

Structure of WALP23 in di-C14:0-PC and anchoring interactions

The secondary structure was for the first 190 ns α-helical and changed drastically with the appearance of the kink in the structure, which was followed by a length adaptation. Indeed, the hydrophobic segment Leu4-Leu20 of the peptide became longer than in regular α-helices. Interestingly, the kink occurred near the interfacial region, which is consistent with the observations that the interfacial region is enriched in irregular structures (48). In addition, we observed that especially the N-terminal Trp-residues were inserted more deeply in the membrane than the closest leucine (Figure 5), which is surprising if we compare the hydrophobicity of the side chains of leucine and tryptophan. The aptitude of amino acids to stretch their side chains towards the bilayer core is called anti-snorkeling as opposed to the snorkeling behavior where the residues buried in the membrane tend to seek the membrane surface by adapting their conformation (49). In contrast, the behavior of the C-terminal tryptophans is neither snorkeling nor anti-snorkeling, probably because this end of the peptide is more profoundly inserted in the membrane than the N-terminus, which is less favorable for anti-snorkeling behavior. Indeed, depending on their

distance from the bilayer core, Trp-residues can adopt either a snorkeling or anti-snorkeling behavior (48,50). Figure 2 illustrates well the change in anti-/snorkeling behavior of the N-terminal Trp-residues with the occurrence of the kink. Furthermore, with the event of the kink, the N-terminal tryptophan orientations became more restricted suggesting a better packing, and hence stronger anchoring properties of the N-terminus of WALP23. Finally, if we consider the changes in potential energies of the amino acids lipid interactions, it is interesting to note that kinking is clearly a favorable event for the Leu4-Ala9 region while it does not affect the energy of the neighboring Trp-residues. This suggests that tryptophans may already be so strongly anchored at the interface that it remains unaffected by the kink.

Tilt angle

We calculated the tilt angle of WALP23 using two procedures, one consisting of a calculus of the angle made by a vector defined by the α-helix, and the other based on ^{2}H NMR quadrupolar splittings fitted to a tilted α-helix in a membrane with the bilayer normal aligned with a hypothetical magnetic field. By this we obtained a few small discrepancies that could be explained by the fact that the fitting procedure assumes no internal motion in a regular α-helix structure and no fluctuations around the average azimuthal rotation angle. However, the difference between the MD-determined tilt angle and the experimental fitted value (chapter 2) is very large, and in order to bridge this gap fluctuations as large as ± 140º around the average rotation angle are required if perfect rigidity of the α-helical structure is assumed. The causes for this discrepancy may be either too short simulation times although 400 ns is quite long (too small fluctuations around average were observed), packing artefacts due to wrong force field parameters in the simulations (see abovementioned), or large fluctuations of the secondary structure parameters which could interfere with the calculation of the experimental values.

Interestingly, the tilt angle was considerably reduced upon kink formation reaching sometimes almost a vertical orientation (see for example Figure 2C).

Another interesting observation is the possible correlation between the fluctuations in bilayer hydrophobic thickness and the tilt angle. Figure 11 illustrates this feature with a plot of tilt angles adopted along the RF simulation versus the hydrophobic bilayer thickness in the region enclosing the 30 nearest lipids. The darkness of the pixels is representative of the frequency of data points in the corresponding area. The distribution of data points shows an ellipsoidal form indicative of a correlation that indicates that the tilt angle decreases with increasing bilayer thickness. This is a strong indication that the tilt angle is sensitive to hydrophobic mismatch. In addition, we noticed that this correlation was even slightly stronger after the appearance of the kink in the α-helix (not shown).

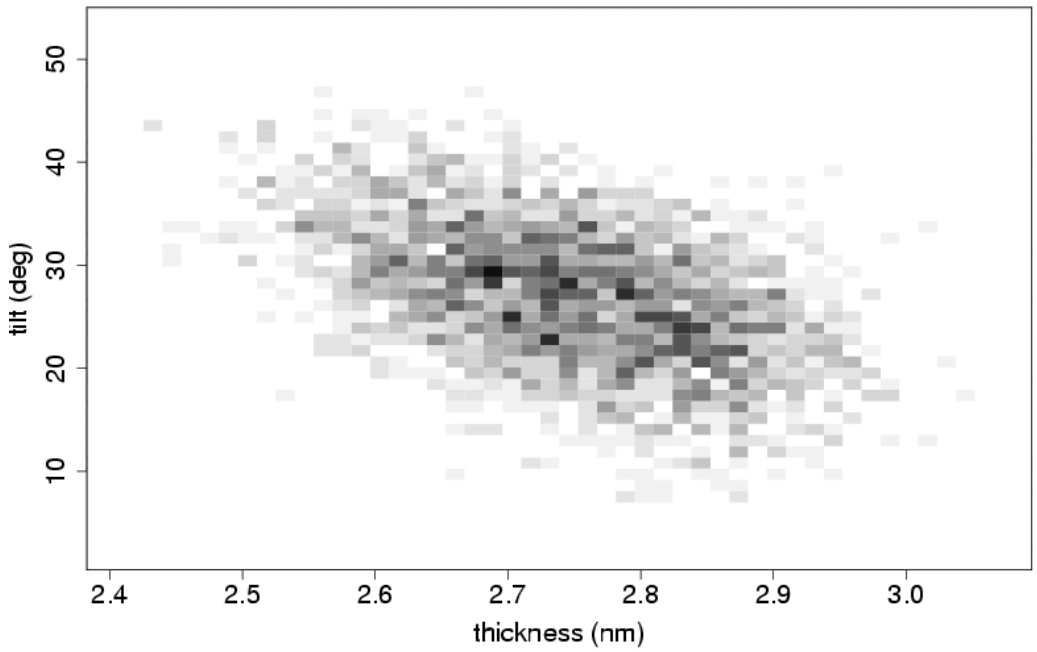

Figure 11. Tilt angles in the RF simulation versus the hydrophobic bilayer thickness of the region enclosing the 30 nearest lipids. The size of one pixel encloses a range of 1.1º in tilt angle by 0.14 Å difference in the bilayer thickness. The darkness of the pixels increases with increased frequency of occurrence of data points in that area.

Rotation angle

It was shown that the nature of flanking residues can influence significantly the direction in which a transmembrane peptide tilts (Chapter 3). In the present work we analyzed this rotation angle by fitting the simulated ^{2}H NMR quadrupolar splittings along the trajectory of not only the RF simulation, but also of 190 ns semi-isotropic PME simulation (see methods). In the case of the RF simulation before the occurrence of the kink and in the complete PME simulation in which the peptide did not experience a kink in the secondary structure, we observed that the rotation angle was not stable for 190 ns (Figure 8). When the peptide lost its α-helical character after 190 ns of simulation in RF experiment, we saw that the rotation angle increased very rapidly to values close to those experimentally determined (Chapter 2) and remained stable for more than 200 ns till the end of the simulation. This means that adopting the final rotation angle has a relaxation time of an order of magnitude of hundreds of ns. The facts that the other PME MD simulation did not reproduce well this parameter and that both RF before kink and PME experiments showed very unstable azimuthal behavior of the non-kinked α-helical peptide emphasize the probability that the occurrence of the kink is an important event that leads to values closer to experimental values.

To our knowledge so far, the only MD study that analyzed the azimuthal angle of model transmembrane peptides before our work was performed on a Lys-flanked KALP-like peptide (51). This study showed that starting several MD simulations with a peptide along the bilayer will lead to a preferred rotation angle after 10 ns. Furthermore, starting the simulations with the polypeptide close to the orientation that

gave the best fit to the observed alanine methyl deuteron splittings, the orientation about the helix axis appeared to be maintained even as the helix tilt deviated significantly from the experimentally observed average (52) Although the trajectories were short for the new computing possibilities, this work gives a good example of how we should with our WALP23/di-C14:0-PC system, investigate the reproducibility of obtaining the azimuthal angle by MD simulations. Unfortunately, as observed in the present study, relaxing processes towards the equilibrium rotational angles are much longer in the case of WALP23, taking hundreds of ns most likely because of the structural kinking event that is unobserved in the case of the lysine-flanked peptide studied by Morrow and co-workers (51).

Long term events and reproducibility issues

The kink formation in the structure of WALP23 seem to have very important implications on structural parameters such as the secondary structure of several amino acids along the sequence, the conformation of the alanines, the hydrophobic length of the peptide, the tilt angle, the more stable orientation of the N-terminal tryptophans and maybe also the rotation angle. Up to now, we have focused our description of the experiments on a 400 ns long semi-isotropic RF simulation, while we also have performed a 190 ns semi-isotropic PME (see methods) simulation as a control. In this second simulation, we did not observe the event of kinking in the α-helical structure yet, suggesting that the probability of occurrence of a kink is small or that the time required for breaking the α-helical structure is in the order or magnitude of several hundreds of ns. Remarkably, after 190 ns of the PME simulation the parameters that seemed to be influenced by the occurrence of the kink compared very well with the RF simulation before the appearance of the disrupted α-helical structure. This observation reinforces the hypothesis that the kink is largely responsible for the evolution and stabilization of the above-mentioned parameters. However, as long as the PME simulation does not reproduce the kink, there is no apparent reason to expect similar parameters as after 190 ns of semi-isotropic RF simulation. Therefore, it is important for reliability issues of the results we presented here to reproduce similar data by for example prolonging the PME simulation for hundreds of ns more, which is the probable time-span for the occurrence of kinking α-helices structures. Alternatively, performing again a semi-isotropic RF simulation of 400 ns may reproduce a kink as well with similar consequences on the structural and dynamical parameters. Finally, a similar experiment could also be realized by reincorporating the kinked peptide in a new di-C14:0-PC bilayer to analyze the same parameters under the same conditions except the starting secondary structure. Obtaining similar structural and dynamical parameters may indicate which parameters can be affected by the kink, and prove also the irreversibility of this event.

Comparison to other MD studies and perspectives

The first systematic study by MD simulations of the response of the transmembrane WALP peptides to hydrophobic mismatch by (20) reported results that were in good agreement with the experimental studies by (21), including the influence on lipid organization. However, these results, which were based on relatively short simulation times, did not show a clear relation between the tilt angle and the hydrophobic mismatch for WALP peptides equally long and shorter than WALP23, whereas ^{2}H NMR studies suggest that increasing the length of WALP from WALP19 to WALP23 in similar lipid bilayers should increase the tilt angle under positive hydrophobic

mismatch (22 and Chapter 2). We could find in the present work that the tilt angle is sensitive to bilayer thickness fluctuations only by prolonging the simulations to hundreds of ns. Nevertheless, the tilt angles we obtain are large compared to experimentally determined ones.

A recent study also predicted smaller tilt angles by investigating the orientations of membrane-bound α-helices that correspond to the lowest solvation energy of the peptide in an implicit membrane system (i.e. the free energy for transferring the helix from vacuum into a given position and orientation in the membrane). The predicted tilt angles for the WALP19 and WALP25 peptides were in agreement with the experimentally determined values by ^{2}H NMR and by infrared spectroscopy for WALP19, and WALP19 and WALP25, respectively (53).

In contrast, a recent MD study (25) in an implicit membrane systems, provided much larger tilt angles that compared well with the ones we obtained with the non-kinked WALP23 in the RF and PME simulations (32.7 ± 8.5º vs. ca. 34-35 ± 6º).

In the case of KALP peptides, a systematic study of the influence of hydrophobic mismatch showed clearly that the tilt angle is sensitive to hydrophobic mismatch (23). A rather weak effect on lipid organization was observed consistent with the weaker influence of KALP peptides on lipid order than equivalent WALP peptides (10). As the bilayer thickness may not increase significantly, tilting will be more important for compensating for hydrophobic mismatch. Therefore, we may expect larger tilt angles for KALP23 in di-C14:0-PC than for WALP23 as is the case in a recent ^{2}H NMR study on WALP23 and KALP23 (Chapter 3). This is not the case if we compare the tilt angle determined by MD for KALP23 to our result with 22.8º and 24.5 ± 7.0º for the tilt angle of KALP23 and WALP23, respectively. This discrepancy suggests that MD conditions to reproduce experimental results or trends for that kind of systems are not optimal yet.

Kandasamy and Larson suggested that the possible aggregation of peptides may decrease tilt as illustrated by the clear reduction of tilt to 8º at a peptide to lipid ratio of 4 to 100 without aggregation. Although at such peptide to lipid ratio aggregation of WALP23 peptides is not shown experimentally, it may still be interesting to perform similar all-atom MD experiments for WALP23 to see whether a reduced tilt would also occur for WALP23 when more than one peptide is present.

The abovementioned simulations on KALP23 were probably sufficiently long for allowing stabilization of the tilt, requiring 50 or more ns of simulation time before reaching equilibrium. Thus, the 10 ns simulations performed in (51) were probably not long enough to reach equilibrium values of the tilt angle that matched the experimental tilt value obtained by ^{2}H NMR on the corresponding peptide. However, even with long simulation times it is known that most widely lipid and force field parameters can lead in MD studies to packing artefacts in peptide/lipid systems as demonstrated by (47). The new parameters developed in that study ensure a less tight packing of the lipids around the peptides. Therefore, it may be worth repeating our experiments with the improved force field and lipid parameters to see whether it makes any difference in influencing the tilt angle.

We saw throughout the present chapter that a special event like the occurrence of a kink in the structure of WALP23 leads to significant modification and stabilization of the tilt and rotation angles, of the hydrophobic length of the peptide, its response to bilayer thickness fluctuations, and of the orientational behavior of the N-terminal Trp-residues. This was observed in none of the previous studies. Since the consequences of the kink are important, it may be very interesting to study the possibilities for this

event and its consequences again with the up-dated MD-parameters by (47) under different conditions including the starting secondary structure, the peptide-to-lipid molar ratio, and the length of simulations.
Future improvements of MD systems as we presented in this chapter will lead to better correlations between experimental and theoretical data, thereby helping to rationalize structural and dynamical parameters involved in lipid-peptide interactions in model membrane systems. Nevertheless, the way we conducted the present study provided a wealth of information on the structure and dynamics of the model system, and may help to design new experiments to understand lipid protein interactions in general.

Acknowledgement

We would like to acknowledge Gaelle Debret from the Équipe de Bioinformatique Génomique et Moléculaire INSERM U726, Université Paris 7, for her help with programming GROMACS tools.

References

1. Arkin, I. T., and Brunger, A. T. (1998) *Biochim Biophys Acta* 1429(1), 113-128
2. Landolt-Marticorena, C., Williams, K. A., Deber, C. M., and Reithmeier, R. A. (1993) *J Mol Biol* 229(3), 602-608
3. Reithmeier, R. A. (1995) *Curr Opin Struct Biol* 5(4), 491-500
4. Sakai, H., and Tsukihara, T. (1998) *J Biochem (Tokyo)* 124(6), 1051-1059
5. von Heijne, G. (1994) *Annu Rev Biophys Biomol Struct* 23, 167-192
6. Wallin, E., Tsukihara, T., Yoshikawa, S., von Heijne, G., and Elofsson, A. (1997) *Protein Sci* 6(4), 808-815
7. Dumas, F., Lebrun, M. C., and Tocanne, J. F. (1999) *FEBS Lett* 458(3), 271-277
8. Killian, J. A. (1998) *Biochim Biophys Acta* 1376(3), 401-415
9. Lee, A. G. (2003) *Biochim Biophys Acta* 1612(1), 1-40
10. de Planque, M. R., Bonev, B. B., Demmers, J. A., Greathouse, D. V., Koeppe, R. E., 2nd, Separovic, F., Watts, A., and Killian, J. A. (2003) *Biochemistry* 42(18), 5341-5348
11. Demmers, J. A., van Duijn, E., Haverkamp, J., Greathouse, D. V., Koeppe, R. E., 2nd, Heck, A. J., and Killian, J. A. (2001) *J Biol Chem* 276(37), 34501-34508
12. Davis, J. H., Clare, D. M., Hodges, R. S. and Bloom, M. (1983) *Biochemistry* 22(23), 5298-5305.
13. de Planque, M. R., and Killian, J. A. (2003) *Molecular membrane biology* 20(4), 271-284
14. Killian, J. A. (2003) *FEBS Lett* 555(1), 134-138
15. Killian, J. A., and Nyholm, T. K. (2006) *Curr Opin Struct Biol* 16(4), 473-479
16. Ren, J., Lew, S., Wang, J., and London, E. (1999) *Biochemistry* 38(18), 5905-5912
17. Webb, R. J., East, J. M., Sharma, R. P., and Lee, A. G. (1998) *Biochemistry* 37(2), 673-679
18. Zhang, Y. P., Lewis, R. N., Hodges, R. S., and McElhaney, R. N. (1995) *Biochemistry* 34(7), 2362-2371
19. de Planque, M. R., Greathouse, D. V., Koeppe, R. E., 2nd, Schafer, H., Marsh, D., and Killian, J. A. (1998) *Biochemistry* 37(26), 9333-9345
20. Petrache, H. I., Zuckerman, D. M., Sachs, J. N., Killian, J. A., Koeppe, R. E., and Woolf, T. B. (2002) *Langmuir* 18(4), 1340-1351
21. de Planque, M. R., Goormaghtigh, E., Greathouse, D. V., Koeppe, R. E., 2nd, Kruijtzer, J. A., Liskamp, R. M., de Kruijff, B., and Killian, J. A. (2001) *Biochemistry* 40(16), 5000-5010

22. van der Wel, P. C., Strandberg, E., Killian, J. A., and Koeppe, R. E., 2nd. (2002) *Biophys J* 83(3), 1479-1488
23. Kandasamy, S. K., and Larson, R. G. (2006) *Biophys J* 90(7), 2326-2343
24. Sparr, E., Ash, W. L., Nazarov, P. V., Rijkers, D. T., Hemminga, M. A., Tieleman, D. P., and Killian, J. A. (2005) *J Biol Chem* 280(47), 39324-39331
25. Im, W., and Brooks, C. L., 3rd. (2005) *Proc Natl Acad Sci U S A* 102(19), 6771-6776
26. Berendsen, H. J. C., van der Spoel, D., and van Drunen, R. (1995) *Computer Physics Communications* 91(1-3), 43-56
27. Lindahl, E., B. Hess, and D. van der Spoel. (2001) *J Mol Model* 7(8), 306-317.
28. Van Der Spoel, D., Lindahl, E., Hess, B., Groenhof, G., Mark, A. E., and Berendsen, H. J. (2005) *J Comput Chem* 26(16), 1701-1718
29. Berger, O., Edholm, O., and Jahnig, F. (1997) *Biophys J* 72(5), 2002-2013
30. Berendsen, H. J. C., Postma, J. P. M., van Gunsteren, W. F., and Hermans, J. (1981) *Interaction Models for Water in Relation to Protein Hydration.*, In Intermolecular Forces, (Pullman, B., Ed). pp. 331-342. Reidel: Dordrecht, The Netherlands.
31. van Gunsteren, W. F. a. B., H. J. C. (1987) *Groningen Molecular Simulation (GROMOS) Library Manual*, Biomos: Groningen
32. Hess, B., Bekker, H., Berendsen, H. J. C., and Fraaije, J. G. E. M. (1997) *J Comput Chem* 18(12), 1463-1472.
33. Miyamoto, S., and Kollman, P. A. (1992) *J Comput Chem* 13(8), 952-962.
34. Berendsen, H. J. C., Postma, J. P. M., van Gunsteren, W. F., DiNola, A., and Haak, J. R. (1984) *The Journal of Chemical Physics* 81(8), 3684-3690
35. Tironi, I. G., Sperb, R., Smith, P. E., and van Gunsteren, W. F. (1995) *The Journal of Chemical Physics* 102(13), 5451-5459
36. Hunenberger, P. H., and van Gunsteren, W. F. (1998) *The Journal of Chemical Physics* 108(15), 6117-6134
37. Smith, P. E., and van Gunsteren, W. F. (1994) *The Journal of Chemical Physics* 100(4), 3169-3174
38. Darden, T., York, D., and Pedersen, L. (1993) *The Journal of Chemical Physics* 98(12), 10089-10092
39. Essmann, U., Perera, L., Berkowitz, M. L., Darden, T., Lee, H., and Pedersen, L. G. (1995) *The Journal of Chemical Physics* 103(19), 8577-8593
40. Anézo, C., de Vries, A. H., Höltje, H.-D., Tieleman, D. P., and Marrink, S.-J. (2003) *J. Phys. Chem. B* 107(35), 9424–9433.
41. Petrache, H. I., Dodd, S. W., and Brown, M. F. (2000) *Biophys J* 79(6), 3172-3192
42. de Planque, M. R., Kruijtzer, J. A., Liskamp, R. M., Marsh, D., Greathouse, D. V., Koeppe, R. E., 2nd, de Kruijff, B., and Killian, J. A. (1999) *J Biol Chem* 274(30), 20839-20846
43. Naarmann, N., Bilgicer, B., Kumar, K., and Steinem, C. (2005) *Biochemistry* 44(13), 5188-5195
44. Nielsen, R. D., Che, K., Gelb, M. H., and Robinson, B. H. (2005) *J Am Chem Soc* 127(17), 6430-6442
45. Gaede, H. C., Yau, W. M., and Gawrisch, K. (2005) *J Phys Chem B Condens Matter Mater Surf Interfaces Biophys* 109(26), 13014-13023
46. Norman, K. E., and Nymeyer, H. (2006) *Biophys J* 91(6), 2046-2054
47. Tieleman, D. P., MacCallum, J. L., Ash, W. L., Kandt, C., Xu, Z., and Monticelli, L. (2006) *J Phys Condens Matter* 18(28), S1221-1234
48. Granseth, E., von Heijne, G., and Elofsson, A. (2005) *J Mol Biol* 346(1), 377-385
49. Chamberlain, A. K., Lee, Y., Kim, S., and Bowie, J. U. (2004) *J Mol Biol* 339(2), 471-479
50. Liang, J., Adamian, L., and Jackups, R., Jr. (2005) *Trends Biochem Sci* 30(7), 355-357
51. Goodyear, D. J., Sharpe, S., Grant, C. W., and Morrow, M. R. (2005) *Biophys J* 88(1), 105-117

52. Sharpe, S., Barber, K. R., Grant, C. W., Goodyear, D., and Morrow, M. R. (2002) *Biophys J* 83(1), 345-358
53. Sengupta, D., Meinhold, L., Langosch, D., Ullmann, G. M., and Smith, J. C. (2005) *Proteins* 58(4), 913-922

Chapter 6

Summary

Protein-lipid interactions play an essential role in influencing the function of membrane proteins. The lipid surrounding can affect in different ways membrane protein structure and activity. In particular, the tilting properties of transmembrane segments of proteins, which adopt in the most cases an α-helical conformation, are very important for the function of the proteins and can be influenced by changes in the lipid composition (See chapter 1). The general principles of such effects are difficult to study by using complex natural membrane proteins in lipid bilayers, because such systems do not easily allow systematic variations in protein parameters. In addition, it is difficult in such systems to characterize the structural consequences of varying lipid or protein composition. Therefore, nowadays, an increasing number of general molecular mechanisms about how proteins sense the lipid environment are being established in model systems composed of designed peptides and synthetic lipids (1). The present thesis is an example of such kind of approach that aims at understanding how membrane parameters like the hydrophobic bilayer thickness, the lipid-protein interfacial interactions and the packing properties of the membrane influence the tilt and azimuthal orientations, and the dynamics of transmembrane segments of proteins. Here, the so-called WALP and analogous peptides were used as mimic of the membrane-spanning parts of proteins in bilayers composed of single-species lipids (Chapter 1) and both peptide and lipid composition were systematically varied to understand better the molecular mechanisms that control lipid-protein interactions. To study these systems, the applicability of a new solid state ^{2}H NMR approach, called GALA (geometric analysis of labeled alanines) is explored throughout the present work. The results and their implications are summarized below.

In **chapter 2**, the tilt angle of the twenty-three amino acids long WALP23 was studied in diacylphosphatidylcholine (PC) bilayers of which the hydrophobic thickness was shorter than or equal to the hydrophobic length of the peptide. The situation in which the peptide's length exceeds the hydrophobic thickness is called positive hydrophobic mismatch and is favourable for a tilted orientation of the peptide. The results showed that a small tilt angle occurs under hydrophobic matching conditions, which increases systematically with decreasing bilayer thickness. However, the tilt angles were too small to fully compensate for the positive hydrophobic mismatch, suggesting that tilting can also be affected by parameters other than the hydrophobic thickness of the membrane like for example the amino acid composition of the peptide. Interestingly, the direction in which WALP23 is tilted (azimuthal or rotation angle) was insensitive to the changes in bilayer thickness. The reason for this preferred rotational angle could be a favourable conformation of the large and bulky flanking tryptophan residues, in combination with a beneficial interaction with the lipid/water interface, where tryptophans have been proposed to anchor (2). In the same chapter, it was shown that the combination of ^{2}H NMR and GALA can be applied to non-oriented samples for determining precisely the tilt and the rotation angle. The major advantages are the fact that it can mimic much better biological membranes, that pH and salt contents can be better controlled under adequate hydration conditions, and that these samples are easier to prepare than oriented samples. In the case of WALP23, eight alanine positions were available for deuterium-labeling in the hydrophobic region, giving more potential data points to use in the analysis. Since this feature would yield more data points than would be required to determine the tilt angle for a regular α-helix, application of this method to WALP23 in addition allowed a detailed analysis of possible deviations from an α-

helical structure. Analysis of the data suggested that in all lipid systems the peptide adopted a very regular α-helix, except in the shortest lipid di-C12:0-PC, where the possibility was suggested of the presence of a kink in the α-helical structure.

The weak sensitivity of the tilt angle to the hydrophobic mismatch raised several questions. For example, can the nature of the flanking residues influence the extent of the tilt and rotational angle? And can these parameters be influenced by the hydrophobicity of the core region? These questions were addressed in **Chapter 3**. Peptide analogues of WALP23 were prepared in which the interfacial tryptophan residues were replaced by Lys (KALP23) and in both these peptides in addition the hydrophobic core of alternating leucine-alanine was replaced by a stretch of polyleucine. These latter peptides were called WLP23 and KLP23, respectively. The tilt and rotation angles of the peptides as a function of hydrophobic mismatch were studied in the same unoriented lipid systems as in Chapter 2, based on four labeling positions for each new peptide. It was found that the tilt angle increased systematically for all peptides upon decreasing the bilayer thickness in a similar way as for WALP23. However, significantly larger tilt angles were obtained for the Lysine-flanked KALP23 than for WALP23, suggesting that interfacial anchoring interactions of tryptophan residues may restrain tilting. This was surprising because we may expect that the stronger anchoring interactions of Trp-residues with the lipid-water interface would in fact cause a larger tilt angle upon changing bilayer thickness. Increasing the hydrophobicity resulted in an increase in tilt angle for WLP23 only, which is the tryptophan-flanked analogue of WALP23. For all peptides the maximum tilt angle obtained was remarkably small (less than 12°), suggesting that further tilting is inhibited, most likely due to unfavourable packing of lipids around a tilted helix. The results furthermore showed that the direction of the tilt is largely determined by the flanking residues: tryptophan- and lysine-flanked peptides were found to have very different rotation angles, which were not influenced significantly by hydrophobicity of the peptides or by the extent of hydrophobic mismatch. Finally, very small changes in the side chain angles of the deuterated alanine probes were observed in both tryptophan-flanked peptides, suggesting that these peptides may deviate slightly from an ideal α-helical structure, and thereby decrease their hydrophobic length to help them incorporating into thin membranes. This last observation for the WALP23 and WLP23 peptides but not for their lysine-flanked counterparts is consistent with the postulated strong interaction of tryptophan with the interface (2).

The importance of membrane interfacial anchoring for peptide/lipid interactions suggests that modifying the physico-chemical properties of the lipid-water interface may influence the behavior of integral membrane proteins. Thus, partitioning of for example small molecules at the lipid/water interface may interfere with the anchoring properties of the transmembrane regions of proteins and thereby influence properties such as tilt and direction of tilt. We tested this hypothesis in **chapter 4** by investigating the effects of 2,2,2-trifluoroethanol (TFE) on the interaction of WALP23 with model membranes of dimyristoylphosphatidylcholine (di-C14:0-PC), which corresponds to slightly positive hydrophobic mismatch conditions.
^{2}H NMR experiments on acyl chain deuterated lipids showed that the addition of amounts as small as 4-8 volume % of TFE to the lipid suspensions significantly

decreased the order in the acyl chains resulting in a reduction of the hydrophobic bilayer thickness. In addition, the presence of TFE abolishes the ability of WALP23 to order and stretch the lipid acyl chains. A striking observation was that the tilt angle of WALP23 was diminished, as shown by ^{2}H NMR and GALA, in spite of the fact that TFE reduces the bilayer thickness. This would lead to an increased positive mismatch, and hence an increase of the tilt angle was expected. As a consequence of the reduction of the bilayer thickness and the 'straightening' of the WALP23 in the membrane, the Trp-residues were more exposed to the aqueous phase as confirmed by Trp-fluorescence quenching experiments using acrylamide. In contrast to WALP23, no influence of TFE was observed on the interactions and tilt orientation of the Lys-flanked analog KALP23 within the bilayer. This implies that the influence of TFE on the properties of transmembrane peptides depends on the nature of the flanking residues and suggests that TFE may act on transmembrane protein segments specifically through membrane-anchoring residues like Trp or Tyr, by disturbing their interactions with the lipid-water interfacial region. Thus, membrane proteins that are rich in aromatic anchoring residues may be more efficiently affected by the presence of TFE or other small amphiphilic solutes, than proteins of which the transmembrane segments are flanked by charged residues like Arg or Lys. A recent study postulated that the ability of TFE and other small alcohols to influence the association state of oligomeric membrane proteins is related both to their anesthetic potency and to their lipid disturbing effect through remodeling of the lateral pressure profile (3). The results presented in Chapter 4 suggest that the interference of TFE with anchoring properties of aromatic amino acids may also be involved in the ability of these small alcohols to dissociate membrane protein complexes (4).

In the studies described in chapters 2-4, potentially important factors for lipid-peptide interactions could be identified by focusing on a few selected parameters only for each experiment. Molecular dynamics (MD) is a complementary technique in the sense that such studies can provide a complete description of the system in one simulation, including not only structural properties of both peptide and lipids, but also the dynamics and energetic parameters of the peptide/lipid interactions, although on relatively short times scales. An earlier MD study on WALP peptides of variable length in PC bilayers of different thickness (5) showed that the bilayer thickness increases monotonically with increasing length of the WALP peptides, and that the peptides tilt in response to hydrophobic mismatch. Although the tilt angles were found to correlate with an earlier experimental study using infrared spectroscopy (6), these findings are not in agreement with the results obtained from ^{2}H NMR studies in Chapter 2 and (7). Also other modeling studies in implicit membrane systems present controversial results about the extent of the tilt angle of WALP peptides (8,9). Since up to now WALP peptides were simulated on too short time scales to reach an equilibrated state and to allow for observations of long-term dynamical processes on MD time scales, **chapter 5** is dedicated to the results of long time scale MD simulations. These were performed on a WALP23/di-C14:0-PC system at a peptide to lipid molar ratio of 1 to 100, which corresponds in experimental studies to a situation wherein no spontaneous peptide aggregation occurs (10). The lengths of simulations we performed were up to 400 ns, which is very considerable and is starting to approach the NMR spectroscopy time scales. In this long simulation we observed a rare event, which is the formation of a kink in the highly α-helical WALP23 and we described the possible implications at the structural and dynamical level.

Consistent with ^{2}H NMR experiments (chapter 4), we observed that the influence of the presence of WALP23 on the order and bilayer thickness decreased with the distance from the peptide. The structure of WALP23 was highly α-helical up to 190 ns. After 190 ns a kink in the α-helical structure occurred at the N-terminal side of the peptide, which seemed to result in stabilization of a variety of important parameters, like the tilt angle, the rotation angle, the Ala side chain conformation, and also the orientation of the Trp-residues. The occurrence of the kink was followed by an increase in effective hydrophobic length of the peptide, due to a decrease of the tilt angle. The change in secondary structure at the N-terminal side of the peptide led also to a change in the relative localization of the amino acids with respect to the membrane-water interfacial region. The N-terminal Trp-residues became more deeply inserted into the membrane than the first Leucine in the hydrophobic sequence of the peptide. The event of kinking was also followed by a clear adoption of a preferential orientation of both N-terminal Trp-residues with in particular the first Trp in the sequence, which had as most frequently occurring orientation its indole ring parallel to the bilayer normal. These results suggested that the N-terminal Trp-residues became more strongly anchored at the membrane-water interface than the C-terminal ones after the kinking of the peptide. Throughout the simulation, WALP23 was slightly more deeply inserted into the membrane on the C-terminal side, which is consistent with earlier experimental observations suggesting that this end of the peptide is more hydrophobic than the N-terminus (10,11).

The tilt angle of the non-kinked peptide was as large as in a previous MD study in implicit membrane systems (8), which was a much larger value than experimentally determined by ^{2}H NMR in Chapter 2. Interestingly, we could observe a correlation between the extent of tilting and the fluctuations in the bilayer thickness, indicating that the tilt angle is sensitive to the hydrophobic mismatch. A striking observation was the significant reduction of the tilt angle upon kinking. However, the tilt angle values remain very large compared to the values obtained in Chapter 2. This was also the case when tilt angles were derived from ^{2}H NMR splittings that were calculated from the simulations. Thus, the large discrepancies between the simulated and experimental values of the quadrupolar splittings could be ascribed to the considerably larger tilt angle of the kinked peptide in the MD simulation, which adopted almost precisely the same rotation angle as determined in Chapter 2. To unambiguously answer the question of what causes the discrepancy between angles that were observed from MD simulations and those obtained from the GALA method requires further studies.

Importantly, other simulations that we carried out on the same system, but that were up to now shorter than 200 ns did not reproduce yet the occurrence of the structural kink, and the different parameters that were stabilized subsequently to the kink did not reach yet their equilibrium. This raises important issues of the time required for events like the kink, stabilization of the tilt, and azimuthal orientation, and of the Trp-residues mobility, and hence the length of simulation that is required for reproducing realistically model membrane systems. But also, this emphasizes the importance of reproducibility of the results as long as MD experiments do not reach lengths that compare with spectroscopic time scales and do not reproduce accurately the experimental values of the measurements as illustrated by the discrepancies between measured and simulated ^{2}H NMR splittings.

Concluding remarks and prospects

Use of GALA

The primary conditions that allow application of GALA to systems like the ones studied throughout this thesis, is that the peptide adopts an α-helical conformation, rotates rapidly around the bilayer normal, but not around its helix axis, and possesses a minimum of four labeled alanine residues in the hydrophobic transmembrane sequence to obtain precise tilt angle values (7,12).

To our knowledge, the first application of ^{2}H NMR in combination with the analysis of the geometry of d_3-Alanines to determine the tilted orientation of transmembrane peptides in lipid bilayers was by Grant and co-workers (12). Peptides corresponding to the putative transmembrane domain of the human EGF receptor with short extra-membranous extensions were found to tilt by approximately 10-14º away from the bilayer normal. We also find in general with our system small angles. However, the approach can also be applied to peptides with larger tilt angles and to other systems than static macroscopically oriented samples and multi-lamellar vesicles (non-oriented sample). An example of this is the application of ^{2}H NMR and GALA to model peptides in bicelles, which adopt tilt angle values between 33-35º with respect to the bilayer normal of the long-chain phospholipids (13). It can also be applied to peptides that associate almost perpendicularly to the membrane normal, i.e. tilt angle values close to 90 º (14). In this latter study, a concentration dependent realignment of the α-helix from a surface-bound orientation (i.e. lying along the membrane surface) to one that was tilted by 30º degrees was calculated using the ^{2}H NMR quadrupole splittings of four d_3-Alanine labels as constraints. These examples of the use of ^{2}H NMR with GALA illustrate how this approach can be very attractive for application to a wide variety of membrane systems, where the tilt angle of the α-helical part of interest encompasses values between 0-90º.

Perspectives

Advantages and complementary aspects of ^{2}H NMR and GALA to other NMR methods

In the introduction, Chapter 1 of this thesis, different elements were described of the use of ^{2}H NMR and GALA that make it an attractive approach to apply to model systems as WALP peptides in PC-bilayers. The technical advantages are the very well defined relations of the ^{2}H NMR quadrupolar splitting with the angle of the labeled bond, and the rotation angle. This allows for very precise information to be obtained with very small errors as illustrated in Chapter 2 and Chapter 3 in comparison to the analysis from a single ^{15}N-label, which allows for tilt angle determination with very large errors in the range of ±20º and no information on the rotation angle (Chapter 1 and ref. 14). The only way to obtain precise information on the azimuthal angle of a transmembrane peptide by ^{15}N NMR is by analysis of the dipolar couplings of multiple NH bonds in terms of PISA (polarity index slant angle) wheels or dipolar waves (15,16). However, this kind of analysis requires ^{1}H and ^{15}N NMR experimental settings that are more complicated to keep under control and in addition the NMR sensitivity of a single ^{15}N nucleus is significantly lower than that of the three equivalent and partially motionally averaged ^{2}H nuclei in the Alanine side chains (see Chapter 1).

Figure 1 illustrates the high precision with which one can detect very subtle differences in tilt and rotation angles. In Figure 1A, the curved arrow indicate the 4º variation in tilt angle for the tryptophan-flanked peptides WALP23 on changing the

bilayer thickness from di-C18:1-PC to di-C12:0-PC, as determined in Chapter 2. In panel B, a schematized representation of the tilted KALP23 is depicted according to the results obtained in di-C12:0-PC (Chapter 3). The panels C and D of the same picture illustrate the subtle and large differences in azimuthal angles between WALP23 and WLP23, and WALP23 and KALP23, respectively. The larger tilt angle and the nearly opposite rotation angle of KALP23 with respect to WALP23 illustrate the importance of the nature of the flanking residues for the way a transmembrane peptide accommodates in a lipid bilayer.

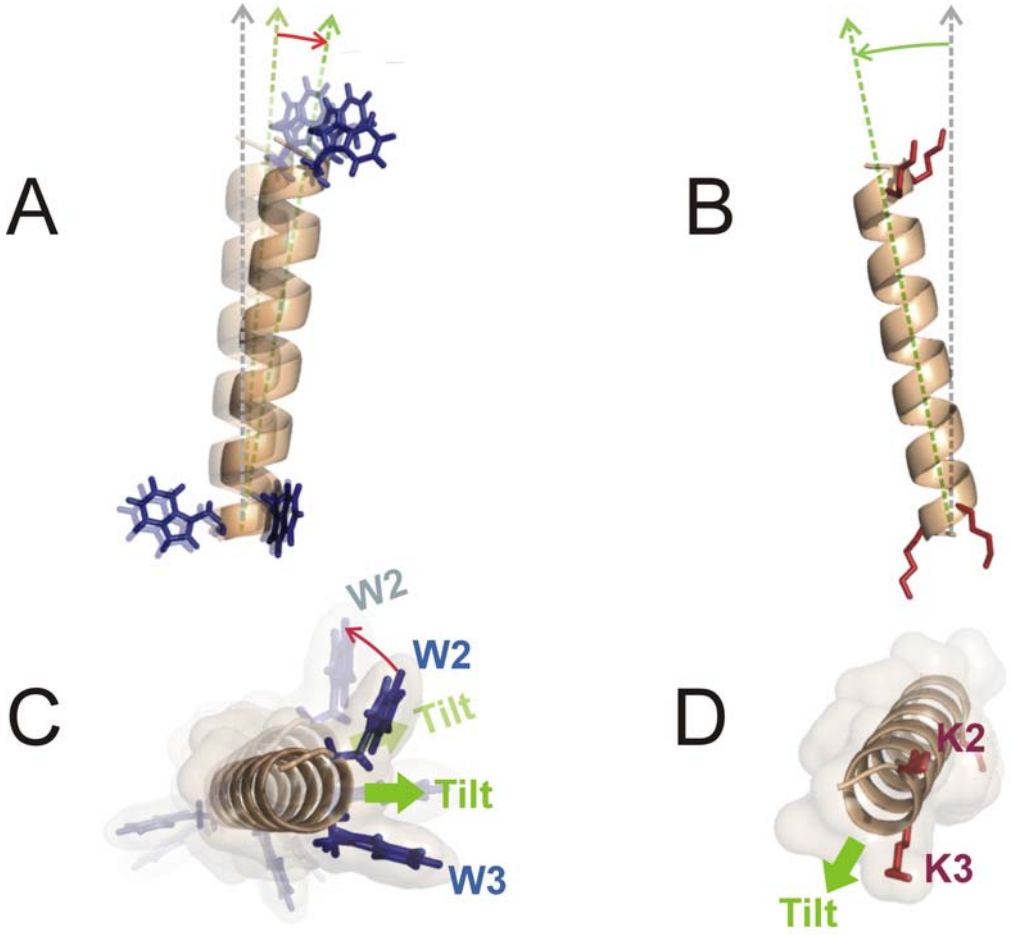

Figure 1. Illustrations of the tilt and azimuthal orientations of model peptides as determined in Chapter 2 and 3 in bilayers of different hydrophobic thickness. Tilted tryptophan-flanked peptides WALP23 in di-C18:1-PC (transparent) to di-C12:0-PC, respectively (A). Tilted KALP23 according to results obtained in Chapter 3 (B). View from the N-terminal side of the α-helical wheel of WALP23 and WLP23 (transparent), illustrating their small differences in rotation angle (C). View from the N-terminal side of KALP23 illustrating the nearly opposite direction of the tilt angle in comparison to the tryptophan-flanked peptides illustrated in C (panel D). The vertical dashed arrows in the background represent the bilayer normal axis, whereas the tilted arrows represent the α-helical axis according to different tilt angles. The curved arrows indicate an increase in tilt angle or alternatively a different rotation angle in panels A and C, respectively.

Applicability to non-oriented samples

The addition of TFE in Chapter 4 was a good example of the benefits of the aptitude to apply ^{2}H NMR and GALA to non-oriented samples. Indeed, the additions the

volatility of TFE makes the use of macroscopically oriented samples unsuitable or difficult to handle for studies as presented in the present thesis.
Except the improvements in packing and hydration properties of the membrane and other advantages described in Chapter 1, the use of non-oriented bilayers enables the study of systems containing lipids that hinder the macroscopic orientability of lipid bilayers between glass-plates (Chapter 2). This will allow the study of more lipid factors that can influence the tilt, and rotation angles of model peptides. We can for instance explore the influence of lipids that may affect the packing properties of the acyl chain regions of the bilayer, like unsaturated PC-species and cholesterol (manuscript in preparation). Alternatively, we may investigate the influence phospholipids that have different headgroup properties than PC-phospholipids, thereby changing the packing properties of the membrane-water interfacial region of the membrane. Enlarging the scope of the application of such method as ^{2}H NMR and GALA in non-oriented lipid bilayers will open the way to study a myriad of parameters in a systematic way.

Applicability to larger systems and more biological systems/proteins
We presented above a large number of benefits from the use of ^{2}H NMR and GALA. However, a principle short-coming if we would apply this methodology to systems that are more biologically representative than model peptides, is that at least four alanine positions along the fragment of interest should be present in order to obtain reliable results. Indeed, in most transmembrane segments of proteins of peptides, the presence of four alanines on the same transmembrane segment is highly improbable.
We can in principle describe two ways to circumvent this problem. The first way is to use the complementarity of ^{2}H NMR/GALA with the use of the ^{15}N NMR chemical shift anisotropy as illustrated in recent work (17,18). Although, this method is not as precise as ^{2}H NMR/GALA, and requires the deduction and exclusion of solutions out of a number of possibilities, a single labeled position suffices to assign approximately the azimuthal angle and the tilt angles within a reasonable range of error of ± 5º. The second way to solve the problem of the scarcity of alanine positions for applying GALA is by performing non-perturbing mutations as exemplified by two recent papers (19,20). The originality of the method described in these papers is based on replacing glycine and isoleucine residues. These mutations were not affecting significantly the tilt and azimuthal orientations of the peptides under scope, and hence the orientational parameters of the biologically relevant peptides were determined very precisely as in our model systems. Thus, applying ^{2}H NMR and GALA in combination with non-perturbing mutations opens very promising perspectives for studying larger systems like membrane proteins.

References

1. Killian, J. A., and Nyholm, T. K. (2006) *Curr Opin Struct Biol* 16(4), 473-479
2. de Planque, M. R., Bonev, B. B., Demmers, J. A., Greathouse, D. V., Koeppe, R. E., 2nd, Separovic, F., Watts, A., and Killian, J. A. (2003) *Biochemistry* 42(18), 5341-5348
3. van den Brink-van der Laan, E., Chupin, V., Killian, J. A., and de Kruijff, B. (2004) *Biochemistry* 43(20), 5937-5942
4. Spelbrink, R. E., Kolkman, A., Slijper, M., Killian, J. A., and de Kruijff, B. (2005) *J Biol Chem* 280(31), 28742-28748

5. Petrache, H. I., Zuckerman, D. M., Sachs, J. N., Killian, J. A., Koeppe, R. E., and Woolf, T. B. (2002) *Langmuir* 18(4), 1340-1351
6. de Planque, M. R., Goormaghtigh, E., Greathouse, D. V., Koeppe, R. E., 2nd, Kruijtzer, J. A., Liskamp, R. M., de Kruijff, B., and Killian, J. A. (2001) *Biochemistry* 40(16), 5000-5010
7. van der Wel, P. C., Strandberg, E., Killian, J. A., and Koeppe, R. E., 2nd. (2002) *Biophys J* 83(3), 1479-1488
8. Im, W., and Brooks, C. L., 3rd. (2005) *Proc Natl Acad Sci U S A* 102(19), 6771-6776
9. Sengupta, D., Meinhold, L., Langosch, D., Ullmann, G. M., and Smith, J. C. (2005) *Proteins* 58(4), 913-922
10. Sparr, E., Ash, W. L., Nazarov, P. V., Rijkers, D. T., Hemminga, M. A., Tieleman, D. P., and Killian, J. A. (2005) *J Biol Chem* 280(47), 39324-39331
11. Nielsen, R. D., Che, K., Gelb, M. H., and Robinson, B. H. (2005) *J Am Chem Soc* 127(17), 6430-6442
12. Jones, D. H., Barber, K. R., VanDerLoo, E. W., and Grant, C. W. (1998) *Biochemistry* 37(47), 16780-16787
13. Whiles, J. A., Glover, K. J., Vold, R. R., and Komives, E. A. (2002) *J Magn Reson* 158(1-2), 149-156
14. Strandberg, E., Wadhwani, P., Tremouilhac, P., Durr, U. H., and Ulrich, A. S. (2006) *Biophys J* 90(5), 1676-1686
15. Opella, S. J., and Marassi, F. M. (2004) *Chem Rev* 104(8), 3587-3606
16. Nevzorov, A. A., Mesleh, M. F., and Opella, S. J. (2004) *Magn Reson Chem* 42(2), 162-171
17. Aisenbrey, C., Sizun, C., Koch, J., Herget, M., Abele, R., Bechinger, B., and Tampe, R. (2006) *J Biol Chem* 281(41), 30365-30372
18. Aisenbrey, C., and Bechinger, B. (2004) *Biochemistry* 43(32), 10502-10512
19. Tremouilhac, P., Strandberg, E., Wadhwani, P., and Ulrich, A. S. (2006) *J Biol Chem* 281(43), 32089-32094
20. Tremouilhac, P., Strandberg, E., Wadhwani, P., and Ulrich, A. S. (2006) *Biochim Biophys Acta* 1758(9), 1330-1342

.

Samenvatting

Biomembranen
De basiseenheid van alle levende organismen is de cel. Iedere cel wordt omsloten en daarbij afgescheiden van haar omgeving door de celmembraan: een vlies dat grotendeels uit lipiden en eiwitten bestaat. Bij eukaryoten (zoals b.v. bij dieren en planten), die meer ontwikkeld zijn dan bacteriën, bevatten cellen naast een kern vaal ook andere interne compartimenten, organellen genaamd, die zich ook met behulp van membranen afschermen van het celsap (het cytoplasma). Voor het goed functioneren van een cel is het belangrijk dat de inhoud van zowel de organellen als van het cytoplasma nauwkeurig wordt gereguleerd. De regulatie van de specifieke cellulaire en intracellulaire samenstelling wordt sterk beïnvloed door de membranen die een selectieve barrière en/of filter vormen voor een groot deel van de moleculen.

Eiwit gereguleerde membraanprocessen
De barrièrefunctie van membranen is te danken aan het waterafstotend karakter (hydrofobiciteit) van de lipide dubbellaag (of bilaag) die het "membraanvlies" vormt. De meeste wateroplosbare (hydrofiel) verbindingen worden niet passief door de membraan gelaten. Bij vele biologische processen is het selectieve transport van hydrofiele verbindingen, grote moleculen (macromoleculen) en ionen (elektrisch geladen deeltjes zoals in zout) door de membranen noodzakelijk. Het transport van deze moleculen wordt hoofdzakelijk uitgevoerd door membraaneiwitten. Behalve transport, zijn membraaneiwitten betrokken bij processen zoals hormonale respons, signaaltransductie en celherkenning die te maken hebben met cellulaire en intercellulaire mechanismen. Tot slot dient de membraan als ankerplaats voor eiwitten die verantwoordelijk zijn voor biochemische reacties zoals katalyse, biosynthese en degradatie van moleculen die door eiwitten worden uitgevoerd.

Structuur van membraaneiwitten
Zoals alle wateroplosbare eiwitten bestaan membraaneiwitten uit aminozuren. In het geval van membraaneiwitten is een groot deel van de aminozuren hydrofoob van karakter waardoor delen van deze eiwitten omgegeven worden door de lipiden in de membraandubbelslag. De termen transmembraanfragment of -segment worden veelal gebruikt om de onderdelen van membraaneiwitten te beschrijven die zich in de lipiden dubbellaag bevinden.
Het contact tussen de hydrofobe segmenten van eiwitten en de lipiden maakt het mogelijk voor het membraan om de functionering van membraaneiwitten te beïnvloeden door de structuur van het transmembraansegment te veranderen. Structuur parameters die van groot belang zijn voor de activiteit van membraaneiwitten zijn de zogenaamde secundaire structuur van de transmembraanfragmenten en hun oriëntatie in de lipide bilaag. De secundaire structuur van transmembraansegmenten neemt heel vaak de vorm van een α-helix (uitgestrekte helix geometrie) in een lipide omgeving. De oriëntatie van de transmembraan α-helices van eiwitten kan gedefinieerd worden door de "tilt" (helling in het Nederlands) -hoek, een hoek tussen de α-helix as en een rechte die loodrecht op het membraanoppervlak staat (de normaal van de bilaag).
Niet alleen de mechanismen waarmee membraaneiwitten hun taak uitvoeren gaan gepaard met veranderingen in de tilthoek, maar ook transmembraansegmenten passen hun tilthoek aan de veranderende lipide omgeving aan.

De tilthoek onderzocht in modelmembranen

Membraan eiwitten zijn meestal grote moleculen die moeilijk in detail en met een systematische aanpak te bestuderen zijn. Daarom heb ik voor mijn promotieonderzoek gebruik gemaakt van modelsystemen die bestonden uit synthetische lipiden en membraanpeptiden. In dit soort systemen kunnen lipiden zoals fosfolipiden spontaan bilagen vormen die de biomembranen kunnen nabootsen. De peptiden die ik heb gebruikt, zijn goede imitaties van transmembraansegmenten van eiwitten in de zin dat deze over de lipide bilaag kunnen steken en omdat hun samenstelling verrijkt is met veel voorkomende aminozuren in transmembraanfragmenten van natuurlijke eiwitten. De voordelen van dergelijke modelsystemen zijn dat de parameters die onder de loep worden genomen één voor één bestudeerd kunnen worden door de samenstelling van zowel de lipiden als van de peptiden te veranderen. Een ander groot voordeel van deze aanpak is de mogelijkheid om specifiek gelabelde aminozuren met magnetisch actieve isotopen in de synthetische peptide te bouwen. De oriëntatie van de magnetisch actieve isotopen zoals deuterium (^{2}H symbool) kan gemeten worden met behulp van de techniek kernspinresonantie spectroscopie of "nuclear magnetic resonance spectroscopy" zoals in het Engels en in het Nederlandse jargon genaamd (NMR spectroscopy, een techniek waarop de principes van MRI berusten).

De tilthoek van transmembraanpeptiden bepaald met behulp van deuterium NMR en moleculaire dynamica

Door de oriëntatie van het deuterium ingebouwd in de aminozuren te meten met behulp van NMR, is het mogelijk om op basis van de α-helix geometrie en met behulp van computerberekeningen de tilthoek van een peptide in een membraan te berekenen. Tijdens mijn promotieonderzoek heb ik een computerprogramma geschreven om de oriëntaties van de peptiden te bepalen aan de hand van de deuterium NMR signalen die ik met gelabelde peptiden heb gemeten.

Met behulp van deze methode heb ik de invloed van de dikte van de lipide bilaag op de tilthoek en de preferentiële richting van de tilt (in dit proefschrift ook de rotatiehoek genoemd) onderzocht. Het resultaat was dat de tilthoek van de gebruikte peptiden gevoelig is voor de membraan dikte, hetgeen bevestigt dat de dikte van de bilaag de activiteit van membraaneiwitten kan beïnvloeden. Maar deze tilthoeken waren klein in vergelijking met de theoretische verwachtingen. Daarnaast is de invloed van de samenstelling van de flankerende aminozuren van de transmembraanpeptiden op de tilt en rotatiehoeken onderzocht. De flankerende aminozuren zorgen namelijk voor de verankering van de transmembraan eiwitten/peptiden aan het lipide/water grensvlak. Het resultaat leidde tot de conclusie dat de grootte van de tilthoek enigszins verandert met de aard van de flankerende aminozuren die zich vlakbij het lipide/water grensvlak bevinden. Een spectaculairder resultaat was dat de rotatiehoek heel sterk beïnvloed wordt door de aard van de aminozuren aan het lipide/water grensvlak. Om verder de invloed van het grensvlak van het membraan op de oriëntatie van de peptiden te verkennen, heb ik vergelijkbare systemen onderzocht met de aanwezigheid van het alcohol trifluoroethanol (TFE). In membraansystemen verdeelt deze verbinding zich grotendeels in het lipide/water grensvlak en daarbij verstoort het de eigenschappen van het membraan in dat gebied. De resultaten in mijn proefschrift tonen aan dat TFE alleen de tilthoek verkleint van transmembraan peptiden die met aromatische aminozuren zoals tryptofaan geflankeerd zijn, maar niet die van lysine geflankeerde peptiden. TFE dient vaak als

model voor onderzoek naar het mechanisme van anesthetica. Mijn resultaten betekenen dat anesthetica zoals alcoholen waarschijnlijk membraaneiwitten anders beïnvloeden wanneer hun transmembraan segmenten met aromatische aminozuren geflankeerd zijn, dan wanneer zij met polaire aminozuren zoals lysine geflankeerd zijn. Tot slot houdt het laatste hoofdstuk van dit proefschrift zich bezig met de moleculaire en atomische mechanismen die bij de lipide/peptide interacties betrokken zijn. Hierbij heb ik gebruik gemaakt van computersimulaties om de moleculaire dynamica van één van de modelmembraan systemen van de vorige hoofdstukken te onderzoeken. Dit laatste hoofdstuk geeft meer inzicht in de dynamische aspecten op atomair en moleculair niveau van zowel de peptide als van de lipiden in model membraansystemen.
Over het algemeen geven de resultaten die in dit proefschrift beschreven zijn een beter begrip voor de interacties die in membranen van belang kunnen zijn. Ook de ontwikkeling van de deuterium NMR biedt perspectieven om de methode bij meer biologische relevante systemen toe te passen zoals transmembraan eiwitten en antibiotica. De moleculaire dynamica kan daarbij ook een belangrijke rol spelen om de dynamische aspecten beter in beeld te brengen dan alléén met NMR.

Acknowledgments, remerciements, dankwoord, teşekkürler

First, I would like to show my profound gratitude to my supervisor Antoinette Killian. Thank you very much Antoinette for all your efforts to guide me through the complexity of biophysical and membrane research. Even in difficult times and in spite of all your responsibilities you managed to create time to help me through the difficult process of graduating. I am confident that your experience and know-how will be for me of great value in my future career. I am deeply grateful to Ben Kruijff who shared generously his ideas about my project showing a permanent interest in my research topic. Vladimir Chupin and Erik Strandberg are thanked for teaching me and assisting me in the use of the NMR spectrometer at the beginning of my project, and Erik especially for the nice work we did together that is described in chapter 2. Thomas Nyholm, and Mobeen Raja are greatly acknowledge for their contribution to the chapter 4 of the present thesis, as well as Erica Kremer for performing important tests. I would also like to thank all other members of Biochemistry of Membranes that I got to know during the last years, but putting an exhaustive list of all the names would be unfair to the colleagues I would next like to mention in particular. I enjoyed very much sharing the office with Hester Hasper, Henry Bouwman, and Anja Rebber and the mental coaching we at least tried to give to each other. Henry, I am very glad we are still in touch in spite of the distance between the US and the NL. I also appreciated very much the patience and calm of Robin Spelbrink and Pieter Rijken and of course their computer tricks to help me out of my software-related problems; sharing the office with them was a pleasure. Dragomir Ganchev will precede me by two weeks with his thesis defence. Dragomir I am glad to still be in touch with you, and I am still impressed and very much interested by the work you did with AFM. Besides gratifying members of Biochemistry of Membranes, I find also important to express how much I feel concerned and sorry about the consequences of the reorganization within the faculty of Chemistry. I wish all the best to every one of you.

Nowadays, scientific research is almost unconceivable without a multidisciplinary approach. Cooperation's are an excellent way to apply several techniques to solve scientific problems. During my thesis, I enjoyed several collaborations some of which leading to a publication, and some fruitful ones providing us more insights and perspectives for future projects. Therefore, I would like to thank Dirk Rijkers and Rob Liskamp for the enormous amount of work that was invested in making peptides. And Dirk, thank you very much for allowing me to do a part of the job under your supervision, and to learn the basics of peptide synthesis. The labeled peptides were used intensively in all my experimental chapters. Patrick Fuchs from the "Université de Paris 7" is not only one of my best friends; he is also a great colleague from whom I learnt very much about molecular dynamics. Working with him is a wonderful pleasure. I also want to express my gratitude to Catherine Etchebest who is the head of the department where Patrick is affiliated. The sharpness of your criticism and analyses helped a lot to clarify the job I did together with Patrick (chapter 5). I hope we will manage to publish the work very soon. I am very grateful to Marc Baldus, from the University of Göttingen who allowed me to be part of the contributors of one of his articles on a topic closely related to my thesis. I enjoyed very much the collaboration with Jaap van Hellemond, Koen van Grinsven, and Aloysius Tielens

from the department of Biochemistry and Cell Biology, at the faculty of Veterinary Medicine.
I would also like to mention collaborations, which did not find their final accomplishment in the form of a publishable work yet. It was a great pleasure to work with Loes Kroon-Batenburg (Crystal and Structural Chemistry), Hans Meeldijk (Electron Microscopy), Alain Milon and Valérie Réat from the "Institut de Pharmacologie et de Biologie Structurale" (Toulouse, France). Although the plans stayed at their nascent stage, I enjoyed very much the brainstorm sessions with Jeroen Geurtsen (Molecular Microbiology), Lucy Rutten (Crystal and Structural Chemistry), and Maarten Egmond (Membrane Enzymology) about the use of NMR for determining the tilt angle of an outer-membrane protein. I have very nice memories of the three-week stay of Frances Separovic (University of Melbourne); thank you very much Frances for teaching me so quickly how to measure NMR relaxation parameters and other essential tricks for the use of the spectrometer: I agree that theories will always remain complex as long as we keep saying they are difficult to understand. Although I did not have the chance to collaborate with Maurits de Planque (Former graduate student of Biochemistry of Membranes, and now University of Oxford), I appreciated very much his efforts to introduce me to the lipid-protein interactions scene during conferences. Thank you very much for your excellent tips about my project and your very nice company at conferences together with Frances.
Since the 1st of June 2006, I am employed in the department of NMR spectroscopy in Utrecht. I am deeply indebted to Rolf Boelens for accepting my candidature in his department; this gave the necessary rest to finish writing my thesis in descent conditions in a period that was very difficult for me at a personal level and to start with a very nice project. I will never forget this very generous decision of yours. The fact that the NMR spectrometer of my previous department was in your building was actually only a good reason for meeting very nice people who were always volunteer to help with questions related to NMR spectroscopy and computational (structure) calculations. I would like to thank Alexandre Bonvin and Aalt-Jan van Dijk for their help with structure calculations. I am very pleased to have the opportunity to work with Alexandre for my new NMR/computational project. Two other persons to whom I absolutely want to express my profound gratitude are Michiel Hilbers and Johan van der Zwan. Without their wonderful technical assistance with the spectrometer, I could not have finished my fourth chapter and much more work that I did not include in my thesis. I am also grateful to emeritus Prof. Rob Kaptein who helped me with project proposals within the Bijvoet Center and for a fruitful collaboration outside the Netherlands. The people I want to thank next were for me during my PhD practically more friends than colleagues. I enjoyed very much the time with Devashih Das, Tammo Diercks, Rob de Jong, Adrien Favier (IBS-Grenoble), Nathalie Sibille (Institut Pasteur de Lille, France), Danny Hsu (University of Cambridge), and Vincent Truffault (University of Munich). And of course I appreciate very much the contact with all my new colleagues at the NMR department, and want to thank them for their strong collegiality over the last years to now. Thank you very much Marc, Tsjerk, and Hugo for the triple Dutch grammar-check of my summary!
During the first three years of my PhD, I got the chance to get involved to some extent in the policy and organization of the Bijvoet Center for Biomolecular Research as a representative for graduate students. This gave me a flavour of other aspects of science than producing and analyzing data. It opened me several chances to collaborate with many of the people I mentioned already above and met friends as

Clasien Oomen (formerly from Crystal and Structural Chemistry) with whom I was co-organizing social events like for example lectures within the Bijvoet Center. I also appreciated very much working with all other members of the graduate-student organizing committee (the "aiopd platform"), and the staff members of the Bijvoet Center for giving us some space to improve our work and training conditions.
And since I am a periodic visitor of the department of Membrane Enzymology (Prof. Gerrit van Meer's department) for their beer tasting moments and events, and in the past for using sometimes some of their technical facilities, I would like to thank them all for their kindness, hospitality and collegiality. Among them, I would like to thank especially Catheleyne Puts, and Guillaume Lenoir; in tough times you helped me often to forget the "heart aches" that prevented me from evolving steadily during the writing process of my thesis.
When I looked at other Dutch theses, I often met the opening sentence: "Promoveren doe je niet alleen…". Considering the length of my acknowledgments and probably the many names I forgot to mention, I think this sounds right and well-tuned into my ears. And this applied also to my private life. I'd also like to thank friends for being simply what they are to me…friends, and my family. Without them my last year would have been unbearable. Among those who surround me in my life out of the work, I will only mention few names for their closer involvement in my thesis or study, some of them being already mentioned above.
Hilmi ve Hande size çok teşekkürler arkadaşlığınız için ve öğrenci zamanlarımda beni kimyanın ve biyolojinin araştırma konuları sevdirdiğiniz için.
Sevgili annecim ve babacım sizi çok özlüyorum: doktoramı bitirince "öğrencilik gibi iş" bitiyor, umarım çok seviniyorsunuz. Hülya, Bahar, et Bülent, je vous adore et vous remercie d'avoir patienté et cru en l'aboutissement de ce travail. Mon très cher frère, nous voilà de nouveau à partager une expérience commune qui aura marquée une bonne partie de nos vies. Un énorme merci à toi Bahar, tu as été vraiment super pendant les durs moment de l'année passée. Cela nous a rapprochés d'avantage.
Graag, wil ik mijn schoonfamilie ontzettend veel bedanken voor de vele goede jaren samen. Jullie weten inmiddels ongeveer veertien jaren al dat ik heel veel, zelfs heel erg veel suiker in mijn thee nodig heb … "zacht en zoet is de mispel" ;-) Met andere woorden (op zijn Suats dan!), is het jullie allemaal gelukt om mij jarenlang het gevoel te geven dat ik bij jullie thuis hoorde. Arnout en Renneke, heel veel dank daarvoor. Adriaan en Esther, Jesca en Reinier ontzettend dank voor jullie geduld, begrip, waardering en vooral de morele steun. Jesca, ik wil je in het bijzonder danken voor jouw onvergetelijke hulp in de voor mij moeilijkste momenten van het afgelopen jaar. Je kunt in alle tijden op mij rekenen!
Même si il m'est très difficile d'accepter les évènements des derniers mois Babette, j'ai vécu mes années avec toi comme inoubliablement belles, candides, et heureuses, malgré quelques fois des douleurs et des déceptions. J'aurais énormément voulu partager l'aboutissement de cette thèse avec toi et éveiller chez toi les mêmes sentiments de fierté que j'ai éprouvé pour ta thèse et bien d'autres choses. Merci pour tout ce que tu as été autrefois pour moi, et pour m'avoir convaincu de reprendre les études aux Pays-Bas. Je te souhaite une vie pleine de richesse spirituelle et de bonheur.

Publications

Chapter 2
Strandberg, E.**, Özdirekcan, S.**, Rijkers, D. T., van der Wel, P. C., Koeppe, R. E. 2nd, Liskamp, R. M., Killian, J. A. (2004) Tilt angles of transmembrane model peptides in oriented and non-oriented lipid bilayers as determined by ^{2}H solid-state NMR. Biophys. J. 86(6), 3709-3721.

Andronesi, O. C., Pfeifer, J. R., Al-Momani, L., **Özdirekcan, S.**, Rijkers, D. T., Angerstein, B., Luca, S., Koert, U., Killian, J. A., Baldus, M. (2004) Probing membrane protein orientation and structure using fast magic-angle-spinning solid-state NMR. J. Biomol. NMR 30(3), 253-265.

Chapter 3
Özdirekcan, S., Rijkers, D. T., Liskamp, R. M., Killian, J. A. (2005) Influence of flanking residues on tilt and rotation angles of transmembrane peptides in lipid bilayers. A solid-state ^{2}H NMR study. Biochemistry 44(3), 1004-1012.

Nyholm, T. K. M., **Özdirekcan, S.**, and Killian, J. A. How protein transmembrane segments sense the lipid environment. Biochemistry (Current Topics). *Minor revisions.*

Submitted manuscripts or in preparation

Chapter 4
Özdirekcan, S., Nyholm, T. K. M., Raja, M., Rijkers, D. T. S., Liskamp, R. M. J., and Killian, J. A. Influence of 2,2,2,-trifluoroethanol on membrane interfacial anchoring interactions of transmembrane α-helical peptides. *Submitted*

Chapter 5
Özdirekcan, S., Etchebest, C., Killian, J. A., and Fuchs, P. F. J. Molecular dynamics on membrane peptides under positive hydrophobic mismatch: insights from long time scale trajectories. *Manuscript in preparation.*

van Hellemond, J. J., Hoek, A., Wichgers Schreur, P., Chupin, V., **Özdirekcan, S.**, Geysen, D., van Grinsven, K. W. A., Koets, A. P., Van den Bossche, P., Geerts, S., and Tielens, A. G. M. The energy metabolism of bloodstream form Trypanosoma theileri in relation to that of other trypanosomes and nutrient availability in the environment. *Submitted*